University of Strathclyde

Department of Pure and Applied Chemistry

Development of a new diagnostic method for Human African Trypanosomiasis using Raman spectroscopy

By

Alexandre Girard

A thesis submitted to the university of Strathclyde, Department of Pure and Applied Chemistry, in fulfilment of the requirements for the degree of Doctor of Philosophy.

September 2018

Declaration

This thesis is the result of the author's original research. It has been composed by the author and has not been previously submitted for examination which has led to the award of a degree.

Signed:

Date:

Acknowledgement

I would like to thank Professor Duncan Graham, Professor Karen Faulds and Dr Annette Macleod for giving me the opportunity to work in their respective research group through a productive collaboration, and for their support and guidance over the past four years. It has been a very exciting and interesting project and I would like to thank them for their trust, that led to an amazing field work opportunity in Guinea.

Many thanks to Barbara Bradley, Paul Capewell, Caroline Clucas and Anneli Cooper at the university of Glasgow for introducing me to the world of biology, for their tremendous help and guidance throughout my PhD and mostly for their patience and kindness in teaching and explaining basic biology to a chemist.

I would especially like to thank, my postdocs and close friends, Dr Samuel Mabbott, Dr Lee Barrett and Dr Steven Asiala for their amazing guidance, advice, support and huge patience during my PhD, as well as for all our pub sessions that helped me go through my bad times (and also good times!). I would like to also extend my thanks to Dr Lauren Jamieson, Dr Kirsten Gracie, Dr Stacey Laing and Corinna Wetherill for their strong help, advice and kindness with my work, thesis writing, and most importantly for our music sessions to overcome the dark moments!!

Special merci to my very good and close friend Etienne “Pascal” Brouillet-Coquillat, along with Dr Andrea Taladriz-Sender, muchas gracias, for their constant support, our 6 nations time, pastis tasting and all the (countless) good time spent outside of work!

Thanks to Richard and Rachel Gregory who welcomed me as a family member and gave me the strength and passion to keep working in science in the UK through the years.

Massive thanks to everyone in the Raman group, particularly Vegas, basketball team (or ski crew now), Sian Sloan-Dennison, Samantha Moreton, Pietro Gancitano, Julie Docherty, Rachael Cameron, Jonathan Simpson, for their support and advice with my work, and making me enjoy every day at work. For all the good time at work and outside work, thank you!

J’aimerai particulièrement remercier mes parents, ma sœur et mes grands-parents pour leur soutien, leur aide et leurs encouragements qui m’ont permis de finir ma thèse. Un grand merci aussi à mes amis de France !

Abstract

Human African Trypanosomiasis (HAT) is a tsetse fly-transmitted parasitic disease found in Sub-Saharan Africa. Although responsible for deadly epidemics throughout the 20th century, a renewed commitment to disease control by the World Health Organisation and partners since 2000 has significantly reduced the number of new cases and motivated a target for the elimination of *gambiense*-HAT by 2030. However, the recent identification of latent human infections, and the detection of trypanosomes in extravascular tissues hidden from current diagnostic tools, such as the skin, has added new complexity to identifying infected individuals. New and improved diagnostic tests, capable of detecting such cases are therefore needed.

This thesis investigates the potential of Raman spectroscopy as a diagnostic tool for HAT. Raman spectroscopy provides vibrational information about the composition of a matrix and could determine the biochemical changes that occurs during the infection, leading to the detection of diseased tissue. Lately, this technique has been extensively used for medical diagnostics and the recent technological advancements have improved the cost, sensitivity and portability of Raman technology, making Raman an attractive tool for the detection of HAT.

The aim of this thesis was to assess and develop a new diagnostic method for *gambiense*-HAT using Raman spectroscopy of the skin. Two sub-species of *Trypanosoma brucei* were analysed and biologically characterised, with the purpose of understanding the surface biological composition of the parasite and to obtain their Raman fingerprint. The skin of *T. brucei*-infected and uninfected mice was then investigated to measure spectral differences using statistical analysis, thus providing information on biochemical changes in infected skin. This technique was then translated *in situ* by analysing infected mice over a time course of infection. Finally, this diagnostic method was tested *in vivo* on human patients in the field in collaboration with the HAT national control active screening program in Guinea. This study investigated for the first time, the application of Raman spectroscopy for the detection of *gambiense*-HAT by targeting the skin of the host. It has demonstrated significant potential to discriminate between infected and non-infected tissue and could represent a unique non-invasive diagnostic tool in the goal for elimination of *T.b. gambiense* disease.

Abbreviations

α	Alpha
AAT	Animal African Trypanosomiasis
ATF	Adipose tissue form
AUC	Area under the curve
β	Beta
BL	Bioluminescence
BSF	Bloodstream form
CATT	Card agglutination test for trypanosomiasis
CCD	Charge-coupled device
cm	Centimetre
CNS	Central nervous system
CSF	Cerebrospinal fluid
CTC	Capillary tube centrifugation
DNA	Deoxyribonucleic acid
ES	Expression site
FFPE	Formalin fixed paraffin embedded
GPI	Glycosylphosphatidylinositol
HAT	Human African Trypanosomiasis
HDL	High density lipoprotein
HE	Haematoxylin and Eosin

IgM	Immunoglobulin M
IM	Intramuscular
IR	Infrared
ISG	Invariable surface glycoproteins
IV	intravenous
L	Litre
LDL	Low density lipoprotein
mAECT	mini anion exchange centrifugation technique
mHCT	micro-haematocrit centrifugation technique
µg	microgram
µL	microlitre
µm	micrometre
µM	micromolar
mg	milligram
mL	millilitre
mM	Millimolar
mW	milliwatt
NA	Numerical aperture
nm	nanometre
NSG	NOD scid gamma
%	Percentage
PC	Principal component

PCA	Principal component analysis
qPCR	Quantitative polymerase chain reaction
s	second
T.b	*Trypanosoma brucei*
T.b. brucei	*Trypanosoma brucei brucei*
T. cruzi	*Trypanosoma cruzi*
T.b. gambiense	*Trypanosoma brucei gambiense*
T.b. rhodesiense	*Trypanosoma brucei rhodesiense*
TL	Trypanolysis test
TLCK	Tosyl phenylalanyl chloromethyl ketone
UV	Ultraviolet
VSG	Variable surface glycoproteins
v/v	Volume/Volume
Wb	whole blood
WHO	World Health Organisation

Contents

Chapter 1 Introduction

1.1 Human African Trypanosomiasis

1.1.1 History

Trypanosoma brucei (*T.b*) is a flagellated protozoan parasite of the order Kinetoplastida, endemic to sub-Saharan Africa. This extracellular parasite resides in the blood and tissue fluids of a vertebrate host where it causes the disease African trypanosomiasis. Human African trypanosomiasis (HAT) or sleeping sickness is caused by two subspecies of *T.b*, *T.b. gambiense* and *T.b. rhodesiense.* The third subspecies, *T.b. brucei*, is only infectious to animals and is one of a group of African *Trypanosoma* parasites responsible for animal African trypanosomiasis (AAT) or nagana in non-human vertebrates.

T.b was first identified as the causative agent of nagana in cattle by David Bruce in 1895,[1] and named in his honour in 1899.[2] This discovery was followed in quick succession by the first observation of trypanosomes in human blood from a European patient in The Gambia by Forde and Dutton in 1902,[3,4] and from isolates taken in North-Eastern Rhodesia (now Zambia) by Stephens and Fantham in 1910.[5] Both parasites located in West and East Africa were at first considered to be separate species, and named as *Trypanosoma gambiense*,[4] and *Trypanosoma rhodesiense*,[5] respectively, then later demoted based on biological similarity to subspecies of *T. brucei*.[6]

Meanwhile, the essential role of the blood-feeding tsetse fly (genus *Glossina*) in the lifecycle and transmission of the parasite between vertebrate hosts was also identified.[7–9] Both male and female tsetse flies feed exclusively on blood and *T.b* can be transmitted via the saliva of an infected tsetse fly during the taking of a blood meal. The frequency and intensity of human exposure to tsetse were thus considered major risk factors for infection.[10] Consequently, the distribution of *T.b* is restricted by the distribution of the tsetse fly vector, which are found across a swathe of sub-Saharan Africa commonly referred to as the tsetse belt. The tsetse flies require specific climatic conditions to survive such as high humidity levels, which are generally found in

tropical forests and mangrove,[11,12] within the tsetse belt, covering an area of approximately 10,000 km^2 between the latitudes of 14° North and 29° South.[13,14] The sub-species *T.b. brucei* is spread throughout the tsetse belt, while HAT is typically limited to more spatially restricted "foci", which are mainly located in remote rural regions. Inhabitants of the rural areas in Africa are subjected to a higher risk of infection due to their activities such as farming, fishing or hunting exposing them to tsetse infected areas, which are generally rich in vegetation and rivers.[11,12,15]

In the early 20th century, HAT was responsible for a number of widespread epidemics that resulted in the death of hundreds of thousands of people.[16] Intense screening of the population combined with the use of adequate treatment and vector control greatly reduced the number of reported cases, nearly eliminating HAT in the early 1960's (Figure 1.1).[16]

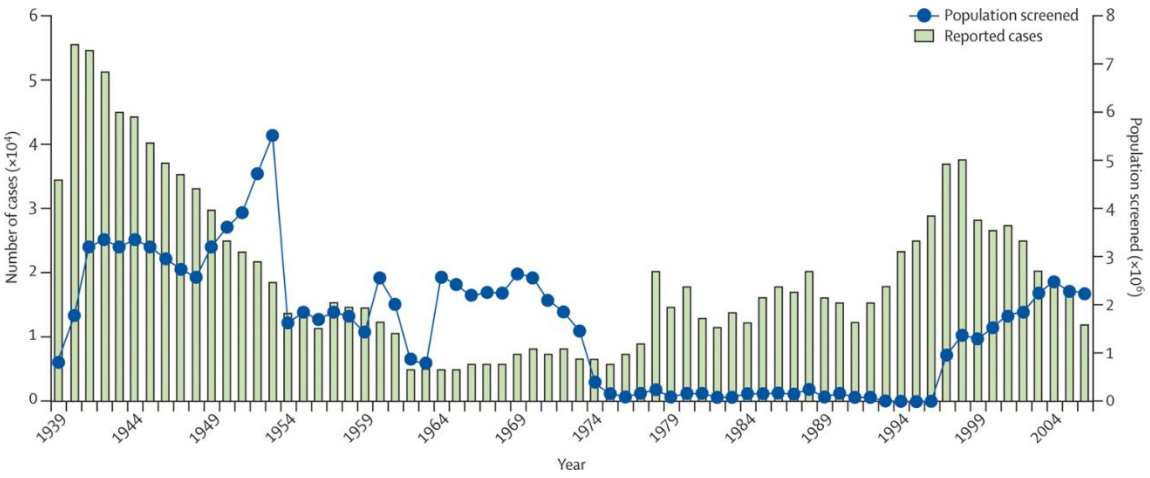

Figure 1.1 Evolution of the number of cases of HAT caused by T.b. gambiense and the population screened in Africa through the 20th century.[17]

However, by the late 1960's many sleeping sickness endemic African countries had become independent, and HAT control programs were deprioritised or were considered untenable.[16] Over time, following a lack of surveillance, recovery of tsetse population, and migration of human population, the disease recrudesced and HAT had reached an estimated 300-500,000 cases by the mid-1990's according to a report produced by the World Health Organisation (WHO) in 1998.[18]

Following a resolution from WHO in 1997, the World Health Organisation (WHO) committed resources to sustained and renew HAT control, and with strong collaboration between international scientific community, more intensive control and treatment programs were installed.[19,20] This intervention successfully brought the number of reported cases to lower than 10 000 in 2009,[19] and in 2012 WHO declared to aim for the elimination of *T.b. gambiense* HAT as a public health problem by 2020, and finally targeting a zero case reported by 2030.[21,22]

Despite the effort deployed, there are still around 60 million people and 55 million cattle at risk of African trypanosomiasis over an area of 10 million km² in the sub-Saharan region.[14,23] With a devastating impact on the economy and social development of African countries, it has been estimated that succeeding in controlling and eliminating human and animal African trypanosomiasis from sub-Saharan countries could potentially return benefits of billions of dollars in terms of agricultural production and human productivity.[24–26]

1.1.2 *Trypanosoma brucei* description and geographic distribution

The two forms of HAT cannot be distinguished morphologically but are separated of the basic of host range, clinical course, geographical range, and by molecular analysis.[6,15,27,28]

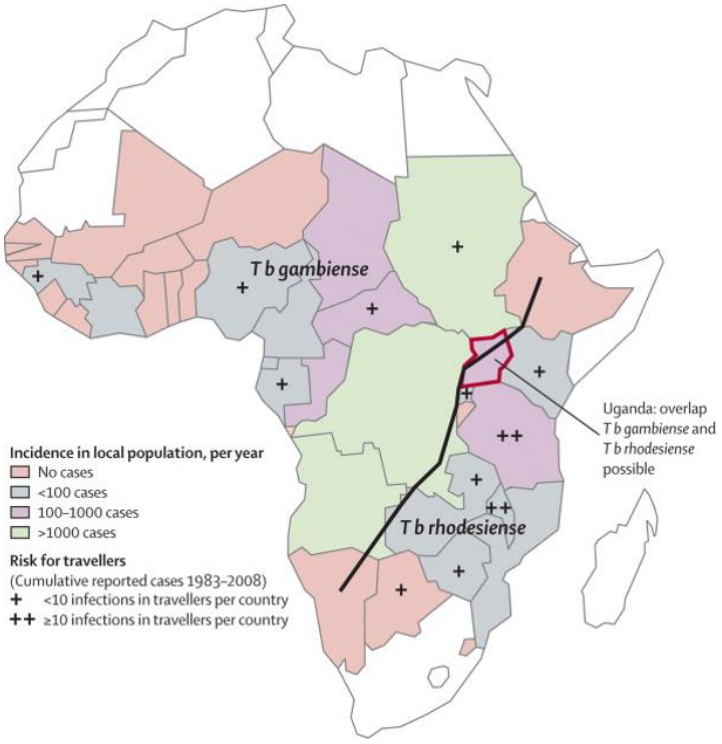

Figure 1.2 Repartition of the two different sub-species of Trypanosoma brucei responsible for HAT (gambiense and rhodesiense) across Africa.[17]

T.b. gambiense is found in the West of Africa (Figure 1.2) and is responsible for 97 % of current reported cases of HAT.[29] This form of trypanosomes typically induce a chronic form of HAT, where the disease progresses slowly and the symptoms can stay latent for months, even years after the initial infection.[30] *Gambiense*-HAT is an anthroponotic disease, which implies that the causing agent of the disease is carried by humans,[15,27] hence limited the transmission cycle to human – fly – human. Further evidences demonstrate the plausible infection of animals by *T.b. gambiense*, suggesting a possible presence of an animal reservoir.[31–33] However, it is still unknown if the disease is transferrable from animal to human.[34]

T.b. rhodesiense is localised in East Africa (Figure 1.2) and despite causing large epidemics in the previous century,[16,35,36] is now responsible for only 3 % of the current cases reported.[29] This sub-species of HAT is more acute than *T.b. gambiense*, and in some cases could lead to the death of untreated patients within weeks. *T.b. rhodesiense* HAT is a zoonotic disease, where the parasites infect preferentially animals, both wild and domestic, constituting the main reservoir for rhodesiense-HAT.[15,27,37] The main transmission routes are animals – fly – animals, from which

human infection can occasionally occur.[27] Hence, population in proximity to national parks and cattle, respectively, are at risk.[38,39] However, some studies have showed that infected domestic animals lead to a lower number of human infection cases.[40]

Only Uganda hosts both forms of HAT parasites in two separated geographical regions (Figure 1.2), where *T.b. gambiense* is located to the north west and *T.b. rhodesiense* is found in the south west.[41,42] In 2005 the barrier separating the two sub-species was only measured as 150 km wide, allowing a risk of convergence, hence disturb the installed diagnostic organisation which requires different evaluation and treatment methods for each.[41] Indeed, it was found recently that two new districts in northern Uganda displayed cases of infection by *rhodesiense*-HAT, manifesting the progressive migration of *T.b. rhodesiense* towards *T.b. gambiense* territory, emphasizing the risk of overlap.[43] This risk will be accentuated due to the recent conflict occurring in the south of Sudan and induced a large movement of population in the north of Uganda that could sustain the disease.[44]

This overlapping would have a disastrous impact as the differentiation of the two forms of HAT are merely based on the different geographical sites and their clinical course, as their morphologies are identical.

1.1.3 *Trypanosoma brucei* interactions with vector - mammalian hosts and associated treatments

1.1.3.1 Morphology and life cycle

Sleeping sickness is a vector-borne disease that is transmitted by the bite of a tsetse fly (genus *Glossina*).[27] The life cycle of T.b involves different biological stages, where the parasite adapts between the host (animal or human) and the vector's environment to develop their growth and multiplication (Figure 1.3).[45,46]

Tsetse fly is being infected when ingesting bloodstream trypomastigote stumpy forms from the infected host during a blood meal.[45] This form of the parasites possesses a dense variable surface glycoprotein (VSG) protecting it from clearance by the host. Bloodstream stumpy form moves toward the midgut of the fly at the start of the infection where they undergo a first differentiation

into a procyclic forms due to the acidic environment of the midgut of the tsetse fly.[47–49] During this differentiation, trypanosomes replace their VSG coat by a procyclin coat.[49] Procyclic trypomastigote forms replicates by binary fission within the midgut and further differentiate into epimastigotes forms.[48,49] Epimastigote forms then migrate toward the salivary gland of the tsetse fly, where they will multiply and then differentiate into infectious metacyclic trypomastigote forms.[50] This new metacyclic form is ready to infect a new host during the next blood meal of the fly, as its procyclin surface coat is replaced by the VSG. It allows the parasites to infect a new host both human or animal. The *T.b* biological cycle in the vector takes around 18 – 35 days, between the infection by bloodstream trypomastigotes and the differentiation into infectious metacyclic forms in the salivary glands of the fly.

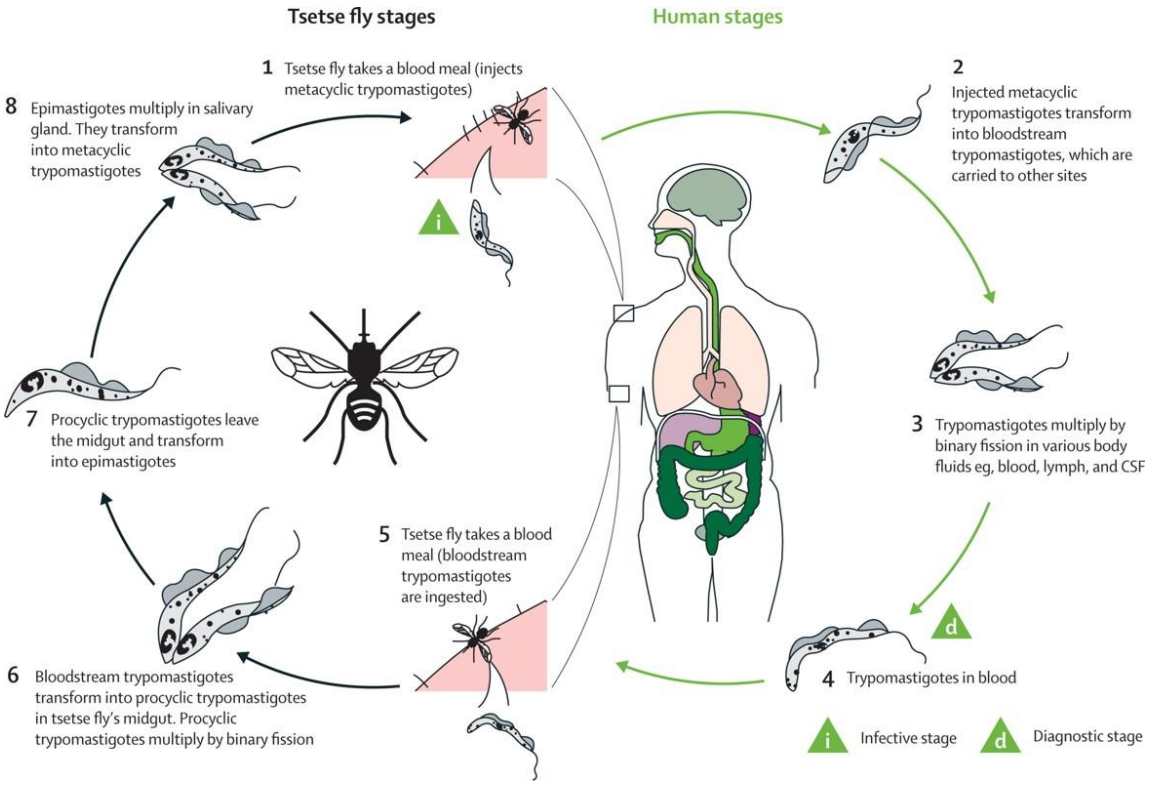

Figure 1.3 Illustration of the life cycle and development of Human African trypanosomiasis in both vector and host.[51]

When an infected tsetse fly bites an individual, it delivers the metacyclic trypomastigotes forms into the skin.[45] As they possess a VSG coat around their surface, they can survive in this new

environment. Metacyclic trypomastigotes replicate at the bite site and then enter the blood via the lymphatic system. During this transition to the blood, metacyclic forms differentiate in long slender trypomastigotes, proliferative, form.[52] This form allows the parasites to maintain the infection within the host by multiplying through binary fission (Figure 1.3). Finally, some of this proliferative slender forms will differentiate into a short stumpy non-dividing form.[52] It was found that the latter differentiation was induced when a high number of parasites was present in the blood.[53] These stumpy forms are adapted to transform into the procyclic forms found in the midgut of tsetse fly, hence ensuring successful transmission of the sleeping sickness back to the tsetse fly during its blood feeding to start a new cycle.

Bloodstream trypomastigotes are not only located in the blood but are also capable of entering the cerebrospinal fluid (CSF) and the brain, as well as being distributed through different organs such as lymph nodes, spleen or liver.[17,54]

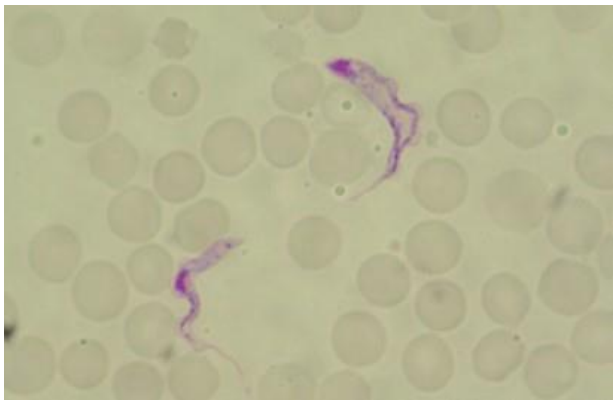

Figure 1.4 Giemsa-stained thin blood film with two bloodstream forms of Trypanosoma brucei: long slender proliferative form (left) and short stumpy non-dividing form (right).[30]

Figure 1.4 displays an example of a microscopic observation of two different bloodstream forms in mammalian blood. The difference in their shape is clearly observed, where the long slender forms proliferate in the blood and the short stumpy form is not dividing and ready for transmission to the tsetse fly. Trypanosomes are usually found in mammalian blood to be a single-shaped cell of 20 – 30 µm long and 2 -5 µm wide, with a single flagellum, running through the cell membrane from the flagellar pocket, that permits the motility of the parasite.[30]

1.1.3.2 Human African Trypanosomiasis disease stages and clinical course

When an infected tsetse fly bites a human being, trypanosomes are released in the blood of the individual. This is the first stage, also known as the haemolymphatic stage.[54] Parasites then replicate at the bite site, where they may cause a chancre, and from here enter the lymphatic system and blood. This chancre has been observed more often for the infection with *T.b. rhodesiense* than for *T.b. gambiense*.[15] During this stage, the lymph nodes may be enlarged and visible at the base of the neck in *T.b. gambiense* infection, a distinction called Winterbottom sign.[15] At this haemolymphatic stage most of the symptoms are non-specific and can provoke fever, malaise, headache, weight loss, enlargement of the spleen or muscle pain,[51] making the early detection of HAT challenging.

The second stage of the disease, known as the meningoencephalitic stage, occurs when the parasites cross the blood brain barrier and reach the central nervous system.[55] For *T.b. rhodesiense*, which is typically a more acute and severe course of infection, this stage can be reached within weeks or months. Although it is difficult to identify the separation between the two stages due to the fast progression of *T.b. rhodesiense* towards the CSF. While for *T.b. gambiense* it can take many years before reaching the second stage of infection.[56,57] The presence of the parasite in the brain leads to serious neurological problems that can remain permanent even after treatment. The main symptoms observed as this stage is a circadian rhythm disruption that leads to sleep disturbance and reverse sleep phases between day and night time. This characteristic daytime somnolence is the originator of the common name for the disease as “sleeping sickness”.[15] Subjects were also shown to manifest a motor or speech disturbance, peripheral motor neuropathy, or psychiatric symptoms such as increased irritability, hallucinations and mental changes.[58,59] If the patient is not diagnosed, and not treated, the course of infection will typically progress to coma, organ failure and ultimately lead to death.[54]

Despite their symptoms similarities, recent studies showed evidences of small distinctions in the clinical course between different regions, where it was observed that *rhodesiense*-HAT was acute in Uganda and chronic in Malawi.[60] These differences were observed after studying the virulence of the parasites within the host, and the difference immune responses between host and trypanosomes. It was proposed that ancestors of the Malawi population have been exposed to

T.b. rhodesiense for a longer period, which confers them a certain tolerance against the trypanosomes. It was further confirmed that the difference in the immune response from the host plays a role in the progression and virulence of HAT.[61]

1.1.3.3 Cases of asymptomatic patients

Following the different observation made regarding the virulence and progression of HAT between hosts, some cases of infected patients with an absence of symptoms or illness, as well as self-curing abilities were reported. Recently, a report by Sudarshi *et al*. mentioned the case of a 62-year-old male that carried *gambiense*-HAT for at least 29 years.[62] It was determined that the infection occurred during his last journey in Africa in 1983, and was only diagnosed in 2012 due to the degradation of his health. It suggests that for at least 29 years, the infection by *T.b. gambiense* was controlled and latent. This case was not isolated, and a larger study was conducted over 15 years on 50 *gambiense*-HAT confirmed infected patients. Among these 50 infected patients, 11 have refused treatment against HAT. It was observed, after a follow up of 15 years, that ten of the patients who refused treatment no longer displayed parasites, suggesting that these patients have been self-cured.[63] These reports indicate that the infection with *T.b. gambiense* is not always fatal and could demonstrate a certain trypanotolerance within human hosts, as it was observed in bovine.[64]

In addition of the evidence of trypanotolerance in certain individual, asymptomatic hosts have been reported. These asymptomatic have been shown to be infected by the parasites but do not display clinical symptoms of the infection.[65,66] Lately, they have been described to not possess visual blood parasites by microscopic observation, while showing positive results to current detection method for *gambiense*-HAT infection.[67–70] A specific study has been performed in Guinea by Ilboudo *et al.* to investigate these asymptomatic carriers.[71] Patients positive with current detection method such as Card Agglutination Test for Trypanosomiasis (CATT), PCR and trypanolysis test (TL), displayed no observable parasites in their blood. It suggested that the blood parasitemia was very low or absent due to the low virulence of *T.b. gambiense* in Guinea. Patients were followed up for two years and four of the 17 patients positive to CATT and TL, developed *gambiense*-HAT. It confirmed that in certain cases, patients do not display any symptoms or any sign of the presence of the parasites in their system but are in fact infected. It

was then suggested that in low prevalence area, these asymptomatic/seropositive carriers needed to be treated as they could act as an undetected human reservoir for *gambiense*-HAT.[69]

The existence of trypanotolerant hosts prove that sleeping sickness is not always fatal and could open to new lead for treatment and diagnosis. However, asymptomatic patients or healthy carriers are a hindrance to the elimination of sleeping sickness. Indeed, they are usually not treated for HAT as they do not display any parasites in their blood, or they do not show any sign of infection.[15,65,68]

Trypanotolerant and asymptomatic patients show that sleeping sickness can progress at a very low virulence rate, and not be detected due to lack of symptoms for a long period of time. These individuals, whether they are detected and refuse treatment, or undetected, present a risk towards the goal for elimination of *gambiense*-HAT by 2030. These patients, mostly asymptomatic carrier, are able to host the disease for a long time, without falling ill, and have been very recently proposed to act like a human reservoir for HAT.[69,71,72]

1.1.3.4 Available treatment against HAT

Drugs to cure HAT have been available since the beginning of the 20th century. They were initially compounds based on arsenic, which often caused undesirable effects to the patient.[73] Progressively, more efficient and less harmful drugs were developed to replace arsenic based treatments. However, they remained toxic, low efficacy and not available orally, which complicates their administration to the patient as it requires specific medical area and equipments.[74]

Recently, WHO and other institutions joined their effort to increase the research for a novel efficient drug, while distributing the current treatment to the affected zone free of charge.[30,75,76] Four main drugs are currently used for treatment of HAT, which are specific to a stage of the disease and of the type of trypanosomes involved (Table 1.1).

Table 1.1 Table describing each drug used in the treatment of Human African Trypanosomiasis, different delivery routes are used: intravenous (IV), intramuscular (IM) or oral.[51]

	First-line treatment	Second-line treatment
Early stage		
T.b.rhodesiense	Suramin (IV)	Pentamidine (IM)
T.b.gambiense	Pentamidine (IM)	Suramin (IV)
Late stage		
T.b.rhodesiense	Melarsoprol (IV)	None available
T.b.gambiense	Eflornithine (IV) plus nifurtimox (oral)	Melarsoprol (IV)

1.1.3.4.1 Early stage treatment

Pentamidine is used for the early stage treatment of HAT induced by the presence of *T.b. gambiense*. It was first used in the 1940s and is still recommended for patients in the haemolymphatic stage of the disease.[15] Its delivery route is via an intramuscular injection, which is easier to apply than intravenously, and has shown great efficiency against T.b. gambiense.[30] Despite its great efficiency and a simpler delivery route, pentamidine remains relatively toxic and can induce different secondary effect such as hypotension, hypoglycaemia or gastrointestinal complications.[17,77]

Suramin is very efficient in eliminating bloodstream stage *rhodesiense* and *gambiense*,[15] however it cannot cross the blood brain barrier and its toxicity is greater than for pentamidine. Complications observed in the use of this drug were renal failure, bone marrow toxicity or neurological complications.[17,54] Suramin also uses an intravenous delivery route, which complicates the administration of the drug to the patient, and its low stability in contact with the air, which makes its conservation a potential issue.[30] This treatment is therefore now only recommended for first line treatment against *T.b. rhodesiense*, although it may be used for *T.b. gambiense*, in the case of pentamidine treatment failure, as it was shown to be efficient against early stage of *gambiense*-HAT.[78]

1.1.3.4.2 Late stage treatment

The treatment for the late stage of HAT is more challenging as, by this point, the parasites are present in the central nervous system (CNS). Therefore, it requires a drug capable of crossing the blood brain barrier in order to efficiently treat the parasites.[51] The most common drug used for late stage infection was Melarsoprol. It has been first administered in 1949 via intravenous injection and has shown great results in treating HAT. Melarsoprol is an arsenic based compound, which has the potential for strong adverse effects. The injections were found to be toxic and painful for the patient, and could lead to encephalopathic syndrome, with a fatal outcome of around 5% of those individuals treated with the drug.[79] Despite these strong complications and the high risk of mortality, it remained widely used for both *gambiense* and *rhodesiense* treatment due to its high efficiency and lack of alternative therapies.

Intra-venous injection of Eflornithine have been widely used and shown to be efficient towards late stage infection of *gambiense*-HAT.[80] This drug displays no activity against *T.b. rhodesiense* and poor access to the CNS, moreover its low reactivity was compensated by increasing the dose's concentration which induces repercussions to the patient's health.[81] Recently, a new combination treatment was obtained for *gambiense*. It is a mixed between the injection of Eflornithine (IV) and Nifurtimox (oral).[82] This combination offers a greater efficiency towards the elimination of *gambiense*-HAT and a lower toxicity compared to Melarsoprol or the Eflornithine monotherapy, reducing mortality from 5.9 % and 2 % respectively, to 0.7 % for the use of combination therapy.[81,83]

With the effort of WHO and diverse institutions, intense research and development are being carried to find new treatment that will provide a safer and more efficient way to cure HAT.[15,30] The delivery method is also being investigated, where an oral drug would be more suitable and easier to deliver to the patient in Africa rather than an intravenous or intramuscular administration. Two potential drugs are of particularly interest, Fexinidazole and benzoxaborole are currently in clinical trials and close to conclusion.[84,85]

Due to the multiple and dangerous adverse effects from each treatment against HAT, it is important that the diagnosis of the patient is accurate. An early diagnosis would allow the use of less toxic drugs and more efficient treatment towards HAT.

1.1.4 *Trypanosoma brucei* surface membrane composition and characteristics

1.1.4.1 Variable surface glycoprotein (VSG)

The bloodstream stage of the parasite (trypomastigote) within the mammalian hosts is covered by a thick and dense layer of a long amino-acids chain, called variable surface glycoproteins (VSG).[51] This layer is an extracellular protein of 50 – 60 kDa linked to the cell membrane via a glycosylphosphatidylinositol (GPI) anchor.[86] It possesses a small C-terminal domain that is attached to the GPI anchor and a large N-terminal domain facing the outside of the membrane (Figure 1.5).[86] VSG forms homodimers on the surface between two units via different linkers. It is estimated that around 1 x 10^7 VSG copies are present around the surface leading to a densely packed layer, around 15 nm thick.[87,88]

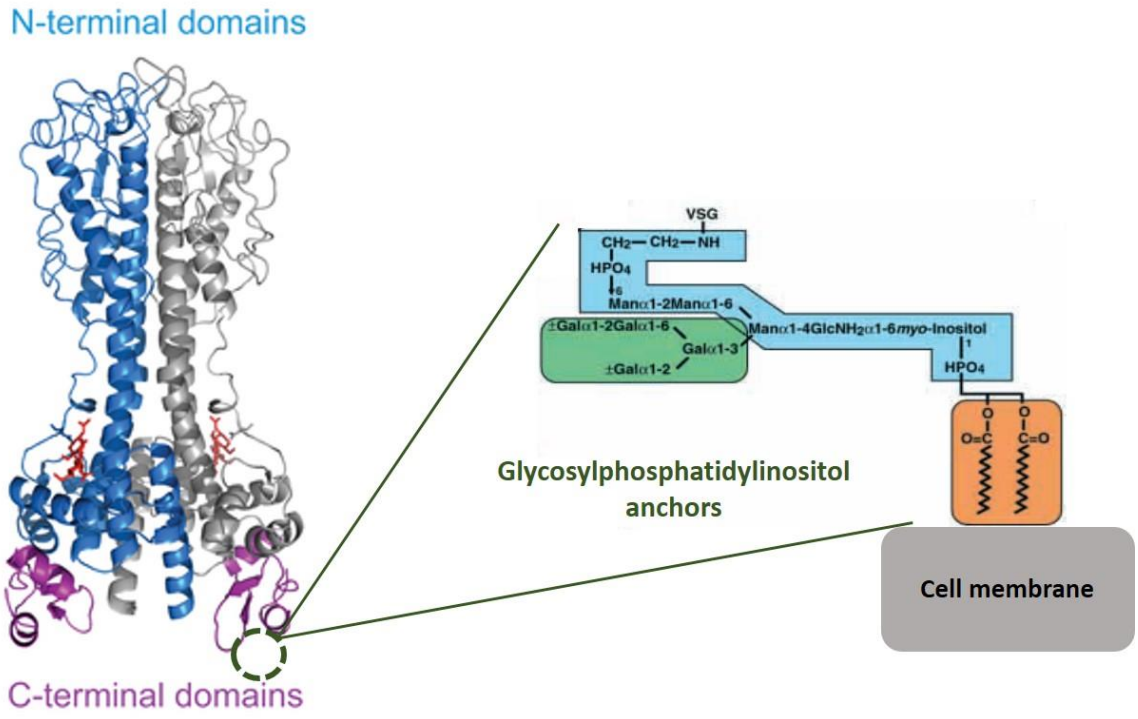

Figure 1.5 Illustration of the structure of a VSG dimer, one monomer in blue and one in grey, forming the N-terminal domain and the two C-terminal domains (purple), covalently attached to the surface of the parasite via a Glycosylphosphatidylinositol (GPI) anchor.[86,89]

Figure 1.5 illustrates the structure of a VSG homodimers. Both N-terminal monomers are shown in blue and grey and their respective C-terminal end in purple, which are further bound to the membrane via the GPI anchor. A N-linked oligosaccharide is shown in red on the N-terminal region. GPI anchor can be found in many eukaryote cells and contains a mixed of lipids, carbohydrates, phosphate and amines groups (Figure 1.5), however, its galactose side chain (shown in green) is unique to VSG.[89] The secondary structure of the protein has been found to be a mixed between α-helical coil, anti-parallel β-sheets and highly conserved cysteine residues.[90–92] The VSG covers over 90 % of the surface membrane and the remaining space is occupied by invariant surface glycoproteins (ISGs) or other non-VSG such as receptors.[86,93]

Trypanosomes are able to change their VSG surface composition throughout their bloodstream life cycle and these variations are noticed within the N-terminal domains, where the sequence of amino-acid is different between each type of VSG, however, the structural conformation of the VSG around the surface remains identical.[92] The variation of composition is not observed structurally but within the sequence of amino-acids in the N-terminal domain. The recycling of the VSG surface coat is a stochastic mechanism as this phenomenon was observed *in vitro*.[94] Hence, it is not triggered by external components or environmental factors such as immune response from the host. This process of replacing the VSG coat occurs through the endocytosis and exocytosis of VSG via the flagellar pocket of the parasite.[95,96] Although, a rapid internalisation and turnover of VSG, facilitated by endocytosis, has been described,[97,98] it was recently determined that trypanosomes are fully replacing their VSG coat within 4 – 5 days following a VSG switch.[99] During this antigenic variation, the surface of the trypanosomes can display two VSG structures, pre-switch and post-switch forms.[100]

Trypanosoma *brucei* possesses about 2000 genes that are related to the synthesis of variable surface glycoproteins,[101] although the parasite can only express one VSG gene at a time.[102] VSG genes are expressed at a specific genetic locations called expression sites (ES) and only one of these ES is activated at a time, leading to the expression of a single VSG gene.[103,104] The recycling and change of VSG surface coat is randomly induced when current ES is silenced and a different site is activated. In addition to possess multiple VSG genes, trypanosomes are able to recombine different genes in order to produce new sequences of expressed surface VSG.[105,106] This repertoire of VSG genes, as well as the recombination of genes, offers a large library of different

glycoproteins that can cover the plasma membrane of the parasite, facilitating antigenic variation.

1.1.4.2 Immune system evasion

This ability of switching the VSG surface composition allows the trypanosomes to efficiently evade the immune response from the host and sustain the infection longer. This high rate of recycling the surface layer, mentioned previously, selectively removes VSG-specific antibodies bound to the cell surface and this, in combination with the ability to switch the expressed VSG, facilitates the evasion of the host's antibody response.[107,108] Moreover, it was demonstrated that trypanosomes expressing two distinct VSG structures, from the pre-switch and post-switch, are also able to avoid recognition from the host's immune response.[109]

IgM and IgG anti-VSG will bind the surface of the trypanosomes and act as a marker for the macrophages in order to eliminate the trypanosomes.[110–112] Once the titre of antibody is high enough against a specific form of VSG, the surface is disrupted and the parasites, that possess that specific VSG antigen, are eliminated by the host's immune system.[15,113,114] Antigenic variation through the stochastic switching of the VSG surface coat ensures that a small number of bloodstream form *Trypanosoma brucei* parasites displaying a different type of VSG are remaining in the blood, invisible the immune response of the mammalian host, and are able to grow and proliferate. The result of this antigenic variation is characterised by successive waves of blood parasitemia as different VSGs arise (Figure 1.6). As parasites are not entirely eliminated, the human host remains infected.[113,114]

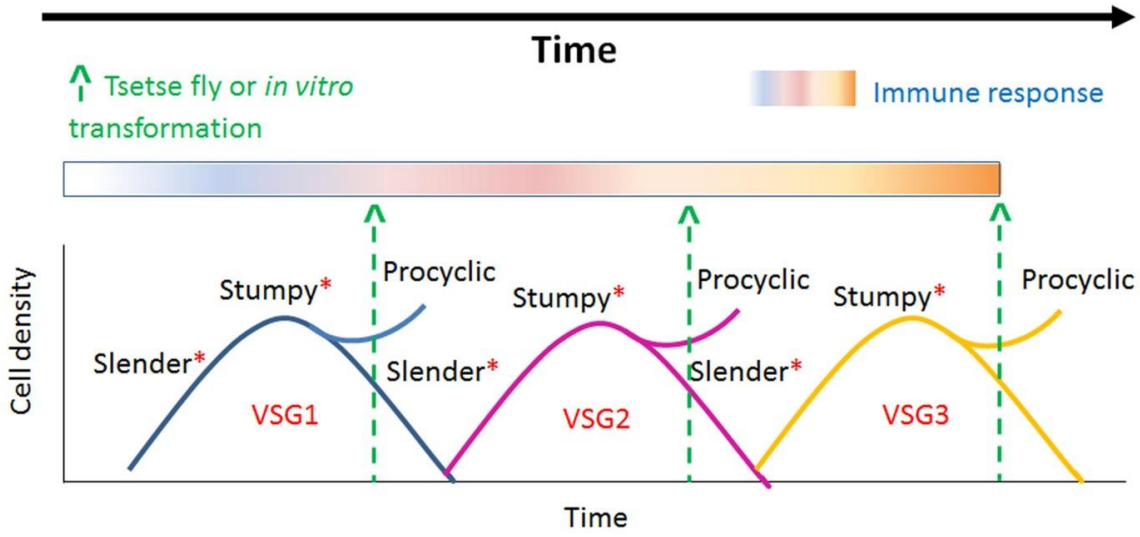

Figure 1.6 Illustration of the blood parasitemia wave due to the elimination of Trypanosoma brucei by the immune system.[113]

Figure 1.6 shows the variation in the blood parasitemia associated with the VSG coat switch and the action of the immune system from the host. It also demonstrates how the morphological changes of the parasites influence the elimination via the immune system. When trypanosomes are injected in the bloodstream from the tsetse fly bite, they have a metacyclic form, which does not permit the division and proliferation of the parasites.[53] Once in the bloodstream, metacyclic parasites undergoes a morphological change to a slender form, where parasites will rapidly grow and replicate. During the slender form, the VSG switch rate will be constant and allow the evasion of the parasites from the immune response. The blood parasitemia then increases to a maximum peak, until trypanosomes are found in a stumpy form that allows the parasites to be transmitted to the tsetse fly.[53,113] In this stumpy form, parasites are not able to divide and replicate and, most importantly they are not capable of switching their VSG coat.[115] As the VSG composition remains constant, the immune system is able to eliminate the parasites that are not transmitted to the tsetse fly from the bloodstream, as they cannot revert to a slender form.[116] However, trypanosomes that possess a different VSG composition and remain in a proliferative form (slender) will survive and will be able to proliferate until reaching another parasitemia peak.

The antigenic variation avoids clearance of the parasites by the host and allows the infection to progress. Constant change of VSG composition prevents the development of an efficient vaccine against trypanosomes,[17] which would be a more efficient and safer method to control and

eliminate HAT. Although, the discovery of trypanotolerant and asymptomatic carriers that can control the progression of the infection opens a new area of research for the development of a successful vaccine against trypanosomes.[117]

1.1.5 Control method for Human African Trypanosomiasis

The difficulties encountered to develop a successful vaccination treatment lead to the use of other methods for the eradication of HAT. It relies on the control of the vector for HAT, tsetse fly, as well as a combination of mass population screening associated with direct treatment.

1.1.5.1 Vector control

One of the control methods is to reduce the population of the tsetse fly by vector control. Controlling the vector carrier of the parasites and the exposure to this vector, the risk of infection can be limited. Various insecticides can be used, but the main method employed is the use of traps against the tsetse fly.[118–120] In the early 20th century, catching flies with a hand net was the main tool used by field workers.[15] Nowadays, the process has been improved to effectively capture a large population of flies by using specifically designed traps which attract them using certain colours, more precisely black and blue.[118,121] These traps can further be impregnated with polymeric adhesives in addition of insecticides to improve their efficiency towards eliminating tsetse flies.

Figure 1.7 Illustration of a tsetse fly trap.[122]

These traps (Figure 1.7) need to be placed near agricultural sites, where most of the tsetse flies are found, in order to have an impact on the prevention of human infection.[15] The cost of this method is relatively inexpensive thanks to the financial support given by WHO to countries in need of such devices. Its efficiency has been improved through the years but this method alone does not provide a strong enough elimination power of the flies, and the use of the traps could be combined with other method such as wide spray of insecticides, bush clearing or release of sterile male flies.[123]

1.1.5.2 Population screening: passive and active surveillance

The surveillance and control of the progression of HAT in the population is performed via two different methods: passive screening and active screening.[124]

Passive screening is used in low-prevalence areas or in the zones where no HAT has been detected for a long time.[15] It is based on the self-presenting patients, where an individual presenting specific symptoms will be diagnosed and treated in a peripheral health centre.[30] This method is preferentially used for the detection of *rhodesiense*-HAT, as no serological test has

been developed for field detection. Due to the non-specific symptoms of HAT and the lack of experience of clinicians in areas where no HAT has been detected, numerous cases of HAT are missed.[125,126] This method has the advantage of having a low cost; however, patients diagnosed with HAT will most likely be in a late stage, with trypanosomes that have reached the brain.[57] Patients and clinicians often do not recognise the symptoms of HAT, and poorly equipped health care centre lead to a delay in the treatment of the patient. It also relies on the health information provided by the country to help the population to recognise the symptoms associated with HAT, however, passive screening often ends with a low attendance at the fixed health centre.[127]

Active screening is based on the activity of a mobile team that will go directly into the villages to perform a large scale screening test on the population.[15] Infected patients will then be directed to local health centres for treatment. This method is relatively costly and requires well trained personnel, but it has shown great efficiency towards eliminating *gambiense*-HAT in certain areas.[128,129] Active surveillance is carried out in areas of endemic prevalence and conducted every six to twelve months to eliminate and prevent any transmission of HAT.[130,131] This method is exclusive to *gambiense*-HAT as efficient serological test have not been developed for *T.b. rhodesiense*. When no HAT cases is detected for a period of five years, mobile team detection method is no longer conducted, and passive surveillance is put in place for the designated area.[15] The mobile teams use the card agglutination test for trypanosomiasis (CATT) for the mass population screening on the field.

The discovery of asymptomatic carriers has complicated the surveillance protocol.[62,65,66] These patients do not develop symptoms of infection by *T.b*, hence they will not be directed towards health care for treatment in a passive surveillance area. Moreover, during active screening, they will show positive results on the diagnosis test but no parasites in the blood to confirm the infection. This poses the question whether to treat or not these unconfirmed patients and these individuals could be asked to return to the health care centre for follow-up investigations, but this method ended with low attendance of patients.[132] Different protocols have been put in place in some countries where a threshold was determined on the diagnosis test, above which patients will be treated whether the infection was confirmed or not.[133] Due to the toxicity of current treatment available, this method is at risk for individuals that do not carry the parasites. The

need of new detection method to address these issues is urgent, as these asymptomatic carriers can act as human reservoir for HAT and jeopardise the elimination of *gambiense*-HAT.[72]

1.1.6 Current detection methods and protocol for the diagnosis of HAT

Different control methods are employed for the detection of *T.b. gambiense* and *T.b. rhodesiense* due to the differences in disease course.

There is no serological screening test available for field diagnostic of *T.b. rhodesiense* due to its acute clinical course and its high antigenic variation.[15] Hence, *rhodesiense*-HAT is controlled through passive surveillance relying on the self-presentation of patients in clinics.[126] Its detection depends on the recognition of non-specific symptoms, such as fever or sleep disturbance, geographical location and blood parasitemia.[134] In contrast with *gambiense*-HAT, the acute infection of *rhodesiense*-HAT produces higher parasite concentration in the blood, allowing easy recognition by microscope using a single drop of blood sample, thus making microscopic observation very reliable for *rhodesiense*-HAT.[10,27]

Due to the aforementioned differences in parasite blood concentration between the two sub-species, different methods are used to identify *gambiense*-HAT. In addition to the recognition of non-specific symptoms, existent serological test can be conducted during passive and active surveillance on the field and participate to the elimination of *gambiense*-HAT.

1.1.6.1 Antibody based detection method for gambiense-HAT: principles and limitations

Card-Agglutination Test for Trypanosomiasis (CATT) test is the gold standard for the method of detection of *gambiense*-HAT on the field. It is only specific to *T.b. gambiense* and has been used for over 40 years.[135] This is a rapid and simple test that can be applied in the field as it does not require specific equipment. CATT is also a low-cost technique that can be provided to African countries. It is based on the blood analysis of an individual and the method consists on measuring the presence of a specific antibody against the VSG LiTat 1.3 of *gambiense* trypanosomes. The whole blood (wb) of a patient, obtained from a blood drop from his finger, is added on the card with freeze dried trypanosomes that display such VSG (CATT-wb). In the presence of the specific

antibody in the blood, the trypanosomes will agglutinate on the card, indicating the infection of the patient.[15]

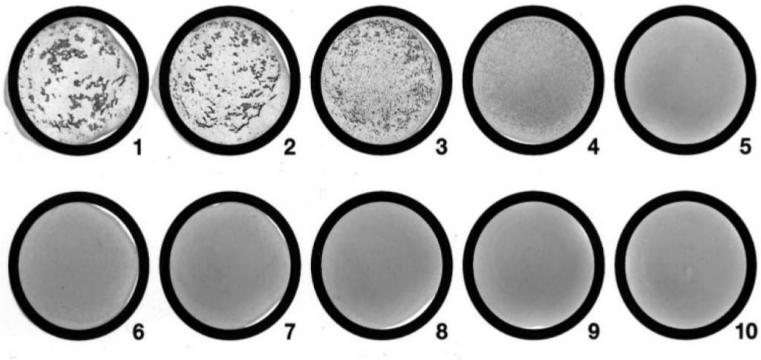

Figure 1.8 Illustration of an example of CATT test realised on ten individuals with serum diluted to 1:4.[136]

Figure 1.8 shows an example of the results that can be obtained with the CATT test on serum diluted. Samples 1 – 3 are deemed positive as the agglutination is clearly observed, whereas sample 4 is considered as weakly positive. Samples 5 – 10 are deemed negative as no agglutination is noticed by visual observation.[136] In addition to being fast and cheap, the CATT has a great sensitivity and specificity (Table 1.2), and allows the testing of up to ten individuals at a time, leading to a fast and large population screened.

Its specificity can be further increased by a series of dilutions (1:4, 1:8, 1:16, …) of the plasma or serum sample obtained from the whole blood (Table 1.2).[15,132] It has been shown that in a low dilution, when using the whole blood or a 1:2 dilution, the agglutination of the parasites is sometimes unstable and can alter the diagnosis.[136] Since this method can be applied on the field, it increases the viability of the population screening. The CATT dilution test on plasma or serum is often performed when blood parasitological observation is negative to confirm the diagnosis.[132]

Moreover, an improved method relying on the card agglutination and the whole blood sample was developed, called Latex-wb. It relies on the same principle as CATT-wb but it targets three different type of VSG: LiTat 1.3, 1.5 and 1.6, with the help of latex particles.[137,138] This technique

targets two more type of VSGs compared to the usual CATT test, hence increasing its specificity towards the detection of *gambiense*-HAT (Table 1.2).

Similar technique based on the detection of antibodies specific to trypanosomes, called immune trypanolysis test (TL), have also been developed to support the result found with CATT.[67,139] The serum of a patient is incubated with serum from a guinea pig, which is rich in complement, and with live *T.b. gambiense* cultured in laboratory. When antibodies specific to the VSG of trypanosomes are present in the patient's serum, it will cause the lysis of the live trypanosomes when associated with the rich complement medium brought from the guinea pig serum. After incubation, the sample is examined by microscopy to observe the state of live trypanosomes and a lack of motility from the parasites result in a positive identification of HAT infection.[139] This method has shown to be highly sensitive and specific to *T.b. gambiense* (Table 1.2) and is a good alternative to confirm results obtained with CATT.

Table 1.2 Summary of the different antibody detection techniques employed for the diagnostic of gambiense-HAT, associated with their respective reported sensitivities and specificities.[140]

Diagnosis methods	Samples	Antigen	Sensitivity	Specificity
CATT-wb	Whole blood	Anti-LiTat 1.3 antibodies	68.8 – 100 %	83.5 – 99.3 %
LATEX-wb	Whole blood	Anti-LiTat 1.3, 1.5 and 1.6 antibodies	67.9 – 100 %	96.1 – 99.2 %
CATT dilution	Diluted blood, serum or plasma	Anti-LiTat 1.3 antibodies	78.8 %	58.5 – 99.5 %
Immune Trypanolysis test	Serum	Antibodies specific to T.b.gambiense	97.2 – 100 %	100 %

Table 1.2 summarises the different techniques available for the detection of antibodies specific to *T.b. gambiense* on the field. Despite the reported good sensitivities and specificities, the current diagnostic methods employed on the field suffer from limitations.

Indeed, the latter described test (TL) has shown greater sensitivity and specificity, but is technically more demanding as its use requires specialised laboratory for the culture of live *T.b. gambiense* and highly trained personnel, and cannot be performed on the field.[140] This diagnostic

method is often performed as a quality control method to confirm the infection, as the test is not rapid.[15,67,140] It would also require a follow-up of the patient found infected, which is difficult to put in place in the rural areas.

Moreover, the CATT test, currently used during active screening of the population, has demonstrated limitations in its accuracy. Despite, its great sensitivity and specificity, many false negative results on the CATT have been reported. This is the case when an individual is infected by a strain of trypanosomes that do not possess the gene of the VSGs targeted (LiTat 1.3). For example, it was observed in Cameroon and Uganda that negative CATT showed a positive parasitology in blood observation, suggesting that patients were infected by a trypanosome strain lacking of LiTat 1.3.[141,142] Similar issues arose for the use the Latex-wb method, where its specificity could be also be affected by lack of certain genes. False negative CATT can also be the result of the prozone effect on the undiluted blood, and the use of a diluted plasma sample can overcome this issue on the field for detection.[15]

Moreover, the number of false positive results reported have been a serious issue in terms of population screening and on the decision whether to treat or not. This problematic is mostly observed in the areas where the prevalence of the disease is low and each national programme possesses its own decision making protocol to set the cut-off point on delivering treatment or not.[15,136] Indeed, CATT dilution is often used to confirm CATT results, and a positive result to a 1:16 dilution indicates that there are enough antibodies against *T.b. gambiense* to confirm the infection. However, patients only positive to 1:4 or 1:8 dilutions remain an interrogation on whether to treat them or not, as the treatment could be toxic. Depending on the country, the cut-off point could be set at 1:8, meaning that patient with only a positive result at 1:4 will not be treated, or it could be set up at 1:16, where only patients with a positive CATT results at 1:16 dilution or higher will receive treatment.[15,133,136] It is possible that some positive cases have been dismissed due to this cut-off point. In an area with a higher prevalence of HAT, it is likely that the limit would be set at a lower dilution. In addition, the false positive result could be the result of a cross reaction with an infection by *T.b. brucei* or different parasitic infections.[67,136] It was also found that antibodies can be detectable with the CATT test even two years after successful treatment of patients, which could potentially also apply to self-cured individuals that may still possess specific antibodies against *T.b. gambiense*.[143]

CATT remains the unique serological test that can be used on the field because of its low cost, simplicity and rapidity. However, these limitations mentioned decrease the efficiency of the active surveillance. Hence, CATT test alone is not sufficient and adequate for diagnosis purposes as it is prone to false positive and negative values, mostly in low HAT prevalence area.[15,144] To confirm HAT diagnosis, the use of additional detection method and tools is required to support the CATT results such as a microscopic observation of the blood in order to visually identify live trypanosomes.[17]

1.1.6.2 Microscopic observation of trypanosomes in blood

The detection of specific antibodies is always associated to the examination of patient's blood for direct observation of trypanosomes.[15] The examination of wet or thick blood films are the method of choice in the field as they are simple, rapid and user-friendly.[140] Wet blood films technique rely on the direct microscopic observation of motile trypanosomes in blood deposited on a glass slide, whereas thick blood film is based on the identification of trypanosomes in a dry and spread blood drop on a glass slide and stained with Giemsa. However, these methods have low sensitivity and the detection limit of thick blood film examination was found to only be 5000 – 10000 trypanosomes/mL of blood (Table 1.3). An alternative method is the examination of the lymph nodes aspirate, where trypanosomes were previously detected. It is a cheap and simple method but its lack of sensitivity is still a drawback to accurately diagnose infected patients (Table 1.3).[15,136]

The sensitivity of blood parasites observation can be enhanced by increasing the concentration of the trypanosomes in the blood sample using a mini anion exchange centrifugation technique (mAECT).[145,146] This technique enables the separation of live trypanosomes from the blood via anion chromatography, where negatively charged blood cells are retained in the column whereas neutral charged trypanosomes can go through. Trypanosomes are further concentrated by a low speed centrifugation prior microscopic examination of the sample. This method greatly increases the sensitivity of the blood parasites detection, as the detection limit has been found to be at 30 trypanosomes/mL (Table 1.3).[15] Furthermore, a similar concentrating method has been developed, called micro-haematocrit centrifugation technique (mHCT).[147,148] This technique has the advantages of being cheaper than mAECT. A small volume of blood taken from the patient is

centrifuged in a capillary tube, separating the white blood cells from the plasma and the erythrocytes. The mobile trypanosomes were found to be in the white blood cells layer, which, by mean of microscopic analyse of the capillary tube, can be observed. This technique has a limit of detection of 500 trypanosomes/mL, which is higher than for mAECT but ten times lower than thick blood films examination (Table 1.3).[15] Its relative low cost and simplicity makes it ideal for field test diagnosis compared to thick blood film examination.

Table 1.3 Summary of the different method for the microscopic observation of trypanosomes in blood samples, associated with their respective sensitivities and detection limits.[15,140]

Diagnosis methods	Samples	Antigen	Sensitivity	Detection limit
Wet blood film	Finger prick blood on a glass slide	Motile trypanosomes	3.9 – 54.2 % [138]	> 10 000 trypanosomes/mL
Thick blood film	Dry blood and Geimsa stained on a glass slide	Trypanosomes	26 – 35 %	5000 – 10000 trypanosomes/mL
Lymph node aspirate	Fresh lymph node aspirate on glass slide	Motile trypanosomes	43 – 77 %	Not reported
mAECT	Blood	Motile trypanosomes	68.8 – 92.1 %	30 trypanosomes/mL
mHCT	Blood	Motile Trypanosomes	39 – 80 %	500 trypanosomes/mL

Table 1.3 summarises the different method employed to directly observed trypanosomes in the blood of an individual and used to support CATT results. However, as mentioned previously for antibody detection methods, these techniques also have limitations for their use on the field. Wet and thick blood film examinations have poor detection limits, which is detrimental for the diagnosis of *gambiense*-HAT, as the blood parasitemia is rather low, and it has been found to be lower than 100 trypanosomes/mL in certain cases.[27] Despite their simplicity and ease to use on the field, these methods lack of sensitivity, often dismissing positive cases. Moreover, the examination of blood film is quite tedious and labour intensive, as located a low number of trypanosomes by microscope is difficult and not accurate. Therefore, it is possible that no trypanosomes would be found in the microscopic observation of the blood sample even in the case of a positive CATT result.[133] This makes the decision on whether to treat the patient or not very challenging, hence the importance on implementing a cut-off line on the CATT results. This

decision is also driven by the fact that the treatment available for the cure of HAT is toxic and can potentially harm individual that do not require treatment due to a false positive result on the CATT test. Increasing the concentration of live trypanosomes in the blood samples has shown a greater sensitivity using mAECT, but it is relatively costly and requires specific equipment such as centrifugation or chromatographic column, as well as the need for electricity.[140] The latter could be a problem in certain rural areas. Despite the similar issues observed for mHCT, such as equipment requirement and electricity, it remains cheap compared to mAECT and easier to use on the field.

Finally, when parasites are being detected in the blood of a patient, it is important to determine the stage of infection of *gambiense*-HAT in order to provide the appropriate treatment.

1.1.6.3 HAT stage determination

Ultimately, the stage of the infection is determined by analysing the cerebrospinal fluid (CSF) obtained by lumbar puncture.[15,149] White blood cells are counted, or microscopic visual observation of trypanosomes is assessed, and will determine whether the patient is in an early or late stage. The white cells counting is undertaken in a cell chamber, and WHO set the stage 2 at the count of five cells per µL in the CSF.[15]

The detection of trypanosomes in the CSF is difficultly achieved by microscope, due to the low sensitivity of the technique, as previously observed with blood samples.[15] The technique can be improved using a modified centrifugation technique mentioned earlier with mAECT, where the detection limit can be lowered to two trypanosomes/mL of CSF.[146]

Lumbar puncture is a dangerous method and requires trained personnel to undertake it. This procedure could induce a risk of infection on the patients when performed in rural settings. Moreover, similar issues with the setting of a cut-off points have been mentioned previously for CATT dilution, as there is no consensus between national program and the area investigated. For example, some countries will use a threshold of 10 cells per µL and others would only consider the patient as in a late stage of HAT with white blood cells greater than 20 cells per µL.[136,150,151]

1.1.6.4 Decision process for diagnosis of gambiense-HAT

Due to the limitations observed in the individual diagnostic method in respect to their sensitivity, specificity or technically challenging set up, different detection techniques are used together in order to establish an efficient diagnostic. Depending on the country where the active surveillance is performed, the type of *T.b* involved as well as the prevalence of HAT, different decision trees can be put in place.[15] Bonnet *et al.* have reviewed the current detection method available for field diagnostic of *gambiense*-HAT and have proposed such decision tree for the elaboration of an efficient and specific diagnostic of *gambiense*-HAT (Figure 1.9).[152]

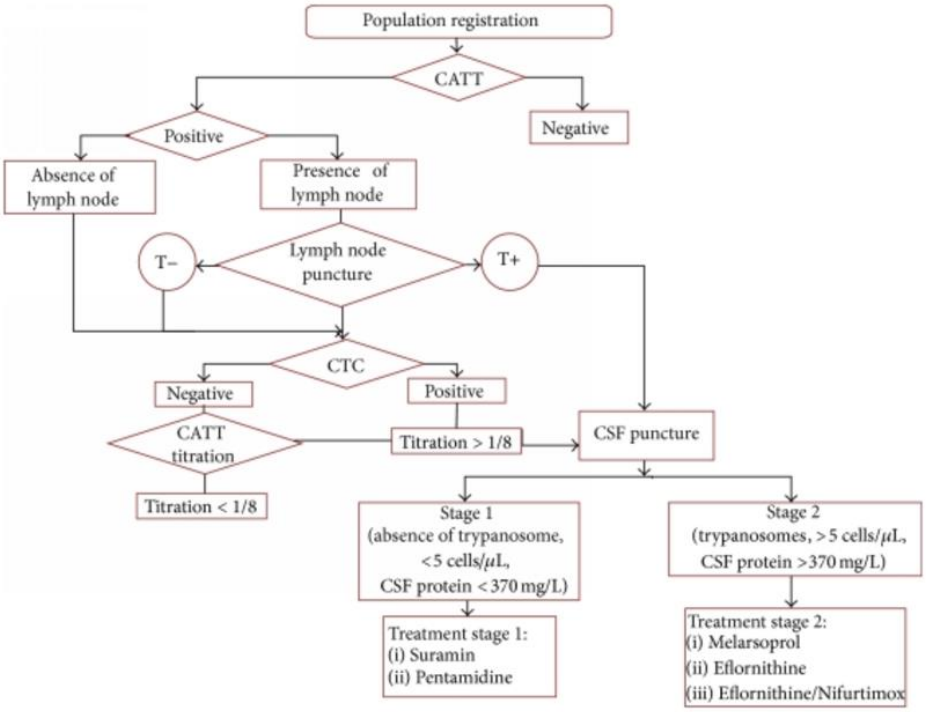

Figure 1.9 Proposed decision tree for the diagnosis of gambiense-HAT.[152]

Figure 1.9 displays the different diagnostic methods to undertake in a specific order to obtain well organised diagnostics.[152] CATT technique remains the first test to perform as it is fast, cheap and simple and allow the screening of a large population. When the antibody titration is positive to *gambiense*-HAT, the second part of the diagnostic process is to find trypanosomes in the blood of the patient. The lymph node puncture could answer to this question,[136] and the presence of trypanosomes observed in the sample by microscopy would confirm the infection and lead to

the stage determination of HAT via lumbar puncture.[15] However, in the absence of enlarged lymph nodes and/or the absence of trypanosomes in the lymph node aspirate, the search for parasites in the blood has to be undertake. As *gambiense*-HAT is characterised by a low blood parasitemia,[27] their concentration need to be increased prior the examination of the sample by microscopy. Here, mHCT technique is proposed (mentioned here as capillary tube centrifugation (CTC) in Figure 1.9), where *T.b. gambiense* are concentrated from whole blood of a patient in capillary tubes and examined by microscopy.[147,148] A positive identification of live trypanosomes lead to the establishment of the stage of HAT.

When no parasites are observed in the blood after centrifugation, CATT titration is performed with a series of dilution on the plasma or serum of the patient.[15] This method increases the sensitivity and specificity of the CATT-wb. Bonnet *et al.* proposed to set the cut-off point at a dilution 1:8 or higher, where individuals remaining positive at this cut-off point would be considered infected by *gambiense*-HAT and their stage would be determined.[152] However, this cut-off point depends on the HAT program of different countries and on the prevalence of the disease in the area investigated. The determination of an accurate cut-off point is still under discussion, as it is dependent on the area examined and the current epidemiological situation in this area. Due to this uncertainty, some *gambiense*-HAT cases could have been missed.

Moreover, the asymptomatic carriers described previously, which display a positive CATT result and negative blood parasitemia,[65,68,69] would be localised at the CATT titration stage in the decision tree in Figure 1.9. As different cut-off points have been set between national control program, it is possible that some asymptomatic cases have been dismissed. The untreated asymptomatic carriers could still act as human reservoir for *gambiense*-HAT and sustain the disease.[69,72] It is important to develop an accurate diagnostic method that could overcome the limitations of the current diagnostic method employed in the field, and specifically detect *gambiense*-HAT as well as identifying the asymptomatic carriers.

1.1.7 New target for detection techniques

The limitations observed in the current detection methods for HAT is a serious issue towards the complete elimination of the disease as well as for efficiently treating infected patients. This is of

particular concern for the group of asymptomatic patients with positive CATT results but negative blood parasitology who may be infected, but currently do not meet the WHO guidelines for treatment.[15]

The current detection methods, CATT, applied on the field relies on blood analysis, which has shown variations and uncertainty in HAT detection. Although *T.b* has historically been considered as an infection of the blood, recent evidence suggests that these parasites may be sequestered in tissues outside of the blood which are currently overlooked during population screening.[54]

It is known that when an infected tsetse fly bites an individual, it firstly delivered the trypanosomes in the skin, where they would undertake morphological changes before entering the lymphatics and blood system.[45] Trypanosomes replicating in the skin at the site of initial infection and the localised inflammatory skin reaction sometimes result in the appearance of a sore or "chancre", that can be used to aid diagnosis of HAT.[51] Other skin lesions have been observed in HAT infected patients, suggesting that *T.b* could also be located and replicating in the skin.[153] Recently, a few investigations have been conducted to analyse the skin as a potential location site for the trypanosomes during HAT infection. Trindade *et al.* showed that trypanosomes were able to survive in adipose tissue in mice.[154]

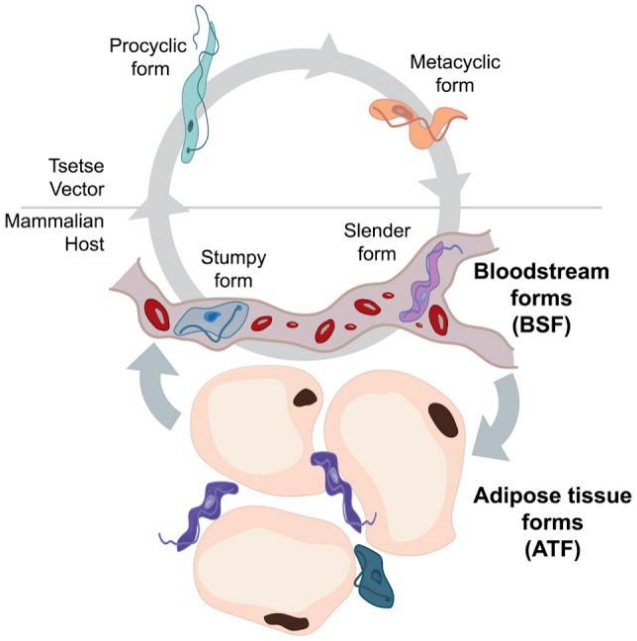

Figure 1.10 Illustration of the trypanosomes transfer between bloodstream and adipose tissue forms during the life cycle of T.b.[154]

This study demonstrates that parasites located in the adipose tissue were different from the ones found in the bloodstream, adding another step in the life cycle of trypanosomes in mammalian hosts (Figure 1.10). They were able to survive and proliferate within the skin, by using the fatty acids as an energy source. Their presence in the adipose tissue and their use of the fatty acids for their replication was potentially related to the weight loss symptoms that are often observed in individuals infected by HAT. Trypanosomes are then able to proliferate in the blood and in the skin of an individual.

This finding was further studied by Caljon *et al.* who confirmed the presence and the proliferation of trypanosomes within the skin of mice at the site of inoculation.[155] It was found that the parasites were able to proliferate in the skin and interacting with adipocyte and collagen. One of the major findings was that trypanosomes were able to be transmitted via the dermis to the tsetse fly during its feeding. However, trypanosomes were only located in the skin at the site of inoculation by the tsetse fly and it does not seem that the blood form was able to re-infect a different area of the skin.

Recently, Capewell *et al.* fully investigated the potential transmission of the parasites located in the skin to the tsetse fly.[156] They demonstrated using a mouse model for *T.b* infection, that parasites were able to cross the blood vessels and extravagate into surrounding tissues, including the dermal layer of the skin. Parasites first appeared in the blood, but they were detected in the dermis 12 days after the initial infection. Bioluminescent trypanosomes were easily tracked with a confocal microscope in the extravascular region, which confirms the previous findings that trypanosomes were able to survive in the skin.

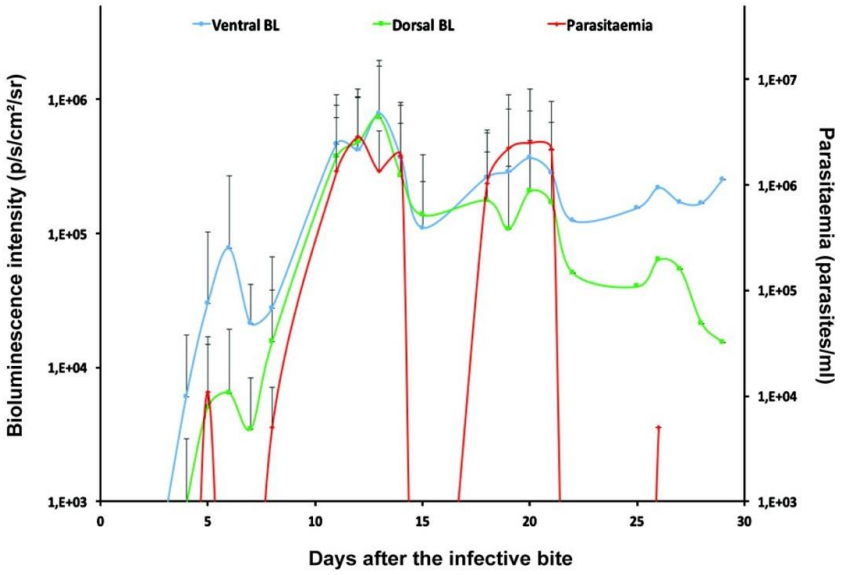

Figure 1.11 Comparison between blood and skin parasitemia. Parasites were measured through their bioluminescence (BL) in the skin.[156]

Moreover, it was also demonstrated that mice with trypanosomes in the skin were able to transmit parasites to the tsetse fly during feeding, even in the absence of detectable blood parasitemia, implicating a role for these extravascular parasites in transmission. This was a major breakthrough in the understanding of the disease, as it would imply that parasites are present in relatively constant numbers in the skin, whereas their numbers vary cyclically in the blood (Figure 1.11). This suggests that patients that have been disregarded because no parasites were found in the blood, could still be infected with trypanosomes in their skin. These patients may therefore be capable of transmitting the trypanosomes, acting as a latent reservoir with in the community and may themselves be vulnerable to developing clinical disease in the future if undiagnosed and

untreated. Such individuals have been proposed by Capewell *et al.*,[156] and others,[72] as an explanation for the historical difficulties in achieving HAT elimination and a current threat to achieving the WHO goal for to interrupt transmission of HAT by 2030.[21,27]

Moreover, old human skin biopsies were also studied by Capewell *et al.*,[156] to observe if the trypanosomes were able to act similarly in human infection. Out of 1121 human skin biopsies obtained from the 1990s, six individuals showed trypanosomes in their skin. However, their skin biopsies were obtained as part of a diagnostic screening programme for *Onchocerca microfilaria* in Democratic Republic of the Congo and were not diagnosed for HAT at the time. This area was endemic for HAT during 1990s and these new evidences of presence of trypanosomes in the skin of individuals confirm the hypothesis of asymptomatic carriers acting as human reservoir for *gambiense*-HAT.[72]

This recent finding in the localisation of trypanosomes in the skin is a major progress towards the elimination of HAT. The existence of the human reservoir is strongly supported by the work of Capewell and Trindade,[154,156] as parasites could be transmitted via the skin of an individual even if the blood parasitemia is very low. As all current detection methods for HAT, including those being used for mass population screening on the field, are based on blood samples, it is possible that patients are being wrongly disregarded and untreated. It is highly probable that some of those untreated are still infected and would sustain the infection in the area.

There is an urgent need for the development of a new diagnostic methods that could answer to the different limitations mentioned with the current techniques employed on the field. Ideally, a non-invasive method would remove any risks for the health of the patient, like for the lumbar puncture mentioned earlier. The ideal technique should be cheap, easy to implement and not requiring highly trained personnel and electricity. Moreover, it should be sensitive and specific enough to avoid the need of blood parasitological examination and should be able to detect the asymptomatic carriers in order to efficiently treat them.[71,72] Hence, the skin offers a new target for the detection of HAT and Raman spectroscopy could play an important role in this area as it is a non-invasive, non-destructive, label free technique, portable, with an easy applicability on the skin. Thanks to recent technical and instrumental development, Raman have been widely used in several tissue for bio-diagnostic. The use of Raman spectroscopy on the skin could potentially overcome the recent issues observed with the current diagnostic techniques.

1.2 Raman spectroscopy

Raman spectroscopy, an optical technique that relies on the scattering of a photon by a molecule, was discovered in 1928 by C.V Raman.[157] Lately, significant improvements in the method and instrumentation have greatly enhanced the sensitivity of the technique, leading to a powerful analytical tool. This spectroscopic technique measures the vibrational and rotational modes of a molecule that has been irradiated by a laser, where the specific energy of each bond allows different molecules to have unique Raman spectra. This advantage leads to extensive applications of this technique in forensic science to identify specific molecules,[158,159] in art,[160,161] or in the food industry.[162,163] Raman is a label free, non-destructive, non-invasive technique and with its high chemical vibrational specificity and intense molecular information within a sample, this analytical method is of great interest for biological sample analysis such as in bio-diagnostic assays.[164,165] Ultimately, the specificity of this analytical technique makes it ideal for the detection of HAT on the skin of an individual and could overcome the limitations observed in the current diagnostic methods employed on the field.

1.2.1 Theory

The principle of Raman spectroscopy is that a molecule is irradiated using a monochromatic light source, such as a laser. This incident energy will disturb the electron cloud, causing a change in polarizability, resulting in excitation to a higher virtual energy state that is lower than the real excited state of the molecule.[166] As a result, there are three main types of scattered light: Stokes, anti-Stokes and Rayleigh scattering.[167] A diagram showing the different energy levels for each type of scattering is shown in Figure 1.12.

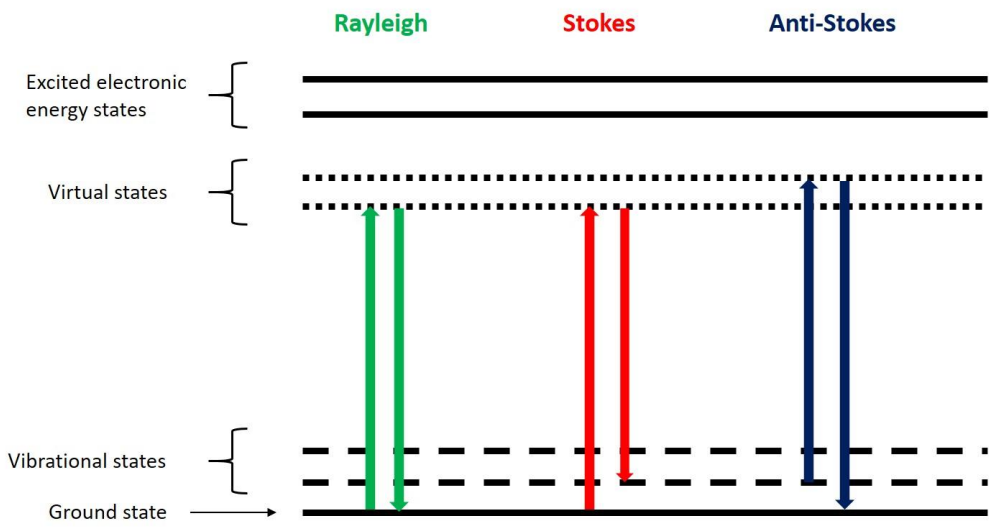

Figure 1.12 Jablonski diagram illustrating the different scattering process.

Rayleigh scattering corresponds to light that has been scattered without any modification of its frequency. This is an elastic process and is observed as an intense peak at the Raman shift = 0 cm^{-1}. When the incident light from a laser disturbs the electron cloud, the electron cloud vibrates and the molecule is promoted to a virtual excited state.[166] The molecule then relaxes to the original ground state with no exchange of energy and, therefore, the scattered photons have the same energy as the incident photons. Rayleigh scattering is the dominant process as only 1 in 10^6 photons is scattered inelastically. The two inelastic scattering processes are Stokes and anti-Stokes scattering, which both give vibrational information about the molecule studied.[168] Some of the incident energy will be absorbed and used for the movement of bonds present in the molecule. When the incident photons excite the electron clouds, it will induce nuclear motion within the analyte. The changes induced in the polarizability during the molecular vibration is required to obtain a Raman spectrum. Some of the incident energy is transferred and will be specific to a vibrational bond. In comparison to elastic scattering, the molecule relaxes to an excited vibrational state. In the case of Stokes scattering, the material is absorbing energy leading to an emitted photon with less energy than the incident photon (Figure 1.12). Whereas for anti-Stokes, the material is losing energy and the emitted photon will have more energy than the incident photon (Figure 1.12). The difference between the incident frequency and the scattered frequency gives the Raman shift. The Stokes scattering peaks will be observed as positive Raman

shifts while the anti-Stokes scattering peak will be in the negative region. Indeed, a molecule that is already in an excited vibrational state will relax to the ground vibrational state after being irradiated. As bonds between different atoms change in energy, the vibration of different bonds results in varying shifts in energy. Therefore, the frequency of each Raman peak corresponds to different bonds in a molecule.

At room temperature, molecules are more likely to be at a ground energy level than in an excited state.[168] Therefore, Stokes Raman scattering will be of a higher intensity than the anti-Stokes scattering. This is described by the Boltzmann equation, which can also be used to predict the energy state of each molecule.[166]

$$\frac{N_n}{N_m} = \frac{g_n}{g_m} exp^{\left[\frac{-(E_n - E_m)}{kT}\right]} \qquad \text{Equation 1}$$

Note: Equation 1 represents the Boltzmann equation where N_n is the number of molecules in the excited vibrational energy level (n), N_m is the number of molecules in the ground vibrational energy level (m), g is the degeneracy of the levels n, m, $E_n - E_m$ is the difference in energy between the vibrational energy levels, k is Boltzmann's constant (1.3807×10^{-23} J.K^{-1}) and T is the temperature.

Since a change in polarizability is required for a Raman signal to be obtained, not every vibration in a molecule is Raman active. Only when the polarizability of a molecule varies in terms of size, shape or orientation, will the vibration be considered as Raman active.[168] In comparison, in another vibrational technique known as infra-red (IR) spectroscopy, a change in the dipole moment is required for a molecule to be IR active. Molecules that possess a centre of symmetry can be either Raman active or IR active, but not both.[166] This is called the mutual exclusion rule.

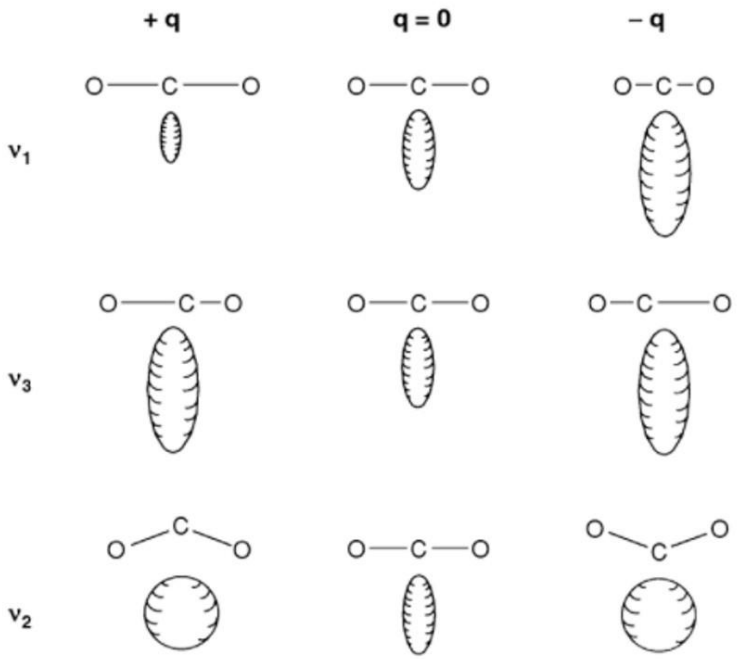

Figure 1.13 Illustration of the different vibration modes and the change in the polarizability of carbon dioxide (CO_2).[168]

Figure 1.13 shows the example of carbon dioxide vibrational modes and the polarizability of the molecule. This is a good example of the mutual exclusion rule as the molecule possesses a centre of symmetry. It is noted that the symmetric stretch ν_1 causes a change in the size of the polarizability of the molecule, which means that this vibration will be Raman active. However, the asymmetric stretch and bending mode, ν_2 and ν_3, do not induce any changes, which means that these vibrations will not be Raman active.

Differently, in molecules without a centre of symmetry this rule does not apply. It is generally observed that symmetric vibrations are more intense in Raman scattering than asymmetric vibrations.[166] The case of water is particularly interesting as the molecule is bend and do not have a centre of symmetry. Hence, its symmetric vibration is strongly Raman active when its asymmetric and bending mode vibrations are weak in Raman scattering. The weak contribution of water in Raman scattering makes the use of Raman spectroscopy ideal for the analysis biological samples.

1.2.2 Instrumentation

The recent advancement in physics and optics has led to the development of high resolution and reliable Raman instruments. A Raman spectrometer can be coupled with a microscope to enhance the resolution of the analysis, which allows the investigation of samples to a bio-molecular level (Figure 1.14).[169,170] Such instruments are capable of obtaining a Raman signal from an area smaller than a micron.[171]

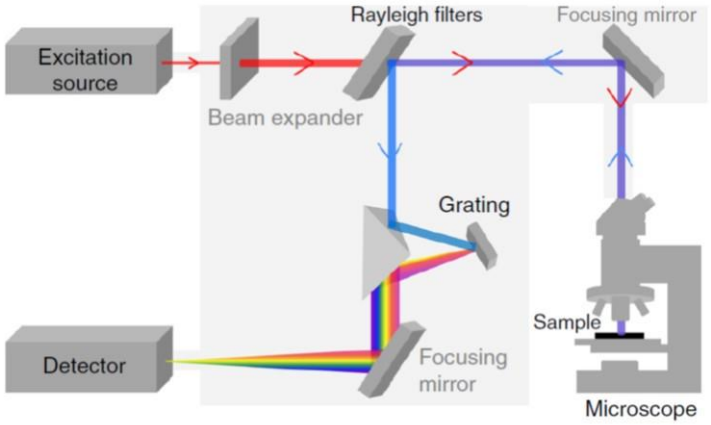

Figure 1.14 Illustration of a typical instrument composed of a Raman spectrometer coupled with a microscope.[172]

Many laser sources are now available offering a broad range of excitation wavelengths, from the near-UV, 488 nm, to the near-IR, 1064 nm.[173] Lasers can be selected depending on the sample being analysed. For example, near-IR lasers are preferentially used for biological studies as it reduces spectral background, the fluorescence and the photodecomposition of the sample.[173–176] The incident laser light is guided to the sample through the microscope. Usually, a band pass filter is used to select a unique incident wavelength. A long pass filter, also called a Rayleigh filter, is often placed before the spectrometer in order to remove the Rayleigh band, where the most commonly used are notch and edge filter.[172,177] Since the elastic scattering is more intense than the inelastic scattering, this can interfere with the readings and so the filter can be utilised to block the scattering at this frequency. In addition to the Rayleigh filter, the scattered light is also diffracted through a grating. As the scattered light is composed of different components of

different frequency, they will be separated through the grating.[173] The grating defines the spectral resolution obtained on the Raman spectrometer. However, a grating that efficiently diffracts the light, hence increasing the resolution of the Raman spectrum, will also reduce the intensity of the Raman bands as well as the spectral range.[172] Finally, the diffracted scattered light reaches the detector, where a multi-channel charge-coupled devices (CCDs) are the most commonly used detectors.[166] They are composed of thousands of pixels that will convert the incident light into electrons. Each electron will be processed and transferred to the readout instrument.[172] In order to improve the signal to noise ratio of the Raman spectrum obtained, CCDs are often cooled down to a cryogenic temperature. At such low temperature, the molecular motion will be almost inexistent, hence reducing the noise.[178]

The addition of a pinhole in the instrument as well as the appropriate microscope objective permit to increase the spatial resolution of the Raman analysis.[172] The size of the aperture of the pinhole determines the amount of scattered light passing through, and acting as a spatial filter where only the scattered light from the irradiated sample will pass and not the scattered light from any other points, thus setting a specific depth resolution within the sample. When a high magnification objective is used, it also increases the lateral spatial resolution for the analysis of sample. This technique is called confocal Raman spectroscopy and allows to perform high resolution images of biological samples.[171,179–181]

1.2.3 Biological applications

Raman spectroscopy is a non-invasive, non-destructive technique and the low interference of water in the spectra make this method promising for the analysis of biological samples such as bio-fluids, cells or tissues. In addition, the development of reliable instrumentation offers many possibilities for the use of Raman spectroscopy in biological investigations. Many studies have shown great potential for the bio-imaging of cellular components.[182–185] In comparison to regularly used fluorescence imaging, Raman is a label free technique, which removes the need for sample preparation.[186] Recently, many investigations have also been performed for the potential use of Raman as a diagnostic method.

1.2.3.1 In vitro and ex vivo investigations

Bio-imaging has been of great interest in order to identify specific components within cells and Raman micro-spectroscopy allows the imaging of a biological sample at a high resolution that can characterise each cellular component.[182,185,187] With the presence of a confocal microscope, it is also possible to obtain 3D images of a singular cell.[180,188] The technique used to image a biological sample is called Raman mapping. The aim is to measure Raman spectra at different points, of a specific step size, across a large sample area.[172,182,189] The sample is interrogated at the laser spot and the successive measurements across a specific area will build a spectral image of the selected region, where the different Raman shifts observed at each measured point will provide information on the composition of the sample. With the development of new instruments, it is possible to obtain a spectrum less than every micron, thus allowing the collection of detailed, high resolution images.[187,190]

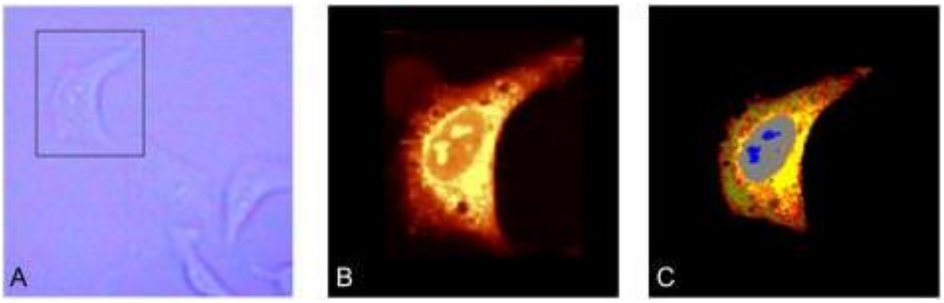

Figure 1.15 Raman mapping of a fixed HeLa cell, (A) Bright field image, (B) Raman image using Raman shifts between 2800 - 3000 cm^{-1} and (C) Raman image built with cluster analysis.[190]

Matthäus *et al.* performed high resolution Raman mapping on fixed HeLa cells in order to compare the resolution between Raman spectroscopy and fluorescence imaging.[190] Raman images were obtained using a point mapping method, where a single Raman spectrum was obtained every 0.5 µm. The resulting Raman image was built using the Raman shifts 2800 – 3000 cm^{-1}, which correspond to the C-H stretch of lipids (Figure 1.15.B)). In Figure 1.15.C), a cluster analysis was performed on the Raman spectra, that allowed a more detailed image to be built, where the nucleus and the different composition of the cytoplasm can be observed. Cluster analysis is a multivariate analysis that allows the investigation the correlation between each individual spectrum and associate them into groups when they are highly correlated. Thus, each

group is associated with a specific colour on the Raman map (Figure 1.15.C)), resulting in the differentiation of each cellular component such as nuclei, mitochondria or cytoplasm. In this study, a strong correlation between Raman mapping and fluorescence mapping of cellular components were obtained, which is of great interest as it would allow characterisation of biological components via a label free technique.

This Raman mapping method allows the detailed investigation of cell components on fixed cells, but also on live cells.[191–194] This opens a new area to permit the tracking of biological processes and pathways within a cell. Such studies were also developed to a diagnostic level using Raman spectroscopy, where different type of cells were able to be differentiated according their respective Raman spectra.[195,196] The ability to differentiate different types of cancer cells from healthy cells or from different stages of the disease has been strongly investigated.[197–201] Ilin *et al.* have also demonstrated that it is possible to track the different stages of differentiation of stem cells.[202]

In addition to cell studies, Raman has been translated to tissue analysis, which has a more complex biological composition. Using point mapping methods or single Raman spectra collection, it has been shown that it is possible to differentiate a healthy from an infected tissue using multivariate analysis.[203–206] As the Raman signal obtained can be complex and difficult to interpret due to the composition of such biological samples, statistical analysis is often used to separate samples. Kendall *et al.* proposed a method of classification of neoplasia in Barrett's oesophagus using Raman spectroscopy.[207] Multiple Raman spectra were obtained from different biopsies and a multivariate analysis was used in order to predict the stage of the disease. This classification would allow the prediction and the diagnosis of Barrett's oesophagus cancer. The method was compared to histopathology observation in order to assess its validity. It was found that the Raman classification method had a sensitivity between 73 % and 100 %, and a specificity of 90 %. This is particularly promising for the use of Raman spectroscopy as a diagnostic tool for *in vivo* studies. Raman was also used to diagnose other types of cancer such as brain,[208] breast,[209] prostatic,[210] lung,[211] or cervical cancer,[212] as well as inflammatory disease.[213]

Raman spectroscopy has therefore shown great potential in biomedical imaging and diagnostic applications, as different disease states can be detected and tracked over time.

1.2.3.2 In vivo applications

The success of the use of Raman spectroscopy as a classification and early detection method for different diseases such as cancer for *in vitro* and *ex vivo* samples has led to the development of more advanced instruments that can perform *in vivo* diagnosis.

Smaller devices have been developed, making them portable, and coupled with a fibre optic probe that allows the investigation of different parts and organs of the body.[214–216] These instruments are now commercially available but are often built in house in order to meet the specific requirements of the research lab. Despite their lower sensitivity and spectral resolution compared to Raman benchtop instruments, their smaller size and their handheld probes make them ideal for clinical studies on patients.[217,218]

Many studies have been conducted for skin analysis using fibre optic Raman techniques and multivariate analysis.[219–222] Schleusener *et al.* investigated the use of Raman spectroscopy coupled with a fibre optic probes for the diagnosis of skin cancer in humans.[223] A total of 104 patients presenting skin lesions were analysed with Raman. Using multivariate analysis, Raman spectra from skin lesions were discriminated from the control Raman spectra obtained from the skin outside the lesions. Raman diagnostic results were then compared with skin analysis performed by dermatologists. A diagnostic accuracy of 73 % and 85 % was obtained respectively for, basal cell carcinoma and squamous cell carcinoma, with the use of Raman spectroscopy compared to normal skin. It appeared that these results were comparable with the accuracy obtained by the method performed by the dermatologists, suggesting that Raman spectroscopy can be a viable alternative for clinical skin diagnosis.

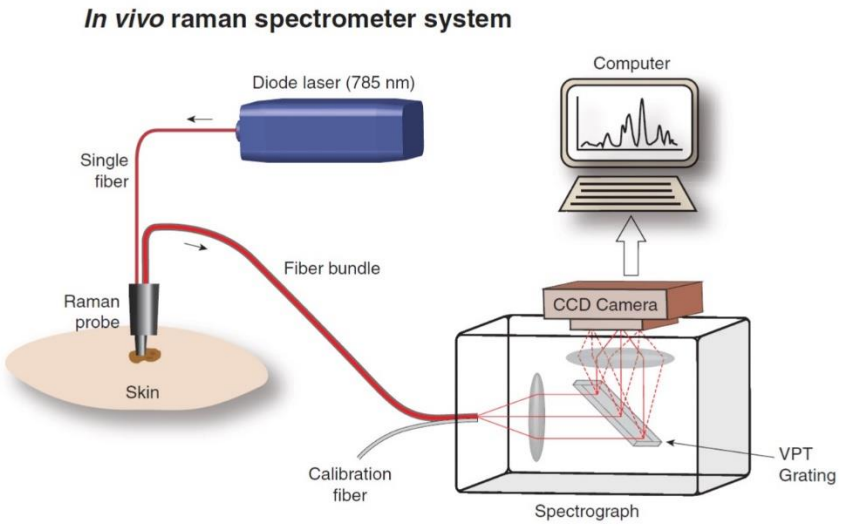

Figure 1.16 Schematic configuration of an in house built Raman instrument, showing the near-IR laser (785 nm) and CCD detectors with Raman fibre optic probes, for in vivo detection of skin cancer.[224]

Lui *et al.* developed a portable Raman instrument coupled with a fibre optic probe in order to perform *in vivo* detection of skin cancer on human patients (Figure 1.16).[224] They selected a near-infrared laser (785 nm) in order to reduce the fluorescence interference and the potential photodecomposition of the skin. Measurements were performed on 453 human patients presenting skin lesions in a hospital over eight years. Different classification and multivariate analysis were conducted on the Raman spectra data sets to assess the efficiency of the diagnostic method. It was found that the Raman *in vivo* measurements offered a high sensitivity and specificity in the differentiation of skin lesions and cancer detection. The diagnostic accuracy was found to be comparable with current clinical examinations. This intensive study performed in a clinical environment demonstrates the great potential of the use of Raman spectroscopy for *in vivo* diagnosis and could potentially be an alternative for the skin biopsies that are the current method of detection for skin cancer.

Further improvement of the probe system led to the development of endoscopic probes that allow analysis of internal organs such as in the oesophagus or in the gastrointestinal region.[225–227] Bergholt *et al.* have evaluated the use of Raman endoscopic technique for the diagnosis of ulcerous lesion in stomach.[225] Raman spectrometer was coupled with a Raman endoscopic probe to allow the measurement of Raman spectra in the stomach of patients. A total of 71 patients were examined and Raman spectra were obtained from normal mucosa, benign and malignant

ulcerous lesions in the stomach of the patients. Statistical classification was used to assess the diagnosis accuracy of the lesions by Raman spectroscopy. It allowed to produce a predictive model by classifying Raman spectra obtained from each tissue. The diagnostic algorithm showed great sensitivity and specificity towards the classification of each lesions and the normal tissue. It demonstrates that the recent technological advancement in the Raman instrumentation allows the use of Raman spectroscopy for assisting clinical and surgical diagnostics.

The reliable use of Raman spectroscopy in the differentiation of cancer cells from healthy cells in different parts of the human body is promising and of great interest for surgical assistance. Indeed, breast cancer was detected by Raman spectroscopy during partial mastectomy, where cancer cells were missed during the first surgery, which led to a second surgery in order to remove the remaining cancer cells.[209,228] Lately, Jermyn *et al.* adapted a Raman instrument to be operational in a surgical room, where it was used during brain surgery (Figure 1.17).[229] Raman spectroscopy was investigated as a possible aid for brain tumour removal during surgery.

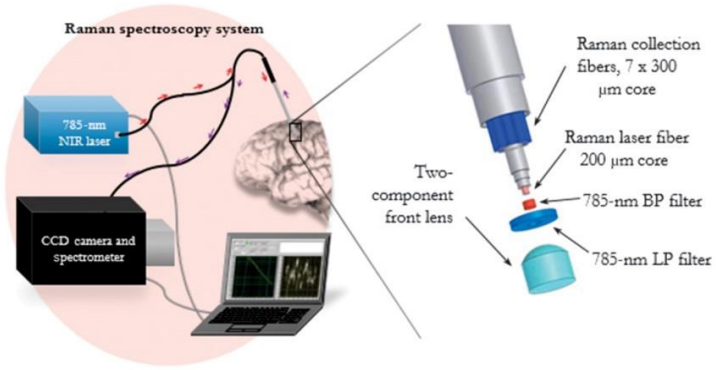

Figure 1.17 Illustration of the instrumental set up used for in vivo diagnosis of brain cancer cells with the near-IR laser (785 nm) and the high-resolution CCD detector with the Raman fibre optic probes. The probe is composed of a band-pass (BP), a long-pass (LP) and a silica based core.[229]

Brain biopsies were obtained and analysed by histopathological staining in order to classify Raman spectra obtained from the brain as normal or cancerous. It resulted in three different groups: normal brain tissue, normal brain tissue with cancer cells (< 90 % of cancer cells present) and dense cancer tissue (> 90 % of cancer cells present). It has been shown that this technique had great sensitivity and specificity towards brain cancer cells, and discrimination between normal brain tissue and brain with cancer cells resulted in a 90 % diagnostic accuracy. Moreover,

it was estimated that brain tissue infiltrated by cancer cells possessing as low as 17 cancer cells/0.0625 mm^2 could be discriminated Raman.[229] This is particularly important as the patient's survival rate depends on the amount of cancer cells remaining after surgery. It appeared that the use of Raman could help increasing the removal efficiency of brain cancer cells. The use of Raman spectroscopy during surgery is a major breakthrough as it opens new possibilities for diagnostics. The high diagnostic accuracy obtained with Raman and the low detection limit of cancer cells in brain tissue detected suggest that Raman spectroscopy could be used to guide surgeon during brain tumour removal and reduce the amount of remaining cancer cells in the brain.

Raman spectroscopy has shown great potential in biomedical applications, such as for use as a diagnostic method. The development of new and high-performance portable Raman instruments allows the translation between *in vitro* and *in vivo* measurements that will be applied in a clinical environment or on field work. Hence, thanks to the recent advancement in the bio-medical diagnosis, Raman spectroscopy could be employed for the detection of Human African Trypanosomiasis. Current diagnostics methods, based on blood samples, for HAT suffer from limitations that could jeopardize the target of elimination of *gambiense*-HAT by 2030.[21,133,141] The recent finding of asymptomatic carriers that can act as human reservoir and sustain the transmission of the disease,[65,69,72] in addition to the capacity of the trypanosomes to proliferate in the skin and to be transmitted to the tsetse fly from the skin,[154–156] offers a new target site for the diagnostic of *gambiense*-HAT. Portable Raman spectroscopy can target the skin in a label free and non-invasive manner, resulting in the rapid detection of *gambiense*-HAT, without the need of skin biopsies.

Chapter 2 Aims

The main goal of this study was to investigate a new detection method for skin analysis using Raman spectroscopy. Ideally it would allow the detection of trypanosome infected patients that otherwise would remain undetected using the current field diagnostic methods.

Different trypanosomes involved in the infection were spectrally and biologically characterised in order to obtain vital information that could be used during the skin study. Parasites were imaged using Raman spectroscopy and the tentative assignment of individual Raman bands allowed the understanding of their composition. As each sub-species are morphologically indistinguishable, their individual Raman fingerprints were obtained and compared to one another, which would assess their spectral discrimination and the identification of such sub-species during skin analysis. Following this study, uninfected and infected mice skin samples were obtained and placed on a calcium fluoride substrate, which allowed their analysis with Raman. Individual samples were mapped several times to obtain a general trend in the biological composition and alteration induced by the infection across the sample. Principal component analysis was performed to discriminate uninfected from infected skin. The resulted Raman fingerprint provided during the analysis allowed the interpretation of each Raman bands and their respective biological association. Finally, the Raman contribution of the parasite during skin investigations was assessed by spectrally comparing the different Raman fingerprints.

This detection method was then translated into *in situ* study, where different infected and uninfected mice were spectrally analysed. The potential of the use of Raman spectroscopy as a diagnostic technique was assessed. Mice infected with different strains of *T.b. brucei* and with *T.b. gambiense* were characterised at different time points and their differentiation investigated. The assignment of Raman bands to biological vibrations allowed to hypothesis on the influence of the infection on the skin. Several experiments were performed to understand the Raman contributions of these biological variations. Then, the detection of sleeping sickness with Raman spectroscopy was compared to other techniques such as blood parasitemia and PCR analysis on the skin.

Finally, this detection method was tested in the field in Guinea using a portable Raman instrument. As part as the medical team responsible for active screening of the population against *gambiense*-HAT in rural areas, it was possible to use Raman spectroscopy along with the current diagnostic methods. Using statistical tools, the data were analysed and the potential of Raman spectroscopy as diagnostic method for HAT was assessed.

Chapter 3 Characterisation of *Trypanosoma brucei* and mouse skin with Raman spectroscopy

All experimental details were described in Chapter 7.

3.1 Aims

The aim of this study was to characterise different sub-species of *T.b* to understand their biological composition, as well as establishing the potential of Raman spectroscopy in the detection of sleeping sickness in mice skin.

Firstly, it was important to study the parasite *in vitro*, and identify its Raman vibrations that could be used for skin studies. VSG surface coat of the parasites was extracted and analysed individually with Raman spectroscopy to provide an idea of the signal that would be obtained from the parasites. Two sub-species of *T.b* were studied: *T.b. brucei* and *T.b. gambiense*. Raman imaging was used to identify the specific molecular vibrations from the parasites for each sub-species and to understand their biological composition. An attempt on assigning individual Raman bands to molecular vibrations was performed to understand the biological information obtained. Different parasites from the same sub-species were then compared to each other in order to assess the possible spectral variations from one parasite to another. From this comparison, Raman fingerprint were obtained for each sub-species and were spectrally compared. The aim was to determine whether it would be possible to identify the type of parasites involved in a skin infection detected by Raman.

Secondly, skin sections were investigated (*ex vivo)* on slides using Raman mapping. It provided information on the skin composition and the changes made by the presence of the parasite. Infected and uninfected maps were spectral compared in order to assess their discrimination. This was the main goal as a positive differentiation between the two skin samples would imply that the detection of sleeping sickness with Raman on the skin is possible. Raman fingerprint

were also obtained to characterise each sample: infected and uninfected skin. A spectral comparison between these two Raman spectra would provide clear biological information on the influence of the parasites in the skin and help to generate hypothesis on the variations observed. Performing a tentative assignment for the Raman bands specific to the infection would help generating hypothesis on the influence of trypanosomes on the skin. Finally, Raman spectra from *T.b. brucei* and skin (infected and uninfected) were compared to assess the contribution of the parasites in the Raman signal specific to the infection and if trypanosomes were detected by Raman in the skin.

Two different lasers were used to undertake this investigation: 532 and 785 nm laser. The 532 nm laser provides better signal and resolution experimentally. It allowed the collection of a large amount of biological information on the difference of composition between samples. The spectral information obtained permit to accurately interpret the molecular changes occurring in the skin due to the infection. Preferentially, a 785 nm laser was used for biological materials as samples are less prone to photodecomposition and this wavelength removed the potential fluorescence background arising from certain biological component. Despite, the reduced intensity and lower resolution of the Raman signal obtained with 785 nm, it provided useful spectral and biological information for the *in situ* study.

3.2 Characterisation of Variable Surface Glycoprotein

The surface of the parasite is composed of a large amount of variable proteins called variable surface glycoprotein (VSG), and to a lesser extent it also contains invariable proteins. The VSG forms a dense packed monolayer around the surface of the parasite, protecting it from the action of the immune system. Through periodically changing the surface VSG it can evade the immune response. However, the change within the VSG mostly occurs through the peptide sequence of the protein. It has been found that a change of surface composition did not affect the structure of the VSG, they still remained closely identical to each other.[92] The peptide sequence changes must occur on the epitope of the VSG in order to avoid recognition by the immune system.

As the VSG was present in a large amount around the surface of the parasite,[89] it was more likely that the Raman information that was obtained, was coming from the VSG composition. It was then important to obtain the fingerprint of a VSG before parasite analysis.

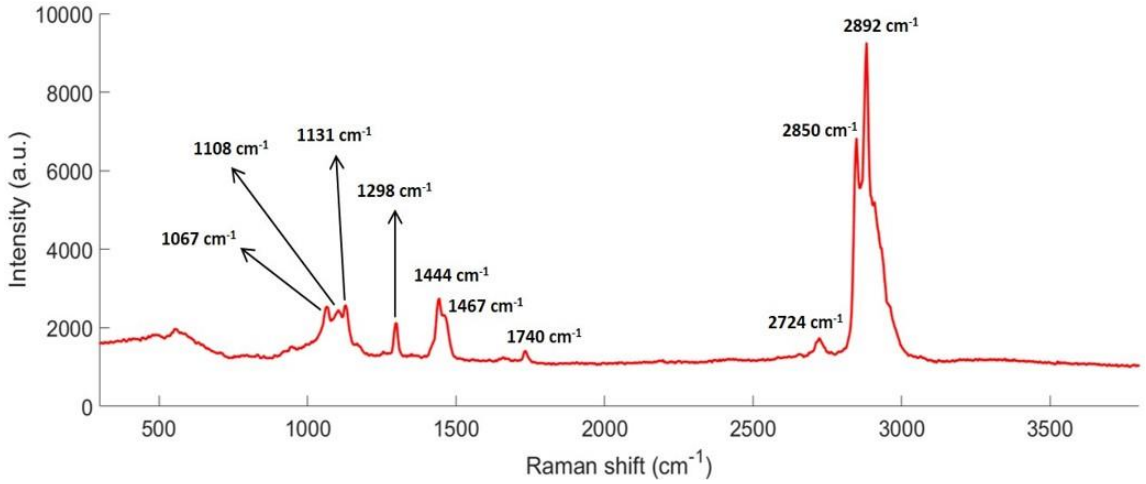

Figure 3.1 Raman spectrum of an extracted VSG using a 532 nm laser wavelength and 1 s acquisition time.

The VSG was extracted from bloodstream trypanosomes and separated from other components. On the surface of the parasite, the VSG was covalently bound via a glycosylphosphatidylinositol (GPI) anchor and was present as a dimer.[230] However, the extraction process removes the GPI anchor from the VSG causing its conformation to become disrupted. The obtained VSG was single

stranded, which could affect the Raman information obtained, but it provided an idea of the Raman signal that could be obtained from a parasite. Figure 3.1 showed the Raman spectrum obtained from the single VSG using a 532 nm laser wavelength. It was obtained with a single spectrum measurement with a 1 s acquisition time.

The result obtained was consistent with a long amino acid chain, and Raman peak assignments are given in Table 3.1. Peaks at 2850 and 2892 cm^{-1} correspond respectively to the symmetric and asymmetric stretch of the C-H bond. The C-C skeletal stretch was characterised by the peaks at 1067 and 1131 cm^{-1}. The presence of an ester group was characterised by the Raman shift at 1740 cm^{-1}. The CH_2 deformation and the C=N stretching was determined by the shifts at 1444 and 1298, and 1467 cm^{-1} respectively.

Table 3.1 Tentative assignment of Raman bands obtained from the measurement of pure VSG. [231–233]

Raman shift (cm^{-1})	Tentative assignments of Raman peaks
2892	CH_2 asymmetric stretch
2850	CH_2 symmetric stretch
2724	C-H stretches
1740	Ester group
1467	C=N stretching
1444	CH_2 deformation
1298	CH_2 deformation
1131	C-C skeletal stretch
1108	Benzoid ring deformation, phenylalanine
1067	C-C skeletal stretch

Establishing the Raman fingerprint of VSG is key, as it acted as a reference when investigating the surface composition of trypanosomes.

3.3 *Trypanosoma brucei*: in vitro study

The species of trypanosome involved in causing sleeping sickness is *Trypanosoma brucei* (*T.b*). Within this species, there are three sub-species that can infect animals or humans. *Trypanosoma brucei brucei* (*T.b. brucei*) is involved in the infection of animals but not in humans. Whereas *Trypanosoma brucei gambiense* (*T.b. gambiense*), and *rhodesiense* (*T.b. rhodesiense*) are involved in human infection. In this study, *T.b. brucei* and *T.b. gambiense* were investigated before investigating their influence in mice skin during an infection.

Parasites were fixed onto calcium fluoride – Raman grade slides in order to avoid fluorescence from glass when probing with a laser as this could result in spectra interference.

3.3.1 Characterisation of *Trypanosoma brucei brucei* biological composition

3.3.1.1 T.b. brucei characterisation with a 532 nm laser

A confocal microscope coupled with a Raman device was used to perform this study. *T.b. brucei* were mapped with using a 532 nm laser. The mapping technique allowed Raman information to be gathered from a large area. This was achieved by taking single point measurements at a defined step size, as shown in Figure 3.2. By using the Raman intensity of an identified peak, a false colour Raman intensity map could be obtained showing its distribution.

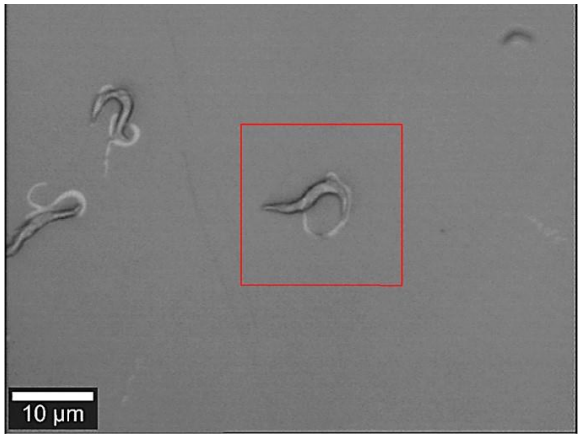

Figure 3.2 White light image of a Trypanosoma brucei brucei (100x lens).

A square was drawn around the parasite (red square in Figure 3.2) showing the area which was mapped (25 x 25 µm). For this experiment, a step size of 0.5 µm was defined. Hence, every 0.5 µm a single measurement was obtained giving a total of 2500 spectra. Interrogation of the sample using a 532 nm laser had the advantage of delivering a high photon energy thus promoting a strong Raman signal. However, due to the energy delivered, samples were often prone to fluorescence and/or sample degradation, which could alter both results and samples.[175,176,234]

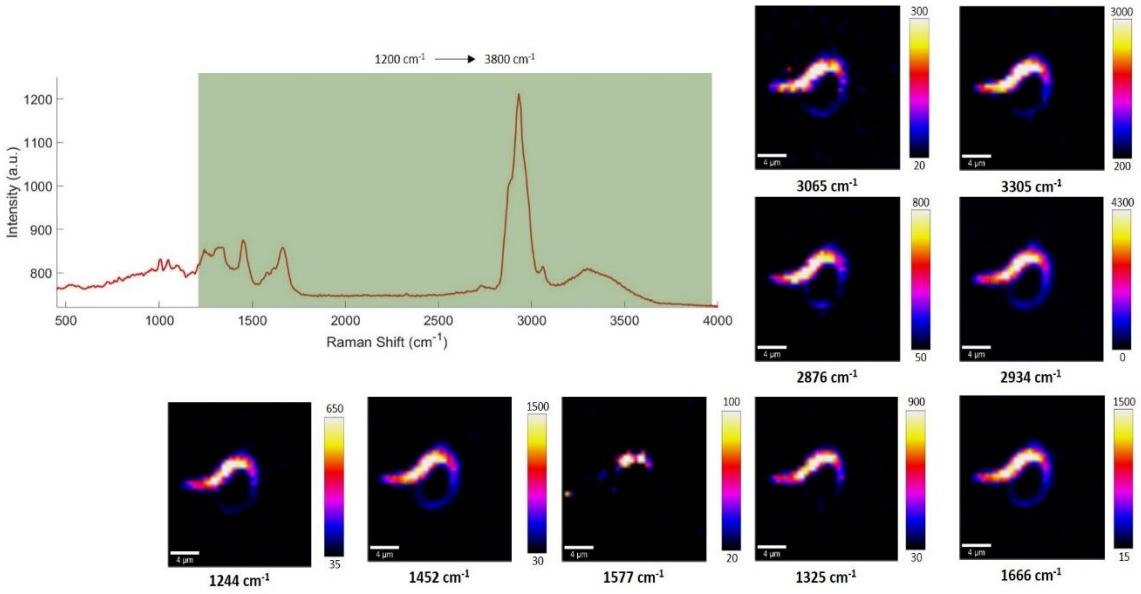

Figure 3.3 Raman intensity maps of T.b. brucei for the high wavenumbers region (1200 – 3800 cm^{-1}) measured with a 532 nm laser, 6 s acquisition time and 100x lens. Each image is associated with their respective intensity bar, which assign a colour gradient from the lowest to the highest intensity, with black showing the lowest intensity and white being the highest intensity.

Figure 3.3 showed the Raman intensity map associated with each Raman bands obtained from *T.b. brucei*. Raman bands from 1200 to 3800 cm^{-1} were shown in this figure. In order to produce these Raman intensity maps, each peak was baseline corrected individually and the intensity bar was set up to specifically show the peak intensity generated by the parasite. The VSG and cellular components from the trypanosomes gave numerous Raman shifts and their tentative assignments were highlighted in Table 3.2. It could be observed on the Raman intensity maps that the main signal was coming from the body of the parasites, where the VSG was densely

packed. It was thought that VSG length was about 15 nm and its compact conformation on the surface,[235] suggested that the majority of the Raman signal observed originated from the VSG protein. It could also be the result of a different focus point, as the main body was thicker than the tail of the parasite. Raman bands above 2800 cm^{-1} have been assigned to the C-H stretch and O-H stretch. The C-H stretch peak had an especially high intensity. Both molecular groups were ubiquitous in proteins and were consistent with long amino acid chains formed by the VSG. The peaks were different from the pure VSG investigated previously, as no identical Raman bands between the two spectra could be observed, possibly due to a different composition in the chain as well as a difference of conformation. Indeed, VSGs only possessed 15-25 % of similar amino acids sequence but they conserved their 3D structure.[92] As the conformation of VSG was different from a pure VSG sequence dried on a solid substrate, the Raman fingerprint was found to be different. The conserved tertiary structure of the VSG around trypanosomes was composed of α-helix coiled coil as well as antiparallel β-sheets.[235] The Raman bands observed at 1244 and 1666 cm^{-1}, have been assigned to Amide III and Amide I vibrations. These vibrations were commonly found in protein analysis, but they were also usually used to interpret the conformation of the protein detected.[236] It was found that both Raman bands were related to β-sheet configuration of proteins.[237,238] It could then be related to the VSG structure of the trypanosomes, but it could also be originating from other proteins within or around the parasite. Two small Raman bands could also be observed at the base of the Raman band 1666 cm^{-1} for the Amide I and were located at 1583 and 1619 cm^{-1}. They could be assigned to the presence of phenylalanine and tyrosine residues within the parasite.[239] Moreover, the peak at 1577 cm^{-1} could also be assigned to the C=C bending mode from aromatic rings, such as for the phenylalanine.[231]

Table 3.2 Tentative assignment of Raman bands for the T.b. brucei Raman bands from 1200 to 3800 cm^{-1} obtained with 532 nm laser. [231–233]

Raman Shift (cm^{-1})	Tentative assignments of Raman peaks
3305	O-H stretch
3065	C-H stretch
2934	CH_2 asymmetric stretch
2876	CH_2 symmetric stretch
1666	Amide I
1577	Nucleic acid modes
1452	CH_2CH_3 deformation
1325	CH_2CH_3 wagging mode in proteins and DNA
1244	Amide III

Other components could also be identified with the mapping of the parasite. The peak at 1325 cm^{-1} was thought to be related to CH_2CH_3 wagging mode in proteins but also in DNA,[231,233] as well as the Raman bands at 1577 cm^{-1} (nucleic acid modes), possibly indicated the detection of DNA residues within the parasites. The latter Raman band was not spread across the parasite but located in two small areas on the Raman intensity map, suggesting that the nucleus was detected. Hence, VSG was not the only protein detected.

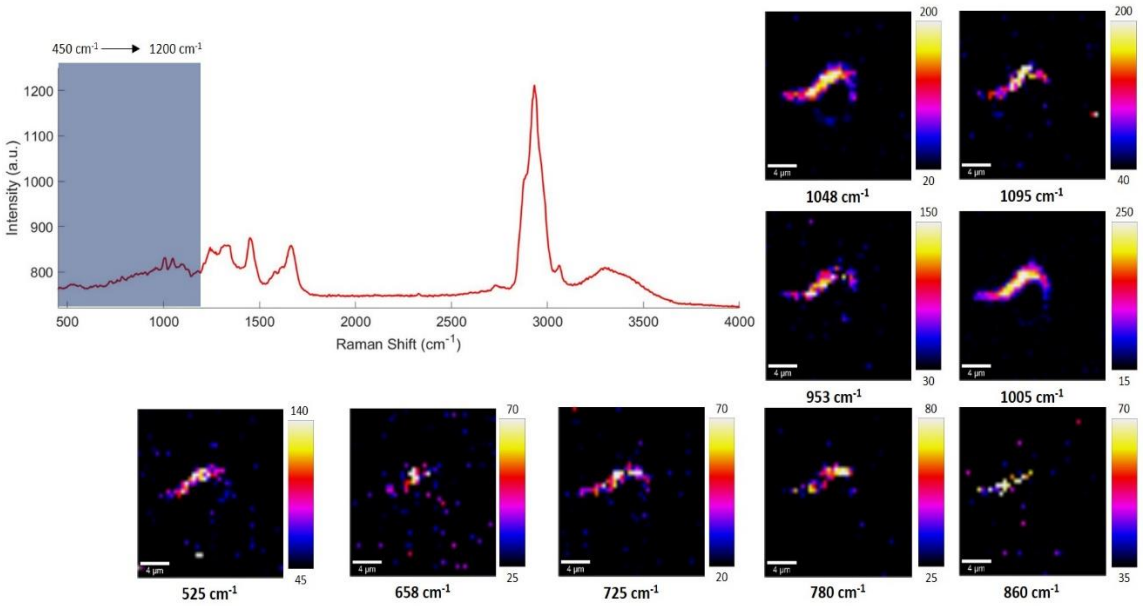

Figure 3.4 Raman intensity maps of T.b. brucei for the low wavenumbers region (450 – 1200 cm^{-1}) measured with a 532 nm laser, 6 s acquisition time and 100x lens. Each image is associated with their respective intensity bar, which assign a colour gradient from the lowest to the highest intensity, with black showing the lowest intensity and white being the highest intensity.

Figure 3.4 provided the Raman intensity maps of the Raman bands from 450 to 1200 cm^{-1} obtained from the *T.b. brucei*. The Raman intensity of the peaks was lower than the previous analysed range (1200-3800 cm^{-1}). However, they gave valuable information about the biological composition of the parasite (Table 3.3). The Raman peak at 953 cm^{-1} provided information on the conformation of the proteins detected, as this peak could be assigned to the presence of CH_3 vibrations of a α–helical protein.[231] The combination of the Raman bands at 953 and 1245 and 1666 cm^{-1}, obtained previously, may be linked to the conformational structure of the VSG.

The VSG was linked to the membrane of the parasite via a GPI anchor.[89] As the surface population of VSG present was high, GPI should then also be present in large amounts. Ideally, it should also be detectable using Raman scattering, despite the dense layer of amino acid chains. The Raman bands at 1048 cm^{-1} (PO_4^{3-}) and 1095 cm^{-1} (PO_2^-) were observed across the entire surface of the trypanosomes (Figure 3.4), and were evident across the surface of the trypanosome, suggesting that the GPI can be identified. Moreover, a phosphatidylinositol, 780 cm^{-1}, and a phosphatidylserine, 525 cm^{-1}, which are structurally very close to GPI have been observed

through the surface of the main body of the parasite. This suggests that GPI could be tracked on the surface of the parasite, despite the dense VSG layer.

Differently, 860 cm^{-1} was assigned to phosphate group vibrations, which could also be linked to the phosphate groups present in the GPI anchor, but the presence of this Raman band was only detected in a small area of the parasite, suggesting the detection of DNA from the nucleus of the trypanosomes. This finding suggested that some intracellular or extracellular components other than VSG could be detected with Raman on the parasites. Moreover, *T.b. brucei* surface composition was not only composed of VSG sequence and proteins. It also possessed numerous fatty acids, lipid and phospholipid residues on its membrane such as phosphatidylcholine, phosphatidylethanolamine, phosphatidylinositol or phosphatidylserine.[240–242] The parasite is capable of using the host biological components like lipids to *de novo* synthesis its own phospholipids depending on its need.[243,244] Such Raman bands associated with phosphate groups could then be associated with the phospholipid layer present in the membrane of the trypanosomes. Importantly, Raman bands at 780 and 525 cm^{-1}, respectively associated with phosphatidylinositol and phosphatidylserine, could also directly relate to their distribution across the membrane of *T.b. brucei*.

Table 3.3 Tentative assignment of Raman bands for the T.b. brucei Raman bands from 450 to 1200 cm^{-1} obtained with 532 nm laser wavelength. [231–233]

Raman Shift (cm^{-1})	Tentative assignments of Raman peaks
1095	C – C stretch, phosphodioxy group (PO_2^-)
1048	C – C stretch proline, PO_4^{3-} symmetric stretching
1005	Phenylalanine
953	ν_s CH_3 of α-helical proteins
860	Phosphate group, tyrosine
780	Phosphatidylinositol
725	C – S protein
658	C – S stretching of cystine
525	Phosphatidylserine or S-S disulfide stretch

Phenylalanine was usually easily detectable in tissue analysis, and it has been tracked here (1005 cm^{-1}) on the entire surface of the parasite due to its large presence in proteins. Similarly, the C-C stretch of proline could also be assigned to the Raman bands at 1048 cm^{-1}, suggesting a large presence of this amino acid as well. Finally, cysteine residues or disulphide bonds between proteins were assigned to the shifts at 725 and 658 cm^{-1}. It was possible that such cysteine residues were detected from the N-terminal site of the VSG. It was demonstrated that cysteine residues were highly conserved between the type of VSG, and were playing an important role in the conformation of the protein.[245]

It was clear that large proteins such as VSG were being identified with Raman. The Raman fingerprint of *T.b. brucei* was different from the one obtained previously with pure VSG because the conformation of VSG has changed. It was thought that amide I and III bands indicated a β-sheet conformation, whereas 953 cm^{-1} suggested a α-helical structure. Moreover, other cellular components were being identified as DNA from nucleus of the parasites, which increased the number of Raman bands obtained. Raman signal could also be coming from the presence of other proteins, such as Invariant Surface Glycoprotein (ISG) or non-VSG proteins, and phospholipids layer from the membrane.[86,240,241] The biological information obtained through the characterisation of the different Raman bands provided an understanding of the molecular

composition of *T.b. brucei*, however, its biological composition may have changed within the sample and the intra-sample variation was assessed by analysing several parasites from the same sub-species. This analysis could also provide a unique fingerprint for this sub-species, which could be used as a reference for the investigation of infected mouse skin, and this work was repeated with a different laser: 785 nm.

3.3.1.2 T.b. brucei characterisation with a 785 nm excitation

This near-IR wavelength has been extensively used for tissue analysis and *in vivo* studies. This was quite advantageous for biological studies to avoid the skin or other tissue to burn during analysis. It also reduced the fluorescence effect that could occur in tissue.

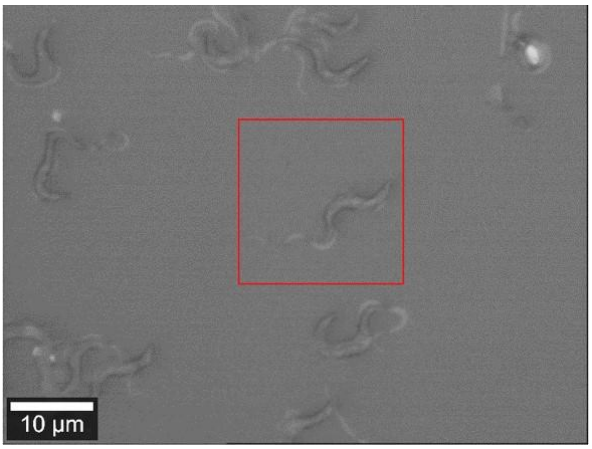

Figure 3.5 White light image of T.b. brucei mapped with 785 nm laser (100x).

Here, a 785 nm laser was used to characterise the parasite composition (Figure 3.5), as it was important to study the Raman information obtained with this wavelength for the further *in situ* tissue analysis.

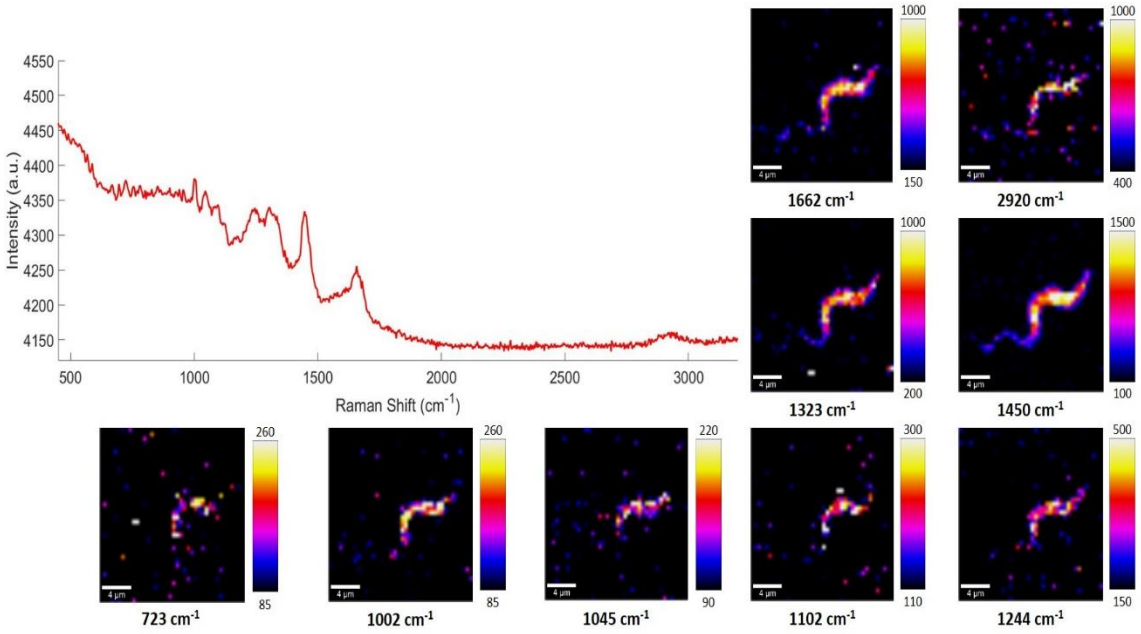

Figure 3.6 Raman intensity maps of T.b. brucei measured with a 785 nm laser wavelength, 6 s acquisition time and 100x lens. Each image is associated with their respective intensity bar, which assign a colour gradient from the lowest to the highest intensity, with black showing the lowest intensity and white being the highest intensity.

Figure 3.6 showed a collection of Raman intensity maps for the study of the *T.b. brucei* with a 785 nm laser. The difference between the 532 nm and the 785 nm excitation was easily recognisable, as the C-H stretching vibrations were less intense with the near-IR excitation. This resulted in only a small peak appearing at 2920 cm^{-1}. It was also clear that the Raman signal at 785 nm was variable, signified by the non-uniform distribution along the parasite when compared with the maps obtained at 532 nm excitation. However, some crucial information about the composition of the parasite could still be obtained. As shown in Table 3.4, the Raman bands were very close to those observed previously, suggesting the information obtained is identical. The Raman bands at 1662 and 1244 cm^{-1} respectively amide III and amide I, still suggested a β-sheet structure on the parasite as observed with 532 nm laser.[237,238] Moreover, the Raman peak at 1102 cm^{-1} (PO_2 stretch) and as well as the band at 1045 cm^{-1} could indicate the presence of the GPI anchor at the base of the VSG on the surface of the parasite. The PO_2 stretch associated with the peak at 1102 cm^{-1} could also be related to the presence of DNA in the parasites. The different phosphate groups tracked may also relate to the phospholipid distribution across the parasite as observed previously with the use of 532 nm laser.[240,241]

Table 3.4 Tentative assignment of Raman bands for the T.b. brucei obtained with 785 nm laser. [231–233]

Raman Shift (cm^{-1})	Tentative assignments of Raman peaks
2920	C-H stretch
1662	Amide I
1450	CH_2 bending mode
1323	CH_2CH_3 wagging mode in proteins and DNA
1244	Amide III
1102	O-P-O backbone stretch of DNA
1045	C – C stretch proline, PO_4^{3-} symmetric stretching
1002	Phenylalanine
723	C – S protein

The presence of phenylalanine (1002 cm^{-1}), as well as proline that could be associated with the peak at 1045 cm^{-1}, was still detected across the surface of the parasite. Cysteine residues, potentially from the N-terminal of the VSG, were assigned to the peak 723 cm^{-1}. These results suggested that, despite the low energy delivered by 785 nm laser, the information obtained about the VSG remained spectrally very close to the one obtained with 532 nm laser. As well as detecting and characterising the VSG on the surface of the trypanosomes, it was also possible that other extracellular proteins and lipids were detected during the analysis. A Raman fingerprint could also be produced for *T.b. brucei* as obtained previously with a 532 nm laser.

The interpretation of the data generated using Raman mapping could often be quite difficult. Care must be taken at the pre-processing stage before generating the false colour peak intensity maps, as shown in Figure 3.7.

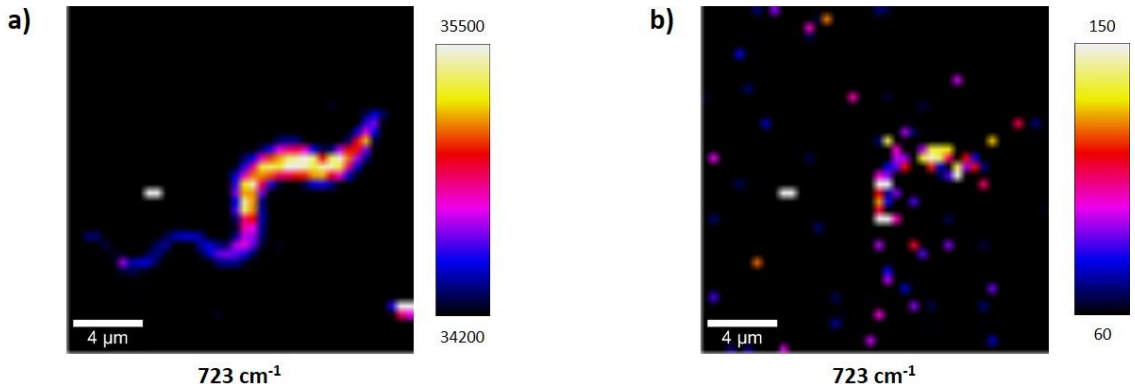

Figure 3.7 Comparison of two Raman intensity map of the Raman peak 725 cm^{-1} for T.b. brucei at 785 nm laser: (a) non-baselined, (b) baselined.

The pre-processing of the acquired Raman data was very important to obtain a real representation of the repartition of a molecular group. The Raman signal was often obtained with an increase in the background noise in the spectrum, and it could lead to a misinterpretation of the intensity map. This was quite crucial for the investigation with 785 nm as in Figure 3.6, it could be observed that there was an increase in the background of the Raman bands present in the region lower than 1500 cm^{-1}. It was then important to baseline each individual peak, or a wrong representation of the C- S stretch vibration would be obtained as shown in Figure 3.7 for the band at 723 cm^{-1}. This Raman peak was having quite a low intensity, the pre-process allowed to track the intensity of the actual Raman peak and not an increase in the background.

The biological composition of *T.b. brucei* has been characterised through their resulted Raman spectra obtained with two different lasers, and a similar investigation was carried out on the human pathogen *T.b. gambiense*.

3.3.2 Characterisation of *Trypanosoma brucei gambiense* biological composition

3.3.2.1 T.b. gambiense characterisation with a 532 nm laser

The same investigation process was performed with the parasite *T.b. gambiense.* This parasite was responsible for the sleeping sickness in human, so it was of interest to study it prior to the *in vivo* experiments.

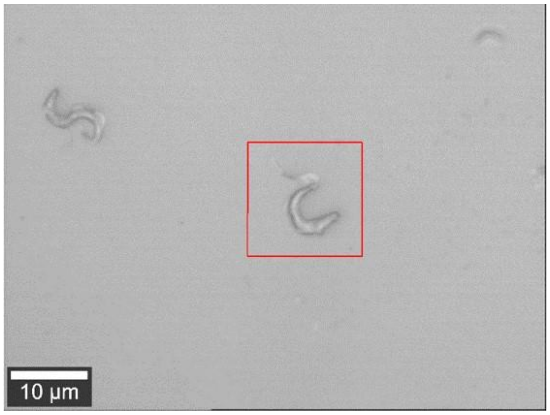

Figure 3.8 White light image of a T.b. gambiense mapped with 532 nm laser (100x).

First, the parasite was studied with a 532 nm laser to obtain strong information thanks to the high energy delivered to the sample by the incident laser (Figure 3.8). The parasite was mapped using the same experimental method as for *T.b. brucei*.

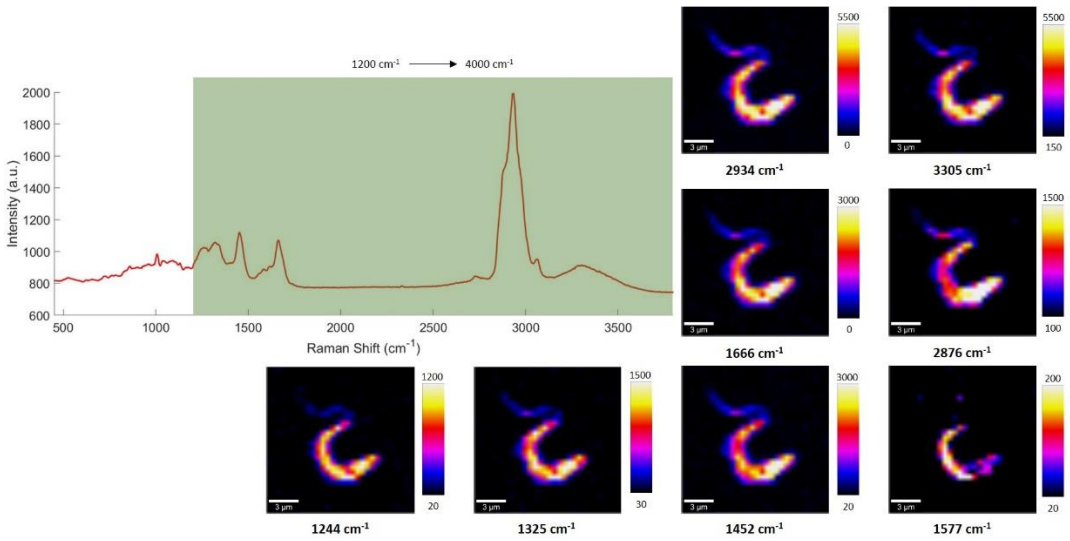

Figure 3.9 Raman intensity maps of T.b. gambiense for the high wavenumbers region from 1200 to 4000 cm^{-1} measured with a 532 nm laser, 6 s acquisition time and 100x lens. Each image is associated with their respective intensity bar, which assign a colour gradient from the lowest to the highest intensity, with black showing the lowest intensity and white being the highest intensity.

The Raman information obtained for the *T.b. gambiense* with 532 nm laser in Figure 3.9 was identical to the one obtained for *T.b. brucei* (Figure 3.3). The Raman bands assignment for the wavenumbers higher than 1200 cm^{-1} were grouped in Table 3.5. The Raman bands at 3305, 2934 and 2876 cm^{-1}, respectively representing the O-H stretch, the CH_2 asymmetric stretch and the CH_2 symmetric stretch, were observed again. They were typically found on proteins or long peptide chains, which correlates with the VSG structure. The possible β-sheet conformation of the VSG was also observed through the peaks at 1666 and 1244 cm^{-1}, which have been associated to amide I and amide III bands.[237,238] Two weak Raman bands could be observed at the base of the Raman band at 1666 cm^{-1} and appeared to be similar to the ones mentioned previously for *T.b. brucei* at 1586 and 1619 cm^{-1}. They were associated to the presence of phenylalanine and tyrosine.[239] The presence of the peak at 1325 cm^{-1} as well as 1577 cm^{-1}, as mentioned previously, also indicated the presence of nucleic acid through CH_2CH_3 wagging mode for the first Raman peak.

Table 3.5 Tentative assignment of Raman bands from 1200 to 4000 cm^{-1} for the T.b. gambiense obtained with 532 nm laser. [231–233]

Raman Shift (cm^{-1})	Tentative assignments of Raman peaks
3305	O-H stretch
2934	CH_2 asymmetric stretch
2876	CH_2 symmetric stretch
1666	Amide I
1577	Nucleic acid modes
1452	CH_2CH_3 deformation
1325	CH_2CH_3 wagging mode in proteins and DNA
1244	Amide III

As mentioned previously, the information obtained was different from the pure VSG, due to the difference of conformation of the VSG around the surface, but also due to the presence of components from the parasite itself. However, the Raman bands, from 1200 to 4000 cm^{-1}, were identical to the one obtained with the *T.b. brucei*. It was possible that the amino acids sequence was different between the VSG from *T.b. brucei* and *T.b. gambiense* but it was not possible to observe this variation by Raman spectroscopy.

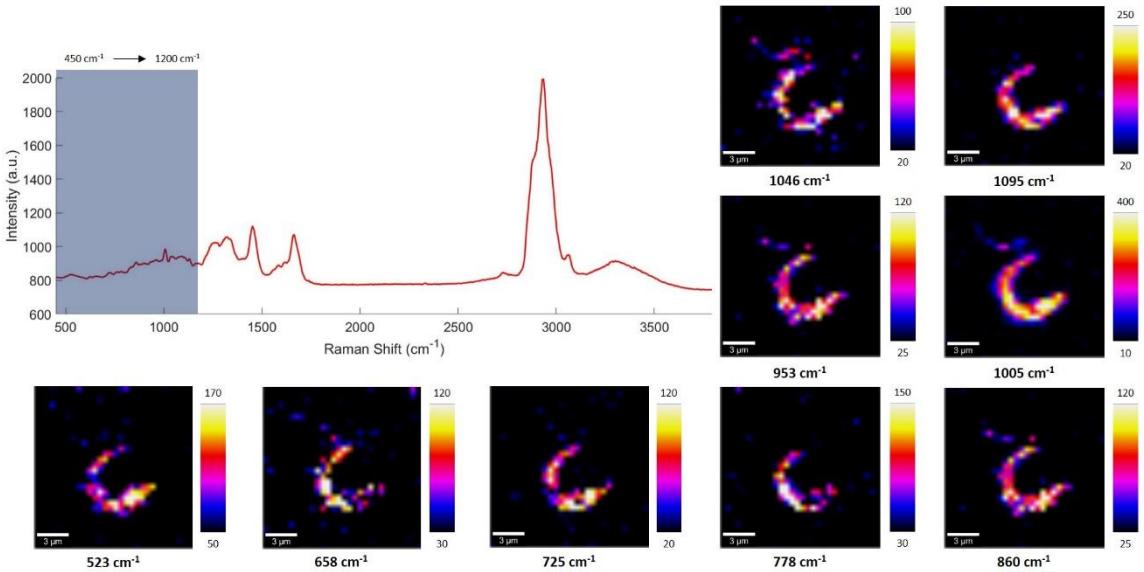

Figure 3.10 Raman intensity maps of T.b. gambiense for the low wavenumbers region from 450 to 1200 cm^{-1} measured with a 532 nm laser, 6 s acquisition time and 100x lens. Each image is associated with their respective intensity bar, which assign a colour gradient from the lowest to the highest intensity, with black showing the lowest intensity and white being the highest intensity.

The Raman intensity maps for the Raman bands present between 450 and 1200 cm^{-1} were represented in Figure 3.10. The intensity of the peaks in this area were lower than those present above 1200 cm^{-1} but their repartition through the parasite could still be followed and assigned in Table 3.6. The Raman bands at 860, 1046 and 1095 cm^{-1} could be assigned to the presence of the phosphate group from the GPI anchor. It was observed that its repartition was all across the parasite structure, which confirmed the identification of the presence of GPI to covalently attached the VSG on the surface. These phosphate groups could also be representative of the presence of a DNA back bone, but its repartition on the intensity map would suggest that in this case, it was associated with the anchor. Finally, the Raman bands at 778 and 523 cm^{-1} have been respectively associated with the presence of phosphatidylinositol and phosphatidylserine, which were structurally very close to the GPI. As mentioned previously for *T.b. brucei* characterisation, the distribution of certain phospholipids present in the membrane across the surface could be performed through the detection of phosphatidylinositol and phosphatidylserine. The other Raman bands such as 860 or 1095 cm^{-1} related to phosphate groups could also be associated with the presence of phospholipids on the membrane of *T.b. gambiense*.[240–242]

Table 3.6 Tentative assignment of Raman bands from 450 to 1200 cm^{-1} for the T.b. gambiense obtained with 532 nm laser.[231–233]

Raman Shift (cm^{-1})	Tentative assignments of Raman peaks
1095	C – C stretch, phosphodioxy group (PO_2^-)
1046	C – C stretch proline, PO_4^{3-} symmetric stretching
1005	Phenylalanine
953	ν_s CH_3 of α-helical proteins
860	Phosphate group, tyrosine
778	Phosphatidylinositol
725	C – S protein
658	C – S stretching of cystine
523	Phosphatidylserine, S – S disulfide stretch in proteins

The α-helical structure of the VSG was also identified with the peak at 953 cm^{-1}.[231] Finally, the highly conserved cysteine residues between VSGs,[245] were also detected through the Raman bands at 658 and 725 cm^{-1}.

The structure and conformation of the VSG could easily be observed with a 532 nm laser excitation. The possible β-sheet and α-helical conformation and the presence of the GPI anchor could be tracked by selecting specific Raman bands. The phospholipid distribution across the surface of the parasites could also be detected via the presence of phosphatidylinositol and phosphatidylserine. The information obtained with *T.b. gambiense* were strongly related with the *T.b. brucei* observed before with a 532 nm laser. This would suggest that the VSG structurally appeared identical between the two sub-species, as demonstrated by Blum *et al.*[92] but their sequence of amino acids could not be differentiated.

3.3.2.2 T.b. gambiense characterisation with a 785 nm laser

As well as a 532 nm laser excitation, T.b. gambiense was also studied with a near-IR laser: 785 nm (Figure 3.11). The method used was the same as for *T.b. brucei*.

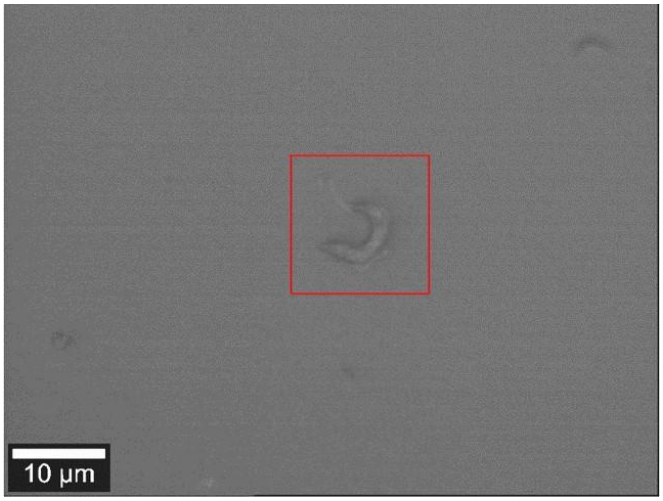

Figure 3.11 White light image of T.b. gambiense investigated with a 785 nm laser (100x).

The use of a near-IR laser wavelength allowed to understand and obtained the fingerprint from the *T.b. gambiense*, which could be used as a reference for future tissue studies.

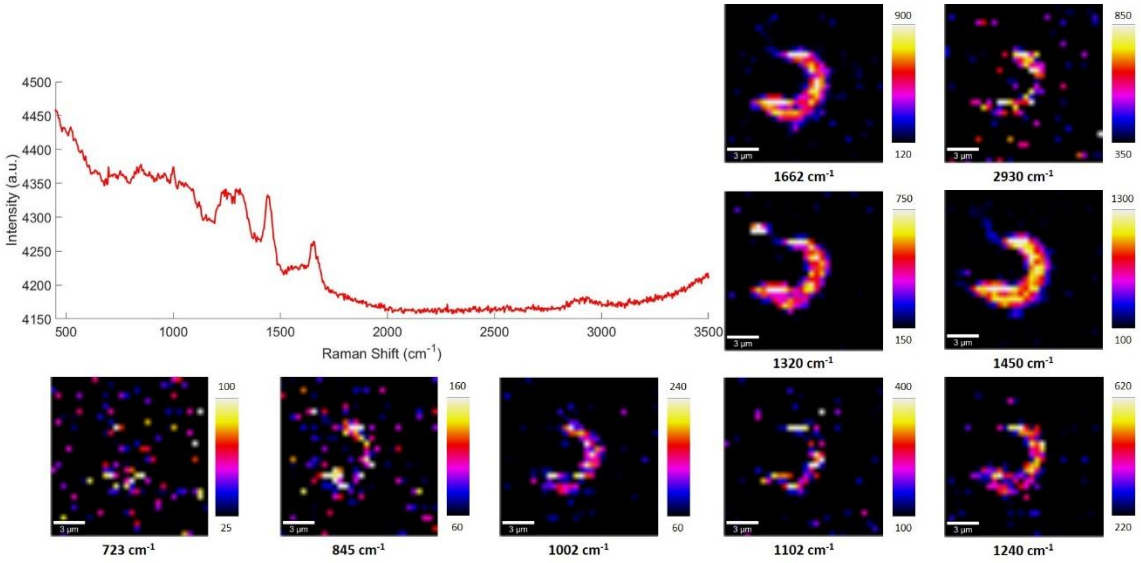

Figure 3.12 Raman intensity maps of T.b. gambiense measured with a 785 nm laser, 6 s acquisition time and 100x lens. Each image is associated with their respective intensity bar, which assign a colour gradient from the lowest to the highest intensity, with black showing the lowest intensity and white being the highest intensity.

Figure 3.12 regrouped the different Raman intensity maps produced with the mapping experiment of *T.b. gambiense* with a 785 nm laser. Each of the Raman bands observed defines

the VSG structure and conformation as it was studied previously with *T.b. brucei*. The C-H stretch vibrations, that was often observed in proteins and peptides, was found at 2930 cm^{-1} (Table 3.7). The CH_2 bending mode and CH_2CH_3 wagging mode at 1450 and 1320 cm^{-1} were also linked to protein structure. The amide III and amide I vibration mode at 1240 and 1662 cm^{-1}, respectively, were identified and could relate to the 3D conformation of the VSG on the surface as β-sheet.[237,238] The Raman peak at 1102 cm^{-1}, which was associated with the PO_2^- stretch, was suggesting that the detection of the GPI anchor and possibly the phospholipids present in the membrane all across the parasites was achieved. The presence of DNA could also be assigned to the Raman peak at 1102 cm^{-1}, combined with the Raman bands at 1320 cm^{-1}.

Table 3.7 Tentative assignment of Raman bands for the T.b. gambiense obtained with 785 nm laser.[231–233]

Raman Shift (cm^{-1})	Tentative assignments of Raman peaks
2930	C-H stretch
1662	Amide I
1450	CH_2 bending mode
1320	CH_2CH_3 wagging mode in proteins and DNA
1240	Amide III
1102	O-P-O backbone stretch of DNA
1002	Phenylalanine
845	C-O-C skeletal mode, polysaccharide
723	C – S protein

Another peak was observed at 845 cm^{-1} and has been identified as a C-O-C skeletal mode from polysaccharides. This was quite interesting as one of the specificity of the GPI anchor was that it possessed a side chain composed of galactose.[89] This could potentially be the assignment made for this Raman peak. This was showing that the specific sugar side chain of the GPI anchor could also be tracked through the mapping experiment. It could also be the identification of the N-linked oligosaccharides present on the sequence of certain VSG.[86]

The characterisation of *T.b. gambiense* gave the same vibrational information as found previously with *T.b. brucei*. However, some peak shifts are observed between the two studies. The C-H stretch was shifted from 2920 to 2930 cm^{-1} with *T.b. gambiense*. Other shifts could be identified at 1320 and 1240 cm^{-1}. Most importantly, there was a new Raman peak observed at 845 cm^{-1} that could be assigned to the presence of the galactose side chain of the GPI anchor. This was not observed previously in *T.b. brucei*, suggesting that there was potentially a structural and sequential differences between the two sub-species that could be differentiated by Raman spectroscopy or that this spectral difference originated from a different VSG sequence due to the constant change of the surface composition.

Overall, the information obtained for the two sub-species with two different excitation wavelengths gave an idea of the structural conformation of the VSG and other proteins around the surface. The GPI anchor and phospholipid residues were also tracked through the surface of the parasite with Raman spectroscopy. The Raman bands remained relatively close between each sub-species, suggesting that even if there was a difference in the amino acids sequence between the two sub-species, the structural conformation of the VSG remained identical, as observed by the work of Blum *et al*.[92] However, the presence of slight differences in the Raman bands at the C-H vibrations and the presence of a new peak associated with the galactose side chain of the GPI anchor or from the N-linked oligosaccharides of the VSG might suggested that the differentiation between the two sub-species or between certain type of VSGs was possible. Indeed, the Raman band at 845 cm^{-1} was not detected using a 532 nm laser, suggesting that a different VSG was present on the surface of the parasite within the *T.b. gambiense* sample. Hence, the spectral differences observed would be attributed to a variation of surface composition of the parasite and would not be specific to a sub-species. The Raman bands being different from the investigation of pure VSG, it was possible that Raman signal was also coming from other components from the parasites other than VSG, such as DNA structure, fatty acids, phospholipids or other protein specific to the trypanosomes (ISG or non-VSG proteins).[86,241–243]

Due to the mapping highlighting the VSG composition of only one parasite, it was important to validate this composition by carrying out a multi-parasite study of the consisting of parasites from the same sub-species. By applying statistical analysis methodologies to the data collected there was a possibility that it would be possible to differentiate between the two sub-species

T.b. brucei and *T.b. gambiense* with Raman spectroscopy. This would allow a positive identification for a type of infection during the diagnostic assay on the skin.

3.3.3 Spectral differentiation between *Trypanosoma brucei brucei* and *gambiense*

The detection of cellular components with Raman could potentially lead to the differentiation between *T.b* sub-species. This was particularly interesting as different treatments were provided depending on the infection with *T.b. gambiense* and *T.b. rhodesiense*.[51] Differentiating *T.b. brucei* and *T.b. gambiense* with the data collected recently, could open a new research approach for the detection of HAT (*T.b. gambiense* or *T.b. rhodesiense*) with Raman. If the invariant components could be detected by Raman, it would potentially allow the differentiation of the two different sub-species, which could be interesting for the diagnosis of the trypanosomiasis. Gadelha *et al.* investigated the proteins located on the flagellar pocket of the trypanosomes and provided an overview of the different surface proteins present across the surface. It was discovered that although the VSG coat is spread across the surface, other proteins are also present, and they are either localised or present themselves in different areas across the membrane.[246] Some of these proteins may be specific to sub-species of *T.b*. However, it was found that the *T.b* species shared a clear majority of these proteins, which could make it difficult to detect a specific signal from one of the sub-species.

Only one VSG gene could be expressed at a time for a single trypanosome, but it was shown that two VSGs could be located on the surface during the recycling.[100,102] Thus, it could potentially lead to some spectral variations across a single trypanosomes, if the information obtained was only coming from the VSG. Moreover, VSG could be changed during the cell culture *in vitro*, which could potentially lead to different signal from different parasites of the same sub-species. The aim of this work was to assess if the difference within the VSG amino acid sequence or other proteins surface composition was detectable by Raman, as observed previously, for multiple parasites of the same group and to identify a possible parasite component that would be specific to one sub-species, which could lead to a clear discrimination and identification of the sub-species involved in the infection.

The principal component analysis (PCA) could be the ideal tool to verify the different variation of signal within one sub-species, and ultimately assess if the two sub-species could be differentiated. This technique reduced the dimensionality of large data sets. By picking out key spectral components which influenced differentiation, the data analysis became simplified. By plotting the scores results against each other in rank of most variation to lesser variation, it could be used to distinguish between spectroscopically similar analytes. The loadings plot also helped to highlight the points within the spectra from which variation has occurred.

Five parasites were mapped, as described previously, for each sub-species, and their respective Raman spectra were analysed with PCA to investigate the possible spectral variations occurring within a sub-species. It was important to first assess if the Raman information obtained from the trypanosomes could vary between cells of the same sub-species.

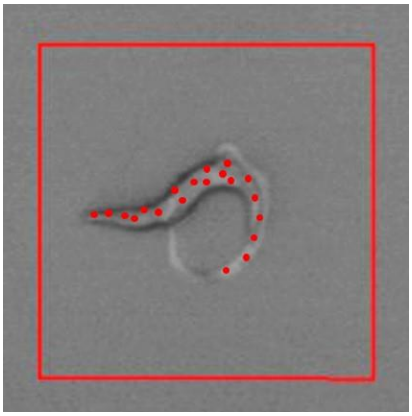

Figure 3.13 White light image (100x) of T.b. brucei mapped within the red square and 20 measurement points (red dots) from this map are taken randomly across the parasite.

An example of the procedure was shown in Figure 3.13, where the parasite was mapped within the red square. Then, twenty measurement points were taken randomly across the parasites from the mapping data set, as shown above. Prior to PCA being carried out the data set was pre-processed. Cosmic rays were first removed. Then data were smoothed using a Savitzky-Golay filter in order to reduce noise interference. Each spectrum was then baseline corrected, and finally the data were normalised to the highest intensity peak and then analysed using PCA.

The resulted PCA plots, for both lasers excitation, for *T.b. brucei* and *T.b. gambiense* were displayed in Appendix 1 and 2, respectively. Results showed that there was no differentiation between parasites of the same sub-species, for both laser excitation, suggesting that the Raman signal obtained from trypanosomes was similar from one parasite to another within the same group. Even if the VSG composition have changed between parasites, its differentiation was not clearly observed by PCA. However, it seemed that across a single parasite, the signal was varying, as multiple data points from single parasite were not grouped. In both *T.b. brucei* and *T.b. gambiense* investigations, the molecular vibrations from the extracellular or intracellular part seemed to indicate a change of composition and conformation across a single parasite. As the spectral information seemed to be identical between cells of the same sub-species, it was interesting to investigate the possibility of differentiating a *T.b. brucei* from a *T.b. gambiense*.

From these findings, where trypanosomes from the same sub-species did not seem to spectrally differ, a Raman fingerprint for each sub-species was produced. Four parasites were mapped, as explained previously, from each of *T.b. brucei* and *T.b. gambiense* sub-species and were averaged into a single Raman spectrum and normalised to the highest peak intensity, providing a fingerprint spectrally representing both sub-species. Then, both spectra were directly compared in order to assess their spectral differences.

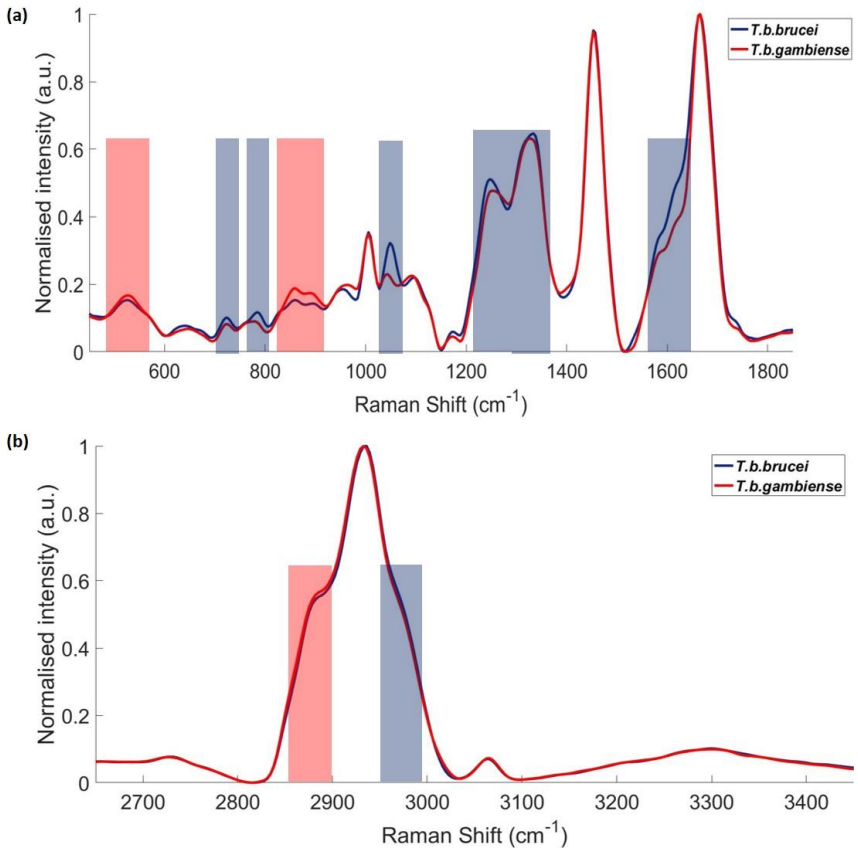

Figure 3.14 Normalised single average Raman spectrum for T.b. brucei (blue), and T.b. gambiense (red) comparing spectral window 450 – 1850 cm^{-1} (a) and spectral window 2650 – 3500 cm^{-1} (b),measured with a 532 nm laser. Blue rectangles highlight the area where the difference is specific to T.b. brucei and red rectangle highlights the area specific to T.b. gambiense.

Both spectral window comparison of the Raman fingerprint between *T.b. gambiense* (red line) and *T.b. brucei* (blue line) were shown in Figure 3.14. The main spectral differences specific to each sub-species were highlighted in blue boxes (*T.b. brucei*) and red boxes (*T.b. gambiense*). It appeared that some spectral variations are clearly observed between the two sub-species. Indeed, a slight spectral variation was noticed in the C-H stretch Raman peak (Figure 3.14.b)). There was a slight increase of the shoulder of the peak in the region 2875 – 2900 cm^{-1} that was specific for *T.b. gambiense*, whereas an intensity increase was observed in the area 2960 – 2980 cm^{-1} for *T.b. brucei*. This was the result of a small shift or variation of intensity in the C-H stretch Raman peak between the two spectra, where it was localised at 2933 cm^{-1} for the *T.b. gambiense* and at 2936 cm^{-1} for *T.b. brucei*, thus, suggesting a different conformation or packing of the different proteins present such as VSG or lipids. This difference in the composition or the

structure of surface proteins seemed to be identified by Raman and could indicate a spectral discrimination between the two sub-species.

In the low wavenumbers region, certain Raman bands were found to be specific to one sub-species, as their intensity differed. A difference in the conformation of the VSG could be observed in their cysteine or disulphide bridge residues that appeared to differ, due to a change of intensity in certain Raman bands at 673 cm^{-1} (C-S stretching mode of cystine), 722 cm^{-1} (C-S (proteins)) specific to *T.b. brucei* and at 529 (phosphatidylserine or S-S disulphide stretch) for *T.b. gambiense*.[231,232] This variations between the disulphide bridge indicated a change in the conformation of surface proteins and possibly a different packing. The Raman bands found at 1247 cm^{-1} (Amide III) and 1334 cm^{-1} (CH_3CH_2 wagging mode),[231,232] specific to *T.b. brucei* were found to be more intense than for *T.b. gambiense* and tend to confirmed the variation in the composition and conformation of such proteins between the two sub-species. Moreover, a more pronounced peak shoulder was observed in the area at 1580 – 1630 cm^{-1} to be specific to *T.b. brucei*. This variation could be associated with an increase of Phenylalanine and Tyrosine present in the parasite, as it was observed previously for the characterisation of both sub-species for a double peaks at 1586 and 1619 cm^{-1}.[239] It could imply a different composition of proteins specific for each sub-species and is supported with more intense Raman bands at 632 cm^{-1} (C-C twisting mode phenylalanine) and 1048 cm^{-1} (C-C stretch proline, PO_4^{3-} symmetric stretching) specific to *T.b. brucei*, and at 859 (tyrosine or phosphate group) for *T.b. gambiense*,[231,232] suggesting a different concentration of certain amino acids in the surface proteins.

Finally, Raman bands associated with phosphate groups were also noticed at different intensity for each sub-species. It was possible that the DNA, as well as the GPI anchor and phospholipid composition of the membrane was tracked. This variation tend to show a different composition and arrangement of the phospholipids in the membrane of *T.b. brucei*, through Raman bands at 784 cm^{-1} (Phosphodiester, DNA) and 1048 cm^{-1} (C-C stretch proline, PO_4^{3-} symmetric stretching), and *T.b. gambiense*, with Raman bands more intense at 859 cm^{-1} (tyrosine or phosphate group) and 893 cm^{-1} (phosphodiester or C-C skeletal).

Overall, it appeared from the comparison between the fingerprint of *T.b. brucei* and *T.b. gambiense* collected with 532 nm laser that both sub-species are spectrally different. The variations in the composition and the arrangement of the biological components of each sub-

species could be detected by Raman, suggesting that a spectral discrimination between the two parasites was possible.

An identical method was employed on the data sets collected with 785 nm laser, where four parasites from each sub-species were mapped and their spectra were averaged into a single spectrum, normalised and compared to each other in order to directly visualise the effect of these spectral variations on their Raman fingerprint.

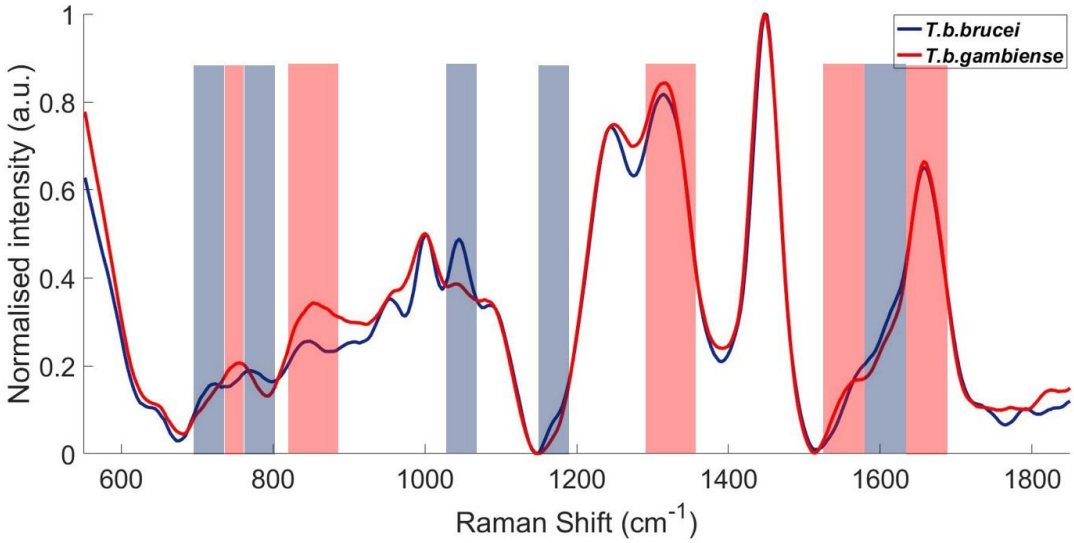

Figure 3.15 Normalised single average Raman spectrum for T.b. brucei (blue), and T.b. gambiense (red) measured with a 785 nm laser. Blue rectangles highlight the area where the difference is specific to T.b. brucei and red rectangle highlights the area specific to T.b. gambiense.

The spectral comparison of the two normalised average spectra from *T.b. brucei* and *T.b. gambiense* were represented in Figure 3.15. where spectral differences were highlighted in blue boxes (*T.b. brucei*) and red boxes (*T.b. gambiense*). As observed for 532 nm laser data, these variations occurred through a difference of intensity between Raman bands. It could be observed that the Raman bands specific to both sub-species were different from those obtained previously with 532 nm, however, they provided similar biological information. It appeared that the biological composition varied between the two spectra, where different amount of amino acids was detected. Raman bands located at 1045 cm^{-1} (C-C stretch proline, PO_4^{3-} stretch) and 1170 cm^{-1} (C-H plane tyrosine, proline) were found to be specific to *T.b. brucei*, when peaks at 755 cm^{-}

[1] (ring breathing tryptophan), 852 cm^{-1} (ring breathing tyrosine, C-C stretch proline ring) and 1560 cm^{-1} (tryptophan) were specific to *T.b. gambiense*.[231,232] In addition, a more pronounced shoulder in the region 1580 – 1630 cm^{-1} (phenylalanine and tyrosine),[239] at the base of the peak at 1657 cm^{-1}, was noticed to be specific to *T.b. brucei*, as observed previously with data collected with 532 nm laser. Similar amino acids such as proline or tyrosine seemed to be present in both parasites, the difference in the Raman bands may suggest a different orientation and arrangement within the proteins and could explain that different peaks were observed. However, the presence of tryptophan appeared to be specific to *T.b. gambiense*. This possible variation in the conformation was supported with the Raman bands at 1318 cm^{-1} and 1657 cm^{-1}, where a slight increase in intensity has been observed specific to *T.b. gambiense*. These Raman bands have been thought to be associated with CH_3CH_2 twisting mode or Amide III (α-helical conformation of proteins) and Amide I vibrations linked to a α-helical conformation of proteins, respectively,[231,232] confirming a conformation change of surface proteins between both sub-species.

Finally, two bands at 771 cm^{-1} (phosphatidylinositol) and 1045 cm^{-1} (C-C stretch proline, PO_4^{3-} stretch) were found to be increased in the *T.b. brucei* Raman fingerprint. There were thought to be associated with the GPI anchor of the VSG and the phospholipid residues from the parasite's membrane. It was possible that the composition of these phospholipids were different between the sub-species or that a less densely packed VSG on *T.b. brucei* allowed their detection, hence suggesting a different arrangement of surface proteins between the two parasites.

Despite the different vibrational information obtained with 785 nm laser compared to the ones observed in the measurements with 532 nm, the two sub-species can be spectrally differentiated. It appeared that a difference composition and conformation within the lipids and proteins of each sub-species is responsible for the discrimination. Such identification could be potentially useful in the diagnostic process in order to choose the appropriate treatment.

3.3.4 Conclusion

In this study, an *in vitro* characterisation of the biological components of two sub-species, *T.b. brucei* and *T.b. gambiense*, was performed with two different lasers. The investigation of a VSG

protein, which was the most represented around the surface of the trypanosomes, provided preliminary biological information and a Raman fingerprint that could be used for the analysis of trypanosomes. However, the preparation of this protein did not allow to keep its natural conformation, leading to different Raman vibrations compared to those obtained on the parasites.

Parasites were initially mapped to produce false colour images of significant Raman bands and various molecular vibrations were tracked across the surface of the parasites. The multiple vibrational information obtained from both sub-species were thought to be mainly coming from the VSG due to its high concentration around the surface of the parasite. Indeed, some indications of its conformation were measured such as its α-helical and β-sheets conformation, as well as its cysteine residues present across its structure, in accordance with previous investigations of this protein. In addition to the VSG, other biological components, such as GPI anchor, phospholipid residues or DNA, were being detected and tracked across the surface of the parasites. Despite the high amount of VSG present on the surface of the parasites, it was still possible to measure other components.

As the recycling and change of VSG protein around the surface is a stochastic event, it was more likely that during the culture of *T.b. brucei* and *T.b. gambiense*, the surface composition had changed. However, it was observed that there was no discrimination between parasites within the same sub-species. Thus, suggesting that the possible change of composition in the VSG was not detected by Raman.

Finally, Raman fingerprints for each sub-species were produced and compared in order to determine if the discrimination of the sub-species could be performed with Raman, which would be a great advantage in the detection of sleeping sickness. It was noticed that the two sub-species were spectrally different, where a different composition of their surface component was detected with a different amount of amino acids and could suggest the presence of different proteins between *T.b. brucei* and *T.b. gambiense*. Furthermore, it was also possible that a different conformation and orientation of surface proteins was measured and could help the discrimination of the two sub-species.

The different investigations performed in this study were critical prior analysis infected skin with *T.b. brucei* as it allowed to obtained Raman fingerprint of the parasites involved in the infection and could be used to detect the parasites in a mouse skin infected.

3.4 Skin investigation: *ex vivo* analysis

Parasites were characterised *in vitro* by Raman spectroscopy and showed strong biological information when they were analysed using either a 532 nm or 785 nm laser. The following study explores the possible application of Raman as a bio-diagnostic tool. By taking advantage of the presence of trypanosomes in the skin, Raman would overcome the limitations of the current blood detection method and provide a non-invasive diagnostic tool.

For this study, mice were infected with *T.b. brucei* and later their skin was removed and embedded in paraffin for preservation. This *ex vivo* pilot study would give preliminary information on whether Raman would be a viable technique for the detection of sleeping sickness in the skin. It provides important spectral and biological information that could help in developing a diagnostic method for sleeping sickness with Raman, as well as understanding the biological impact that the parasites have on the skin. The aim was to assess whether the infection of mice by *T.b. brucei* affected the skin composition by comparing infected and uninfected samples, and if these changes could be detected by Raman. The discrimination between infected and uninfected skin provided insight into how the skin biological composition was affected by the infection and whether this variation could be attributed to the metabolic processes resulting from the trypanosomes in the skin or to a direct contribution from the parasites to the Raman signal. A comparison between the Raman bands, associated with their tentative assignment, obtained gave information on the molecular differences observed in the samples. Finally, using the Raman fingerprint of *T.b. brucei* obtained during the *in vitro* experiment it was possible to assess if the parasites themselves were contributing to the Raman signal, hence making this technique more specific to sleeping sickness.

3.4.1 Sample preparation: Paraffin spectral interference and removal

Glass slides could not be used as a substrate for this study as they confer a spectral background when illuminated with a 532 nm or 785 nm laser, which could interfere with the biological Raman signal. Raman grade CaF_2 was found to the most efficient substrate compared to IR polished CaF_2, magnesium fluoride or potassium bromide.[247] CaF_2 does not display any spectral background or fluorescence.

Tissue samples were prepared and fixed using formalin, then embedded in paraffin (FFPE). This allows the tissue to be chemically suspended in one state and also preserves the samples for long periods of time.[172] This method of conservation is used worldwide for clinical sample preservation. However, the method has a few limitations when being used in tandem with a Raman instrument. Fixation using formalin can affect the chemical composition of the tissue, causing the lipids present in the sample to become cross-linked.[248] Potentially this could affect the Raman signal, which requires effective interpretation of the lipid residue signal. The presence of paraffin is also inconvenient because it gives a strong Raman signal that overlaps with the signal from the tissue sample.[172]

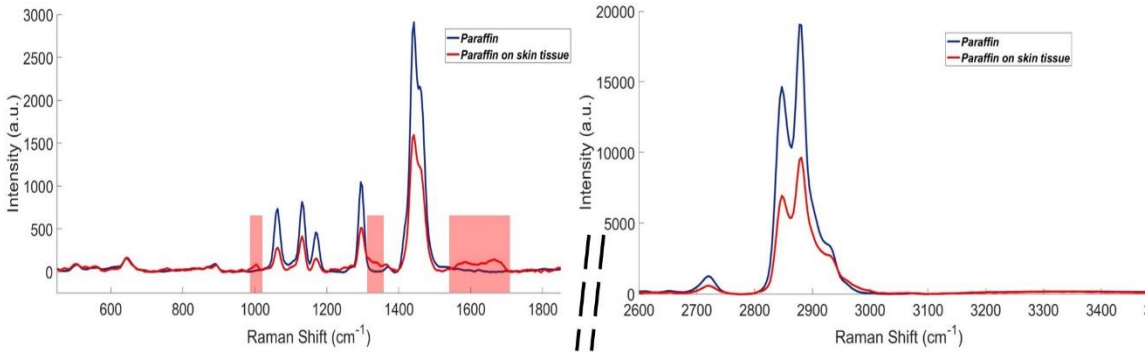

Figure 3.16 Spectrum of paraffin from sample preparation measured with 532 nm laser with 1 s acquisition time on the slides (blue) and on the tissue (red). Raman skin tissue signal is highlighted with red boxes.

An example of the interference from the paraffin is shown in Figure 3.16 where two spectra collected from the skin samples are displayed. The Raman signal from the paraffin is very intense and provides very sharp peaks. Those intense peaks are located at 1063 and 1131 cm^{-1} (C-C

skeletal), 1173 cm^{-1} (C-H bend), 1294 cm^{-1} (CH_2 deformation), 1442 and 1462 cm^{-1} (CH_2 bending mode), 2721 cm^{-1} (C-H stretch), 2847 cm^{-1} (CH_2 symmetric stretch) and 2881 cm^{-1} (CH_2 asymmetric stretch).[231,249] These Raman bands are similar to those reported in the literature.[172,249] Although, some Raman bands from the skin could be observed through the paraffin signal (highlighted by the red regions), it is easily observed that the paraffin peaks were so intense that they masked the skin signal, and they could potentially overlap with the biological sample. Hence, prior to Raman analysis of the sample, the paraffin was removed.

A chemical removal methodology was employed to remove the paraffin from the skin sample.[250] Incubation of the tissue, previously attached to the substrate, with xylene was used to remove the paraffin. Sequential washes with ethanol and water were then performed to remove residual xylene that could affect the Raman signal.[172]

3.4.2 Discrimination of *T.b. brucei* infected skin compared to uninfected with PCA

Spectral differences between infected and uninfected skin were investigated to assess if the detection of sleeping sickness with Raman spectroscopy was possible.

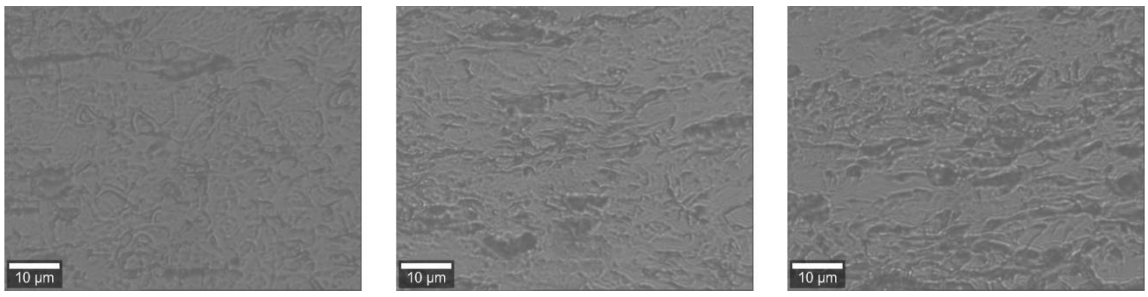

Figure 3.17 White light image of T.b. brucei infected mouse skin with a 100x lens.

Samples were then placed on a CaF_2 slides and the paraffin was chemically removed using xylene (Figure 3.17), before Raman analysis. Each of the infected and uninfected skin samples were mapped, using a 50 x 50 µm area and a 2 µm step size, for a total of 625 spectra, and with an acquisition time of 1 s for 532 nm and 3 s for 785 nm.

All maps were then analysed using PCA in order to identify a difference between infected and uninfected samples. However, skin is a complex biological matrix with varying composition across its surface. Therefore, a potential difference between two maps could not only come from the infection, but also from different biological composition within the skin area. This could lead to a misinterpretation of the data. So, each infected and uninfected skin sample was mapped multiple times to obtain general information on the composition of the skins surface. Each map was then averaged into a single spectrum, in attempt to observe a general trend in the change of composition only specific from the infection without being affected by the different area within the skin. All spectra were normalised to the highest peak intensity prior to analysing them using PCA.

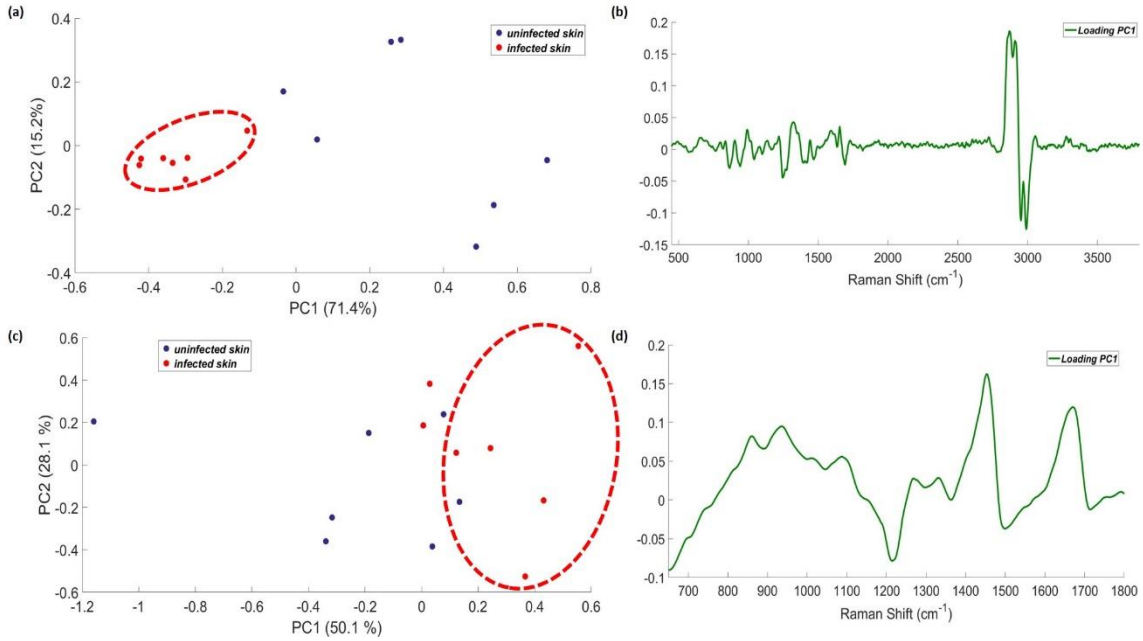

Figure 3.18 Principal component analysis of the averaged and normalised spectra of T.b. brucei infected (red dots) and uninfected mouse skin (blue dots) samples, measured with a 532 nm laser. (a) Scores plot of PC1 versus PC2 (infected data points were circled for clarity), (b) PC1 loading spectrum, and 785 nm laser (c) scores plot of PC1 versus PC2, (d) PC1 loading spectrum.

Seven averaged maps from each of the skin samples were analysed using PCA. The spectral window of the data collected with 785 nm was reduced to 650 – 1800 cm^{-1} because no spectral

information was obtained in the high wavenumber region. It appeared that the analysis with both wavelengths could spectrally differentiate the infected from uninfected skin.

Figure 3.18.a) shows the resulting scores plot of PC1 versus PC2 for 532 nm laser and it can be observed that infected samples (red dots) formed a cluster and were well discriminated from the uninfected group (blue dots). The fact that the data points were well grouped together indicated that the biological changes resulting from the infection were continuously present across the skin. Data points from the uninfected skin were dispersed across PC2, indicating a map to map variations possibly due to different biological composition across the skin. The discrimination between infected and uninfected samples was not affected by this variation.

The loading spectrum of PC1 in Figure 3.18.b) indicated that the main Raman bands explaining the spectral discrimination of data collected with 532 nm laser, were 2953 and 2989 cm^{-1}, which represent the C-H stretch. It can therefore be hypothesised that the parasites within the system appeared to alter the C-H vibrations. It was explained previously that the fixation and the chemical dewaxing can affect the lipid residues that were also identified in this wavenumber region. However, the modification should be constant between infected and uninfected as the protocol used was the same. Hence, this change in the Raman bands at this position can only be because of parasites present in the skin. It is not the result of the Raman identification of the fingerprint of *T.b. brucei* obtained during *in vitro* study as it gave Raman bands at 2876 and 2934 cm^{-1}. This change is the consequence of a change in composition within the skin because of the infection. It was described that *T.b. brucei* is able to use the surrounding matrix of the skin, such as fatty acids and lipids, as an energy source to synthesise its lipid composition.[154,243] It is possible that this disruption within the lipid and protein composition of the skin is seen via the shift of the Raman peak in the C-H region. This is emphasised with the contribution of the Raman bands at 942 cm^{-1} (C-C stretch backbone proline), 1248 cm^{-1} (Amide III), 1273 cm^{-1} (Amide III α-helix), 1392 cm^{-1} (C-N stretching), 1421 cm^{-1} (CH_2 bending mode of proteins and lipids), 1470 cm^{-1} (C=N stretching) and 1694 cm^{-1} (Amide I),[231–233] which suggests an alteration of the protein/lipid composition and arrangement in the skin due to the presence of the parasites. In addition, Raman bands at 575 cm^{-1} (Phosphatidylinositol), 864 cm^{-1} (phosphate group or tyrosine, proline) and 1041 cm^{-1} (C-C stretch proline, PO_4^{3-} stretch),[231,232] also agree with a variation in the phospholipid or DNA composition in the skin due to the phosphate group vibrations. However,

these assignments could also be attributed to the phospholipid components and the GPI anchor of the VSG from the surface of the trypanosomes,[89,240,241] hence measuring a direct spectral contribution from *T.b. brucei* in the differentiation of infected skin. It suggests that the spectral differentiation of the infection was potentially the result of a combined contribution from the parasites as well as the changes induced in the skin by the metabolism of the parasites.

Differently, scores plot of PC1 versus PC2 of the 785 nm data (Figure 3.18.c)) also showed a differentiation between uninfected skin group (blue dots) and infected group (red dots). This separation was not as clear as for the data collected with 532 nm as some data points from each group were mixed. However, data sets from the uninfected group were more spread out, suggesting a similar map to map spectral variation as observed previously. The spectral information specific to the infected group (Figure 3.18.d)) demonstrated similar biological modification, as for the analysis with 532 nm, about the variation of lipid/protein composition and arrangement with Raman bands found at 937 cm^{-1} (C-C stretch proline and protein backbone (α-helix)), 1012 cm^{-1} (tryptophan), 1087 cm^{-1} (C-C stretch lipids, PO_2^- stretch), 1269 cm^{-1} (Amide III, α-helix), 1333 cm^{-1} (CH_3CH_2 wagging mode in proteins), 1455 cm^{-1} (CH_2CH_3 deformation) and 1672 cm^{-1} (Amide I).[231,232] Similarly, the potential direct contribution from the surface of the parasites or from the alteration of phospholipid or DNA composition in the skin could be identified with the Raman bands at 860 cm^{-1} (phosphate group or tyrosine) and 1087 cm^{-1} (C-C stretch lipids, PO_2^- stretch).[231,232] Furthermore, for both lasers' analysis seemed to indicate an increased presence of certain amino acids such as proline, tyrosine and tryptophan in the infected skin.

It must be mentioned that the signal to noise ratio and the sensitivity of the CCD were very low when using the 785 nm laser compared to the 532 nm instrumentation. This instrumental limitation led to the use of a more comprehensive pre-processing protocol and may have affected the resolution of the Raman bands obtained from the skin, hence altering the biological information detected. The extensive processing that has been carried out on the data made it particularly difficult to interpret the biological variations and to draw any solid conclusions, as the quality of data collected using 785 nm was poor. This difference in biological information and signal resolution obtained between 532 and 785 nm lasers could be observed with the loading spectra of PC1 for both wavelengths. While Figure 3.18.b) displayed multiple Raman bands,

through a shift or an increase in intensity, to explain the discrimination of the data collected with 532 nm, Figure 3.18.d) showed that an increase in intensity of Raman bands, which were broader and less resolved, was specific to the infected skin group in the differentiation.

Despite the instrumental limitations experienced for the analysis with 785 nm, it was observed that both lasers used for this investigation were able to discriminate infected from uninfected skin. This finding was promising as it implied that Raman could be used for the detection of sleeping sickness by targeting the skin of an infected host. Biological information obtained from the statistical analysis suggested that the presence of the parasites affected the conformation and composition of the skin matrix. *T.b. brucei* seemed to metabolise its surrounding matrix, such as lipids or proteins, in order to proliferate, and this alteration was detected by Raman. Some Raman bands related to phosphate groups and phosphatidylinositol were suspected to be associated with a direct contribution from the parasites in the Raman signal. The detection of the infection by Raman being a success, it was also important to investigate and understand the origins of these biological variations.

3.4.3 Investigation of the biological variation induced by *T.b. brucei* in the skin during infection

Statistical analysis gave a clear differentiation between infected and uninfected skin and outlined the spectral differences involved. It allowed an overview of the biological implications in the skin due to the presence of *T.b. brucei*. Each map run previously for each group were averaged into a single Raman spectrum, specific to infected and uninfected skin, and normalised. This unique Raman spectrum for infected and uninfected provided a fingerprint for each state of the skin. Their spectral comparison gave a more general representation and understanding of the biological variations occurring across a larger section of the skin.

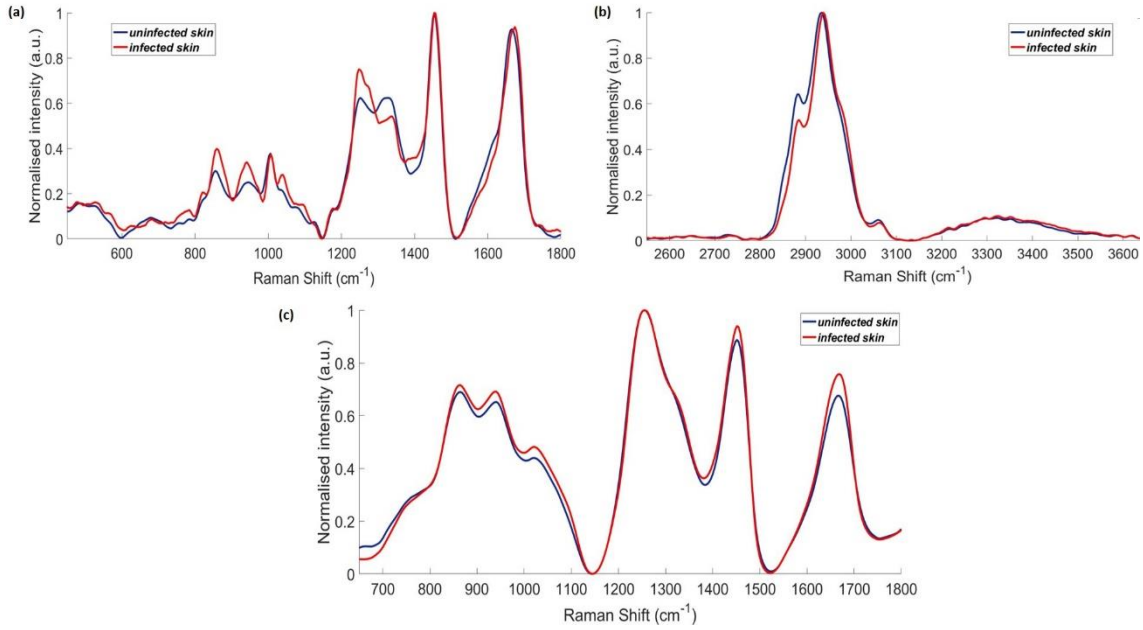

Figure 3.19 Normalised Raman fingerprint from uninfected (blue line) and infected (red line) mouse skin, measured with a 532 nm laser, showing the spectral window 500 - 1800 cm^{-1} (a), and 2550 - 3700 cm^{-1} (b), and measured with 785 nm laser (c) spectral window 650 – 1800 cm^{-1}.

Figure 3.19 displayed the spectral comparison of the Raman fingerprint of infected and uninfected skin obtained with 532 and 785 nm laser. The spectral window of the Raman spectra collected with 532 nm were split between 550 – 1800 cm^{-1} (Figure 3.19.a)) and 2550 – 3700 cm^{-1} (Figure 3.19.b)) and averaged separately for better visualisation of the spectral differences between infected and uninfected skin. It is observed in Figure 3.19.a) and c) that the spectral differences resulted from an increase in intensity of certain Raman bands specific to the infection, whereas in Figure 3.19.b), an increase in intensity was also observed, but a shift in the Raman peak of the C-H stretch was noticed between the two spectra. Thus, the discrimination between infected and uninfected skin was confirmed, and a variation in the level of certain biological components as well as in their composition was suggested.

An increase in intensity specific for the infection was observed for the Raman bands at 785 cm^{-1} (backbone O-P-O), 820 cm^{-1} (PO_2^- stretch (DNA)) 859 cm^{-1} (phosphate group, tyrosine), and 1041 cm^{-1} (C-C stretch proline, PO_4^{3-} stretch) and 1096 cm^{-1} (PO_2^- stretch) in Figure 3.19.a) as well as in Figure 3.19.c) for the data collected with 785 nm laser with a Raman bands at 864 cm^{-1} (phosphate group, tyrosine) and 1087 cm^{-1} (C-C stretch lipids, PO_2^- stretch).[231–233] This increase in intensity for phosphate group vibrations, observed at both wavelengths, could suggest an

increased presence of DNA within the skin, or a variation in the level of phospholipids present in the skin due to the influence of *T.b. brucei*.

Interestingly, further evidence for an alteration of the lipid composition was provided by this spectral comparison of the Raman fingerprint. Data collected with 532 nm in the high wavenumber region (Figure 3.19.b)) showed a shift in the Raman band for the C-H stretch from 2936 cm^{-1} (uninfected skin) to 2939 cm^{-1} (infected skin), suggesting a change in the lipid/protein composition and conformation in the skin. This shift observed could also be the result of a variation of intensity with peaks present in this region. It was supported with the increase in intensity of Raman bands at 942 cm^{-1} (C-C backbone, proline) 1248 cm^{-1} (Amide III) and its shoulder at 1273 cm^{-1} (Amide III α-helix) and a decrease in intensity of the Raman peak at 1339 cm^{-1} (CH_2CH_3 wagging mode in collagen) observed in Figure 3.19.a).[231–233] Additionally, data collected with 785 nm laser (Figure 3.19.c)) demonstrated an increase in intensity that similarly explained an alteration of lipid/protein levels in the skin, associated with the Raman bands at 937 cm^{-1} (C-C stretch proline and protein backbone (α-helix)), 1020 cm^{-1} (C-C stretching), 1333 cm^{-1} (CH_3CH_2 wagging mode in collagen), 1451 cm^{-1} (CH_2CH_3 deformation) and 1668 cm^{-1} (Amide I).[231–233] Previous studies have described how bloodstream *T.b. brucei* uses glucose as its main energy source,[251,252] but are also capable of using lipids such as low density lipoproteins (LDL) and high density lipoproteins (HDL).[253,254] Lately, Trindade *et al.* showed that adipose tissue form of *T.b. brucei* changed their main carbon source to lipids and fatty acids.[154] It was possible that the presence of *T.b. brucei* in the skin resulted in an up-regulation of the release of lipids and fatty acids from adipocytes to support their proliferation. Such an increase of lipid concentration in the skin was then detected by Raman through the increase in intensity of certain Raman bands, which were specific to the infection.

Moreover, this up-regulation of lipids in the skin was further supported by the presence of a new Raman peak, very close to 1666 cm^{-1} (Amide I), at 1674 cm^{-1} in Figure 3.19.a), which was thought to be associated with a specific lipid: cholesterol.[255] At a lesser extent, it could also be observed that the Raman band at 530 cm^{-1} was slightly increased compared to the uninfected skin spectrum (Figure 3.19.a)), and could be associated with cholesterol ester as a Raman band was found at 538 cm^{-1} in cholesterol ester spectrum.[255] Cholesterol is a lipid transported by LDL and HDL to the cells and to the liver, respectively.[256] The cholesterol attached to the LDL is taken up

by the parasite and allows membrane synthesis and multiplication. It was previously shown that the concentration of cholesterol, LDL and HDL was decreased in the serum of animals infected with *T.b. brucei*.[257,258] Adipose tissue form *T.b. brucei* may have induced an up-regulation of the release of lipids and lipoproteins in the skin for their proliferation, which resulted in an increase in intensity of Raman bands associated with lipids and particularly cholesterol. Interestingly, similar findings about cholesterol were obtained in mice infected with *Trypanosoma cruzi* (*T. cruzi*), which leads to the parasite disease called Chagas disease in South America. It was found that during the infection of mice by *T. cruzi*, the cholesterol level increased in the heart, pancreas and mostly in white adipose tissue.[259] Even if both parasites possess a different life cycle and mechanism of infection, it is possible that the infection by *T.b. brucei* could also lead to an increased level of lipids such as cholesterol in the skin. It would be interesting to specifically measure their concentration in the skin to confirm the results obtained with Raman spectroscopy. This increase of cholesterol could also be associated with a direct detection of the trypanosomes in the skin as described previously with the phosphate that could be related with the GPI anchor and phospholipid residues from the membrane surface. Indeed, it was previously observed that the flagellar part of *T.b. brucei* was mainly composed of cholesterol, and that it could be tracked all across the parasite after being uptaken.[260,261] The amount of cholesterol may have increased within the membrane across the parasites, as they are located in a rich lipid environment. However, the metabolism and influence of the adipose form trypanosomes in the skin are still unknown as they have been discovered recently.

This Raman peak at 1674 cm^{-1} could also be associated with an Amide I vibration, suggesting a different conformation in protein composition in the skin. Similarly, it appeared that the presence of the parasites in the skin also altered certain amino acids. The infected spectrum collected with 785 nm laser (Figure 3.19.c)) displayed a slight decrease in intensity for the Raman band at 755 cm^{-1} that was thought to be associated with tryptophan.[231,232] Moreover, the shoulder between 1580 – 1630 cm^{-1} of the Raman peak at 1666 cm^{-1} was less pronounced in the infected skin than in the control spectrum obtained with 532 nm laser (Figure 3.19.a)). It was previously thought that these two small Raman bands located at the base of the Raman peak at 1666 cm^{-1} could be associated with phenylalanine and tyrosine,[239] and would suggest a decrease of their concentration in the skin. This alteration in amino acid suggested that protein

composition and conformation have varied during the infection, thus establishing that the trypanosomes were affecting the skin composition through their metabolism or that the infection led to a rearrangement in the skin matrix.

However, these amino acids may have been detected individually and not as part as proteins. Indeed, previous studies in the serum of infected animals showed that *T.b. brucei* was able to catabolise these three amino acids leading to a decrease of concentration of such amino acids.[262–264] It is supposed that this metabolic process is detected by Raman, due to the decrease in intensity of Raman bands associated with tryptophan, phenylalanine and tyrosine. Similarly, certain Raman bands, thought to be associated with proline showed an increase in intensity, suggesting a higher concentration of proline in the infected skin. Such alteration of proline concentration in serum has been demonstrated previously.[262] Furthermore, this variation observed spectrally for these amino acids could result of the interaction of *T.b. brucei* with the surrounding skin matrix, which has led to a change of composition and conformation due to their presence.

Finally, the spectral discrimination of infected from uninfected skin appeared to be the result of both the interaction of the parasites with the skin environment *via* its metabolism as well as its surface membrane components being detected by Raman and explained the differentiation of the infected skin. Data collected with 532 and 785 nm lasers seemed to provide similar information on the biological variations induced by the parasites. Certain Raman bands appeared to be similar between both wavelengths such as 1254 cm^{-1} (for 785 nm laser) and 1248 and 1273 cm^{-1} (for 532 nm laser). Only a single peak was obtained at this region with the near-IR laser because of the low spectral resolution given by the instrument and these two Raman bands observed at the same region with 532 nm laser could not have been separated, as previously observed with PCA loadings. Biological modifications were easily detected and the tentative assignment of Raman bands specific to the infection provided a good understanding of the influence of the parasites on the skin. The alteration of the lipid and protein composition of the skin observed with the increase in intensity of related Raman bands was in agreement with previous finding on the mechanism of adipose tissue form *T.b. brucei*. Moreover, it was suspected that the surface membrane of the parasites also contributed to the Raman signal through the phosphate and cholesterol vibrations.

3.4.4 Investigation of the spectral similarities between Raman fingerprint of *T.b. brucei* and infected-uninfected skin samples

Infection of the skin by *T.b. brucei* was detected and differentiated from uninfected skin by Raman. The spectral differences and the tentative assignment of specific Raman bands provided a good comprehension of the influence that the parasites had on the skin matrix. Some Raman bands were suspected to be related to the surface membrane of the trypanosomes. Comparing the Raman fingerprint of *T.b. brucei* with skin samples (infected and uninfected) could help determining the spectral contribution of the parasites in the Raman signal specific to the infection.

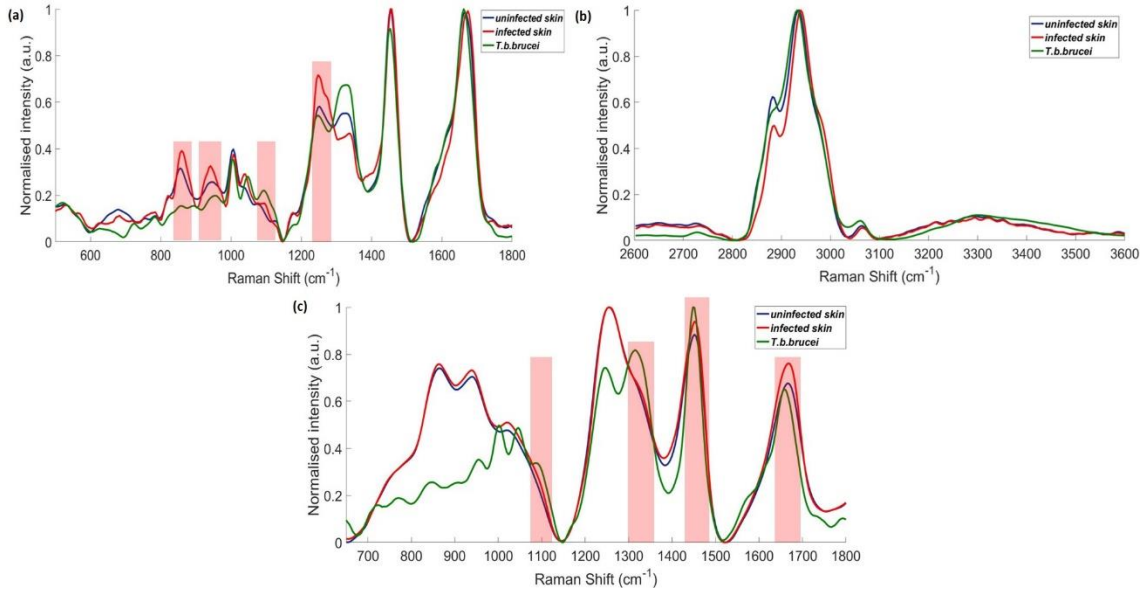

Figure 3.20 Comparison of Raman fingerprint of T.b. brucei (green line), infected mouse skin (red line) and uninfected mouse skin (blue line) obtained with 532 nm: spectral window 500 – 1800 cm^{-1} (a) and spectral window 2600 – 3600 cm^{-1} (b), and with 785 nm laser spectral window 650 – 1800 cm^{-1} (b). Suspected contribution of T.b. brucei Raman signal in the infected skin spectrum are highlighted with red boxes.

Figure 3.20 shows the comparison between the Raman fingerprint of *T.b. brucei* with skin samples collected with 532 and 785 nm. The spectral window for the data collected with 532 nm was split into two different regions, 500 – 1800 cm^{-1} (Figure 3.20.a)) and 2600 – 3600 cm^{-1} (Figure 3.20.b)), and averaged separately in order to clearly observed the spectral similarities between

T.b. brucei and infected skin Raman fingerprints. The *T.b. brucei* Raman spectrum was collected for both laser using a 6 s acquisition time whereas the skin samples were measured with 1 s for 532 nm laser and 3 s for 785 nm laser, which could make the estimation of the contribution of *T.b. brucei* to the Raman signal of infected skin difficult but the relative intensities should be unaffected. Their qualitative comparison would provide an idea of their possible contribution. It was observed that some Raman bands specific to the infected skin signal were related and influenced by the direct detection of the parasites in the skin, which are highlighted with red boxes in Figure 3.20.

Raman fingerprints collected with 532 nm were displayed in Figure 3.20.a) and four Raman bands from infected skin were suspected to be related to *T.b. brucei*. The peaks at 859 cm^{-1} (phosphate group, tyrosine) and 1096 cm^{-1} have been related previously to phosphate groups in the infected skin Raman spectrum.[231,232] This band showed an increase in intensity compared to the healthy skin, and was similar to the one obtained in the fingerprint of *T.b. brucei*. It is possible that it is related to the phospholipids present on the surface of the trypanosomes,[240,241] and due to the presence of *T.b. brucei* in the skin, the intensity of these two Raman bands increased in the infected Raman spectrum. Moreover, Raman bands at 942 cm^{-1} (C-C skeletal, proline) and 1248 cm^{-1} (Amide III), as well as previously reported 859 cm^{-1} for tyrosine, were also similar to the fingerprint of *T.b. brucei*.[231–233] They could be related to the VSG proteins located around the surface of the trypanosomes. There was no correlation observed in Figure 3.20.b), for the high wavenumbers, as the shift of the C-H stretch Raman peak between infected and uninfected skin did not seem to be related with the Raman peak observed for *T.b. brucei*.

Figure 3.20.c) illustrated the comparison of the fingerprint of *T.b. brucei* and both skin samples collected with 785 nm laser and displays a Raman peak at 1087 cm^{-1} that was thought to be associated with C-C stretch of lipids or phosphate groups.[231,232] It could be observed that the intensity was slightly increased compared to the healthy skin and was similar to a Raman band from *T.b. brucei*. As mentioned for the data collected with 532 nm, it could also be linked to the GPI anchor and phospholipid residues from the membrane of the trypanosomes. Similarly, the contribution of the surface protein of the parasites such as VSG could be related to the Raman bands at 1333 cm^{-1} (CH_3CH_2 wagging mode), 1451 cm^{-1} (CH_2CH_3 deformation) and 1668 cm^{-1} (Amide I), as they showed an increase in intensity in the infected skin.[231–233]

It appeared that some Raman bands had similarities with the fingerprint of *T.b. brucei* for both laser measurements, as they have shown to have an increase in intensity in the infected skin Raman fingerprint and could be related directly to the presence of the trypanosomes. However, there was a significant spectral overlap between the skin spectra (uninfected and infected) with the spectrum of *T.b. brucei*. Hence, it was unclear whether the surface proteins of the parasites were contributing to the Raman signal obtained in the infected skin. Moreover, the Raman fingerprint of *T.b. brucei* was obtained *in vitro* from a bloodstream form. It was possible that, by adapting its metabolism to the skin environment, the surface composition of the parasite (adipose form) has changed. Therefore, it was plausible that the Raman signal from *T.b. brucei* may have changed during the infection of the mouse.

3.4.5 Conclusion

Both mouse skin samples, uninfected and infected, were analysed with two different lasers after successfully removing the paraffin from the skin. Raman mapping allows the analysis of a small area of the skin, but multiple maps were performed across the sample in order to obtain a general view on the biological information of the skin. Skin is a complex matrix and is subject to high variability in its composition depending on the area investigated. This variation could alter the analysis. To avoid this interference, each map was averaged into a single spectrum and gave a general trend on the biological composition of a specific area. The infection was successfully detected spectrally by using PCA, which showed clear differentiation between infected and uninfected skin. It was then possible to detect the infection through multiple spectral variations between both skin samples, and individual Raman bands were tentatively assigned to molecular vibrations which could provide an understanding of the biological information obtained. However, instrumental limitations were observed for the laser 785 nm and a more comprehensive pre-processing of the data sets had to be performed. This technique then reduced the spectral resolution of the Raman spectra, hence limiting the amount of information collected as well as making it difficult to draw conclusions, compared to the use of a 532 nm laser.

Raman fingerprints were produced for uninfected and infected skin and were compared with each other to identify the biological variations induced by *T.b. brucei*. It was then detected that

the lipid/protein composition and conformation were disrupted by the presence of the infection through Raman bands that showed an increase in intensity specific to the infected skin. Moreover, increased intensity for phosphate group vibrations tend to demonstrate that phospholipids and DNA were present in a higher amount during the infection. The alteration of the skin matrix, mostly lipids and proteins, observed between the two samples was in accordance with the hypothesis that *T.b. brucei* was able to interact and metabolism the surrounding skin matrix for its proliferation. Furthermore, a Raman band was measured at 1674 cm^{-1}, for the data collected with 532 nm laser, was thought to be associated with cholesterol. Interestingly, it was previously demonstrated that bloodstream trypanosomes were able to use cholesterol for their growth, hence reducing its concentration in blood. It was hypothesised that the presence of *T.b. brucei* might increase the level of cholesterol in the skin, as it could have been observed in the infection with a different parasite, *T.cruzy*. An alteration of the level of amino acids such as proline, phenylalanine and tyrosine were also noted in the infected skin, suggesting a variation in the protein composition induced by the infection. However, the method employed to characterise the spectral comparison between infected and uninfected aimed to average multiple maps to obtain a single Raman spectrum in order to understand and observe a general trend in the biological variations across the skin. This method could induce some shift in the Raman bands that could be misinterpreted during the biological assignments. Although, it had indicated that the lipid/protein composition of the skin was affected by the presence of the parasites, the Raman band 1674 cm^{-1} was associated with cholesterol. This Raman band could have also been associated with Amide I vibration, measuring a different conformation of proteins in the skin, and averaging multiple maps may have induced this peak to shift from its original location, as the skin is a complex matrix and different area would provide a different Raman bands around this shift. Nevertheless, it was interesting to observe that cholesterol was possibly associated with an infection with *T.b. brucei*, as it had been previously related to a different trypanosomes infection.

Differently, the presence of the parasite within the skin is most likely trigging an immune response from the body and could lead to an inflammation of the skin. Lieber et *al*. have investigated the Raman signal obtained from the inflammation of the skin compared with cancer cells in human skin.[222] They have found that specific Raman signal for inflamed tissue were

following in the following shift region: 768 – 782 cm^{-1}, 789 – 814 cm^{-1}, 1178 – 1188 cm^{-1}, 1300 – 1356 cm^{-1} and 1643 – 1671 cm^{-1}. Raman bands specific to the infection displayed here an increase in intensity at 1339 cm^{-1} for the data collected with 532 nm laser and 1333 and 1668 cm^{-1} for 785 nm laser. It is possible that this increase in Raman intensity observed in the infected skin spectrum compared to the uninfected was due to the immune response from the host. The presence of the parasites in the skin would lead to the inflammation of the skin and the response from the host, by releasing different biological residues, could also explain the discrimination obtained through the biological composition of the sample.

Finally, Raman fingerprint of both skin samples and *T.b. brucei* were qualitatively compared to identify the possible contribution of the parasites in the Raman signal of infected skin. Certain Raman bands from the infected skin were found to be similar to the fingerprint of *T.b. brucei*, resulting in an increase in intensity compared to the uninfected skin. Although, it was possible that these Raman bands indicated a direct detection of the parasites, there was a significant spectral overlap between the parasite and the skin (uninfected and infected), which made it unclear whether these peaks resulted in the direct identification of the parasites in the skin.

3.5 Conclusion

In vitro and *ex vivo* investigations were extremely important and valuable before performing *in situ* studies for the diagnosis of sleeping sickness as it provided preliminary data on the parasites and the infection of mouse skin. It allowed the comprehension of the biological composition and repartition of the parasites as well as assessing whether Raman could be a viable tool for the detection of sleeping sickness on the skin.

Two different lasers wavelengths were used for this study; 532 nm that can generate a strong Raman intensity due to the energy of the photons focussed onto the sample, and a 785 nm laser that allowed reference spectra of the parasite and the skin, before *in situ* tissue analysis, to be obtained. Indeed, this wavelength is preferentially used for biological analysis as it reduces fluorescence background from biological components. However, the use of this laser and the

spectral information obtained were limited due to the low signal to noise ratio and the poor spectral resolution obtained during the acquisition. It led to the use of strong pre-processing steps, which affected the Raman spectra and made their interpretation challenging.

Two sub-species of *Trypanosoma brucei*, *T.b. brucei* and *T.b. gambiense*, were mapped and multiple molecular vibrations were tracked across the parasites. It appeared that the VSG coat, its GPI anchor and phospholipid residues were detected, and the conformation of the surface proteins was measured. Despite the multitude of biological components detected, the Raman signal of parasites within a sub-species remained similar. It was shown by using PCA that parasites from the same sub-species could not be spectrally discriminated, thus suggesting a similar composition and/or conformation of the surface proteins. It was possible that the composition of the VSG had changed between parasites, however, it did not seem to be affecting the Raman signal. Interestingly, Raman fingerprint of *T.b. brucei* and *T.b. gambiense* were compared and displayed some spectral differences. This was particularly important as it would suggest that the parasites could be differentiated with Raman, leading to a more accurate diagnosis of the disease if the parasites were detected in the skin. The determination of the biological composition of the trypanosomes and the differentiation between sub-species were very promising for the use of Raman as a detection method for sleeping sickness. However, it would be interesting to reproduce this investigation with parasites from different culture forms (e.g. adipose tissue form) as well as determining and quantifying the biological composition of each sub-species using a different analytical method such as mass spectrometry in order to confirm these findings.

Following the investigation of trypanosomes, mouse skin sections were examined with Raman to assess if the detection of the infection on the skin could be achieved. It was found that the detection of sleeping sickness was successfully performed with Raman. The use of PCA for the analysis of different Raman map from uninfected and infected skin showed clear differentiation of the infection. As multiple maps were performed across the skin, it suggested that the biological changes induced by the infection were present homogeneously along the sample. Raman fingerprints for uninfected and infected skin samples were produced and compared to investigate the biological variations detected. It was found that an increase of certain Raman bands was specific to the infection. Although, the discovery of parasites in the skin is very recent

and its impact on the skin biological composition is not yet understood, the tentative assignment of the Raman bands specific to the infected skin provided some hypothesis on these variations. An alteration of the lipid and protein composition was spectrally identified, which was in accordance with previous work demonstrating that adipose form trypanosomes were able to use lipids and fatty acids for their proliferation. Particularly, a Raman band that was thought to be associated with cholesterol was identified in the data collected with 532 nm laser. It was suggested that the infection led to an increased amount of cholesterol in the skin, as it could have been observed in a different parasitic disease caused by *T. cruzi* (Chagas disease). Furthermore, a variation in the level of certain amino acids was detected as it was demonstrated in animal serum and could be related to the metabolism of the trypanosomes or a change in the protein composition and conformation of the skin induced by the infection. Such findings were important for the understanding of the impact that the parasites have on the skin. Raman spectroscopy should be combined with other analytical techniques to measure these levels in the skin to confirm these hypothesises.

The study of trypanosomes and the murine skin with Raman spectroscopy provided possible explanation of the biological variation observed during the infection but more investigations are needed to understand the mechanism of action of the parasites within the skin. Nonetheless, it was shown that Raman spectroscopy was able to discriminate the infection in the skin of mouse. Raman bands obtained for both lasers, such as 860 or 937 cm^{-1} for example, specific to the infected skin could be used to provide an indication of the infection for the *in situ* mouse study.

Chapter 4 *In situ* analysis of mice infected by *Trypanosoma brucei* with Raman spectroscopy

All experimental details were described in Chapter 7.

4.1 Aims

Analysis of mouse skin *ex vivo* has shown that it was possible to differentiate infected from uninfected skin. A few Raman bands have been identified as specific to the presence of the parasites within the animal. It is important to confirm these findings by studying the potential of Raman spectroscopy to detect sleeping sickness in mice. This *in situ* study would provide vital information for the potential use of this technique in the field.

The main aim of this work was to transfer the differentiation technique from a microscope coupled Raman spectrometer to a portable Raman instrument. The detection of the parasitic infection in the skin could lead to application in the field and a comparison with current detection techniques was assessed.

Mice were infected by different strains of *T.b. brucei* and *T.b. gambiense* and were analysed post-mortem at different time points. The detection of the infection with Raman was assessed and the biological variations induced by the presence of the parasites in the skin were investigated by assigning Raman bands to molecular vibrations. Further experiments were performed to understand these variations such as infecting immunodeficient mice or injecting directly the parasites under the skin. Finally, the Raman detection technique was compared with other detection method such as blood parasitemia and PCR analysis.

4.2 Methodology

Previous *in vitro* and *ex vivo* experiments were performed with an Alpha 300 R Witec instrument, which allowed imaging and high spatial resolution measurements. This instrumentation was not adapted for field analysis as it was very large and requires a constant power supply and stable benchtop. It is also quite expensive compared to a portable Raman instrument and it would be inconvenient to take measurements from a patient with a microscope. A smaller and more portable instrument was needed for this study. In addition to being more transportable, it provided a larger laser spot size (1.5 mm diameter according to the supplier compared to a µm diameter size with a microscope). The spectral resolution of the signal and the amount of information obtained was reduced, but a larger area could be irradiated. As the signal obtained was different from the *in vitro* study, it was difficult to operate a direct comparison of the Raman data from each study. However, trends in the signals could be compared.

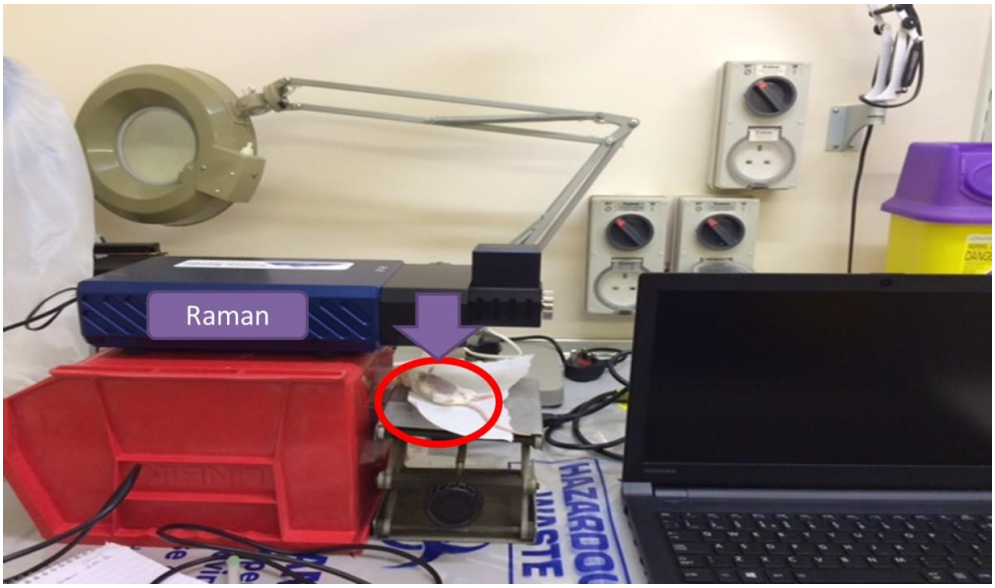

Figure 4.1 Illustration of the instrumental set-up of a benchtop Raman instrument for in situ mouse analysis.

Figure 4.1 showed the instrumental set up for the *in situ* analysis. The Raman instrument – a Snowy Range Instruments (model Sierra 2.0) with a 785 nm laser – was placed on a stable support that allowed the irradiation of the mouse and controlled with a computer. The laser used was 785 nm, as this minimised fluorescence from the skin and the risk of skin burn. The focal point of the laser was obtained with a silica standard and adjusted if needed depending on the size of the mouse studied. This instrumental set up was easy to install and transport to any location when compared with previous microscope-based instruments used. Measurements of the mouse skin was performed post-mortem.

Prior to each measurement, fur from the mouse was removed to directly irradiate the skin, as hair can burn and interfere with the Raman signal, and alter the information obtained. A cream hair-removal product was used to chemically remove hair from the skin. This method was preferentially employed compared to the use of a razor because of the risk of cutting the skin leading to bleeding; this is an important biological hazard when infected blood is involved. The use of cream reduced this risk. However, it could potentially alter the chemical composition of the skin as hair is chemically removed, or residual cream in the skin could interfere with the biological signal. The cream was left in contact for the shortest time possible, which was 5 min, and mice were thoroughly washed with water to remove any residual cream product.

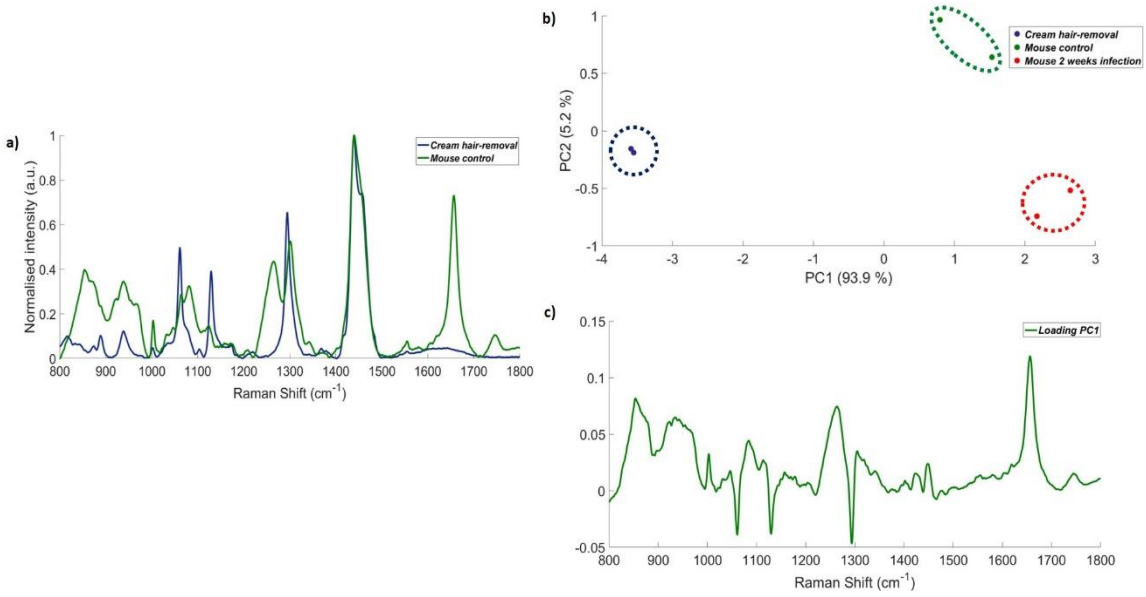

Figure 4.2 Investigation of the effect of the cream hair-removal on the mouse skin. (a) Spectral comparison between mouse control skin and cream normalised Raman signal, (b) PCA scores of PC1 vs PC2 between cream (blue), control mouse skin (green) and skin infected with T.b. brucei 247 (red) and each group circled for clarity, (c) PC1 loading spectrum. Spectra were acquired with a 785 nm laser, 45 mW and 60 s acquisition time.

Figure 4.2 showed the comparison between mouse skin and cream Raman signal. It was important to assess if residual cream was present in the skin after removing the hair. The direct spectral comparison did not show any signal from the cream hair-removal (blue) in the mouse spectrum (green) in Figure 4.2.a). The Raman fingerprint of the cream hair-removal product could be identified by four sharp and intense Raman bands at 1061 (C-C plane), 1129 (C-C skeletal), 1295 (CH_2 deformation) and 1440 (CH_2 and CH_3 deformation) cm^{-1}. In order to confirm this, a statistical analysis between the cream hair-removal and an uninfected and infected mouse skin was performed with PCA. There was clear separation observed between the cream Raman spectrum (blue) and mouse skin signal (green and red) in the PCA scores plot (Figure 4.2.b)). It appeared that the fur was successfully removed from the skin without leaving any chemical traces of the cream that could alter the Raman spectral information.

Another potential issue was discovered during the initial experiments measuring the Raman signal from the skin. It was found that when the abdominal skin region of a mouse was investigated, Raman signal was also obtained from the organs present below the skin. This gave a strong fluorescence background in the spectrum and did not allow for long acquisition times

to be used. It has been found previously that some organs such as liver and spleen give strong fluorescence, which can obscure Raman signal.[233] This background increase was mostly obtained on infected mice, and was thought to be due to a strong enlargement of the spleen.

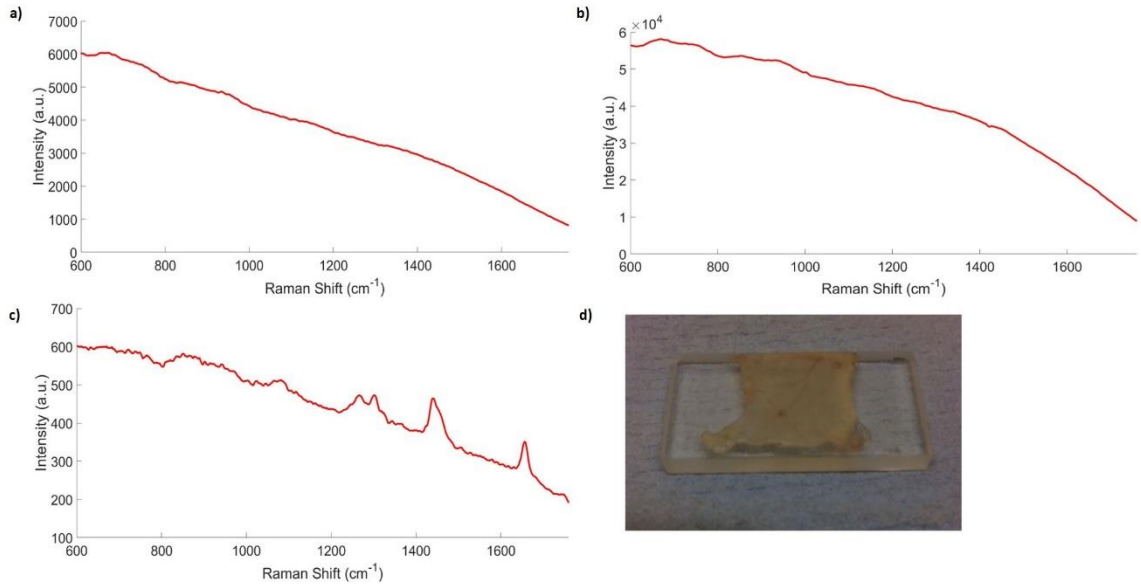

Figure 4.3 Investigation of the Raman fluorescence signal obtained from the skin and internal organs. (a) Mouse abdominal skin Raman signal measure with 1 s acquisition time obtained near the sternum area, (b) Mouse abdominal skin Raman signal measured with 30 s acquisition time obtained near the sternum area, (c) Mouse abdominal skin Raman signal measured with 1 s acquisition time obtained near the tail region, (d) Illustration of mouse abdominal skin placed on CaF_2 slides. All spectra were measured with 785 nm laser, and 45 mW power.

This increase in background led to a diminution of Raman bands as they became swamped under the background fluorescence, which altered the biologically relevant information obtained. It would also not help to measure a large area of the skin to obtain a good representation of the signal, as measurements taken near the spleen would have an increased background. Figure 4.3 showed a few examples of the different Raman signals obtained. Figure 4.3.c) shows a Raman spectrum of the mouse abdominal skin measured with a 1 s acquisition time near the tail area and where Raman bands were easily distinguished, and Figure 4.3.a) and b) provided an example of the increase of the background in the Raman spectrum measured with 1 and 30 s acquisition times respectively, obtained near the sternum area where the spleen is located. The difference between spectrum a) and c) were quite notable. The intensity was increased to up to a 10-fold,

and Raman bands were not present, due to an increase in fluorescence background even if the acquisition time was identical.

Originally, measurements were taken with a 60 s acquisition time in order to obtain maximum information from the skin. However, as shown in Figure 4.3.b), the CCD was nearly saturated with a 30 s acquisition time in certain areas of the skin. The CCD for this instrument had a limit of ~60000 counts. All measurements were preferentially taken with a 30 s acquisition time (unless stated otherwise) to avoid the fluorescence background or CCD saturation.

Given it was shown that signal could be obtained from organs below the skin, it was important to assess if this signal would alter the results. Hence, after measurements, the abdominal skin was removed from the mouse and placed on a calcium fluoride slide (Figure 4.3.d)) and separate sets of measurements were taken, where only skin signal had been measured. This helped for a comparison of the two different methods and assessing if the signal from the organs affected the results.

Another means of avoiding the fluorescence background from the abdominal organs was to investigate a different area of the skin. The abdominal skin was originally of interest because trypanosomes were known to be present in adipose tissue.[154] It was also found experimentally that the hair from the abdominal region was quite easy to remove. However, it has been shown that trypanosomes could also be present in the dorsal region and still infect tsetse flies.[156] This gave a new region for investigation, with measurements taken from muscle tissue that surrounds the spine. These muscles are thicker than the skin from the abdominal region and reduced the fluorescence signal from organs that could alter the Raman spectra obtained. Spectra showed that the muscles had little fluorescence when measurements were taken (data not shown). This allowed a longer acquisition time to be used to increase the Raman signal.

The comparison between two different skin areas could help investigate the best way to detect the disease in an infected mouse and discover a preferential location of the parasite within the skin.

4.3 Preliminary investigation of mouse infected by *T.b. brucei* gvr35 and the related biochemical changes in the skin

BALB/c mice were infected with a *T.b. brucei* gvr35, which was a specific strain within the parasite sub-species. The infection of mice with this strain has been studied previously, and has shown that the parasites were present in the brain after 7 days post-infection.[265] It was thought that, if the parasites were able to cross the blood brain barrier after 7 days, they would also be located in the skin at this stage. Another *T.b. brucei* strain, *T.b. brucei* 247, was investigated in mice, and this strain has been found to be present in the skin after 12 days.[156] This meant that the use of gvr35 could potentially provide a faster skin infection by the parasites, and a greater concentration of the parasite in the skin for Raman measurements.

Prior to any Raman measurement, the parasitemia of the mouse was followed and measured to ensure its infection by the parasites. This technique was based on the method developed by Herbert *et al.*,[266] which counted parasites in a drop of blood on a glass slide with a microscope, and then allowed an estimation of the number of parasites per mL of blood. The value obtained for blood parasitemia was the logarithmic value of the concentration of parasites in the blood, which then allow its estimation.

The aim of this work was to investigate whether Raman spectroscopy could detect infected mice *in situ,* and to optimise the experimental and data analysis procedures for future experiments.

4.3.1 Two weeks post-infection analysis of mouse skin

T.b. brucei gvr35 infected BALB/c mice were taken after two weeks of infection, and Raman measurements were obtained from their abdominal region. Ten spectra were taken across the skin region for each mouse type: uninfected and infected. Individual Raman spectra were obtained using a 60 s acquisition time and 45 mW laser power. This allowed for a good representation of biological changes that the presence of the parasite could induce across the skin. The data set was then analysed using PCA.

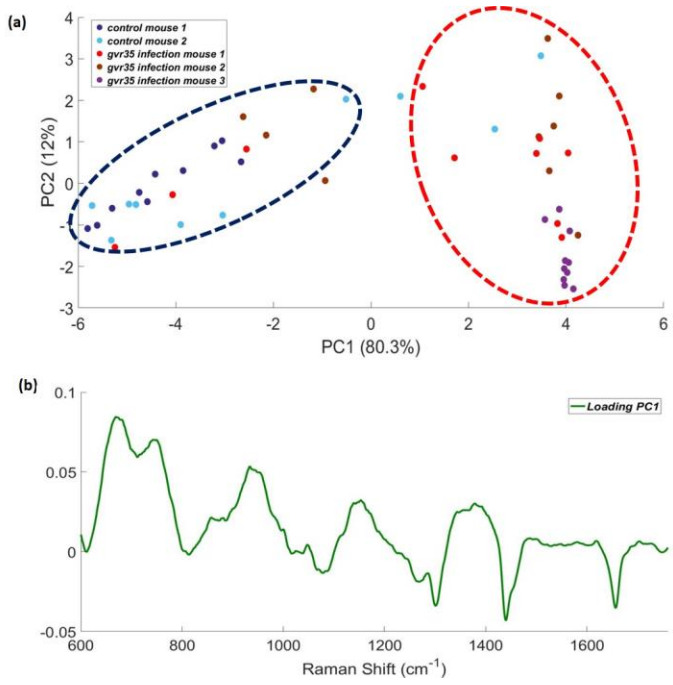

(c)

Two weeks infected mouse	Estimation of parasitemia (number of parasites/mL of blood)
Mouse 1	3.2×10^7
Mouse 2	6.3×10^7
Mouse 3	1.3×10^8

Figure 4.4 Principal component analysis of two control mice (dark and light blue) and three infected mice (red, brown and purple) measured at 2 weeks post-infection with ten Raman spectra each obtained on the abdominal region with a 785 nm laser, 45 mW and 60 s acquisition time. (a) Scores plot of PC1 versus PC2, (b) PC1 loading spectrum, (c) estimation of the blood parasitemia.

Figure 4.4 displayed the statistical analysis of two weeks post-infection mice versus uninfected mice. The main separation occurred across PC1, and accounts for 80.3 % of the co-variance of the data set. Control and infected groups were circled in blue and red respectively for clarity. It could be observed that most of the spectra from the infected mice were discriminated from the control group and located in the positive side of PC1. However, there were some spectra that were mixed up with the control data set and were not well separated. The same observation could be made with one of the control animals, which has some data points spread across PC1 within the infected group. It appeared that the infected mice 1 and 2 possess data points that were spectrally identical to the control measurements, whereas infected mouse 3 seems to be completely separated. According to the blood parasitemia estimation shown in Figure 4.4.c), the three mice were infected by T.b. brucei gvr35. However, infected mouse 3 had more parasites in its blood, which could explain why this infected mouse was clustered and well discriminated, as it maybe was that more parasites had entered the skin. Spectral variations observed between the infected group indicated that biological changes and the reaction towards the infection may be different between mice or the different mice took different amounts of time to respond to

the infection, leading to different levels of parasites in the skin. The latter explanation would suggest that biological variations associated with parasites invading the skin were the same between mice, but that a different invasion rate of the trypanosomes would lead to different level of Raman signal. Moreover, the presence of data points from infected mouse 1 and 2, which had a lower blood parasitemia than infected mouse 3, in the control cluster could suggest that the biological changes induced by the infection were localised, and not observable across the entire skin area for these mice. It was also possible that the trypanosomes were heterogeneously spread in the skin and may form patches. Despite these variations between infected animals and the presence of a few control points in the "infected" area of the score plots (Figure 4.4.a)), it appeared that the infected skin could be differentiated from a control skin.

The loading spectrum in Figure 4.4.b) provided the spectral differences that were specific to the infected mice. It appeared that there were Raman bands that could define the separation. The Raman bands at 670 cm^{-1} (porphyrin or tryptophan), 750 cm^{-1} (porphyrin or tryptophan), 858 cm^{-1} (proline or tyrosine), 879 cm^{-1} (hydroxyproline), 934 cm^{-1} (C-C backbone, proline), 1153 cm^{-1} (C-C, C-N vibration) and 1378 cm^{-1} (CH_3 band) cm^{-1} were responsible for the discrimination between uninfected and infected mice.[231–233] Porphyrin has been associated with red blood cells. A study has shown the presence of porphyrin in human red blood cells with the Raman bands at 669 cm^{-1}, as well as 752 cm^{-1}.[267] Here, the two Raman bands 670 and 750 cm^{-1} specific to the infected skin group could be associated with the presence of blood cells in the skin. In addition, other Raman bands specific to the infection such as C-C backbone and C-N vibrations seemed to indicate an alteration of the biological components of the infected mouse skin, relating to a change of lipid/protein composition due to the presence of the parasites in the skin.[154] This result tends to confirm the measurements and interpretation made previously during the *ex vivo* study. This analysis demonstrated the biological changes observed in the presence of the infection and shows that these changes could tend to be inconsistent across the skin. Most of the data points from infected mice were separated from the control, however, it appeared that some areas remain indistinguishable.

All spectra obtained from individual animals were averaged into a single Raman spectrum. These spectra were normalised and compared to each other to identify the spectral variations between each group. This method allowed the biological variations observed previously within an

individual animal to be reduced and helped a general trend to be observed in the biological changes due to the infection within each mouse.

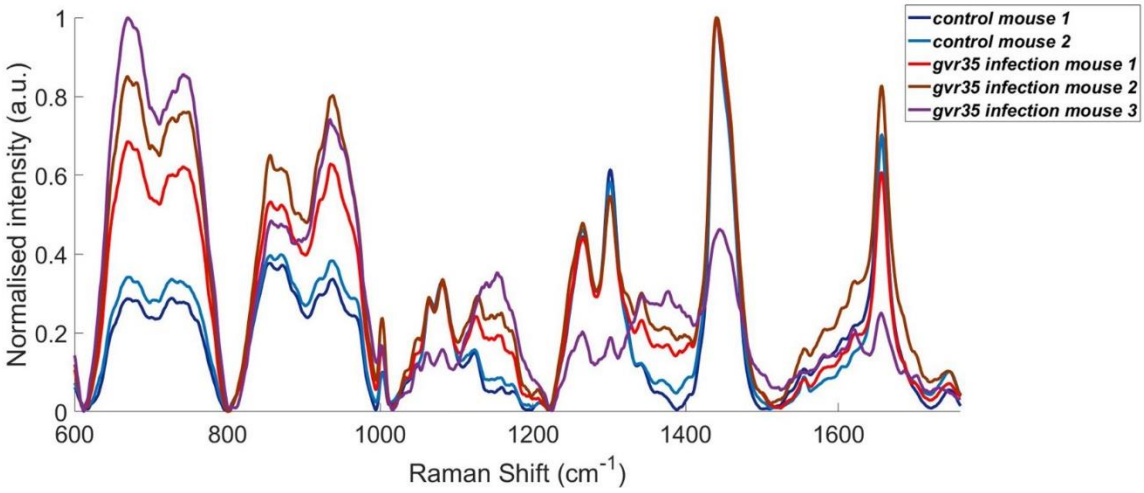

Figure 4.5 Spectral comparison between Raman spectra of uninfected and two weeks infected mice, averaged and normalised, measured with 785 nm laser, 45 mW and 60 s acquisition time on the abdominal skin region.

A comparison of the averaged Raman spectra helped demonstrate the general change that occurred across the skin during the infection. These spectral differences could be observed in Figure 4.5. According to this spectral comparison, there was an increase in the Raman intensity of certain peaks for the infected mice. These Raman bands were localised at 670 cm^{-1} (porphyrin deformation observed in human red blood cells, or tryptophan), 728 cm^{-1} (ring breathing of tryptophan), 742 cm^{-1} (tryptophan), 856 cm^{-1} (proline, tyrosine), 876 cm^{-1} (hydroxyproline), 935 cm^{-1} (C-C backbone, proline), 1003 cm^{-1} (phenylalanine), 1047 cm^{-1} (proline, PO_4^{3-} stretch).[231–233] It appeared that the presence of the parasites in the skin increases the presence of peaks associated with certain amino-acids such as phenylalanine, tyrosine, tryptophan and proline, which could be related to a high variation in proteins. These amino acids are the most Raman active, and support the observation of an increased concentration of proteins in the skin. Moreover, there were two other regions identified as specific to the infected mice, where the intensity was only slightly increased, at 1126 cm^{-1} (C-C/C-N stretching of proteins/lipids), 1159 cm^{-1} (C-C/C-N stretching proteins), 1343 cm^{-1} (CH_3CH_2 wagging collagen) and 1379 cm^{-1} (CH_3 symmetric of lipids).[231–233] This could relate to the rearrangement of the skin matrix in the

presence of trypanosomes, where the biological conformation and composition is affected by the parasites. Indeed, *T.b* was shown to be able to interact with lipids and fatty acids for their metabolism as well as collagen.[154,268] This increase in intensity of Raman bands associated with protein/lipid composition could described an up-regulation, induced by the parasites, of such biological components release by the host for the metabolism and the proliferation of the trypanosomes. This increase in intensity could also relate to the surface protein carried by *T.b. brucei* such as VSG.

The Raman peak observed at 670 cm^{-1} was especially interesting. It has been found to be related to porphyrin that is present in red blood cells.[267] Porphyrin complexes were related to heme and the increase in intensity suggested that this component was more present in the infected skin. Given that porphyrin was related to red blood cells, this could suggest that when the parasites crossed blood vessels to enter the skin, blood cells were released into the skin. The identification of several Raman bands that have increased in intensity was a promising starting point to set up a method to detect parasites in skin. Unfortunately, no specific peaks for the infection were observed, which could have led to a clearer, or faster identification of the infection, but the identified peak intensity differences could be used to develop a peak ratio method to detect the presence of the parasite in skin.

It was also observed that the Raman fingerprint of infected mouse 3 was different from the other infected mice. There was a decrease in intensity observed for Raman bands located in the 1200 – 1800 cm^{-1} wavenumbers region for this mouse. This indicated a clear change in the biological composition between infected mice, suggesting that mice could act and respond differently to infection by *T.b. brucei*. Nonetheless, this spectral variation did not affect its discrimination towards the control mice.

4.3.2 Three weeks post-infection analysis of mouse skin

The differentiation between control mice and two weeks infected mice was possible with Raman spectroscopy. It was achieved by taking measurements on the abdominal region. This further investigation aimed to confirm these findings by analysing mice that had been infected by the parasites after three weeks and to confirm if the infected skin gave the same spectral

identification. In addition, the dorsal region of the mouse was analysed in order to compare it with the abdominal region, and finally, the influence of fluorescence from the organs was assessed.

4.3.2.1 Investigation of the abdominal skin region of three weeks infected mice by T.b. brucei gvr35

The abdominal skin of mice was analysed after three weeks of infection in order to confirm the spectral differences obtained with two weeks infected mice. The method of acquisition was changed slightly, with five spectra acquired with a 30 s acquisition time across the skin. This was to help reduce the fluorescence interference that occurred in some instances. The skin was also removed and placed on a calcium fluoride slides to investigate the potential influence of the organs' fluorescence on the Raman spectrum. Five spectra were taken across the mounted skin sample with a 60 s acquisition time.

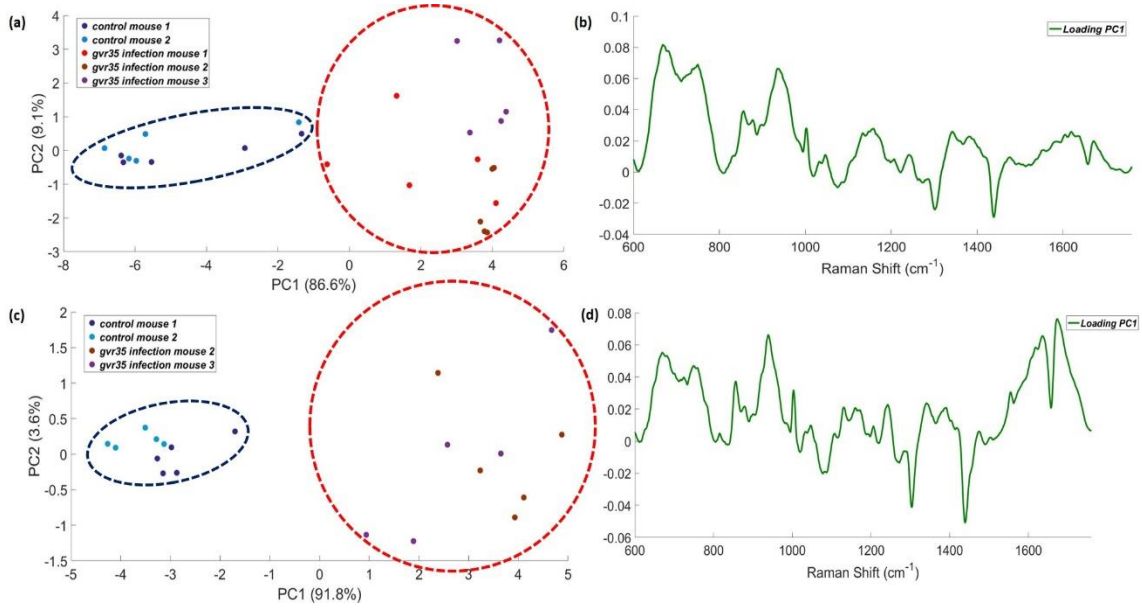

Figure 4.6 Principal component analysis of uninfected (dark and light blue) versus three weeks infected by T.b. brucei gvr35 mice (red, brown and purple) Raman spectra measured on the abdominal skin region of the animal: (a) PCA scores plot PC1 vs PC2, (b) PC1 loading spectrum, and on the abdominal skin placed on a CaF_2 slides where only two infected mice were analysed (brown and purple): (c) PCA scores plot PC1 vs PC2, (d) PC1 loading spectrum. All spectra were obtained with 785 nm ,45 mW, and 30 s acquisition time for abdominal skin ((a) and (b)) and 60 s acquisition time for abdominal skin on CaF_2 slides ((c) and (d)).

Figure 4.6.a) and b) showed the PCA scores and the loading spectrum of PC1 for the data obtained on the abdominal skin region of mice. Mice were analysed three weeks after infection by the parasites. The separation between infected and uninfected mice was clearly observed across PC1 (86.6 %). Each data point from the infected group was well discriminated from the control and were respectively circled in red and blue. In Figure 4.4.a), some data points from control and infected were not well separated. This suggested that the infection had progressed after a further week; which suggested parasites were now more present and dispersed across the skin, and/or the biochemical changes that their presence induced was more homogeneous. Each individual infected mouse appeared to also be clustered away from controls. Biological changes measured within their skin was found to be constant across the area investigated. However, it appeared that spectral differences existed between each infected mouse, suggesting that animals may respond differently to the infection, or that the parasites did not invade the skin at the same rate. Estimation of the blood parasitemia showed that the three mice were infected and had more parasites in their system than for the two week infection (Table 4.1). It indicated that infected mouse 3 had a lower parasitemia than the other two mice, and in Figure 4.6.a) it appeared that this mouse was slightly separated from the other two mice. This appeared to confirm that the biochemical changes observed in the Raman spectra were correlated to the state of infection of the animal and to its biological response.

Table 4.1 Estimation of the blood parasitemia of the three mice infected by T.b. brucei gvr35 and analysed at three weeks post infection.

Three weeks infected mouse	Estimation of parasitemia (number of parasites/mL of blood)
Mouse 1	1.3×10^8
Mouse 2	1.3×10^8
Mouse 3	3.2×10^7

The shape of the loading spectrum of PC1 for the three week infection (Figure 4.6.b)) was similar to the spectrum obtained previously for the two week infection. Given this similarity, the time of infection could potentially be tracked, as the same Raman bands were specific to the infection, but their intensity was increasing over time. According to Figure 4.6.b) Raman bands that

characterised the infection were found at 669 cm^{-1} (porphyrin or tryptophan), 750 cm^{-1} (porphyrin or tryptophan), 856 cm^{-1} (proline, tyrosine), 876 cm^{-1} (hydroxyproline), 935 cm^{-1} (C-C backbone of proline), 1002 cm^{-1} (phenylalanine), 1046 cm^{-1} (proline, PO_4^{3-} stretch) and 1159 cm^{-1} (C-C/C-N stretching) cm^{-1}.[231–233] The Raman bands specific to the infection obtained here were similar to the ones measured previously for two week post-infection analysis. The variation between each data set was also reduced according to the scores plot, suggesting that the biochemical changes were more homogeneous and easily identified across the infected skin after a longer infection time.

It was described previously that some interferences could be measured due to the fluorescence signal given by some organs. To address this, skin was removed from the mice and placed on CaF_2 slides before Raman measurements in order to obtain signal from the skin alone. The resulting PCA analysis was shown in Figure 4.6.c) and d). The scores plot showed a clear separation between infected and uninfected mice across PC1 (91.8 %). The differentiation of infected and uninfected isolated skin on CaF_2 substrate appeared to be more efficient than direct measurement of the abdominal region (Figure 4.6.a)) with control data points well grouped. The PC1 loading spectrum for this experiment was similar to Figure 4.6.b). The same specific Raman bands were observed, and new ones could be identified because the interference from the organs was removed. According to this loading spectrum, the Raman bands that explained the differentiation of the infected group were identical to the ones found previously in Figure 4.6.b) with the addition of two more pronounced Raman bands at 1132 cm^{-1} (C-C skeletal) and 1243 cm^{-1} (Amide III) cm^{-1}.[231–233] The contribution of these Raman bands was hidden during the direct measurement of the animal, possibly due to the interference from internal organs. They indicated an alteration of protein structure within the skin due to the infection. It was possible that the contribution from the proteins carried by *T.b. brucei* were detected. The shape of the Raman peak at 1658 cm^{-1} (Amide I) was found to be different as well. The region at 1580 – 1630 cm^{-1} at the base of this band was contributing to spectral changes resulting from infection. This characteristic was also observed during the *ex vivo* investigation was thought to be related to phenylalanine and tyrosine,[239] however this increase was found to be specific to the uninfected skin. The variation in this region was not as clearly observed on the abdominal skin (Figure 4.6.b)), hence it was possible that the alteration of these amino-acids seemed to be characteristic

of the skin infection by the parasites as the interference from internal organs were removed, due to their increased presence. A more pronounced Raman band was also found at 1555 cm^{-1} and could be associated with porphyrin or tryptophan.[231]

The difference between the two methods of measurement, however, was not large. The interference caused by the organs may have obscured some of the signal from the skin, but it did not affect the differentiation between uninfected and infected. Many of the same Raman bands were still vital in this separation such as, for example, 856 and 935 cm^{-1}. Similar Raman bands were also observed in the infected mouse skin during the *ex vivo* investigations and seemed to also correlate to the infection in the *in situ* work. Hence, there was no need to remove the skin from the mouse to obtain a detection method.

Each of the data sets that were used for the PCA in Figure 4.6.a) were averaged into a single Raman spectrum in order to clearly identify a general trend in the spectral differences between uninfected and infected mouse.

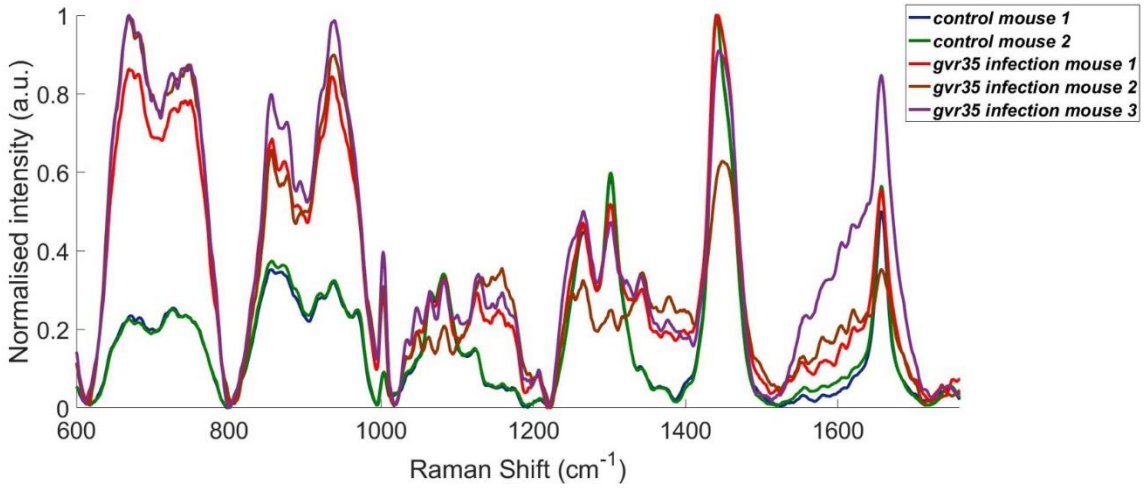

Figure 4.7 Comparison between Raman spectra of uninfected and three weeks infected mice, averaged from five spectra and normalised, measured with 785 nm laser, 45 mW and 30 s acquisition time on the abdominal skin region.

The comparison between the unique Raman spectra for each mouse displays the same spectral differences observed previously with two week infected mice (Figure 4.7). An increase in intensity for certain Raman bands could be observed. It was found that the presence of the

parasites within the skin was determined by an increase in intensity of Raman bands at 669 cm^{-1} (porphyrin deformation observed in red blood cells, or tryptophan), 728 cm^{-1} (ring breathing of tryptophan), 750 cm^{-1} (tryptophan or porphyrin), 856 cm^{-1} (proline, tyrosine), 876 cm^{-1} (hydroxyproline), 936 cm^{-1} (C-C backbone, proline or hydroxyproline), 1003 cm^{-1} (phenylalanine), 1034 cm^{-1} (phenylalanine) and 1047 cm^{-1} (proline, PO_4^{3-} stretch).[231–233] The tentative assignment of the different Raman shifts suggested an augmentation in the presence of Porphyrin (red blood cells) in the infected skin. This provided further evidence in support of the previous conclusion where it was thought that blood cells were released in the skin when the parasites crossed the blood vessels. From the data obtained, it appeared to be specific to the presence of trypanosomes. An increase in concentration of amino-acids like tryptophan, phenylalanine or proline was also observed.

Other Raman bands at 1127, 1159, 1208, 1343, 1379 and 1555 cm^{-1} could potentially be specific to the infection, and could respectively be associated with C-C/C-N stretching, C-C/C-N stretching, tryptophan or phenylalanine, CH_3CH_2 wagging, CH_3 symmetric of lipids and ν(C=C) of porphyrin or tryptophan.[231–233] The Raman peak at 1657 cm^{-1} (Amide I) also displayed a larger shoulder in the region 1580 – 1630 cm^{-1} for the infected skin. This region was thought to be associated with the presence of phenylalanine and tyrosine.[239] This increase in intensity for such molecular vibrations could be associated with the proteins present in *T.b. brucei* such as VSG. It was also possible that it was the result of the animal host response to the infection causing the release of different proteins.

The results obtained were consistent with those obtained from the two-weeks post-infection mice. The presence of the parasite in skin could be followed *via* the intensity of certain Raman bands when the measurements were taken on the abdominal skin region. It appeared that Raman was indeed detecting an increase in red blood cells and specific amino-acids within the skin associated with the infected animals. The presence of these Raman bands seemed to increase with the time of infection. It was observed in the PCA scores plot that the infected data points were less variable for a three week infected mouse than for a two week infected mouse. It was thought that the biochemical changes induced by the infection were more homogeneous across the abdominal skin at a longer infection time. It could also suggest that trypanosomes do not invade the skin at localised areas but seemed to be represented across the abdominal region

with time. Nonetheless, *in situ* Raman spectroscopy was able to detect trypanosome infection in mice by targeting the abdominal skin region for measurement.

A different skin region, such as dorsal skin, was analysed and compared to the abdominal skin in order to find the best location to perform the Raman measurements.

4.3.2.2 Investigation of the dorsal skin region of three weeks infected mice by T.b. brucei gvr35

The same experimental method was employed for the dorsal region as for the abdominal skin. Five spectra were obtained across the skin with an acquisition time of 30 s. The fluorescence influence was reduced in this region, suggesting that muscles, underneath the skin, were less prone to auto-fluorescence than spleen or liver.

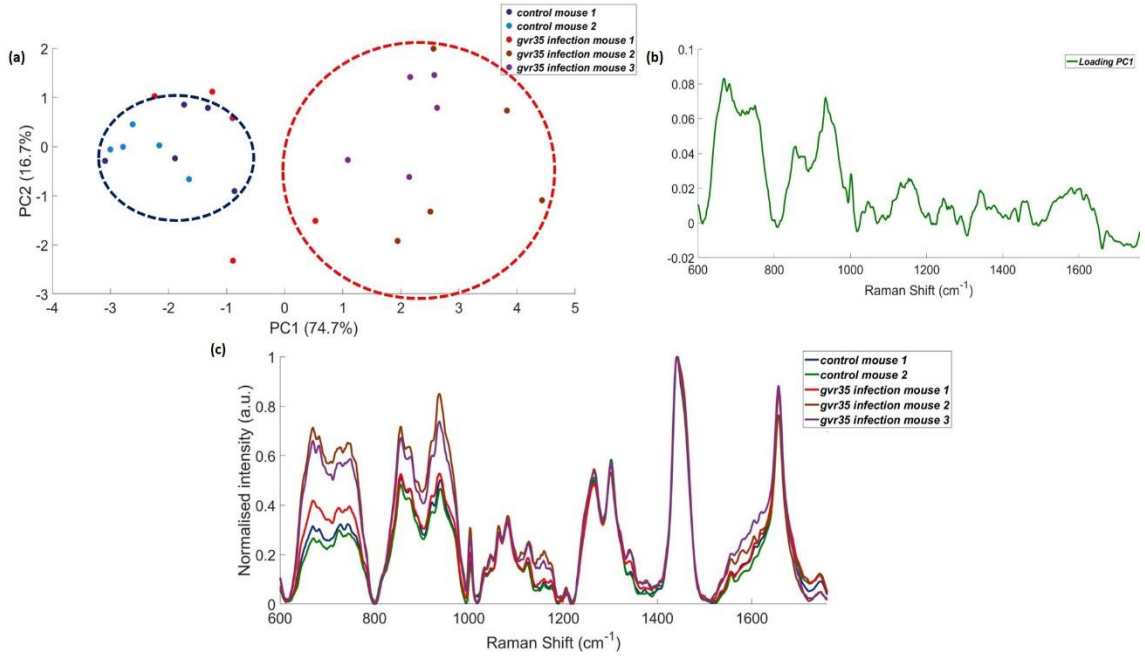

Figure 4.8 Principal component analysis of uninfected versus three weeks infected mice Raman spectra measured on the dorsal skin: (a) PCA scores plot PC1 vs PC2, (b) PC1 loading spectrum, (c) Five Raman spectra from each mouse were averaged and normalised, and spectrally compared. All spectra were obtained with 785 nm, 45 mW and 30 s acquisition time.

The resulting PCA scores plot in Figure 4.8.a) showed that infected and uninfected data sets were differentiated along PC1. The percentage of variation explained was 74.7 %, which was slightly

lower than that obtained with abdominal skin measurement. Both control and infected groups were circled, respectively in blue and red, for clarity and to show the trend of separation. This suggested that the Raman spectra might be more variable on the dorsal skin than on the abdominal region. This could further be observed within the infected data sets, where data points for each mouse were not well grouped. It was also noted that the first infected mouse (red dots) was not differentiated from the control mice. Despite this variation, the other two infected mice were well differentiated across PC1, and the loading spectrum was identical to the one obtained for the abdominal skin region. Hence, even though the data sets were slightly more variable, it was still possible to detect the presence of the parasite in the dorsal skin, as well as in the abdominal skin. Shown in Figure 4.8.b), the Raman bands specific to the infection on the dorsal skin were identical to the ones found in the abdominal region. Similar biochemical changes were observed between the two skin regions. This was confirmed when single averaged Raman spectra were compared to each other in Figure 4.8.c). An identical increase in intensity of certain Raman bands, as for the abdominal region (Figure 4.7), was observed here.

Dorsal skin measurements were more variable than the abdominal skin measurements but a similar pattern in the Raman peak intensities was observed, and the detection of the infection could still be performed. Moreover, the lower discrimination between dorsal infected and uninfected skin compared to abdominal skin was in correlation with adipose tissue being a reservoir for trypanosomes.[154] Since adipose tissue was more present in the abdominal region than in the dorsal region, trypanosomes could then be preferentially located in the abdominal region. This was supported by the Raman measurements, where the discrimination between infected and uninfected skin was clearer when abdominal skin was analysed.

4.3.2.3 Raman spectral comparison between dorsal and abdominal skin measurements

The data obtained from the measurement of the abdominal and dorsal skin were analysed and compared with PCA to find an ideal location to detect the infection. Each single averaged Raman spectrum obtained previously in Figure 4.7 and Figure 4.8.c) were combined and analysed. Each spectrum represented measurements for either dorsal or abdominal skin with a 30 s acquisition time.

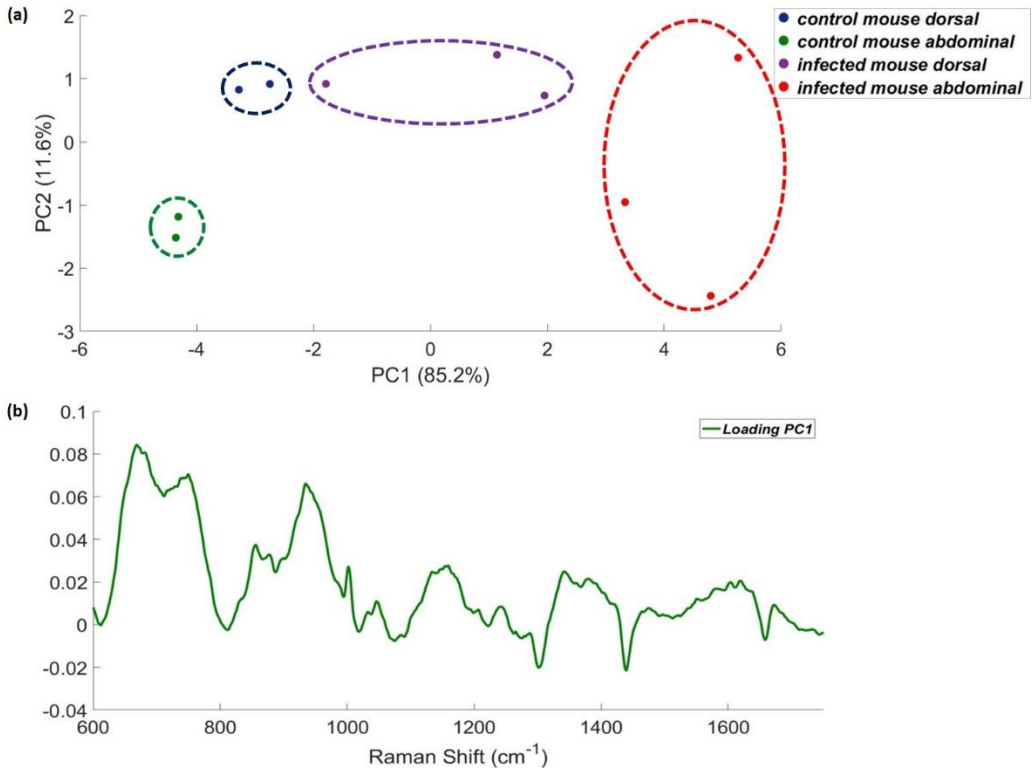

Figure 4.9 Principal component analysis of single averaged Raman spectra measured on the dorsal or abdominal skin for uninfected versus three weeks infected mice with 785 nm laser, 45 mW and 30 s acquisition time: (a) PCA scores plot PC1 vs PC2 (each group were circled for clarity), (b) PC1 loading spectrum.

A clear differentiation was obtained across PC1 (85.2 %) on the scores plot when comparing infected and uninfected mouse skin (Figure 4.9.a)). It was observed that control group from dorsal and abdominal measurements were clustered and well differentiated from the infected group. In addition, these were also separated from each other indicating a different biological composition in the two regions, which could relate to the amount of body fat or the different proteins or lipids present in each area. The interference from internal organs was also different, where internal organs such as liver or spleen could contribute to the Raman signal in the abdominal region, and dorsal muscle could contribute in the back skin. Despite the different biological area investigated, it appeared that infected skin, both dorsal and abdominal, were well discriminated from the control group, suggesting that the biochemical changes induced by *T.b. brucei* was generalised and homogeneous across the whole skin organ. Moreover, the abdominal

skin group was better differentiated from the control group than the dorsal skin on the scores plot. This suggested that the effect of the infection on the skin was stronger in the abdominal area, most likely due to a larger presence of parasites in the adipose tissue.[154] Nonetheless, it appeared that the presence of the parasites could be detected in both dorsal and abdominal skin.

4.3.2.4 Conclusion

The detection of mice infection by trypanosomes was demonstrated by analysing their abdominal skin region. Within one mouse, each Raman measurement appeared to be slightly spectrally different according to the PCA scores plot for two weeks infection. Trypanosomes may not have been homogeneously spread in the skin and might have formed localised patches, which could have also affected the resulting biological changes induced by their presence. However, the overall infected data group was clearly differentiated from control, suggesting that there were Raman bands specific to the infection being present. Hence, each individual measurement from a mouse was averaged into a single Raman spectrum before analysis to mitigate slight variations across the skin and to obtain a better visualisation of the spectral differences induced by the presence of the parasites. After a further week after infection, identical spectral variations were observed and Raman measurements within a single mouse were more consistent, indicating that biological variations were homogeneous across the skin area. It appeared that after 3 weeks trypanosomes had spread throughout the skin. Spectral differences between uninfected and infected skin were clearly identified when comparing single averaged Raman spectrum, hence principal component analysis would not necessarily be required for future analysis.

Moreover, both dorsal and abdominal skin provided an interesting area to detect the infection of the mouse by the parasites *via* Raman spectroscopy and using PCA. Identical biological changes were observed during the infection of the mouse skin, whether analysis was performed on the dorsal or abdominal skin, and these were characterised through identical PC1 loadings, which allowed the discrimination between infected and uninfected group mice. These spectral variations between uninfected and infected mice were further confirmed by the direct spectral comparison of averaged single Raman spectra from each mouse, where identical Raman bands

displayed an increase in intensity during the infection. When both skin areas were compared using PCA, it appeared that abdominal skin allowed a better differentiation of the infected against the control measurements. The abdominal skin would then be preferred for future analysis. Interestingly, it was found that adipose tissue was a preferential reservoir for the trypanosomes in the skin.[154] A clearer and stronger discrimination of the abdominal infected skin hence suggested that the Raman signal obtained could be directly related to the presence of the trypanosomes as more adipose tissue can be found in this area compared to dorsal area.

This preliminary *in situ* analysis on infected mice also provided spectral information specific to the infection and tentative assignment of these Raman bands helped understand the biological influence of the parasites in the skin. Many Raman bands associated with lipids and proteins, as well as amino acids, suggesting that the infection led to a change in the composition and conformation of such components. It was known that trypanosomes could adapt their metabolism to their surrounding media and could interact with collagen, and particularly lipids and fatty acids in the skin.[154,268] Their related Raman bands displayed higher intensity during the infection, which could describe an increase amount of proteins/lipids. It was possible that trypanosomes present in the skin induce an up-regulation of the release of certain biological components for their metabolism and proliferation. In addition, a response from the immune system from the host could also be measured and translated to this intensity increase. This increase could also be related to the presence of the parasites and their associated VSG surface coat and could be measured by Raman during the infection, suggesting a direct detection of the trypanosomes. Moreover, the alteration and up-regulation of proteins composition were also supported by the Raman bands associated with amino acids such as tryptophan, tyrosine, phenylalanine and proline. Surprisingly, the variation in intensity of peaks associated with amino acids is different from the *ex vivo* observation, where a decrease in intensity was observed, suggesting that the alteration in proteins or amino acid may also originate from other region than the skin during the infection.

Differently, it was shown that trypanosomes were able to use amino acids such as tryptophan, tyrosine and phenylalanine for their metabolism, inducing a decrease in their concentration in the host, while parasites released indolepyruvate, hydroxyphenylpyruvate and phenylpyruvate respectively.[262–264] These catabolites were structurally close to their respective amino acids. It is

possible that Raman was detecting such increase in concentration of these catabolites. An increase of the concentration of proline was also observed in the serum of infected voles.[262] It would then confirm previous work on the alteration of amino acids induced by *T.b. brucei* observed in serum and plasma of infected animals.[262,265] However, it could not be determined whether the Raman bands associated with these amino acid were related to free amino acid or amino acid present in proteins.

Moreover, the Raman bands at 669 cm^{-1}, as well as 750 or 1555 cm^{-1}, were thought to be associated to porphyrin.[231,267] This component was related to the composition of heme in red blood cells. The passage of the parasite from the blood vessel to the skin could result in the release red blood cells in the skin and led to its detection with Raman spectroscopy.

Finally, another interesting Raman peak was located at 876 cm^{-1} and was assigned to hydroxyproline. This Raman band has also been found to be related to choline and the presence of phosphatidylcholine.[231,269] These phospholipids have been shown to be extensively represented across the membrane of *T.b*.[240,243] This detected Raman peak could therefore also be attributed to the choline from this phospholipid, indicating the direct detection of the presence of the trypanosomes in the skin via phospholipids located on its membrane. Choline has also been previously associated with the presence of parasites in mice.[265] Indeed, *T.b. brucei* was able to use phospholipids, such as phosphatidylcholine, for growth and membrane production. This would result in a reduction in the concentration of phosphatidylcholine, and an increase in the concentration of choline in mouse plasma.[265]

4.4 Investigation of mouse infected by *T.b. brucei* 247 and the related biochemical changes in the skin

4.4.1 Two and three week post-infection Raman measurement on mice infected by *T.b. brucei* 247

A different strain of *T.b. brucei* could be used to infect mice. *T.b. brucei* gvr35 was used, due to its potential ability to enter the skin early, which could lead to skin biological modification at an

earlier post-infection time point. *T.b. brucei* 247 has been found to enter the skin 12 days post-infection, and possessed a low virulence towards the mouse, which meant that the infection is less likely to lead to the death of the mouse.[156]

It was interesting to investigate the Raman information obtained with a different strain compared to gvr35 over the time of infection. It would allow assessment of whether biological variations observed by Raman after infection were different because of an infection with a different strain. Moreover, *T.b. brucei* 247 have been used previously for the *in vitro* and *ex vivo* study, which permit comparison of Raman fingerprint from *T.b. brucei*, *ex vivo* skin and *in situ* measurements to understand the Raman signal obtained specific to the infection. Mice were analysed after 2 and 3 weeks of infection.

The abdominal skin region of mice was analysed by obtaining ten spectra across the skin. Each of these data sets were averaged into a single spectrum and spectrally compared to one another.

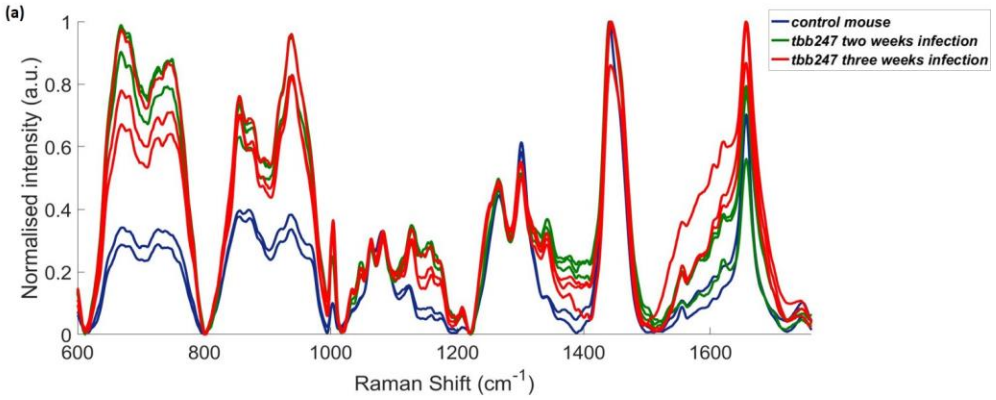

(b)

Mice samples	Estimation of parasitemia (number of parasites/mL of blood)
Two weeks infection 1	2.5×10^8
Two weeks infection 2	2.5×10^8
Two weeks infection 3	1.3×10^8
Three weeks infection 1	5×10^5
Three weeks infection 2	5×10^7
Three weeks infection 3	4×10^6

Figure 4.10 Comparison of averaged and normalised Raman spectrum of (a) two control mice (blue), three mice two weeks after infection (green) and three mice three weeks after infection (red) by T.b. brucei 247 measured on the abdominal region, with a 785 nm laser and 60 s acquisition time, (b) comparison of the estimation of blood parasitemia in mice.

As spectral differences between each state were clearly identified, it was not necessary to use a statistical tool such as PCA. Figure 4.10 showed the direct comparison of the Raman spectra obtained from uninfected and infected mice by *T.b. brucei* 247 at two time points, two and three weeks post-infection. It was notable that infected mice were easily distinguished using their respective Raman signal. The same increase in intensity as observed previously was present here. However, it did not appear that there was a clear spectral difference correlated to the length of time after infection; there was no relation between the increase in intensity of certain peaks and the time points. It appeared that there were variations between each mouse investigated, suggesting that different mice may respond to the infection differently. Raman bands specific to the infection were observed at 669 and 750 cm^{-1} (porphyrin or tryptophan), 1159 cm^{-1} (C-C/C-N stretching of proteins), 1343 cm^{-1} (CH_3CH_2 wagging) and 1379 cm^{-1} (CH3 symmetric (lipids)), which were more intense at 2 weeks post infection than at 3 weeks. One should consider that the presence of the parasites in the skin could be cyclic, as observed in the blood,[113] and that it would not be possible to observe a constant increase in the Raman bands. A cyclic presence of the parasite in the skin could also induce cyclic biological changes, which would relate to the difference in signal observed between the two time points, and these Raman bands might be associated with the presence of the parasites.

However, the Raman peak at 1657 cm^{-1} and its shoulder (1580 – 1630 cm^{-1}) and, to a lesser extent the Raman peak at 1555 cm^{-1}, were more pronounced at the late stage of the infection, which could indicate a gradual increase in their intensity according to the length of infection. Raman is then providing multiple peaks for biological information from the skin about the stage of the disease, that combined, help the detection of the infection. It was more likely that a combination of the biological changes in the tissue, as well as the presence of the parasites were measured with Raman. Some of the Raman bands, 938, 1003, 1555, 1580 – 1630 or 1657 cm^{-1} appeared to be related to the length of infection of the mouse. All specific Raman bands to infection and their tentative of assignments were grouped in Table 4.2.

Table 4.2 Tentative of assignment of the Raman bands specific to the mouse infected by T.b. brucei 247.[231–233]

Raman bands (cm^{-1})	Tentative of assignments
669	Porphyrin or tryptophan
680	Ring breathing of DNA bases
728	Ring breathing of Tryptophan
750	Porphyrin or tryptophan
856	C-C of proline, tyrosine
876	Hydroxyproline
938	C-C backbone, proline
1004	Phenylalanine
1034	Phenylalanine
1048	Proline, PO_4^{3-} stretch
1128	C-C/C-N stretching of proteins/lipids
1159	C-C/C-N stretching of proteins
1208	Tryptophan, Phenylalanine
1343	CH_3CH_2 wagging
1379	CH3 symmetric (lipids)
1555	ν (C=C) Porphyrin or Tryptophan
1580 – 1630 shoulder	Phenylalanine, Tyrosine
1657	Amide I

The Raman bands, and their associated biological information, obtained for infection with *T.b. brucei* 247 were similar to the ones identified with a *T.b. brucei* gvr35 infection during the preliminary *in situ* investigation, suggesting that the biochemical changes occurring due to the presence of *T.b. brucei* were constant. An increase in intensity related to certain amino acids was measured. Porphyrin was still detected, which could possibly suggest that the parasites crossed the blood vessel. The detection of infected animals was as successful with this strain as with the previous strain, using the same Raman shifts for detection. It appeared that the spectral

information obtained between different strains of trypanosomes was similar. This served as evidence that this method of detection could potentially be used to detect any strain of trypanosome infection.

4.4.2 Raman bands comparison between in vitro *T.b. brucei*, *ex vivo* and *in situ* skin infected by *T.b. brucei* measurements

Beside the detection ability of Raman, these results could be compared with the those obtained previously *in vitro* and *ex vivo* to have a better understanding of the information obtained. As different instruments and experimental settings were used, the spectral comparison between each spectrum cannot be performed. A qualitative analysis is shown in Table 4.3 between the Raman bands of *T.b. brucei* fingerprint obtained *in vitro* (section 3.3.3), the Raman bands that were found to be specific to the infected skin compared to uninfected in the *ex vivo* study (section 3.4.3) and the Raman bands previously found specific to infected skin *in situ*.

Table 4.3 Comparison between each Raman bands specific to the skin infection and T.b. brucei obtained with a 785 nm laser during in vitro, ex vivo and in situ experiments. Similar Raman bands between in situ mouse and T.b. brucei fingerprint are highlighted in green, and similar Raman bands between in situ mouse and ex vivo skin measurements are highlighted in yellow.

Raman peaks specific to infected mouse *in vivo* (cm^{-1})	Raman peaks specific to infected skin *ex vivo* (cm^{-1})	Raman peaks of *T.b.brucei in vitro* (cm^{-1})
669		
728		720
750		770
856	864	850
876		
938	937	956
1004		1002
1034	1020	
1048	1087	1045
1128		1091
1159		1170
1208		1247
1343	1333	1315
1379		
1555	1451	1448
1657	1668	1658

Table 4.3 regrouped the different Raman bands that were found to be specific to the infection by *T.b. brucei*. These results were difficult to compare because instrumentation used to obtain them was different which could lead to some shifts in the location of the Raman bands, but it could give an indication as to what the Raman measurement was detecting *in situ*. Furthermore, it was explained in the *ex vivo* study that spectra obtained with 785 nm were poorly resolved.

Interestingly, four Raman bands were found to be similar between mouse *in situ* measurements and *T.b. brucei* fingerprint (green). There was a slight shift observed (<5 wavenumbers), but this was to be expected from the difference in instrument used. Moreover, there were two Raman bands that were found to be similar between *in situ* and *ex vivo* skin measurements (highlighted in yellow).

Raman bands similar between *in situ* and *in vitro* experiments have been thought to be associated with certain amino acids such as phenylalanine (1004 cm^{-1}) or proline (856 and 1048 cm^{-1}) as well as to Amide I (1657 cm^{-1}) in the *in situ* measurements.[231–233] It was possible that these similarities in the Raman bands could suggest a direct influence of the parasites in the Raman signal due to its surface proteins such as VSGs. However, it was explained previously that the Raman fingerprint of *T.b. brucei* possessed a strong spectral overlap with the fingerprint of the skin, hence it was difficult to draw conclusions on these similarities and to certify that the trypanosomes were directly detected and contributing to the Raman signal of infected skin. Also, it was found in the *in vitro* experiment on the parasite that the Raman signal obtained was mainly obtained from the surface components like phospholipids and VSG. These surface components were more likely to be different than the previous study as the VSG coat was periodically replaced to enable *T.b. brucei* to adapt to a new environment: skin.[99,154] Therefore it was possible that the Raman fingerprint from the parasites in the skin was different from the parasites mounted on slides.

Differently, Raman bands at 856 and 938 cm^{-1} (proline and tyrosine) for *in situ* spectrum and 864 and 937 cm^{-1} (phosphate group, tyrosine and proline) for *ex vivo* shows some consistency in the biochemical changes observed between the two experiments. Although, Raman bands at 856 and 864 cm^{-1} were separated by more than five wavenumbers, the shape of the two peaks combined between the two spectra seemed to be preserved. It could suggest that these biological changes were detected during the *ex vivo* study and seemed to be also tracked during the *in situ* measurements.

Surprisingly, there was little similarity between *in situ* and *ex vivo* Raman bands, with only two Raman bands found in both Raman spectra. Given that the laser spot used during *ex vivo* experiments had a size of μm^2 whereas in the *in situ* it was mm^2, the information obtained would be expected to be different. In addition to the low signal to noise ratio and poor resolution obtained with 785 nm during ex vivo study, the change of instrumentation may have induced a shift in certain Raman bands, leading to the differences observed. Moreover, it was also discovered in this study that there could be some variation in the body response between mice, which could explain why the Raman bands were dissimilar.

In conclusion, Raman spectroscopy was able to detect infection by the trypanosomes in the skin of mice. The signal specific to the infection was not dependent on the strain of the trypanosomes, as signal was similar for the two strains studied. Two different time points were compared, and their respective Raman signal did not seem to be correlated with the length of infection. However, certain Raman bands such as 669 and 750 cm^{-1} (porphyrin or tryptophan), 1159 cm^{-1} (C-C/C-N stretching of proteins) and 1343 cm^{-1} (CH_3CH_2 wagging) were more intense at two weeks post infection. It could indicate that the presence of trypanosomes in the skin is cyclic, and it would be interesting to investigate how the parasites cross the blood vessels and if it led to a release of blood in the skin.

Comparison with previous data did not allow for an entire match of the findings obtained with skin *ex vivo*. Only two Raman bands were found similar here. The different instrumentation could explain this situation. Also, it was observed during the *ex vivo* experiment that the spectral resolution obtained was lower due to the CCD, and it was possible that some Raman bands were not observed previously. In addition, it was not possible to certify if the parasites were detected and directly contributing to the Raman signal of infected skin because of the strong spectral overlap between the two spectra mentioned during the *ex vivo* study and to the possible change of surface proteins of trypanosomes in the skin compared to the *in vitro* culture that could change its Raman fingerprint. Hence, the similarities in the Raman bands might have arisen from the animal's physiological response and not the parasites themselves.

4.5 Investigation of mouse infected by the human pathogen *T.b. gambiense*

4.5.1 Spectral differences between mice infected by *T.b. gambiense* compared to uninfected

T.b. gambiense primarily infects humans and is the main cause for HAT. However, some animal infections by *T.b. gambiense* have been reported in pigs in Africa,[31] suggesting that it was possible to infect mice with this sub-species in order to test the Raman diagnostic method on a human pathogens. It was not known whether *T.b. gambiense* present in pigs could be transmitted and infect humans, but it could provide an understanding of its influence on the biochemical changes

in the skin.[31] Mice were infected with this parasite and the information obtained with Raman spectroscopy would define whether the infection could still be detected in the skin, and if the response was similar to *T.b. brucei* infection.

Mice were infected with *T.b. gambiense*, of the strain TOBO, but due to the inability to infect animals, the concentration of parasites in the blood was only increased after a few weeks. The three infected mice were analysed after six, seven and eight weeks post infection respectively, which is much longer than the infection time of *T.b. brucei*. There were no parasites found in the blood on the day of the analysis, but the spleen of the three mice were enlarged, suggesting that the mice were still infected with the trypanosomes. Indeed, hosts infected by *T.b* displayed an increase in the size of their spleen.[270,271] The visual observation and counting of trypanosomes in a drop of blood with a microscope, blood parasitemia,[266] provided values that corresponded to the logarithmic values of the estimated concentration. Hence, when no parasites were observed, like in this case, it gave a blood parasitemia of zero, however, it indicated that the concentration of parasites in the blood was lower than 1.0×10^4 parasites/mL, and not zero.[266] The same method used for *T.b. brucei* detection was applied and the spectra obtained from each mouse were averaged into a single Raman spectrum and normalised to the highest peak intensity to be compared.

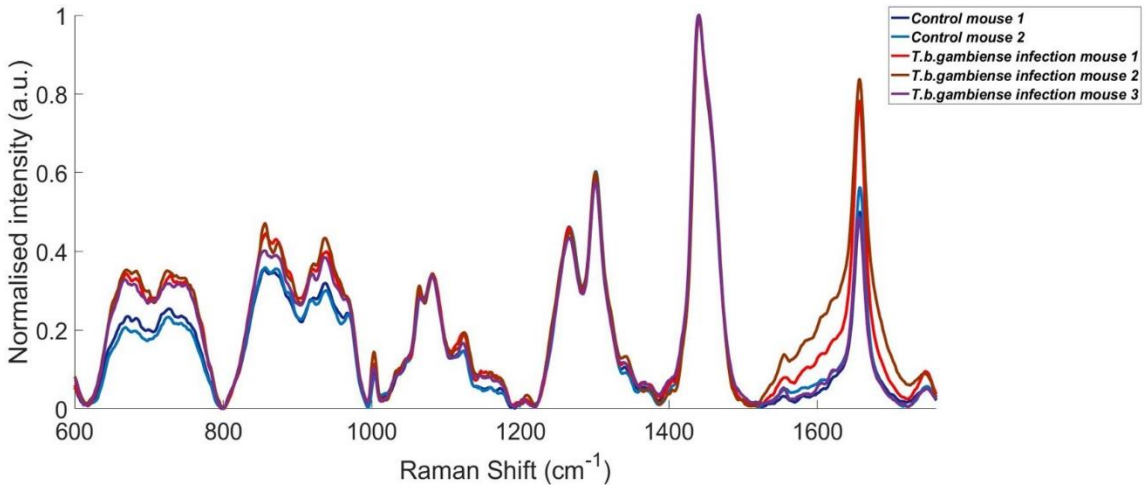

Figure 4.11 Comparison of averaged and normalised Raman spectra obtained from uninfected (dark and light blue lines) and infected (red, brown and purple lines) mice by T.b. gambiense, respectively analysed at six, seven and eight weeks post-infection, measured on the abdominal region, with a 785 nm laser, 45 mW and 30 s acquisition time.

The infection of the mouse by the parasites was still detectable with Raman spectroscopy as an increase in intensity was noticed on certain Raman bands (Figure 4.11). These increases at specific frequencies were similar, but less pronounced, to those observed previously with a *T.b. brucei* infection.

The Raman bands specific to the infection were found at 670 cm^{-1} (porphyrin or tryptophan), 728 cm^{-1} (tryptophan), 750 cm^{-1} (porphyrin or tryptophan), 856 cm^{-1} (C-C of proline, tyrosine), 874 cm^{-1} (hydroxyproline), 937 cm^{-1} (C-C backbone, proline), 1003 cm^{-1} (phenylalanine), 1126 cm^{-1} (C-C/C-N stretching of proteins/lipids), 1159 cm^{-1} (C-C/C-N stretching of proteins), 1208 cm^{-1} (tryptophan or phenylalanine), 1343 cm^{-1} (CH_3CH_2 wagging mode), 1555 (ν(C=C) porphyrin or tryptophan) and 1657 cm^{-1} (Amide I).[231–233] These Raman bands were similar to those obtained previously with a *T.b. brucei* infection. A more pronounced shoulder for the peak at 1657 cm^{-1} (1580 – 1630 cm^{-1}) was also observed, which was thought to be associated with phenylalanine and tyrosine. The infection with *T.b. gambiense* appeared to trigger the same biological changes in the skin. The Raman bands related to certain amino acids such as tryptophan, proline and phenylalanine, as well as porphyrin, displayed an increase in intensity. However, some spectral differences obtained previously were not as intense for certain peaks such as 1128, 1159, 1208, 1343 and 1379 cm^{-1} for example, when some Raman bands are absent such as 1034 and 1048 cm^{-1}. These spectral variations, whether there were related to a small shift in the peak, to a lower

intensity or to an absence of certain Raman bands, between the infection with different sub-species could indicate that a discrimination between was achieved with Raman. However, as shown by the blood parasitemia, it appeared that *T.b. gambiense* was less virulent in animals than *T.b. brucei*, suggesting that biological changes might not be as intense. The low parasitemia could indicate a low or no presence of the parasites in the skin, and any biochemical reactions from the host or influenced by the parasite itself would be reduced, hence the less pronounced spectral variations. Nonetheless, certain Raman bands described previously were present and more intense than the control spectra, suggesting that the detection was still achievable. It was thought that the Raman signal specific to the infected would be in correlation with the number of parasites present in the skin, as more parasites would have a stronger influence on the skin and led to more biological changes, as observed for *T.b. brucei*.

4.5.2 Spectral comparison between *T.b. brucei* and *T.b. gambiense* infection

It was shown that Raman was able to detect the infection of mice with the human pathogen *T.b. gambiense*. The spectral identification of the infection was identical to the infection by *T.b. brucei*, but were less intense than for *T.b. brucei* infection, suggesting that the Raman signal could be related to the amount of trypanosomes present. Raman measurements from both infections are compared below to understand these differences.

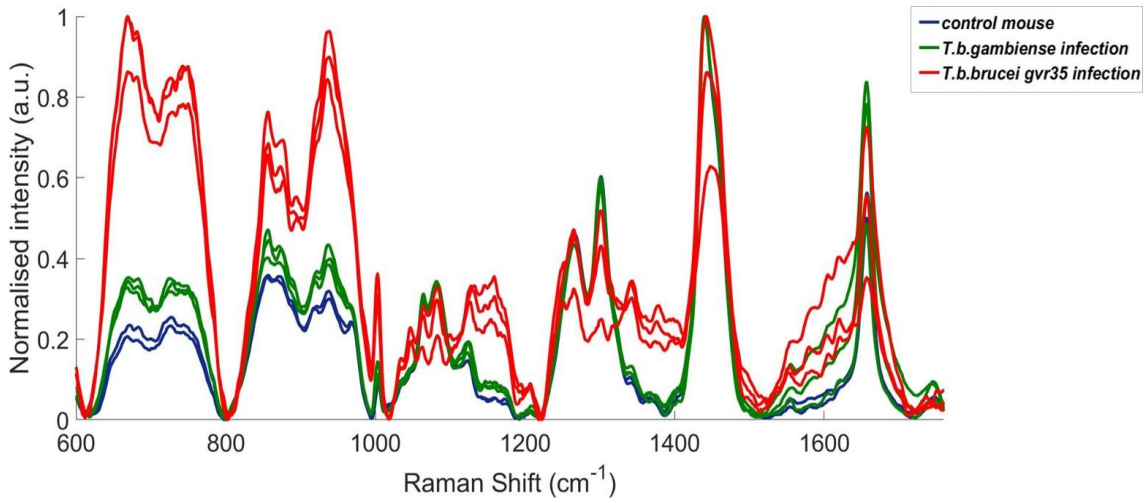

Figure 4.12 Comparison of averaged and normalised Raman spectra of uninfected mice (blue lines) and T.b. brucei gvr35 (red lines) and T.b. gambiense (green lines) infected mice measured on the abdominal skin, with a 785 nm laser, 45 mW and 30 s acquisition time.

The Raman spectral information obtained from two different sub-species was compared in Figure 4.12. The mice infected with *T.b. brucei* gvr35 were analysed at three weeks post-infection, whereas *T.b. gambiense* was analysed six weeks, or more, post-infection. Due to the ability of *T.b. brucei* gvr35 to cross the blood brain barrier at an early stage of the infection, it was assumed that the number of parasites in the skin was likely greater than *T.b. gambiense*, even at these time points.

Raman bands specific to the infection increased gradually from uninfected, to *T.b. gambiense* infected and then *T.b. brucei* infected mice. A qualitative analysis of a small area of the mouse skin by immunohistochemically staining the parasites with a specific antibody anti-ISG65 revealed that no parasites could be observed in the skin for *T.b. gambiense* infection, whereas *T.b. brucei* were found in the skin. This was a visual observation of a small portion of skin, and some parasites may have been miscounted or be present in a different area of the skin but it demonstrates that *T.b. brucei* was present at high concentration in the mouse skin, whereas a low amount or no *T.b. gambiense* was noted. Hence, the difference in the relative intensity between the two sub-species seemed to correlate to the number of parasites present in the skin. A higher concentration of parasites induced a stronger biological response from the host and *T.b* also altered the skin composition more through its metabolism, which could relate to a stronger increase in intensity for Raman bands specific to the *T.b. brucei* infection.

It was not clear and confirmed that Raman was able to directly detect the parasite in the skin, but it seems that the Raman bands specific to the infection were correlated with the number of parasites in the skin. Moreover, the Raman band changes following infection were similar between the two sub-species, indicating that most of the changes in Raman signal observed was coming from the biological changes induced in the skin, rather than a direct detection of the trypanosomes. Hence, the detection method did not seem to be specific enough towards the trypanosome sub-species in order to identify which *T.b* was infecting a host. However, it was interesting to consider what type of information was manifested in the Raman spectra: a response from the host such as an immune response, or several parasites detected in the skin for example.

4.6 Investigation of the biological changes contributing to the spectral differences in the infected Raman signal

It has been shown that Raman spectroscopy was able to differentiate infected from uninfected mice by taking measurements on their abdominal skin. Since the spectral differences observed were very clear and the detection technique seemed to be reliable, it was important to understand the source of the spectral differences whether the parasites were directly contributing to the Raman signal or if a biological response from the host, or a biochemical change induced by the parasites was responsible for the Raman spectral differences.

4.6.1 Examination of the contribution of trypanosomes in the skin to the Raman signal specific to the infection

4.6.1.1 Comparison between mice infected by T.b. brucei 247 and gvr35

The infection of the mice was performed with two different strains of *T.b. brucei*: 247 and gvr35. It was previously thought that *T.b. brucei* gvr35 would be present in a higher concentration in the skin than *T.b. brucei* 247. Although the same spectral differences were observed with the two type of infection when compared to uninfected mice, a direct comparison coupled with a

measurement of the number of parasites present in the skin could give an indication whether the biological information obtained with Raman was directly related to the presence of the parasites.

Table 4.4 Semi-quantitative measurements by immunohistochemically stained trypanosomes to determine the number of parasites present in the skin of uninfected and infected mice. Total number of extravascular parasites are highlighted in blue for controls, red for T.b. brucei gvr35 and green for T.b. brucei 247.

mouse ID	Infection time		HPF-1	HPF-2	HPF-3	HPF-4	HPF-5	HPF-6	HPF-7	HPF-8	HPF-9	HPF-10	total
C1	N/A	intravascular	0	0	0	0	0	0	0	0	0	0	0.00
		extravascular	0	0	0	0	0	0	0	0	0	0	0.00
C2	N/A	intravascular	0	0	0	0	0	0	0	0	0	0	0.00
		extravascular	0	0	0	0	0	0	0	0	0	0	0.00
GVR35 I1	Day 14	intravascular	1	0	1	0	0	0	0	1	0	0	3.00
		extravascular	0	0	0	0	0	1	1	1	0	0	3.00
GVR35 I2	Day 14	intravascular	0	0	0	1	1	0	0	0	0	0	2.00
		extravascular	1	1	1	1	0	1	0	0	0	1	6.00
GVR35 I3	Day 14	intravascular	0	0	0	0	0	1	0	0	0	1	2.00
		extravascular	1	1	2	1	1	1	2	2	1	2	14.00
247 I1	Day 14	intravascular	1	1	2	1	1	1	1	2	1	1	12.00
		extravascular	1	0	0	0	0	1	0	0	0	1	3.00
247 I2	Day 14	intravascular	1	1	1	1	2	2	1	1	1	2	13.00
		extravascular	0	0	0	0	0	0	0	0	1	1	2.00
247 I3	Day 14	intravascular	0	0	1	0	0	0	1	1	1	1	5.00
		extravascular	1	1	1	1	1	1	1	1	1	1	10.00

Table 4.4 showed the semi-quantitative measurements of the number of parasites present in the skin of mice. After the Raman measurements, a small area of the skin was removed to be analysed by microscopy. An antibody, anti-ISG65, was used to target the trypanosomes present in the sample. This immunostaining targeted the invariant surface glycoprotein (ISG) 65 that was present in all the *T.b*. The observation of the sample and parasite counting were made by eye, and ten different areas of the sample were investigated to provide a better representation of the presence of the parasites in the skin. Measurements were semi-quantitative as the exact number of trypanosomes was not reported. Instead, an ordinal score was used to assess the presence of trypanosomes in the skin, where 0 showed no presence of parasites, 1 showed low number of parasites (<20 trypanosomes) and 2 showed a moderate number of parasites (20 – 50 trypanosomes). Two different locations within the skin were investigated, the intravascular and extravascular regions.

It could be observed in Table 4.4 that the number of parasites present in the system was variable between the type of infection (strains used) and between each mouse. The data showed that

mice infected by *T.b. brucei* gvr35 possessed more parasites in their skin than in the blood vessel. However, mice infected by *T.b. brucei* 247 generally had more parasites in their system, by combining intravascular and extravascular data. This suggested that these two different strains act differently in mice.

The data obtained from Raman measurements on the abdominal skin of two weeks infected mice with these two different strains can be compared, which would provide information as to whether the number of trypanosomes in the system influenced the Raman signal obtained. Ten spectra were obtained across the abdominal region of two uninfected and three infected mice for each strain at two weeks post-infection, and with a 60 s acquisition time. These measurements were then averaged into a single Raman spectrum for each mouse and normalised to the highest peak before being analysed.

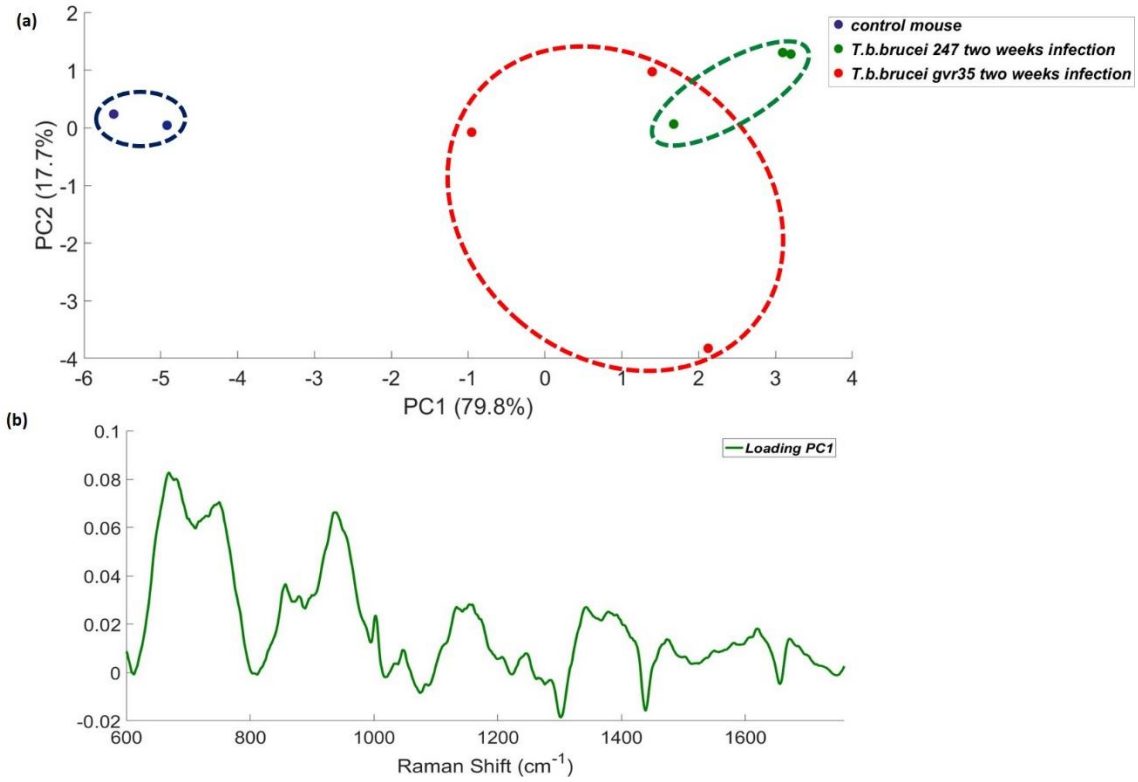

Figure 4.13 Principal component analysis of averaged and normalised Raman spectra of uninfected versus two weeks infected mice by T.b. brucei 247 and T.b. brucei gvr35 (circled for clarity) measured on the abdominal skin, with a 785 nm laser, 45 mW and 60 s acquisition time: (a) PCA scores plot PC1 vs PC2, (b) PC1 loading spectrum.

When both infections were compared statistically, it first appeared that the infected mice were well separated from the uninfected mice across PC1 on Figure 4.13.a). The differentiation was quite clear, and it could also be observed that both types of infection could be separated into two groups, circled in red for *T.b. brucei* gvr35 infection and in green for *T.b. brucei* 247 infection. Mice infected by *T.b. brucei* 247 appeared further separated from mice infected by *T.b. brucei* gvr35. Using data provided by Table 4.4, it was known that more parasites were present in the host, both intravascular and extravascular measurements, in the mice infected by *T.b. brucei* 247; it was possible that the Raman bands explaining this differentiation were directly related to the number of trypanosomes. Figure 4.13.b) provides the Raman bands specific to the differentiation of the two types of infection, and they were matching those obtained previously for the differentiation of uninfected and infected mice, as reported in Table 4.2. This showed that the increase in intensity of these Raman bands was related to the number of trypanosomes present in the mouse, but it did not correlate with the number of parasites found in the skin. These results tend to confirm the previous observation, that the detection technique was not specifically discriminating *T.b. gambiense* from *T.b. brucei* but was measuring the amount of biological variations induced by their presence, hence correlating to their number.

An intra-dermal injection of trypanosomes can be performed to investigate the relation between the Raman measurements and the number of parasites present, as well as their possible direct contribution to the Raman signal specific to the infection.

4.6.1.2 Intra-dermal injection of trypanosomes in mouse

Concentrated solution of parasites in serum were injected intra-dermally in an uninfected mouse. This injection formed a blister on the dorsal skin, where Raman measurements were taken, and compared with a normal skin signal. This investigation was performed to help understand whether the Raman bands specific to the infection were related to the number of trypanosomes present in the skin. It would also show whether the Raman signal from trypanosomes was contributing to the Raman spectrum from the mouse. In addition to the blister measurements, two types of control spots were measured for this experiment. First, measurements were performed on an area of the uninfected skin. Second, a solution of serum with no parasites was injected in the skin. Serum contains a certain amount of proteins, and it

was important to compare it to the serum containing trypanosomes. This experiment allowed the removal of the biological response from the host by injecting directly the trypanosomes in the skin. The injection of serum and trypanosomes were made in the dorsal region, as the skin is thicker and made the injection easier. Three Raman spectra were obtained for each spot: one control skin, two control serum blisters and two trypanosomes blisters; with a 60 s acquisition time. The three measurements were then averaged into a single Raman spectrum, representing each location, and normalised before analysis.

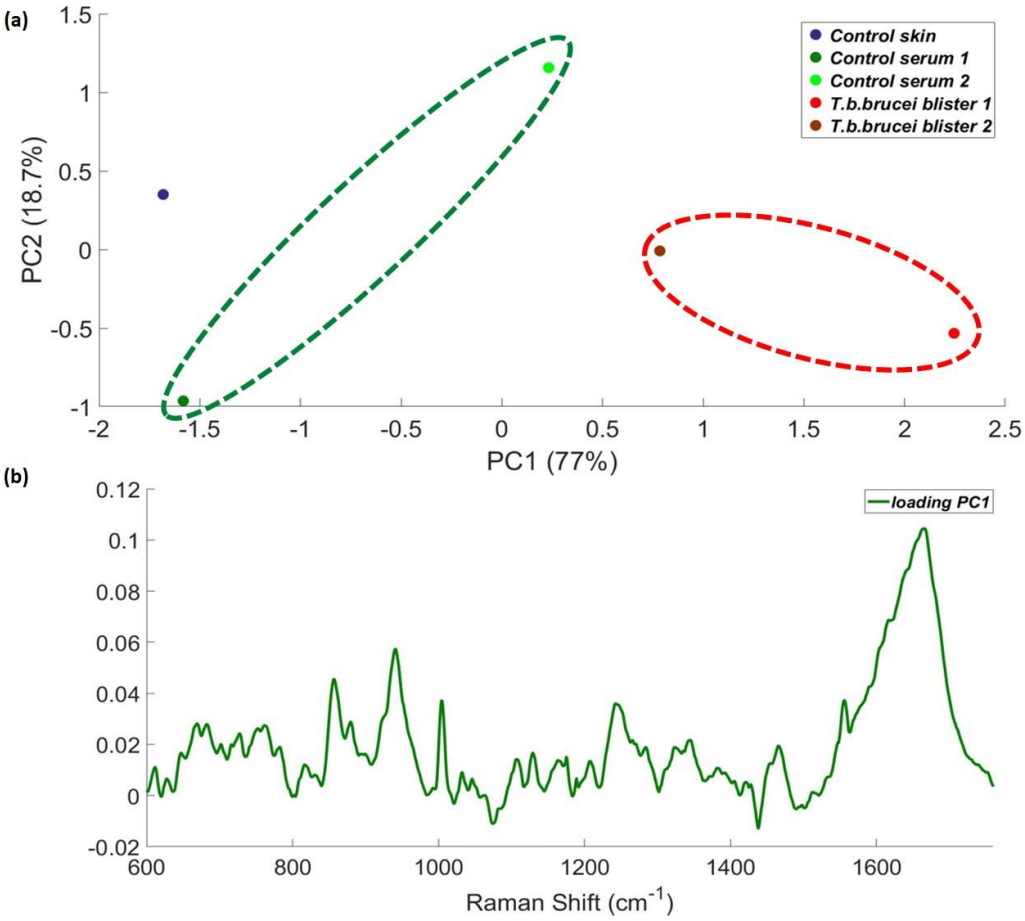

Figure 4.14 Principal component analysis of averaged and normalised Raman spectra of normal skin (blue) and blisters formed of serum (dark and light green) and serum containing trypanosomes (red and brown) on the dorsal skin, measured with a 785 nm laser, 45 mW and 60 s acquisition time: (a) PCA scores plot PC1 vs PC2 (serum and T.b. brucei blisters are circled for clarity), (b) PC1 loading spectrum.

Figure 4.14.a) provided the scores plot for the comparison of the biological composition of the skin and blisters. Two repeat injections were performed for the normal serum and the serum containing trypanosomes due to the difficult nature of this technique. Indeed, the liquid injected might not have remained stable, and may have readily dispersed into other body parts. It could be observed that the blisters containing parasites were clearly differentiated across PC1. Blisters containing normal serum were also separated from the skin measurement. This gradual separation from normal skin, to normal serum and to serum containing parasites could be explained by the increasing prevalence of proteins in the skin.

The Raman spectral differences seemed to be associated with an increase in the amount of proteins, which was related to an increased number of trypanosomes in the blisters. Figure 4.14.b) displayed Raman bands specific to the discrimination located at 857, 880, 941, 1004, 1242, 1345, 1555 and 1666 cm^{-1} with also the shoulder of the last peak more pronounced in the region 1580 – 1630 cm^{-1}. These Raman bands were similar to previous investigations for mice infection (Table 4.2), with a slight shift for some peaks. These Raman bands were thought to be associated with amino acids like proline, tyrosine, tryptophan or phenylalanine and amide bonds in proteins. It appeared that the discrimination correlates with an increasing concentration of such biological components in the blisters. To a lesser extent, the Raman bands at 669, 728, 753, 1046, 1129 and 1208 cm^{-1} were also found in the loading spectrum of PC1 and were also responsible for the discrimination of infected mouse skin previously.

The increase of protein concentration through the different samples could be linked to the proteins contained in the serum but also those on the surface of the trypanosomes. The discrimination observed between control serum and serum containing trypanosomes could be explained by an increase in number of proteins from the surface of the parasites. The Raman bands obtained here cannot certify that the trypanosomes were specifically detected, as it seems to be related to protein concentration. As the Raman bands explaining the discrimination of the blisters were similar to those obtained for the detection of parasite infection in mice, it was possible that the increase in intensity of these peaks observed previously correlated with the presence of parasites in the skin, through the detection of their surface proteins.

Combining this result with the investigation of the number of parasites in the skin between *T.b. brucei* 247 and gvr35 indicated that the Raman detection of the mouse infection was linked with

the detection of trypanosomes in the host associated with biochemical changes in the skin induced by the presence of the parasites. Indeed, it was shown that the number of parasites present in the host intravascular and extravascular areas influenced the Raman signal obtained. Due to the lack of a specific Raman bands for *T.b. brucei*, different from the skin, it could not be certified that the parasite itself was contributing to the Raman signal of the infected mice or quantify it. In addition, amino acids or proteins found on the surface of trypanosomes could also be observed in skin biological composition, which did not help for a direct identification of the contribution of trypanosomes in the Raman signal. Hence, it was more likely that the spectral differences observed in the infected mice were correlated with an increased concentration of proteins/lipids, possibly through the VSG surface coat of the parasites, resulting of a combination between the number of trypanosomes present in the host, and their influence on the skin matrix due to their metabolism, and a biochemical response from the host due to the infection.

4.6.2 Investigation of the immune response contribution to the Raman signal specific to the infection

It has been shown that the spectral differences observed in the Raman spectrum of an uninfected and infected mouse can be related to the increased number of parasites in the host extravascular and intravascular areas, as well as a biochemical response from the host due to the infection. Some of the Raman bands could be associated with a response from the mouse related to the infection. In order to investigate the potential influence of host response in the detection of sleeping sickness, a genetically modified mouse was infected with *T.b. brucei*. Specific mice, called NOD scid gamma (NSG) mice, were developed in laboratory to be immunodeficient. When infected by parasites, there would be no immune response from these mice, which might influence the Raman signal obtained. This experiment gave a better understanding of the possible immune response detected with Raman measurements.

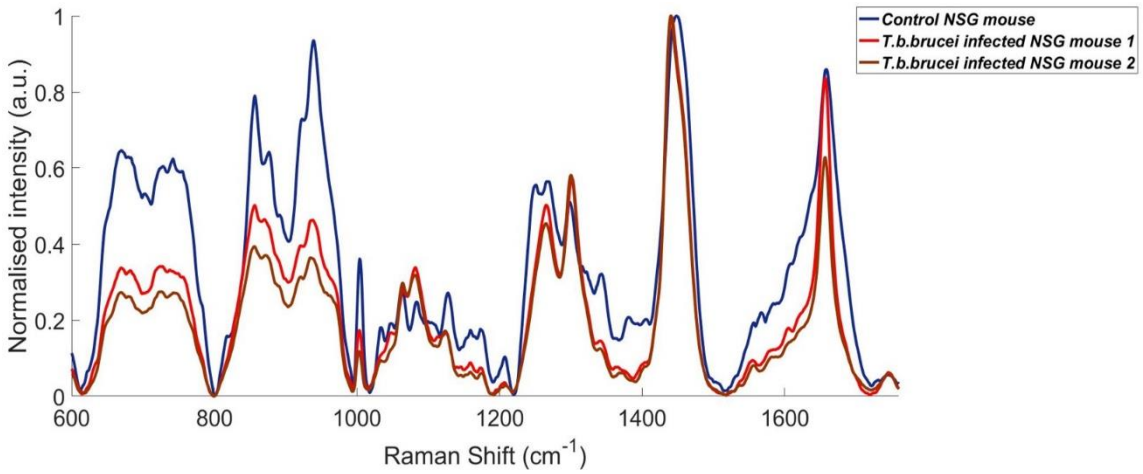

Figure 4.15 Comparison of averaged and normalised Raman spectra obtained from uninfected (blue lines) and infected NSG mice (red and brown lines) measured on the abdominal skin region, with a 785 nm laser and 30 s acquisition time, 45 mW.

The Raman measurements were made as previously described. Five spectra were obtained across the abdominal skin region, then averaged into a single Raman spectrum and normalised for comparison. Figure 4.15 shows the spectral comparison for the infection of immunodeficient NSG mice. It appeared that the signal differences obtained here showed an opposite trend compared to those observed previously for the infection of BALB/c mice. Indeed, a reduction of Raman peak intensity was noticed instead of an increase. This was intriguing as the same Raman bands that were specific to the mouse infection before were here found to be related with the control NSG mouse. The trend in the change of signal was difficult to interpret, as the presence of trypanosomes should increase, or at least slightly increase the intensity of previous Raman bands, and not reduce the signal associated with previous measurements with trypanosomes. NSG mice are very expensive and this experiment could not have been repeated to confirm the results. The low numbers of mice used for this experiment did not allow a conclusion on the involvement of the immune response and comparison with previous investigations to be made.

It was difficult to draw conclusions related to the immune response influence on the Raman signal in an infected, immunocompromised mouse. However, it was possible that this host's response could potentially be measured with Raman, as well as the number of trypanosomes present, because of the change of signal observed with infected NSG mice. This reduction of signal may indicate that the immune response contributes to the Raman spectra observed. It was possible that this reduction in intensity is related to the metabolism of the parasites. Indeed,

parasites might metabolise surrounding proteins or lipids for their proliferation, which could induce a drop in their concentration. Previous increase in intensity in the Raman signal, could then be related to the immune response from the host, which by producing proteins to clear the parasites induced an increase of concentration of overall proteins in the skin.

This effect was also investigated in a different way by verifying if skin inflammation could also contribute to the Raman signal obtained in the infected mice skin. In a previous study, it was found that trypanosomes in the skin led to mild inflammation.[156] The skin samples previously stained to measure the number of parasites present in the skin for the two weeks infected mice with *T.b. brucei* 247 and *T.b. brucei* gvr35 were also analysed for the presence of immune cells. The inflammation score was measured semi-quantitatively, as performed previously for the number of parasites in the extravascular and intravascular region.

Table 4.5 Semi-quantitative measurements of the skin inflammation present in uninfected mice and mice infected by T.b. brucei 247 and T.b. brucei gvr35, and T.b. brucei infected NSG mice, at two weeks post-infection.

mouse ID	Infection time	HPF-1	HPF-2	HPF-3	HPF-4	HPF-5	HPF-6	HPF-7	HPF-8	HPF-9	HPF-10	total	average	SD
Control mouse #1	N/A	1	1	1	0	1	0	0	0	0	0	**4.00**	0.40	0.52
Control mouse #2	N/A	0	0	0	0	1	1	0	0	0	0	**2.00**	0.20	0.42
T.*b.brucei* gvr35 #1	Day 13	0	1	0	0	1	0	0	0	0	0	**2.00**	0.20	0.42
T.*b.brucei* gvr35 #2	Day 13	0	0	0	1	1	0	0	0	0	1	**3.00**	0.30	0.48
T.*b.brucei* gvr35 #3	Day 15	1	0	0	0	0	0	0	0	0	0	**1.00**	0.10	0.32
T.*b.brucei* 247 #1	Day 13	0	0	1	0	0	1	0	0	0	0	**2.00**	0.20	0.42
T.*b.brucei* 247 #2	Day 13	0	0	0	0	0	0	0	0	0	0	**0.00**	0.00	0.00
T.*b.brucei* 247 #3	Day 14	1	1	0	1	1	1	0	0	0	0	**5.00**	0.50	0.53
T.*b.brucei* NSG mouse #1	Day 13	0	0	0	0	0	0	0	0	0	0	**0.00**	0.00	0.00
T.*b.brucei* NSG mouse #2	Day 14	2	0	0	0	0	0	0	0	0	0	**2.00**	0.20	0.63

Each skin sample was stained with Haematoxylin and Eosin (HE) stain to measure the number of inflammatory cells present in the skin. Ten different areas of each samples were investigated to have a better representation of the skin inflammatory response. This method was semi-quantitative, and each measurement was represented by either 0 (absent or only rare leukocytes present), 1 (mild inflammation – low numbers of mixed inflammatory cells present) or 2 (moderate – moderate numbers of mixed inflammatory cells). Table 4.5 grouped the measurement for the control and infected mice. Surprisingly, there was no difference in inflammation state between control and infected skin. Control skin samples were already inflamed before the infection by the parasites, and infected skin did not show an increase in

concentration of inflammatory cells in the presence of trypanosomes. This suggested that the spectral differences observed in the Raman spectra between control and infected BALB/c mice were not influenced by the inflammatory response from the mouse. The detection method was therefore specific to sleeping sickness, as it would be related to the number of trypanosomes in the host, and not a general inflammatory response from the host that could be caused by any disease. Also, infected NSG mice, which were immunodeficient, showed one small area where some inflammatory cells were found, which was difficult to explain, as they should not have such immune response. Moreover, there seemed to be variations in the inflammation state between infected mice, as observed previously with the number of parasites, which could result from mice to mice variations between their biological response during infection and could explain some spectral variations between mice observed previously.

According to this investigation, Raman signal seemed to only be related to the number of trypanosomes present in the host. It is difficult to interpret and conclude on the results obtained with NSG mice, but the spectral differences observed could indicate that immune response contributed to the Raman spectral changes. It would be interesting to repeat this experiment with a larger number of mice. Nonetheless, inflammatory cells in the skin due to the presence of trypanosomes did not influence the Raman signal specific to the infection, which indicated that the detection of sleeping sickness in the skin was specific. However, H&E stained measures general inflammation response in the skin. It is possible that the presence of trypanosomes in the skin induced a more specific immune response, as suggested by the experiment with NSG mice, like the presence of antibodies or macrophages, that could be detected by Raman. This would require a different and specific method for measurement.

Other possible interactions of trypanosomes with the host should be investigated such as the use or release of certain biological components in the host. Their measurements could provide more information on the biochemical changes that were occurring in the skin, and also could confirm whether the number of parasites in the host was the only contributing factor. Indeed, the presence of parasites in the system could also disturb the production of certain molecules and proteins, which could influence the spectral differences observed in the infected spectrum. It has been found that trypanosomes were able to use lipids from their host such as fatty acids

and phospholipids for their growth.[154,243] It would require much further investigation to identify the components involved, and how to measure any change.

4.6.3 Conclusion

The detection of sleeping sickness in mice *in situ* was successful, as Raman spectral differences were observed between uninfected and infected mice. It was, however, interesting to understand what drives these spectral changes at a biological level as it would determine whether the detection method was specific to sleeping sickness.

According to experiments performed to investigate the spectral changes, it was observed that the number of trypanosomes present in the host, in the extravascular and intravascular area, was related to the increase in Raman signal related to the infection. The intra-dermal injection of parasites confirmed these findings, as some Raman bands that were used to detect the infection were also found to be present in the measurements of serum containing parasites, at a higher extent than in the normal serum. This finding demonstrated that Raman spectroscopy was able to inform the number of parasites, through an increased concentration of proteins, present in the host, which makes the detection method specific to sleeping sickness. However, the infection of mice with *T.b. gambiense* displayed no parasites in the blood or in the skin, and the increase in intensity of Raman bands was similar to those obtained with *T.b. brucei*. This suggested that, in addition to the number of parasites, a specific biochemical change induced by the infection was detected such as an immune response or a host response. It could also demonstrate that the parasites were not directly detected, as suggested by the intra-dermal injection, but that the biochemical variation induced by the parasite infection was proportional to the number of parasites located in the skin or blood. This would explain why the spectral differences observed with *T.b. gambiense* were identical but less intense than for *T.b. brucei*.

It was known that the presence of parasites in a body triggers several immune responses from the host.[114] Semi-quantification of inflammatory cells in the skin did not show any progression of inflammatory response during the infection. The same response was also present in the control skin and the differentiation between control and infected mice with Raman was not affected by the presence of such cells in the skin. The use of immunodeficient mice was inconclusive, as

spectral differences were observed with infected skin, but the intensity trend was the opposite of what was found with non-immunodeficient mice. However, it was possible that it was indicating a role of the immune response of the host in the Raman signal of infected mice. The reduction in intensity observed could be related to the lack of immune response, indicating a lower release of biological components in the host. Hence, the measurements would relate to the metabolism of the surrounding skin matrix by the parasites, leading to a drop in the concentration. It was reported that specific immune response such as an increased concentration of IgM is related to the infection by T.*b*,[272] and could contribute to the Raman signal. It would be interesting to determine and quantify such response from the host in addition to the use of NSG mice. Further analysis should be performed such as inducing skin inflammation or studying a different skin disease in order to assess the specificity of this detection method.

The increase in intensity of Raman bands have been discussed previously, and it was possible that parasites induced an up-regulation in the release of biological components such as lipids for their proliferation. Different biological changes could also be induced and detected by Raman spectroscopy due to the interaction of trypanosomes with biological components from the host. Parasites were able to release soluble form of their surface membrane coat, VSG, into the system in order to regulate the immune response.[273] This release of large proteins from the parasite could also be detected by Raman in the skin, resulting in the increase in intensity of Raman bands observed. Interestingly, the release or use of lipids/proteins, VSG, catabolites or amino acids may be proportional to the number of trypanosomes present in the host. It would confirm the previous finding where mice with more parasites in the overall extravascular and intravascular area were more discriminated. Moreover, parasites also required nutrients from their host, and were able to regulate their production to use them for their growth. For example, polyamine synthesis could be up-regulated by the host, as they were essential for the growth of trypanosomes within the system.[274] Other nutrients could be of interest, such as glucose and certain amino acids,[262,264,275] iron/heme[276,277] and fatty acid.[154] Such increase of synthesis could be measured with Raman spectroscopy, and could explain some of the spectral differences observed between uninfected and infected skin in the Raman spectra.

It was very challenging to identify the biological changes induced by the parasites in the skin. Most of the studies performed on the metabolic process of *T.b* was done in the bloodstream, but

it was demonstrated that trypanosomes in the skin were different from this form.[154] Parasites could adapt to a new environment and use different components for their growth and metabolism and it was possible that the biological changes observed in the bloodstream could be different than in the skin, due to different nutrients used or metabolism.[251,278] This finding being very recent, the interaction of the parasite with the surrounding skin matrix was not well understood yet. Additional analytical methods such as fluorescence spectroscopy would be required to support the observations made by Raman spectroscopy. The investigation for the biological changes induced by the presence of the parasites in the skin needs to be further pursued. It was important to assess the specificity of the detection technique towards sleeping sickness. Nonetheless, Raman spectroscopy was successfully used for the detection of mice infected by *T.b. brucei* and *T.b. gambiense*.

4.7 Relation between the biological variations induced by the parasite and time of infection of mice infected by *T.b. brucei*

A time study experiment was performed to track the evolution of the infection with Raman spectroscopy. It helped shed light on how the skin was affected by the presence of the parasites and helped determine the rate at which the infection spreads. This investigation also allowed us to obtain preliminary data on how early this method could detect the infection. It was important to understand how early the infection could be detected.

This experiment was performed in the same way as before, but a different type of mouse was used: mouse C57/Black6J. This mouse has black hair instead of white like for BALB/C mouse. This change helped us understand whether the black pigment on the skin could affect the Raman detection of sleeping sickness.

Mice were culled at different time points after the infection, and Raman spectra were obtained from their abdominal skin. Five measurements were made across the skin area and averaged into a single Raman spectrum and normalised prior analysis with PCA.

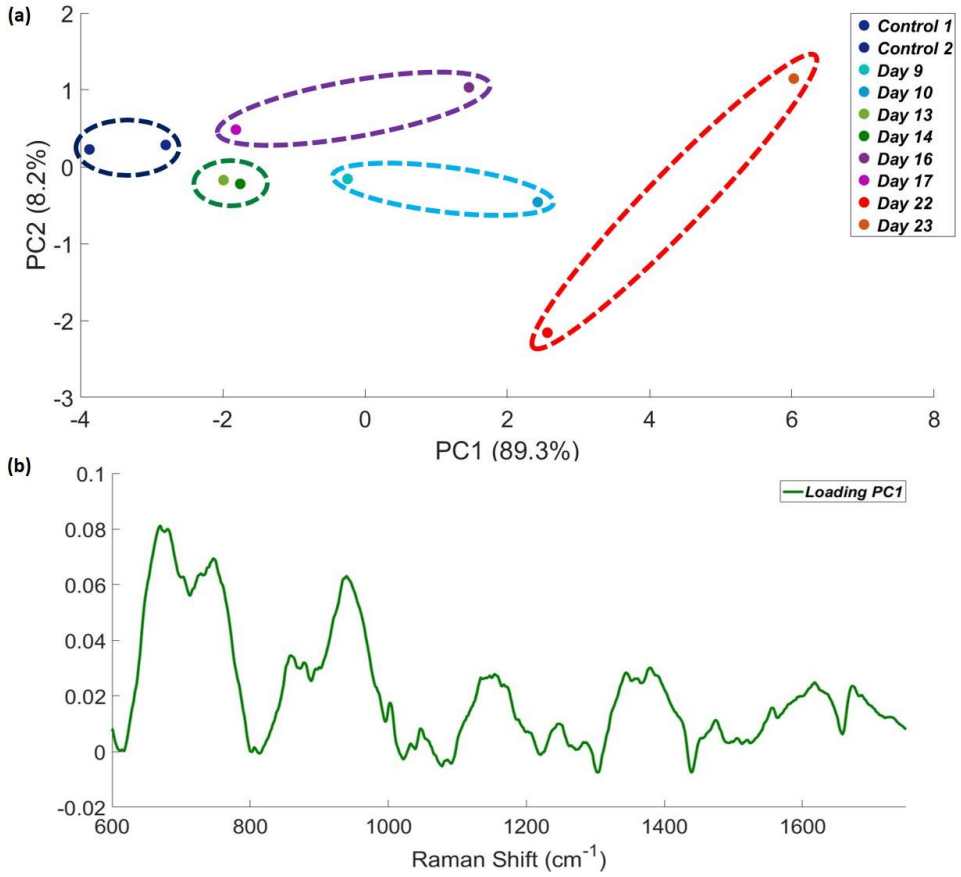

Figure 4.16 Principal component analysis of averaged and normalised Raman spectra measured at different time post-infection from the abdominal skin of C57/Black6J mice measured with a 785 nm laser, 45 mW and 30 s acquisition time: (a) PCA scores plot PC1 vs PC2, (b) PC1 loading spectrum.

It can be observed in Figure 4.16.a) that the black pigment in the skin did not affect the Raman measurements. The scores plot still showed a differentiation between infected and uninfected skin across PC1. The detection of the infection was still reliable with Raman spectroscopy. Measurements were performed at different post-infection time points but close analysis days, such as day 9 – day 10 for example, were circled for clarity. Infected mice were discriminated from the control mouse and it seemed that the spectral variation, hence biological changes, were cyclical through the time of infection, as suggested previously. For example, day 9 – day 10 were more differentiated than day 13 – day 14, suggesting variations within the biological composition of the skin, ending with a strong discrimination at a late stage of infection. Slight variations also occurred between analysis performed within 24h. It is possible that *T.b. brucei* influence on the

host could vary between animals. It would be interesting to increase the number of replicates to obtain an average response from mice.

The same Raman bands observed previously (Table 4.2) were still present in Figure 4.16.b) and played a role in the discrimination of the infected mice throughout the infection time. Interestingly, it appeared that there was a variation in the signal depending on the post-infection time point. According to the scores plot, the early time of infection (day 9 and 10) and the longest time of infection (day 22 and 23) were more separated from the control skin. Whereas middle time points (day 13, 14, 16 and 17) were closer to the uninfected cluster. This suggested that perhaps the presence of trypanosomes and the biological changes induced by their presence in the skin were cyclical, as observed in the blood.[113] The Raman intensity was varying through time, but was still different compared to the control mice. This infection cycle in the skin, as well as the spectral variations obtained, could be linked to the action of the immune system to eliminate the parasite, reducing their numbers. In addition to the response from the host's immune cells, trypanosomes were able to interact with the immune response and to control their proliferation through the release of chemical components such as VSG or indolepyruvate, by the parasites at high blood infection peak, as mentioned before.[264,273]

This cycle observed in the blood was most likely occurring in the skin as well. Raman spectroscopy was able to follow the evolution of the disease according to Figure 4.16.a). The biological information obtained could either be measuring the number of parasites in the skin, the immune response or the release of chemical molecules by the parasites, as each of these responses appear to be cyclical. Even at an infection trough, Raman could still detect the infection in mice.

4.8 Comparison of the Raman detection method with current detection techniques

Most of the current detection methods for sleeping sickness such as CATT test and PCR were based on blood analysis.[135,279] With the use of Raman spectroscopy, analysis of the skin has been shown to hold potential as a new approach for the detection of sleeping sickness. It was possible

to differentiate an uninfected mouse against an infected one, as well as track the evolution of the infection through a time study. In contrast to the current method, Raman analysis of the skin was non-invasive, and did not require any skin biopsy or blood extraction from a patient. It was interesting to compare this Raman detection method with the current methods, as Raman could be easily used in the field.

4.8.1 Blood parasitemia measurements versus Raman analysis of skin

Trypanosomes were found in the blood at various concentrations, as it has been found that the number of parasites in the blood is cyclical.[113] Given that the number of parasites could be very low and that blood parasitemia was based on a visual observation, this method could not be considered as reliable as a detection method. This technique was used as a qualitative assessment of the infection of a mouse in the laboratory.

Using the time study previously performed, a blood parasitemia was obtained on the mice prior to each Raman measurement for comparison. After normalisation of Raman spectra, it was found that the Raman peak at 1442 cm^{-1} had often the highest intensity. Each Raman peak specific to the infection was compared to this peak *via* an intensity peak ratio method. The resulting value obtained from the parasitemia and the intensity peak ratio were plotted against each other for comparison. The blood parasitemia value displayed on the chart correspond to the logarithmic value of the estimation of the number of parasites in a mL of blood.

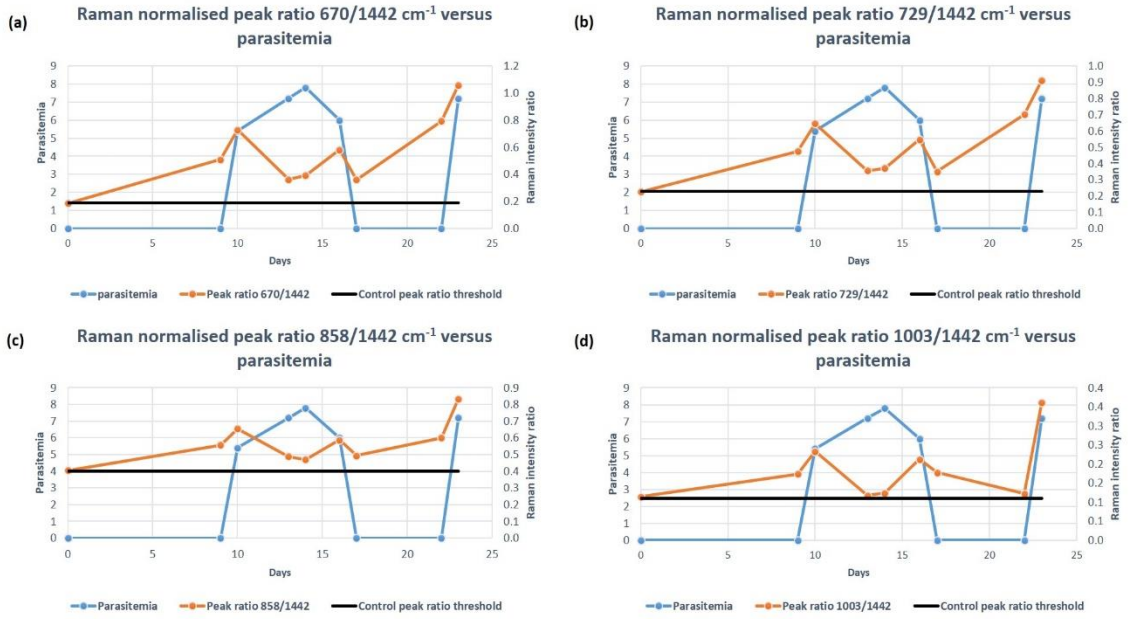

Figure 4.17 Comparison between blood parasitemia (log value of estimated concentration of T.b. brucei in blood) and Raman peak intensity ratio measurements, (a) 670/1442 cm^{-1} peak ratio comparing (porphyrin or tryptophan)/(CH_2 bending mode), (b) 729/1442 cm^{-1} peak ratio comparing (tryptophan)/(CH_2 bending mode), (c) 858/1442 cm^{-1} peak ratio comparing (proline, tyrosine)/(CH_2 bending mode) and (d) 1003/1442 cm^{-1} peak ratio comparing (phenylalanine)/(CH_2 bending mode).

A few examples of peak ratios are shown in Figure 4.17, but the same trend was observed with the other Raman bands at 878, 940, 1003, 1047, 1154, 1248, 1344, 1380, 1474 and 1557 cm^{-1} and offered more possibility to detect an infected mouse. The Raman peak at 1442 cm^{-1} (CH_2 bending mode) appeared to be constant, and often the highest peak intensity across each analysis and was chosen to be the reference peak for the ratio. Examples shown above display the variation in porphyrin, tryptophan, proline, tyrosine and phenylalanine over the time of infection compared with the number of parasites in mouse blood. The cyclical presence of the parasite in the blood was noticeable in this study, where the parasitemia reached a peak at day 14 (6.3×10^7 parasites/mL) and finally dropped down to zero at day 17 (concentration lower than 1×10^4 parasites/mL) before increasing again at day 22. The Raman measurements on the skin also showed a variation through the days, but more data for a long-term infection would be required to investigate whether it reaches a constant value, or the variation continues.

Contrary to the blood parasitemia values that could drop to zero, Raman peak ratio varied but did not drop below the control value, which indicated that the infection could still be detected

through time with Raman. Control threshold was represented by a constant black line in Figure 4.17 and displayed the ratio value obtained from the uninfected mouse for each peak. Any Raman ratio values higher than the threshold were considered as infected. Raman peak ratio also varied, as the blood parasitemia, but did not seem to follow the trend of blood parasitemia. This observation suggested that the biological information detected with Raman was not influenced by the blood or the concentration of trypanosomes in the blood. Only the skin variations were measured.

Moreover, parasites were observed in the blood at day 10 with a visual observation with a microscope whereas Raman indicated an infection from day 9 with any of the Raman bands investigated. This showed that the Raman detection method could detect the infection earlier than the blood observation. This was particularly interesting as microscope observation of blood was often used to confirm the presence of trypanosomes after being found positive on the CATT test. Failure to find parasites in the blood could lead to the non-treatment of the individual, as its CATT test would be considered as false-positive, although blood obtained from patient was often centrifuged and concentrated through a column in order to increase the concentration of parasites in the blood and simplify their findings. Raman measurements on the skin appeared to be a viable alternative to detect the infection.

Blood analysis such as CATT test was widely used for population screening, and at the moment, was the gold standard method of detection.[129,135] Despite the success of the CATT test to efficiently detect infected individuals, this method had its limitations, where false positive or negative could arise, and search for trypanosomes in the blood needed to be performed to confirm the results. However, as observed in Figure 4.17 their presence was sometimes not detectable with a microscope. The use of the skin as a target for the detection of the disease was a good alternative to eliminate all of these different potential issues that could be raised with the use of CATT test or blood parasitemia. Raman measurements on mice skin have been shown reliable and demonstrated good sensitivity over blood parasitemia. Even when parasites were not detectable in the blood, Raman was able to differentiate an infected from an uninfected mouse. This would make this new detection method a strong alternative for field detection of sleeping sickness. Examination of infected mice at a time of infection lower than day 9 should be performed to determine if it could be detected earlier. Moreover, only one mouse per time point

was analysed here, and it would be necessary to perform more repeats at each time point in order to assess the reproducibility of the trend observed.

4.8.2 Quantitative Polymerase Chain Reaction of parasites in the skin versus Raman spectroscopy

Polymerase Chain Reaction (PCR) was a newly developed method for the detection of parasites in blood. It has dramatically increased the sensitivity and the specificity of the detection method compared to CATT, as it returns 99% sensitivity and 97.7% selectivity in blood.[280] However, such a detection technique could not be used in the field due to the equipment requirement, and the possibility of contamination that could occur in a non-controlled environment. With PCR being the most accurate detection method, this technique was applied on the skin sample from the mouse time study. After each mouse analysis with Raman, a small area of the skin was obtained for PCR measurements. The comparison between Raman and PCR would provide information on the sensitivity of the developed method.

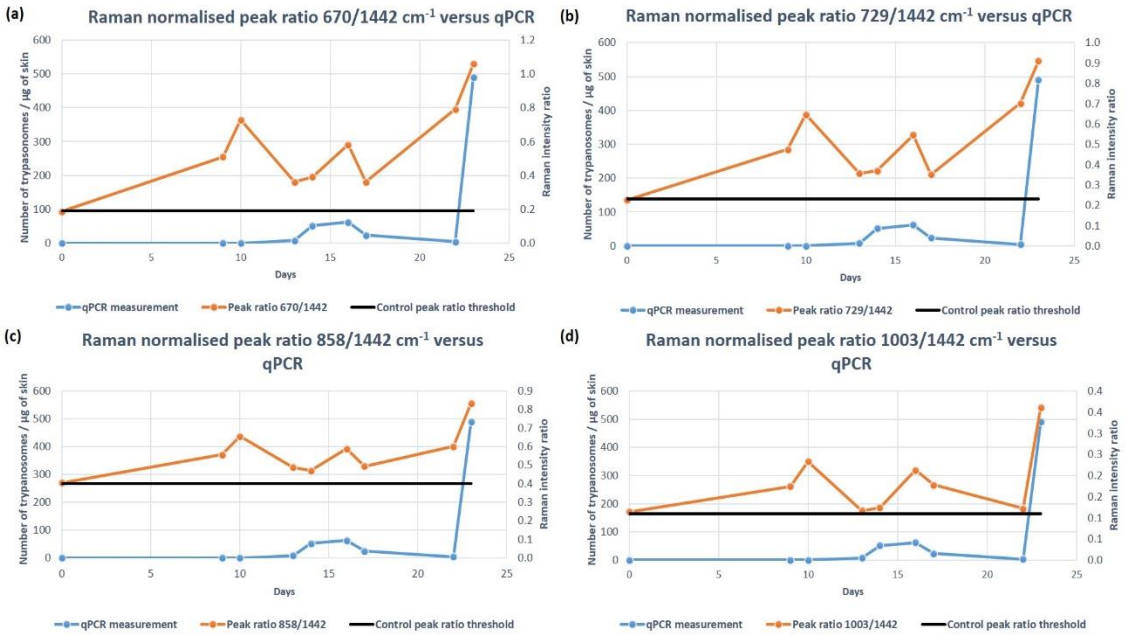

Figure 4.18 Comparison between qPCR measurements and Raman peak intensity ratio measurements, (a) 670/1442 cm^{-1} peak ratio comparing (porphyrin or tryptophan)/(CH_2 bending mode), (b) 729/1442 cm^{-1} peak ratio comparing (tryptophan)/(CH_2 bending mode), (c) 858/1442 cm^{-1} peak ratio comparing (proline, hydroxyproline)/(CH_2 bending mode) and (d) 1003/1442 cm^{-1} peak ratio comparing (phenylalanine)/(CH_2 bending mode).

The values obtained with the different methods were plotted against each other and shown in Figure 4.18. It appeared that the qPCR measures of parasites were also cyclical, further suggesting that the number of parasites present in the skin varied through time. The concentration of parasites in the skin reached a peak between day 14 and 16 and dropped off at day 22. A similar observation was made for the Raman measurements, but the variation observed seemed to occur at a faster rate. Another explanation for this cyclical trend observed was the heterogeneous distribution of the parasites through the skin. It was possible that trypanosomes formed patches in the skin and were not homogeneously distributed across the skin. This would introduce variation between each skin sample obtained. Multiple skin samples should be obtained from each mouse in order to have a more accurate view on the presence of trypanosomes in the skin.

According to the qPCR data, trypanosomes were observed in the skin at day 13 (8 trypanosomes/µg of skin) whereas Raman detected the infection at day 9. The skin sample obtained at day 9 or 10 did not show any parasites according to PCR but it was possible that

trypanosomes were present in the mouse skin in a different area because of their heterogeneous distribution. Nonetheless, according to the data shown in Figure 4.18, the infected mouse at day 9 displayed no trypanosomes in its skin. As Raman was detecting at day 9 a biological variation specific to the infection, this indicated that the spectral variations were also influenced by biochemical changes in the skin and not only presence of parasites. The Raman detection method was detecting the infection before qPCR did. The other Raman bands that have been found specific to the infection showed a similar trend as in Figure 4.18. The variation observed with these Raman bands did not relate to the number of trypanosomes in the skin. However, the Raman peak located at 1557 cm^{-1} (porphyrin or tryptophan) seemed to follow the same variation as qPCR (Figure 4.19).

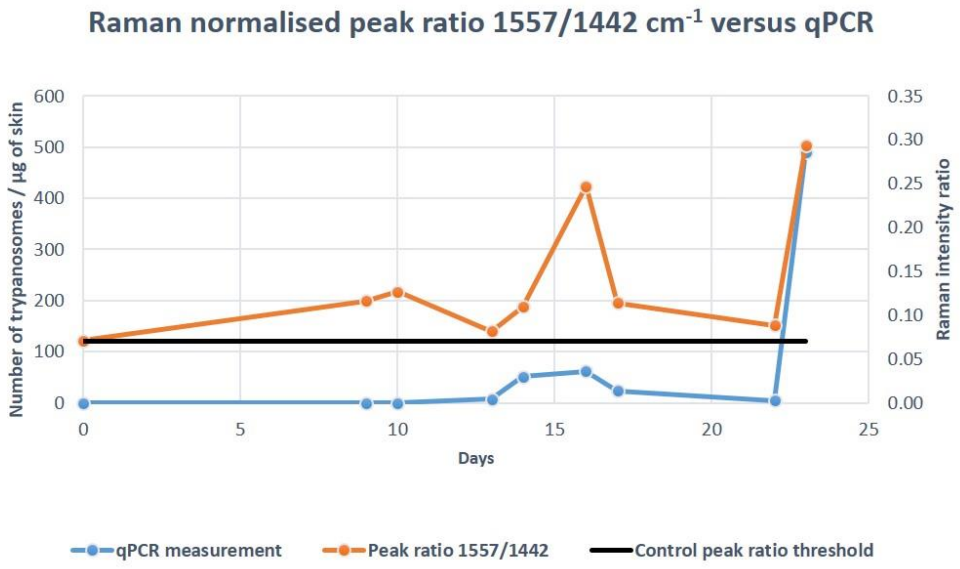

Figure 4.19 Comparison between qPCR measurements and Raman peak intensity ratio for 1557/1442 cm^{-1} associated with (porphyrin or tryptophan)/(CH_2 bending mode).

The Raman peak at 1557 cm^{-1} is associated with either tryptophan or porphyrin.[231,232] It was shown in Figure 4.19 that between day 13 and day 22, the Raman peak ratio followed the same trend as qPCR. Hence, it was possible that this specific Raman peak ratio was directly related to the number of parasites in the skin. Before day 13, there was an increase in the ratio observed that was not measured with qPCR. The presence of porphyrin in the skin could indicate the presence of blood in the skin due to the parasites crossing blood vessels, or it could be related

to the heme that the parasites needed to grow.[276,277] This Raman band, through its tryptophan assignment, could also be associated with the presence of trypanosomes surface proteins, hence showing a direct detection of the parasites in the skin. Given these results, Raman could be more sensitive than qPCR for the direct detection of trypanosomes in the skin. Moreover, it could also be related to the presence of indolepyruvate released by the parasite, as its concentration would increase with the number of trypanosomes in the host.

PCR assays, performed in blood for the detection of sleeping sickness, have demonstrated good sensitivity and specificity.[279,280] It has been used in Cameroon to confirm the infection of CATT positive patients with no observable parasites in their blood.[70] However, a routine use of PCR assays for the diagnosis of this disease in endemic areas was limited due to its relatively expensive cost. The use of this type of assay also required specific equipment and infrastructure to reduce contamination, which cannot be provided in the field for mass population screening. The finding that Raman spectroscopy could detect the infection in the skin prior to qPCR (Figure 4.18) shows that Raman could serve as a good alternative or complementary detection technique for field measurements.

It would be necessary to repeat this experiment with an increased number of mice analysed per time point to demonstrate reproducibility and reliability in the Raman detection. More skin samples should also be obtained for each mouse for qPCR measurements to assess the distribution of trypanosomes across the skin, and to validate whether Raman can detect the infection before parasites invade the skin. According to these preliminary results, it appeared that Raman measurements could detect the infection earlier than the visual observation of blood samples and for the PCR analysis of skin, hence before *T.b. brucei* entered the skin.

4.9 Conclusion

Raman spectroscopy was successfully translated from *in vitro* to *in situ* mice applications. Despite obtaining subtly different spectral information between each study, which could be linked to the instrumental changes and the potential interaction with internal organs, it was still possible to differentiate an infected from uninfected mouse. Moreover, Raman bands that were found specific to the infected mice were slightly different than those obtained previously during *ex vivo*

studies. Although, Raman bands at 856 and 938 cm^{-1} and their associated shape seemed to be similar to the previous study, suggesting that a similar biological information was measured. This difference in the Raman spectra could be explained by the contribution from other organs to the Raman signal or to the variation of responses observed between mice.

Different strains of *T.b. brucei* and different sub-species of *T.b* were used to infect mice without any changes in their Raman spectra. Comparing individual Raman spectra allowed the detection of the infected skin through an increase in intensity of certain Raman bands. The different trypanosomes used did not change the biological information, which meant identification of the trypanosome sub-species present in the system was not possible. However, certain Raman bands, which were found specific to the infection, were absent or did not show the same increase in intensity for *T.b. gambiense* compared to *T.b. brucei*. It was thought that the low number of parasites present in the host due to *T.b. gambiense* being less virulent was the result of this variation and not a discrimination between sub-species.

The number of parasites present in the host could be followed with Raman as it was visually observed that more *T.b. brucei* 247 were present in the host, extravascular and intravascular region, than *T.b. brucei* gvr35 and their correlated Raman spectra were different. It appeared that even if gvr35 infected mice possessed more parasites in the skin than 247, the latter infection was more discriminated. Raman peak changes may have arisen from biochemical changes induced by the parasites in the host and seemed to be stronger when more parasites were present. These spectral differences were linked to the Raman bands specific to the infection, suggesting that the information obtained was directly correlated with the presence of the trypanosomes in the host, both intravascular and extravascular. Biochemical variations induced by parasites in the intravascular region may have been transferred to the skin, which makes them detectable by Raman. It was also shown previously that the parasite was able to use some lipids and fatty acids present in the surrounding tissue in order to use them for its growth and VSG production. This action on the tissue composition could change the Raman signal compared to a control skin. An increasing concentration of trypanosomes would likely increase these biological changes, leading to the potential Raman detection of their presence. This was further supported by the presence of Raman bands associated with amino acids, showing a change in the protein composition and concentration. These amino-acids could also be the result

of the detection of certain metabolites from the trypanosomes. Further studies should be performed to measure it.

Furthermore, the direct detection of the trypanosomes in the skin was not clearly identified due to high spectral overlap between the fingerprint of parasites and the signal from the skin. However, it seemed that an immune response from the host was detected by Raman, suggesting that the infection is measured with a combination of a biological response from the host, an alteration of skin composition by the parasites, and potentially the contribution of the surface proteins of the trypanosomes. It would be interesting to compare the Raman signal obtained from the detection of sleeping sickness with a different skin disease, such as malaria or a specific inflammatory reaction to understand the biological information obtained as well as to determine whether the detection method was specific to sleeping sickness.

Raman analysis also demonstrated that the presence of the trypanosomes in the skin or their influence on the biological composition could be cyclical. It appears that their presence varied due to the response from the immune system. These measurements were correlated with what was observed with blood parasitemia, as trypanosome concentration was found to be cyclical in those measurements as well. Despite these variations, the infection was always able to be detected by Raman. As the first time point was taken at day 9, this could be considered as the limit of detection. However, lower time points could be further investigated in future studies.

The direct comparison between the results obtained with Raman, blood parasitemia and PCR on the skin confirmed that the effect or the presence of trypanosomes in the skin was also cyclical. However, the trend was different. The Raman peak ratio curve did not exactly follow the blood parasitemia. Visual observation of parasites in the blood is a part of the mass population screening as well as CATT test. As blood parasitemia (log value of the estimated concentration of parasites in blood) drops down to zero at certain time points, some patients may be considered false positive to the CATT test and not be treated, which does not make this method very reliable. However, Raman peak ratio values were always different from the relevant control value, which indicated that the detection of the infection was still possible even when no parasites were present in the blood-based measurement or in the skin when compared with PCR values. Using Raman could help detect these individuals in order to give them the appropriate treatment. It would be interesting to measure Raman at earlier time points and determine when the infection

could be detected in the skin, but also at longer time points, in order to understand if the biological information remains cyclical or if it reaches a plateau.

Raman appeared to be a good technique for the detection of sleeping sickness using the skin as a target. However, it would need to be optimised by understanding the chemical reactions that are induced by the presence of trypanosomes in the skin. An opportunity was given to test this application on the field by following a medical team during active screening of the population for *gambiense*-HAT.

Chapter 5 Field application of the Raman detection method: Guinea (Africa)

Raman spectroscopy has proven to be able to detect infection by parasites in the skin of mice. The spectral differences were easily identified and allowed the differentiation between infected and uninfected mice. An opportunity was awarded to test *in vivo* this new detection technique in the field by taking measurement on humans.

5.1 Aims

It was offered to our team to run a pilot study of the Raman detection method in Guinea (Africa). Guinea has been affected by Human African Trypanosomiasis (HAT) due to the infection by *T.b. gambiense*. Tremendous efforts were being made by the World Health Organization (WHO) and by the Guinean government to perform mass population screening and treatment of HAT, with the objective of eliminating the disease by 2030.[21,22]

Figure 5.1 Map of Guinea in Africa, the region where the medical performed the active screening control is shown in the red rectangle: Forécariah region.

The health ministry was organising multiple population screens across the country. A health mobile team was sent to small villages in rural places, where the access to health care was poor, to test the population using the CATT test. Patients that tested positive would then be sent to a small health centre. They were further tested to assess the stage of the infection by meeting with a medical practitioner, who also performed a lumbar puncture. Once the stage of the disease was determined, patients received treatment on site before being sent back to their respective villages.

Our team was invited to follow one of the mobile teams in order to test the *in vivo* Raman detection during population screening. The population screening was performed in the region of Forécariah, highlighted in red in Figure 5.1.

Figure 5.2 Photo taken during the Guinea trip of the organisation and set up for the screening of the population for HAT, photo on the left shows the set up and the electricity supply for the field lab, and photo on the right shows a CATT test being performed in the field.

The HAT test was carried out throughout the day as illustrated in Figure 5.2. A blood analysis was performed with the CATT test, and visual observation of the blood with a microscope was performed in order to detect the parasitic infection. At the end of this three weeks of screening, every positive patient was brought to Forécariah to a health centre for more tests, and to receive the appropriate treatment.

Over one week, each positive testing person was further tested, and their stage of infection was determined. Raman measurements were taken during this week at the health centre, and not in the villages, before the patients received the treatment.

The primary aim of this work was to detect individuals infected by *T.b. gambiense* and to treat them, but there were two other scientific aims during this field investigation. First, skin biopsies were obtained from every infected patient in order to confirm that parasites were present in human skin, as this has only been confirmed in animals.[154,156] The skin biopsies and their analysis will help to corroborate this theory. Every patient positive for the CATT test, even if no parasites were found in the blood, was invited to the health centre for a skin biopsy. The second aim was to obtain Raman measurements from every infected individual, and from uninfected individuals (CATT negatives or relatives) and to assess if Raman could be used to detect HAT in the field.

5.2 Methodology of the field Raman detection method

The same Snowy Range instrument, model Sierra 2.0, 785 nm laser used for the mouse study was taken to Africa to take measurements on patients. Protocol used for this experiment was explained in chapter 7.

Figure 5.3 Photos of the instrumental set up (left), measurement set up (centre) and Raman adaptor (right) to keep measurement protected from the light and to keep a constant focal point.

As shown in Figure 5.3, the Raman instrument was placed on a stable table to take measurements on patients. This reduced the skin area where information could be obtained. Two different skin areas were investigated: the back of the hand and the inside forearm from the

wrist to the elbow. Five measurements were taken on both skin areas. For the data to be reproducible, it was necessary to keep the focal distance identical between measurements and between patients. This focus point was measured with a silica slide, where the intensity of the Raman peak was the highest. An adaptor, shown in the right photo of Figure 5.3, was then printed with a 3D printer (Ultimaker 2+ 3D printer, UK), with its length identical to the focal distance. This adaptor was placed on the device, where the laser comes out, and allowed the distance to be identical between measurements. Another advantage of this adaptor was that it allowed the acquisitions of Raman spectra without disturbance from ambient light; making it like taking measurements in a dark room.

Another potential issue for this study was the effect of the laser on the human skin. Indeed, as measurements were obtained from human patients, there were safety regulations to follow to avoid burning the skin. The laser power and the acquisition time needed to be considered. There exists a calculation for the maximum exposure time of the laser on the skin. The laser power to be used was dependent on the laser, whether it was pulsed or continuous wave, its wavelength and the exposure time. The calculations were done according to the documented "British Standard – Safety of laser product" published in 2004.

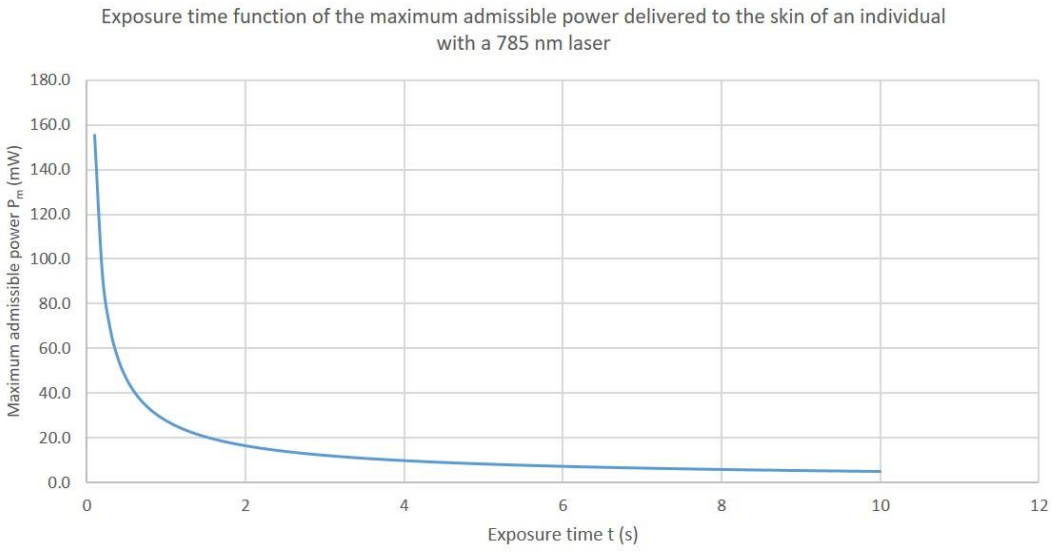

Figure 5.4 Graph showing the maximum admissible power P_m (mW) that can be used as a function of the exposure time t (s).

The curve obtained in Figure 5.4 showed the maximum laser power that could be used for the measurement on human skin with a 785 nm laser wavelength as a function of the acquisition time. Any parameters that fell below the curve were considered to be safe. It was decided to perform Raman measurements with an exposure time of 5 s and a laser power of 5.7 mW on both the hand and forearm.

Table 5.1 Table showing the number of patients tested according to their status: uninfected or infected.

Group	Number of patients
Uninfected	10
Seropositive	7
Stage 1	4
Stage 2	14
Total	**35**

The details of the patients that were tested were grouped in Table 5.1. During this study, it was possible to obtain Raman measurements from 10 uninfected and 25 infected individuals at various stages. Infected patients were positive for the CATT test with titre higher than ¼ dilution. Within the infected individuals, seven people did not show any parasites present in the blood during the visual observation with a microscope and were then considered as "seropositive". The stage of the infection was determined with a lumbar puncture, where the white cell concentration was measured. An individual that had a concentration of white cells in its cerebrospinal fluid (CSF) less than 5 white cells/mL or trypanosomes were not found in the CSF was considered to be at stage 1. If the concentration was greater, the individual was in stage 2. It was found that four patients were in stage 1 and 14 people were in stage 2.

5.3 Skin biopsies: Search for trypanosomes

Every skin biopsy was analysed to search for the presence of extravascular parasites. Two different methods of staining were employed. The first test was performed by staining human skin with giemsa, and the second test was done by immunostaining the skin samples with an antibody anti-ISG65 specific to the trypanosomes. Later, polymerase chain reaction (PCR) was

performed on the skin biopsies to amplify the sensitivity and the accuracy of the detection of trypanosomes in the skin.

(a)

Infection class	Positive for skin parasites
Stage 2 patient	14/14
Stage 1 patient	4/4
Seropositive	6/7

(b)

(c)

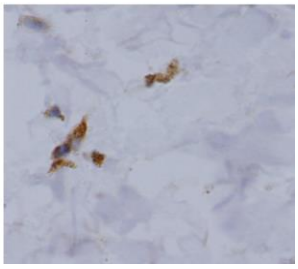

Figure 5.5 Results for the presence of extravascular trypanosomes in the skin biopsies after staining and PCR experiments, (a) number of skin biopsies which were positive for extravascular parasites, (b) Giemsa stained at 60x magnification, (c) anti-ISG65 immunohistochemistry staining at 60x magnification.

The first aim of this field investigation was successful, as parasites were found in the skin of infected individuals, after performing both staining and PCR experiments. Figure 5.5.b) and c) showed skin images obtained after staining and provided evidence that the parasites can cross the blood vessel and enter the skin during the infection. However, one skin biopsy was negative for the presence of the parasites. All stage two and stage 1 patients, as well as six out of seven seropositive individuals, had parasites in their skin, but one of seven seropositive did not have parasites in the skin biopsies. This could suggest that trypanosomes do not always enter the skin, but it could also mean that the area that was biopsied did not have parasites. The parasites might have been present elsewhere in the skin. Indeed, the skin is the largest organ in the human body, and the area that was punctured for the biopsy was only 2 mm^2, which was an extremely small area compared to the whole organ. In addition, parasites may preferentially be located in certain area of the skin, as it was observed in animals.[156] This could explain why one biopsy was found to be negative. Parasites may have been present but not in the skin area that was targeted.

It was also possible that the patient with a negative biopsy may have not been infected at all. As no parasites were found in the blood nor the skin, he might have been false positives for the CATT test, or he may have been infected in the past and still have antibodies against trypanosomes present in his system.

This discovery of parasites in the skin of patients that showed no parasites in their blood was shown for the first time and was very important, as it would allow them to be treated and cured. Normally, they would not have been considered as infected and then treated because they did not have parasites present in their blood. It also opened a new area of research for the detection of Human African Trypanosomiasis, by targeting the skin instead of the blood. Combined with the positive results from Raman in mice skin, this method could be optimised to be used a screening detection method in the field.

5.4 Raman measurements

As mentioned previously, Raman spectra were obtained on the back of the hand and on the volar surface of the forearm of a patient, with an acquisition time of 5 s and a laser power of 5.7 mW due to safety regulations. Five measurements were made across the hand or forearm.

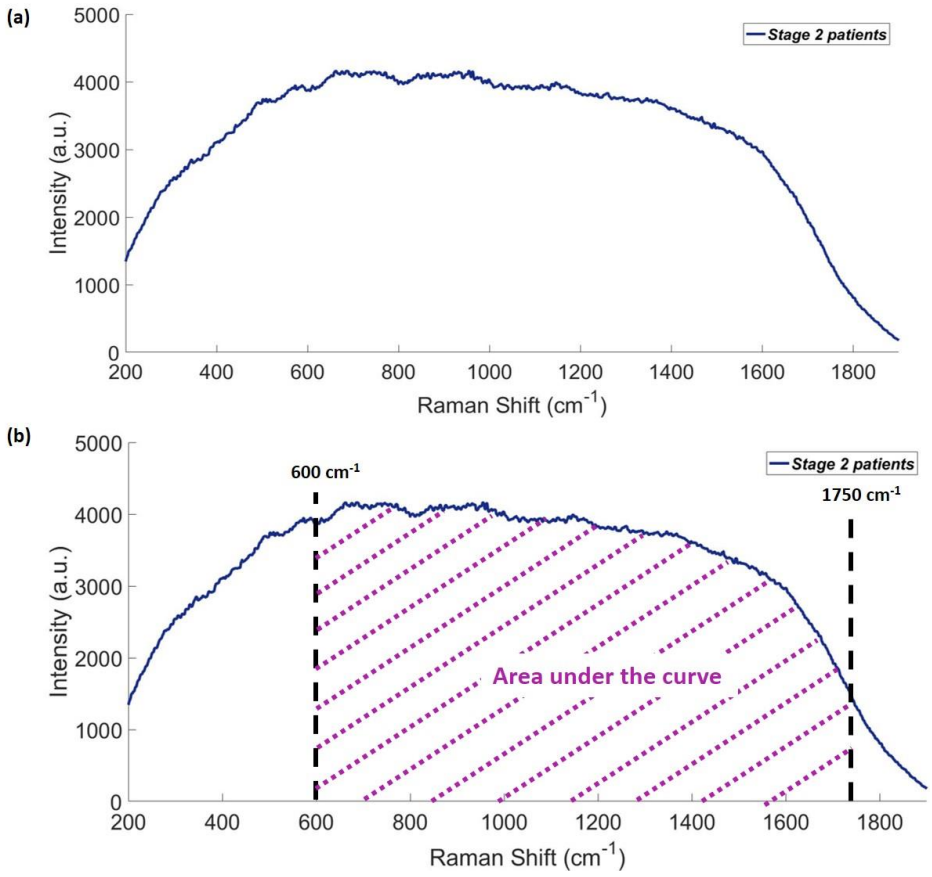

Figure 5.6 Example of a raw Raman spectrum obtained from a stage 2 patient (a) and the description of the calculation of the area under the curve (purple) of the Raman spectrum within specific Raman shifts (600 – 1750 cm^{-1}) (b) taken on the back hand measured on this patient, with a 5 s acquisition, 785 nm laser and 5.7 mW laser power.

The parameters employed (exposure time and laser power) were lower than for the investigation on mice. Hence, the resulting Raman spectra did not show any clear Raman bands as were observed previously. The increase presence of melanin in the skin could have also been responsible for the spectra showing no distinctive Raman bands. Indeed, melanin strongly absorbed light in the visible region, which made the Raman analysis of the skin quite challenging. Figure 5.6.a) displayed an example of a raw Raman spectrum obtained from a stage 2 patient on the back hand. This spectrum was one of the five replica that were measured for each patient, before being processed. No Raman bands could be observed in this spectrum. Hence, it was not possible to treat and analyse these data obtained during the field study using the same process as previously described for the mouse study. Interestingly, variations in the fluorescence signal detected between each measurement were observed experimentally. The calculation of the area

under the curve (AUC) of each Raman spectrum could then be performed to analyse these variations and assess whether they could be specific to the infection. Figure 5.6.b) illustrates the process of calculation of the AUC of the Raman spectrum of a stage 2 patient. Each Raman spectrum was individually smoothed with a savitzky-golay filter, then the x-axis was reduced to 600 – 1750 cm^{-1} and the AUC value was determined. A single value for this area was obtained for each spectrum and were simply compared between the different group of healthy and infected individuals.

5.4.1 Comparison of the area under the curve values measured on the forearm of uninfected and infected patients

As mentioned previously, five replicas were obtained for each patient, resulting in a total of 50 Raman measurements for the uninfected group. Differently, only the patients that were confirmed to be infected via the blood analysis and/or the skin biopsy were included in this study (Figure 5.5), hence providing 120 Raman spectra for the infected group. Comparing these two groups would help to differentiate control versus infected skin. For both group (uninfected and infected), the mean value of AUC and the standard deviation of the data set was calculated and compared.

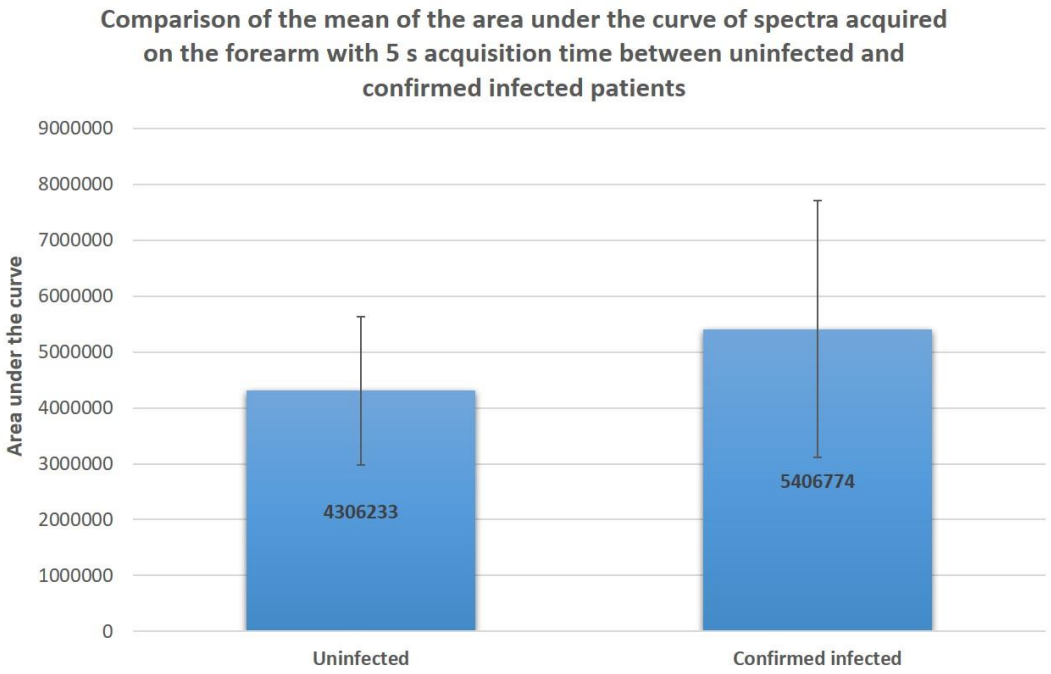

Figure 5.7 Comparison of the mean value of the AUC for each uninfected and infected group, from the Raman spectra obtained from the forearm and with a 5 s acquisition time (785 nm, 5.7 mW).

The comparison between the mean of the AUC values for each uninfected and infected group was displayed in Figure 5.7. A difference between the value of uninfected and infected patients was clearly observed. It appeared that the infected skin led to an increase of the fluorescence signal measured with the Raman instrument, hence an increase of the AUC value. The presence of the trypanosomes in the skin seemed to have induced biochemical changes within the skin matrix, which was related to a higher fluorescence signal measured. This observation was very interesting as it would suggest that the changes induced in the skin by the parasites could be detected by Raman, with a different and more suitable instrument for *in vivo* studies that could overcome the fluorescence background due to the presence of melanin or other biological components.

Despite the clear difference between the mean AUC values, the standard deviation calculated for each data set were found to be quite large. Indeed, both standard deviations showed strong variance in the data set and were overlapping with each other. Thus, suggesting that the mean difference observed would not be significant enough to differentiate uninfected and infected patients using AUC values. Due to this strong variation within the data set, it was important to

determine if the difference between uninfected and infected mean AUC value was statistically significant and would describe a pattern that could be used to differentiate the two groups. A student t-test was then performed to assess whether the mean of the two group were statistically different. The resulted test demonstrated that the difference between the two mean values was statistically significant ($t(151) = 3.9$, $p = 0.0001 < 0.05$). According to the p value obtained, it was clear that the difference was not a random effect due to the variance of the data set and showed that infected skin could be differentiated from control skin using the AUC values.

It was demonstrated in Figure 5.7 and with the use of a student t-test that an increase in the fluorescence background detected in the Raman spectra obtained from the forearm of a patient was specific to infected skin. It implied that the presence of the parasite in the skin induced a strong change in the biochemical composition resulting in an increase in the fluorescence. However, AUC values could not be used in the field to detect HAT patients, as it could lack of specificity, it was however setting the basis for further optimisation of the Raman detection method. Indeed, the difference in AUC values has demonstrated that a detectable biochemical change was occurring in the skin and could potentially be detected with Raman spectroscopy.

5.4.2 Comparison of the area under the curve values measured on the hand of uninfected and infected patients

Similarly, the same data processing and analysis was performed on the Raman spectra obtained from the hand of the patients. As demonstrated previously with the measurements made on the forearm, the biochemical changes induced by the infection resulted in an increase of the AUC values. These changes, as well as the distribution of trypanosomes across the skin, could vary between the targeted skin area analysed and between individuals, hence altering the spectrum obtained. For this model's application, it was important to find an area of the skin where the biological changes and the presence of trypanosomes were constant between individuals, and specific to the infection by trypanosomes.

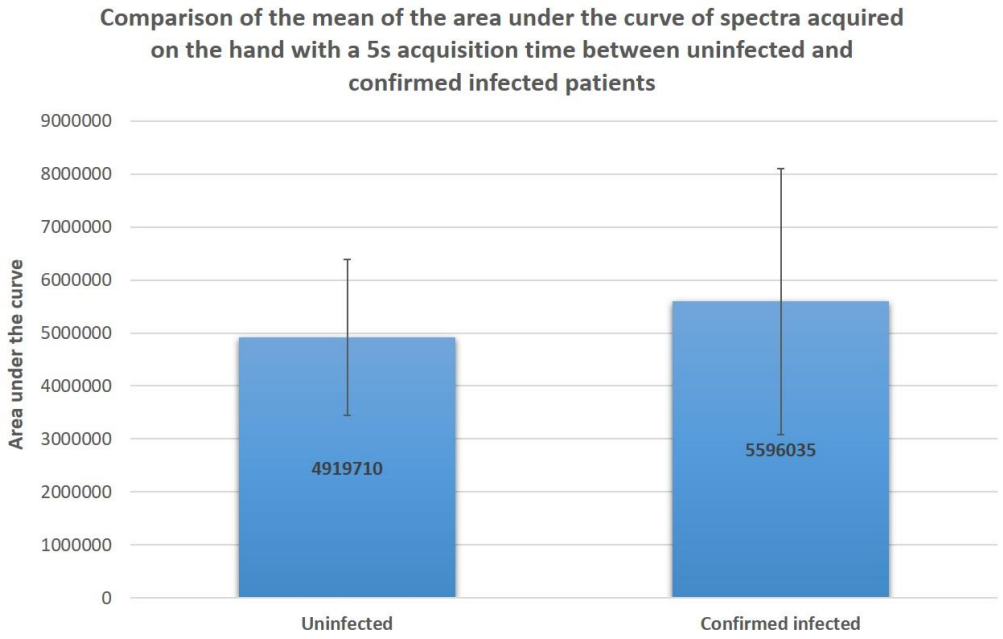

Figure 5.8 Comparison of the mean value of the AUC for each uninfected and infected group, from the Raman spectra obtained from the hand and with a 5 s acquisition time (785 nm, 5.7 mW).

Figure 5.8 displayed the comparison of the AUC mean value for both uninfected and infected data sets. Identically to the AUC data set obtained from the forearm, a difference between the mean AUC value of uninfected and infected patients was observed. Infected skin corresponded to an increased value of AUC compared to normal skin. Moreover, their respective standard deviations showed a strong variance within the data set and were also overlapping, suggesting that this difference might not have been specific.

A student t-test was also performed on the two data sets to determine if this change in the AUC values was statistically significant. According to this test, the hand data were also found to be statistically significant ($t(150) = 2.2$, $p = 0.03 < 0.05$), demonstrating that the infection led to an increase of the fluorescence during the measurements. It further demonstrated that the biological composition of the skin was changing during the infection by the trypanosomes and could potentially be detected with Raman. These results were promising and further optimisation of the method to overcome the fluorescence influence to obtain Raman signal will be undertaken.

Furthermore, the investigation of two different locations on the skin showed a similar trend about the influence of the infection in the skin; the changes seemed to be the same across the skin. However, the spatial distribution of the trypanosomes across the skin was still unknown and it was not determined if parasites were present in the targeted area with Raman, suggesting that the biochemical changes induced by the infection could be present along the skin even in the absence of trypanosomes. In addition to the optimisation of the Raman technique, it would be interesting to investigate the distribution of the trypanosomes across the skin, as well as the biological changes induced by their presence, to find an optimum target for the Raman detection. The biochemical variations occurring in the skin might be stronger with the presence of trypanosomes in the skin area analysed with Raman.

Overall the translation of Raman from mouse study to human measurements delivered positive outcomes. The separation between infected and uninfected patients with their AUC values was found to be statistically significant for both targeted skin area. The data analysis of the field data was based on the fluorescence background, instead of Raman bands like in the mouse study, but it demonstrated that the infection could potentially be detected with Raman. The use of AUC values could not however be used in the field as it might not be specific to HAT but in this study, a proof of concept for the use of Raman has been demonstrated and indicated that further development was required for the Raman technique to be used on the field. Indeed, the instrument used for this study, a Snowy Range Instruments benchtop, was not explicitly designed for such measurements. It was not able to overcome the presence of melanin and to measure Raman bands from the skin. Nonetheless, the trend in differentiation observed was very promising, and optimisation of the method with a more appropriate instrument would make the use of Raman very interesting for the detection of HAT.

Differently, the data obtained in the field was also analysed using of a trained statistical model, which could make the method of detection more efficient and improved the trend observed previously with the AUC values. In addition, having a more thorough and robust data set would allow for the creation a model through a trained statistical method, which could further ameliorate the differentiation between infected and uninfected patients.

5.5 Statistical model

An attempt was made to use machine learning to process the data sets obtained in the field. Despite the small amount of data available, the use of machine learning would allow for the creation of a statistical model to predict whether a Raman spectrum corresponded to an infected or uninfected patient.

In collaboration with Dr Simon Babayan at Glasgow University, an attempt was made to use a prediction model to analyse the Raman data and assess the reliability of Raman spectroscopy as a method of detection. After consideration, it was decided to use Extreme Gradient Boosting (xbg) as an algorithm to obtain the model. The low sample size limited the use of other techniques, and xbg was thought to be more suitable for this study. This method allows for the investigation of the variation within data sets by classifying them. Part of the data set is pre-determined into different classes (model), and the rest is used to test this model by assigning each data point to a class. Two groups were set up: infected and uninfected. Patients were primarily assigned to a group identified as control (uninfected) or where trypanosomes were observed in their skin biopsy (infected).

The sample size was small but the number of variation (Raman wavenumber) is relatively high and can make the model unstable. Wavenumbers were then clustered according to their correlation between each Raman spectrum. It means that data set is run primarily to identify correlation between variation of the wavenumbers, it would allow to cluster similar ones and reduce the dimension of the data set.

To assess if the model was robust and accurate, 70% of the Raman spectra of each group were considered as known (trained model). They were the model to be tested. The remaining 30% of each class were considered as unknown and were tested against the model to assign them to one of the two groups. The accuracy of the assignment was then calculated. This process was repeated multiple times by changing the data within the model and the data to be tested in order to obtain a better reproducibility. For example, a given spectrum that was part of the model building set, then moved to the unknown set in the second iteration. This helped build a better model and to assess the reproducibility within the data. It allowed determination of whether all

Raman spectra followed the same trend of spectral correlation within one group. Five Raman replica from each patient's forearm, obtained from their forearm, were only averaged (no smoothing nor baseline correction) and their x-axis reduced to 600 – 1750 cm^{-1} before building the model.

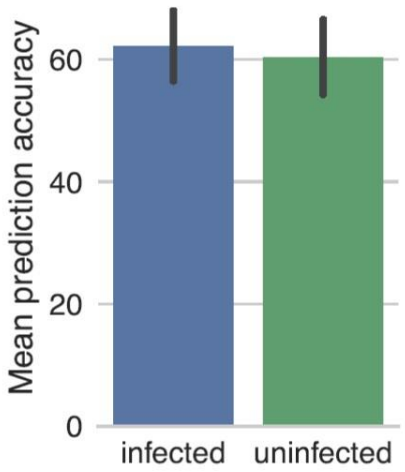

Figure 5.9 Mean prediction accuracy for data classification of patients using Extreme Gradient Boosting between uninfected and infected groups.

The mean prediction accuracy for the assignment of patients between uninfected and infected group was shown in Figure 5.9. The test of the model shows around 60% prediction accuracy for the uninfected and infected groups. This was very promising results as the sample size for the model was relatively small. The model was based on the Raman measurements obtained on the forearm of patients. It displayed a relatively strong prediction accuracy considering the instrument used and the amount of data obtained. It seemed that there were still some variations within the data sets that did not allow for clear classification, but this could be improved with a larger data set. It was also correlating with the results obtained previously with the AUC values. As the data were not baseline corrected in this study, the model was based on the fluorescence background on the spectra. It seemed that the trend observed previously, where an increase of fluorescence was related to the infection, was confirmed and could be used to classify the data set.

This was preliminary data as the model could be worked on and the method of detection optimised, but the prediction accuracy obtained suggest that Raman spectroscopy could be a good alternative for the detection of HAT.

5.6 Conclusion

This method of detection was tested in the field by following a health mobile team in Guinea. The aim of this team was to perform population screening in a specific area of Guinea, and Raman would be tested on patients prior to the start of their treatment. Patients, that were confirmed infected by CATT test and blood parasitemia, were investigated. The stage of their infection was determined after by measuring white cell counts in cerebrospinal fluid. The main interest of this trip was the investigation of seropositive patients. These patients were positive for the CATT test, often at low titre, and negative to blood parasitemia. Due to their low titre at the CATT test and the absence of trypanosomes in the blood, they were considered as false positives and not treated. However, if parasites were located in their skin, they would still be infected, and could possibly die but also infect other tsetse flies, acting as reservoir for HAT. The objective was then to confirm the presence of the parasite in the skin via skin biopsies, and to use Raman to determine if they could be detected as infected.

One of the main achievements of this journey to Africa was the discovery of trypanosomes in the skin of *gambiense*-HAT patients, confirming previous work in mice. All stage 1 and 2 patients were found to have parasites in their skin biopsies through immunostaining and PCR experiments. Moreover, six out of seven patients considered as seropositive also displayed trypanosomes in their skin, thus showing that such seropositive individual could act as a reservoir for HAT. One patient did not show any parasites in the blood nor the skin. As the skin is the largest organ in the body, it was possible that parasites were present in very low numbers and were located elsewhere than at the area of the skin biopsy; it was not known whether the parasites would be homogenously or heterogeneously distributed throughout the skin.

Raman measurements, on both hand and forearm, did not show any distinguishable Raman bands, probably due to the presence of melanin in the skin that absorbed the incident light and increased the fluorescence background. Thus, hiding the Raman signal that could have originated

from the skin. Nonetheless, a variation in the fluorescence intensity was observed between measurements, and their potential specificity towards the infection was investigated by calculating the AUC of each Raman spectra. The comparison of the mean AUC values of uninfected and infected patients showed that infected skin had their AUC value increased. It was confirmed by performing a student t-test on the data sets, which demonstrated this increase was statistically significant for both skin area analysed. It suggested that the infection by trypanosomes resulted in the change of the biochemical composition in the skin, inducing an increase of fluorescence measured. This was very interesting results as it would imply that the infection could be measure via the skin with Raman spectroscopy. This finding offered a new research area to optimise the Raman detection, as it would provide a fast, non-invasive method to detect HAT in the field. Unfortunately, the Raman information obtained was hidden by the fluorescence background due to the instrument used and the presence of melanin. This could be ameliorated by using an instrument built specifically for tissue, *in vivo* studies, that could also overcome the presence of melanin or other fluorescent components by using an excitation wavelength closer to the IR region. Due to these spectral limitations, it was difficult to conclude on the success of the detection of HAT with Raman in the field, but the use of AUC values gave promising preliminary data for the detection of HAT by targeting the skin.

A machine learning method was also applied to analyse the Raman data measured. It was a trained method, as opposed to the untrained PCA, and allowed the creation of model against which unknown data could be tested. Due to the small sample size and low spectral resolution obtained due to the instrument used, the model was quite unstable, but it could give an idea as to whether Raman should be investigated in the future as a potential detection method. The model demonstrated a mean prediction accuracy of around 60% for both infected and uninfected data. This means that the model created and the test data, which were both obtained in the field, showed a good correlation between them; it was possible to predict from a Raman spectrum whether the patient was infected or uninfected with a fair level of accuracy.

The Raman technique was tested *in vivo* on host's skin and, despite the spectral limitation observed, showed a great potential to become a reliable detection technique. Mouse study and field investigation gave promising data that serve as a good starting point for further optimisation of the method. A different instrument should be used to ameliorate the biological information

obtained, mainly for the field study, such as a more portable Raman to access different part of the skin. The understanding of the biological changes induced by the infection and the distribution of the trypanosomes of the skin would also help increase the sensitivity of the method as to provide an ideal skin area for the detection. Further investigations should also be performed on the analysis of the data sets obtained in Guinea, as different methods could provide a better discrimination of the different groups.

Chapter 6 Conclusions

Human African Trypanosomiasis is a vector borne parasitic disease that has been causing the death of thousands of people during the 20th century and likely more before its discovery. Due to the combined effort of WHO and diverse institutions this disease came under control in the early 1960s but recently have resurfaced. The use of vector control and mainly passive and active screening have slowed and reduced the number of infected individuals by detecting them and providing them the appropriate treatment. Thus, making the target of elimination of *gambiense*-HAT achievable by 2030. Different detection methods were used based on blood analysis such as CATT and have shown to be reliable and allowed the screening of rural population, which are difficult to reach. However, the recent breakout of the disease led to think that there could be an unknown reservoir for *gambiense*-HAT that had sustained the disease. Cases of trypanotolerant individuals that were able to self-cure and most importantly asymptomatic carriers, that carried the infection without developing any symptoms and proving themselves to be negative according to current diagnostic methods and were not treated, led to the conclusion that trypanosomes had a different impact and possibly different life cycle between patients. The latter cases were of most concern as they showed that a human reservoir exists for *gambiense*-HAT as they remained infected and could transmit the disease to tsetse flies. More recently, it was discovered that trypanosomes were, in addition to the blood and other organs, also located in the skin, mostly adipose tissue, and could still be transmitted to tsetse flies without being present in the blood. Study of old human skin biopsies obtained in Democratic Republic of Congo showed evidences of parasites in the skin and confirmed the presence of a human reservoir. This new location site would explain the case of asymptomatic carriers and were overlooked during diagnostic tests, which could jeopardise the elimination of *gambiense*-HAT. The need for the development of new methods has arisen to target the skin area and reach the elimination goal.

Raman spectroscopy is a non-invasive, non-destructive and label free technique, and has been shown to be reliable in bio-diagnostics. Many studies have demonstrated its use in cancer detection in different organs such as the skin, and, thanks to recent technological development, has been able to be used *in vivo* and for example to assist surgeon during medical interventions.

This work has proposed and shown the development of a diagnostic method for *gambiense*-HAT by targeting the skin with Raman spectroscopy.

This investigation has not been performed previously so it was important to explore the different aspects of the disease from *in vitro* to *in vivo* applications. Different sub-species of *T.b*, *T.b. brucei* and *T.b. gambiense*, that are responsible for the infection of animals and humans respectively have been analysed *in vitro* with Raman. This work had been performed to understand the biological composition of the parasites as well as to assess the possible spectral differentiation of the two types of trypanosomes, which could lead to a more specific detection method. High resolution Raman mapping allowed to track certain biological components such as DNA, phospholipids and the VSG coat surface. As the latter was present at high concentration around the surface it was thought that most of the Raman signal would be originated from this protein layer. Despite the ability of trypanosomes to change periodically the composition of its VSG, it was not spectrally identified between cells of the same sub-species. However, by using the Raman fingerprint specific to each sub-species, it appeared that they were spectrally different. It would suggest that it would be possible to differentiate both *T.b. brucei* and *T.b. gambiense*. These results could lead to further work by investigating the other sub-species *T.b. rhodesiense*, that is the other human infective parasite, and other parasites infecting animals such as *T. vivax* and *T. congolense*, as a detection that could characterise the parasite involved in the infection would help to provide the appropriate treatment. However, it was unknown whether the surface composition of VSG within the same sub-species or between sub-species was different, and the spectral differences could not be linked to a specific biological component. It would be interesting to study more closely the surface composition and organisation of the parasites with different methods. Fluorescence spectroscopy could help track individual components and comparing it with Raman information, as well as mass spectrometry that could be used to determine the composition and structure of VSG and provide more insight on the differentiation observed with Raman. In previous studies, it was demonstrated that the surface protein layer is affected by the environment, and it would be important to culture the trypanosomes in different media. For example, bloodstream trypanosomes, as used here, could be compared with adipose tissue form trypanosomes with Raman in order to obtain the fingerprint of these parasites that are present in the skin as well as determining the biological variations.

Mice skin samples were then analysed on CaF_2 substrate to understand to first determine if the infected skin could be detected and to understand the biological variations induced by the presence of the infection. Raman mapping technique was used to characterise different area across the sample and provided a general trend of the biological variations. Infected and uninfected skin were found to be spectrally different by PCA, meaning that the use of Raman spectroscopy for skin diagnostic is possible. Raman fingerprint obtained from each sample demonstrated that protein and lipid composition were affected during the infection. It is possible that the parasites were using their surrounding skin matrix for their metabolism and proliferation, thus leading to these biological alterations. In addition, trypanosomes needed specific nutrients for their growth such lipids and fatty-acid, their presence in the skin could reveal an up-regulation in the release of such components by the host induced by the parasites. It would explain the increase in intensity observed for Raman bands specific to proteins and lipids. Such differences in protein composition in the skin could also be originated from the presence of the parasites and their direct contribution to the Raman signal. However, the comparison between each fingerprint did not provide clear conclusion on their contribution. The spectral overlap between *T.b. brucei* and the skin was too important to confirm this hypothesis. These results were quite promising as it was demonstrated that Raman was able to spectrally detect the infection in the skin as well as providing some information on the biological changes induced by the parasites. It would be interesting to repeat this investigation on multiple skin samples from different mice. It was possible that the biological implications of the infection may vary between host, and the use of different skin sample would allow to assess it, in addition of obtaining more data to confirm these findings. The alteration of the skin by the parasites was still unknown as their presence in the skin have been recently identified but the tentative assignment of the different Raman bands provided some hypothesis for these changes. It would be important to closely investigate these variations in order to understand their spectral differences detected with Raman. Fluorescence spectroscopy and mass spectrometry could also help identifying variations in composition and concentration of specific biological components, which could corroborate the findings obtained with Raman. By knowing the biological variation specifically induced by the presence of the parasites in the skin would make the Raman detection method more specific to HAT, as specific Raman bands could be identified. Skin samples analysed were infected with *T.b. brucei* and, in the future, it would be interesting to compare it with an

infection with *T.b. gambiense* or *T.b. rhodesiense*, as they could potentially have a different interaction with their surrounding environment.

Following the success of the *ex vivo* skin detection of the infection, Raman was applied *in situ* on post-mortem mice with the use of a portable instrument. It was clearly shown that the detection of the infection was achieved and characterised by an increase in intensity of certain Raman bands. The spectral information was slightly different from the *ex vivo* study, probably due to the different instrumentation and resolution employed and due to the contribution from other organs such as spleen or liver to the Raman signal. Nonetheless, the tentative assignment of Raman bands specific to the infection seemed to indicate similar changes in the protein and lipid composition. With a better understanding of the biological variations from *in vitro* and *ex vivo* studies, it would be possible to determine whether the infection is only detected through the change in composition and conformation of protein/lipid or if specific metabolites are released by the trypanosomes in the skin that could be detected by Raman. It was shown that different strains of the *T.b. brucei* sub-species, as well as *T.b. gambiense*, infecting mice were detected and provided similar Raman information. Hence, it was not possible to specifically identify the sub-species involved in the infection. A different signal was obtained for *T.b. gambiense* but it was thought that it was the result of a less virulent infection of this sub-species in animals, and with the result obtained it was not possible to clearly conclude on the possible differentiation of sub-species. This observation was supported by comparing the number of parasites present in the host, intra-vascular and extra-vascular, which showed that the increase in intensity of specific Raman bands correlated to this number. Different experiments were performed to understand the origin of the Raman signal specific to the infection obtained in addition to the alteration of lipids and proteins in the skin. Intra-dermal injection of parasites displayed a similar increase in intensity of Raman bands as observed in infected mice, but it could be related to the increase of protein concentration resulting from the presence of the VSG coat in the blisters. The direct detection of trypanosomes within the skin could not be proven but it was interesting to observe similar spectral changed between infected mice and the blister containing trypanosomes. Moreover, it appeared that an immune response from the host was also measured during the infection as immunodeficient mice infected with *T.b. brucei* showed a decrease in their Raman signal. Finally, a cyclical presence of the parasites in the skin have been determined, similar to

blood parasitemia, during the time study, and it was possible to track the progression of the infection through time with Raman. Raman detection technique was also compared to blood parasitemia and qPCR on the skin and was proven to detect the infection before these two techniques. However, the number of mice used in this study was too low to assess the reproducibility and the variation in biological responses between mice, to fully assess the early detection of the infection by Raman. It was also possible that qPCR did not detect parasites earlier because trypanosomes were located on a different area of the skin than the one analysed. In the future, it will be important to increase the number of repeats per time points and to add earlier time points to determine when the infection can be detected. This *in situ* has proven that the detection of sleeping sickness with a portable Raman instrument was achievable. More work needs to be performed to obtain a full animal model for the detection of the infection. The contribution of the immune response by the host will also have to be assessed in addition to the presence of the parasites and its influence on the skin matrix, which would determine the specificity of the method. A different parasitic disease or a different skin infection could be studied to assess it. It will also be interesting to investigate live animals, where the infection could be tracked on the same host and biological alterations and responses could be detected with Raman through time. In addition, it is currently unknown if the treatment for HAT are efficient in the elimination of the parasites located in the skin, it could be assessed by tracking the progression of the infection on live animals before and after treatment.

The opportunity to test this method on the field was given, and by using the same instrument as for the *in situ* study, Raman spectra were obtained from human skins. Raman spectra did not display any visible Raman bands due to strong autofluorescence from the skin. Despite the absence of spectral information, a variation in the fluorescence between measurements was observed. The comparison of the AUC values between control and confirmed infected patients showed an increase of the AUC for the latter group, thus demonstrating a change within the biochemical composition in the skin that could be tracked with Raman. This method of data analysis could not be used on the field due to its lack of specificity, but it showed great potential for the establishment of a diagnostic method targeting the skin. The difference between AUC mean values seemed to indicate that a change within the biological composition of the skin was occurring. Moreover, it appeared that the raw Raman spectra from control and infected patients

could be classified by using a trained statistical model. It would be important to increase the number of patients from the field in order to obtain a more representative and robust model. The use of a different instrument could provide Raman spectral information about the state of the skin and potentially ameliorate the field detection by overcoming the autofluorescence of the skin, mostly due to the presence of melanin.

Overall, it has been demonstrated that Raman spectroscopy could be used in the detection of HAT by targeting the skin of the host. The method was developed through *in vitro*, *ex vivo* and *in situ* experiments and has shown to be quite reliable. Further work needs to be performed by increasing the number of repeats of the different experiments to make the animal model more robust and to assess the specificity of the detection method. It will also be important to understand the biological influence that the parasites have on the skin, how trypanosomes spread across the skin and if their mode of action is identical between hosts. Raman analysis supported with other analytical techniques such as fluorescence or mass spectrometry could achieve it. In addition, previous works have investigated the concentration of metabolites or amino-acids in blood, serum or urine of animals due to the infection by *T.b. brucei*, and the use of Raman on these samples could be explored and in association with skin analysis could provide a more accurate detection method for HAT. The use of Raman spectroscopy was shown for the detection of *gambiense*-HAT, but it could also be translated for *rhodesiense* cases, that also affect humans. Moreover, animals are also at risks with an infection by *T.b. brucei* or *T.b. rhodesiense*, and cause economic problems, as well as acting as a reservoir for human infection in the case of *rhodesiense*, and the application of Raman for the detection of infection in animals should also be investigated. Differently, this technique could also be tested for different skin parasitic infections such as Chagas disease, malaria or leishmania. For example, Chagas disease is caused by a trypanosome, *T. cruzi*, and relation between this infection and sleeping sickness was made during this work due to the possible increase of cholesterol in the skin due to the presence of *T.b. brucei*. Raman spectroscopy could then be applied to such parasitic infections to expand the use of this technique and this investigation would also allow to assess the specificity of the diagnostic method demonstrated here. Finally, trypanosomes have also been located in other organs such as spleen, liver or lymph nodes, which could provide a different site for the detection of HAT with Raman. Indeed, Special Offset Raman Spectroscopy (SORS) is a Raman technique

that allows the interrogation of an area deeper than the skin or organs such as spleen that was known to be a reservoir for trypanosomes. It was for example used for the analysis of bones through the skin and could be applied here to target such organs and provide a different detection site.

The development of a detection method for HAT with Raman has opened a new research area for the investigation of the skin as a potential site for the diagnostic of the disease. It has proven to be quite promising and its use on the field could help identify asymptomatic carriers and reduce the human reservoir, which would contribute to the elimination of *gambiense*-HAT. Importantly, this technique could also be applied to other parasitic disease present in the skin, making the use of Raman spectroscopy an interesting tool for bio-diagnostic in the future.

Chapter 7 Experimental

7.1 Extraction and preparation of variable surface glycoprotein

This experiment was carried by Dr Annette Macleod's group at the university of Glasgow.

1 - 2 x10^8 bloodstream trypanosomes were chilled on ice, centrifuged at 2500 g for 10 min, washed in an isotonic buffer and resuspended in 300 µL of 10 mM sodium phosphate buffer, pH 8.0, containing 0.1 mM TLCK, 1 µg/mL leupeptin, and 1 µg/mL aprotinin. After 5 min at 37 °C, the mixture was cooled on ice and centrifuged (14,000 g, 5 min). The supernatant was applied to a small (0.2 mL packed gel) DE52 anion exchange column equilibrated in a 10 mM sodium phosphate buffer, pH 8.0. The sVSG was eluted from the DE52 by adding 4 x 200 µl 10 mM sodium phosphate buffer, pH 8.0. The entire column eluate (1.1 mL; containing about 50-100 µg sVSG) was concentrated on a Microcon YM-10 concentrator (Millipore, Watford, UK) and diafiltered into water by adding 0.5 mL water and spinning five times. The diafiltered (de-salted) sVSG is recovered from the filter in 100 µL water which can be stored frozen.

The solution was then spotted onto a glass slide and left to dry. This step was repeated three times in order to increase the concentration of VSG onto the slide.

7.2 Trypanosomes preparation: *T.b. brucei* and *T.b. gambiense*

The culture of trypanosomes was performed by Dr Annette Macleod's group at the university of Glasgow.

Trypanosoma brucei brucei and *Trypanosoma brucei gambiense* bloodstream form cell cultures were cultivated in HMI-9 medium supplemented with 20% (v/v) Serum Plus™ media supplement. An additional 1 % of human serum was added for the culture of *T.b. gambiense*. Cultures were maintained in vented lid flasks in a 37 ^oC, 5% CO_2 incubator and sub-passaged every 2-3 days to maintain a cell density of ~10^5-10^6 trypanosomes per mL.

HMI-9 media modified – Iscove's Modified Dulbecco's Medium (IMDM) supplemented with; 1 mM hypoxanthine, 50 µM bathocuproinedisulfonic acid, 1.5 mM cysteine, 2 mM sodium pyruvate, 160 µM thymidine, 200 µM 2-mercaptoethanol, 1.4 mM glucose, 125 µM adenosine, 125 µM guanosine, 30 µg/ml kanamycin, 1 mg/ml methyl cellulose, 20% (v/v) Serum Plus™ Fetal Bovine Serum media supplement. Filter sterilised. Stored in 500 ml aliquots at 4 ^{o}C.

Trypanosomes were fixed with 10% formalin on Raman grade calcium fluoride slides (Crystran Ltd, UK). Prior Raman analysis, slides were gently washed with a few drops of water deposited and removed with a 1 mL pipette.

7.3 *Ex vivo* mice skin samples

7.3.1 Preparation and fixation of mice skin samples

Mice skin samples extraction and fixation were performed at the university of Glasgow by Dr Annette Macleod's research group.

Infected mouse was culled at day 15 post infection with a blood parasitemia level at 7.8. Then, 2 cm^2 skin samples removed from the abdominal area for both infected and uninfected mice. Skin samples were fixed in 10% neutral buffered formalin prior being processed into paraffin blocks. Paraffin embedded skin samples were cut into 2.5 microns section and placed on a CaF_2 slides (Crystran Ltd, UK).

7.3.2 Paraffin chemical removal protocol

Mice skin samples were preserved in formalin, paraffin embedded and fixed onto Raman grade calcium fluoride slides (Crystran Ltd, UK). Prior to Raman analysis, samples were dewaxed to remove the paraffin. Samples were placed in a bath of xylene (Sigma-Aldrich, UK) for 15 min. This step was repeated twice. Samples were then washed successively with 90% ethanol (v/v), 70% ethanol (v/v) and then water, within a period of 5 min each. Wash steps with water were repeated three times.

7.4 *In vitro* and *ex vivo* Raman spectroscopy

All Raman *in vitro* and *ex vivo* experiments were performed with an Alpha 300 R Witec confocal Raman microscope (Witec, Germany) equipped with a 532 nm laser, coupled with an Andor CCD camera (DV401-BV) with a 600 l/mm grating (spectral resolution of 3 cm^{-1}), and a 785 nm laser, coupled with an Andor CCD camera (DU401-BR-DD) with a 300 l/mm grating. The microscope was equipped with a 100x (0.9 NA) lens. The spectral range used was 200 – 4000 cm^{-1}. Before any measurements, instrument was calibrated using a silica, where the Raman peak was set to 520 ± 0.5 cm^{-1}, by adjusting the laser wavelength on the Witec control software toolbox (Witec, Germany).

7.4.1 Raman measurement of pure VSG

Sample was measured with a 532 nm laser, a 100x (0.9 NA) lens, 1 s acquisition time and 25 mW power.

7.4.2 Raman mapping of Trypanosoma brucei

7.4.2.1 Trypanosoma brucei brucei and Trypanosoma brucei gambiense Raman mapping

532 nm: Samples were analysed using a 532 nm laser, at 9 mW, a 6 s acquisition time and a spectral centre of 2500 cm^{-1}. Parasites were mapped with a 0.5 µm step in x and y. Prior the production of the Raman intensity maps, cosmic rays were removed from each spectrum using cosmic ray removal tool for the Witec project software. Raman intensity maps were produced on the Witec project software by selecting individual Raman bands.

785 nm: Samples were analysed using a 785 nm laser, at 78 mW, a 6 s acquisition time and a spectral centre of 2200 cm^{-1}. Parasites were mapped with a 0.5 µm step in x and y. Prior the production of the Raman intensity maps, cosmic rays were removed from each spectrum using cosmic ray removal tool for the Witec project software. Raman intensity maps were produced on the Witec project software by selecting individual Raman bands.

7.4.2.2 Principal component analysis

Principal component analysis was performed with Matlab 2016a (Mathworks®, UK) and a homemade statistical toolbox. For each map, 20 spectra were selected randomly across the trypanosomes to give the best representation of the map.

7.4.2.2.1 *Trypanosoma brucei brucei* PCA comparison

532 nm: Five maps were chosen for this analysis, representing 20 spectra for each parasite for a total of 100 Raman spectra, and were imported in Matlab. The data sets were pre-processed as follow: cosmic rays were removed using a length factor 5, spectra were smoothed with Savitzky-Golay smoothing method with a polynomial order of 2 and spectral window of 9, data were baseline corrected with a smoothing parameter of 10^5 and asymmetry parameter of 0.01. Each spectrum was then normalised to the highest peak intensity, mean centre and analysed with PCA.

785 nm: Five maps were chosen for this analysis, representing 20 spectra for each parasite for a total of 100 Raman spectra, and were imported in Matlab. The data sets were pre-processed as follow: cosmic rays were removed using a length factor 7, spectra were smoothed with Savitzky-Golay smoothing method with a polynomial order of 3 and spectral window of 13, spectral window was reduced to 552 – 1850 cm^{-1}, data were baseline corrected with a smoothing parameter of 10^4 and asymmetry parameter of 0.001. Each spectrum was then normalised to the highest peak intensity, mean centre and analysed using PCA.

7.4.2.2.2 *Trypanosoma brucei gambiense* PCA comparison

532 nm: Five maps were chosen for this analysis, representing 20 spectra for each parasite for a total of 100 Raman spectra, and were imported in Matlab. The data sets were pre-processed as follow: cosmic rays were removed using a length factor 5, spectra were smoothed with Savitzky-Golay smoothing method with a polynomial order of 2 and spectral window of 9, data were baseline corrected with a smoothing parameter of 10^6 and asymmetry parameter of 0.01. Each spectrum was then normalised to the highest peak intensity, mean centre and analysed using PCA.

785 nm: Five maps were chosen for this analysis, representing 20 spectra for each parasite for a total of 100 Raman spectra, and were imported in Matlab. The data sets were pre-processed as follow: cosmic rays were removed using a length factor 7, spectra were smoothed with Savitzky-Golay smoothing method with a polynomial order of 3 and spectral window of 13, spectral window was reduced to 552 – 1850 cm^{-1}, data were baseline corrected with a smoothing parameter of 10^4 and asymmetry parameter of 0.001. Each spectrum was then normalised to the highest peak intensity, mean centre and analysed using PCA.

7.4.2.3 Trypanosoma brucei brucei and Trypanosoma brucei gambiense Raman fingerprint comparison

532 nm: Four maps of each sub-species were chosen for this analysis, representing 20 spectra for each parasite for a total of 80 Raman spectra, and were imported in Matlab. The data sets were pre-processed as follow: cosmic rays were removed using a length factor 5, spectra were smoothed with Savitzky-Golay smoothing method with a polynomial order of 2 and spectral window of 9, data were baseline corrected with a smoothing parameter of 10^4 and asymmetry parameter of 0.01. Each data sets from each sub-species were then averaged into a single Raman spectrum, to obtain their Raman fingerprint. Raman spectra were then split between two spectral windows, 450 – 1850 cm^{-1} and 2550 – 3550 cm^{-1} and were normalised separately to the highest peak intensity.

785 nm: Four maps of each sub-species were chosen for this analysis, representing 20 spectra for each parasite for a total of 80 Raman spectra, and were imported in Matlab. The data sets were pre-processed as follow: cosmic rays were removed using a length factor 7, spectra were smoothed with Savitzky-Golay smoothing method with a polynomial order of 3 and spectral window of 13, spectral window was reduced to 552 – 1850 cm^{-1}, data were baseline corrected with a smoothing parameter of 10^4 and asymmetry parameter of 0.001. Each data sets from each sub-species were then averaged into a single Raman spectrum, to obtain their Raman fingerprint. Then, each Raman spectrum was normalised to the highest peak intensity.

7.4.3 *Ex vivo* mice skin analysis

7.4.3.1 Raman mapping and PCA of uninfected and infected skin

532 nm: Both skin samples were mapped in square dimensions (50 x 50 µm) using a 2 µm step in x and y, for a total of 625 spectra, using a 532 nm laser, 12 mW, with a 1 s acquisition time and a spectral centre of 2450 cm^{-1}. Seven maps for each skin samples were imported into matlab and pre-processed as follow: cosmic rays were removed using a length factor 5, spectra were smoothed with Savitzky-Golay smoothing method with a polynomial order of 2 and spectral window of 9, spectral window was reduced to 500 – 3600 cm^{-1} and data were baseline corrected with a smoothing parameter of 10^4 and asymmetry parameter of 0.01. Each map (625 spectra) were then averaged into a single Raman spectrum for both samples, total of seven Raman spectra for each uninfected and infected skin and normalised individually to the highest peak intensity. Data set was mean centre before being analysed using PCA algorithm.

785 nm: Both skin samples were mapped in square dimensions (50 x 50 µm) using a 2 µm step in x and y, for a total of 625 spectra, using a 785 nm laser, 78 mW, with a 3 s acquisition time and a spectral centre of 2200 cm^{-1}. Before being imported into matlab, all maps had some of their cosmic ray removed using Witec project software. Seven maps for each skin samples were imported into matlab and pre-processed as follow: cosmic ray were removed using a length factor 17, spectra were smoothed with Savitzky-Golay smoothing method with a polynomial order of 3 and spectral window of 15, and the spectral window was reduced to 650 – 1800 cm^{-1}, data were baseline corrected with a smoothing parameter of 10^4 and asymmetry parameter of 0.01. Each map (625 spectra) were then averaged into a single Raman spectrum for both samples, total of seven Raman spectra for each uninfected and infected skin and normalised individually to the highest peak intensity. Data set was mean centre before being analysed using PCA algorithm.

7.4.3.2 Raman fingerprint comparison between uninfected and infected skin samples

532 nm: Seven maps from each skin samples obtained previously were processed as mentioned before. Each data sets from uninfected and infected skin were averaged into a single Raman

fingerprint, representing one spectrum for each state of the skin. Spectral window was divided in two separate section, 550 - 1800 cm^{-1} and 2550 – 3700 cm^{-1} and were normalised separately to the highest peak intensity before comparison.

785 nm: Seven maps from each skin samples obtained previously were processed as mentioned before. Each data sets from uninfected and infected skin were averaged into a single Raman fingerprint, representing one spectrum for each state of the skin. Then, normalised to the highest intensity peak before comparison.

7.4.3.3 Raman fingerprint comparison between skin samples and Trypanosoma brucei brucei

532 nm: Each Raman fingerprint obtained from skin samples and *T.b. brucei* were processed as explained previously. Spectral window was separated between, 500 – 1800 cm^{-1} and 2600 – 3600 cm^{-1}, and spectra were normalised separately to the highest peak intensity before comparison.

785 nm: Each Raman fingerprint obtained from skin samples and *T.b. brucei* were processed as explained previously. Spectral window was reduced to 650 – 1800 cm^{-1} and spectra were normalised to the highest peak intensity before comparison.

7.5 *In situ* investigation

7.5.1 Blood parasitemia

A small blood sample was taken by means of venepuncture of the superficial vein of the tail. A drop of blood was placed on a microscope slide and a square coverslip 22 x 22 mm placed on top of the sample to make a wet smear.

The sample was allowed to settle for 1 minute to allow any Brownian movement to stop (the only movement should be the motility of the trypanosomes), then it was placed on a microscope and a number of fields were observed using a 40x lens.

Using the system and charts devised by Herbert et al.,[266] several fields were observed and matched with the chart to give an antilog value. From the antilog value, a fairly accurate estimation can be made of the number of trypanosomes /ml of blood.

7.5.2 Immunohistochemical staining and semi-quantitative evaluation of trypanosomes in mice skin samples

This experimental procedure was carried out by Dr Annette Macleod's group at the university of Glasgow.

Paraffin embedded skin samples were processed for immunohistochemical staining using a polyclonal rabbit antibody raised against the invariant surface glycoprotein 65 (ISG65) (M. Carrington, Cambridge, UK) using a Dako Autostainer Link 48 (Dako, Denmark) and were subsequently counterstained with Gill's Haematoxylin.

Stained skin samples were then assessed by two pathologists blinded to group assignment and experimental procedures. Presence of parasites defined as intravascular and extravascular was evaluated in 10 randomly selected high-power fields at 40x magnification with a 0 to 3 semi-quantitative grading scale (0 = no parasites detectable; 1 = low numbers of parasites (<20); 2 = moderate numbers of parasites (20 < 50); 3 = large numbers of parasites (>50)). An average parasite burden score was calculated for each sample.

7.5.3 Histopathological assessment of inflammation in the skin

This experimental procedure was performed by Dr Annette Macleod's research group at the university of Glasgow.

Paraffin embedded skin samples were stained with Haematoxylin and Eosin (HE). Semi-quantitative assessment of cutaneous inflammatory cell was performed by two pathologists blinded to group assignment and experimental procedures. The extent of mixed inflammatory cell infiltration in the skin was evaluated in 10 randomly selected high-power fields at 40x magnification on a 0 to 3 grading scale (0 = no inflammation or only few scattered leukocytes; 1 = low numbers of inflammatory cells; 2 = moderate numbers of inflammatory cells; 3 = large

numbers of inflammatory cells). An average inflammation score was calculated between the 10 high-power fields for each sample.

7.5.4 Raman analysis of mice skin *in situ*

7.5.4.1 Raman measurements on mice skin

All Raman analysis were performed using a Snowy Range benchtop (Snowy Range instruments, UK), model sierra 2.0, 785 nm laser (100 mW). The spectral range of the measurement was 200 – 2000 cm^{-1} with a spectral resolution of 4 cm^{-1}. All measurements were performed using the bottom aperture of the instrument.

The instrument was elevated from the bench, and a plate holder was placed underneath the aperture, which could regulate the distance between the sample and the aperture. Prior any measurements, instrument was calibrated with a Silica slide, which provided the optimal focus point of the laser. This distance was measured and applied during the analysis of mice in order to keep the working distance identical between each experiment.

BALB/C and NSG mice, controls or infected with *T.b. brucei* 247 or gvr35 and *T.b. gambiense*, were shaved using a hair removal cream (Veet®). Cream was spread with fingertip across the abdominal or dorsal region and left for less than 10 minutes, usually 6 minutes, to work in order to avoid any skin damage. Cream was removed with a wet paper towel, ensuring that a large portion of skin was cleared from hair. Then, the skin area shaved was washed thoroughly under a running tap water to remove any residual hair removal cream from the skin area.

Mice were then placed on the plate holder and the working distance was defined. Raman spectra were obtained with three acquisitions, at 30 and 60 s acquisition time and 45 mW, and ten or five replicates were obtained across the skin depending on the experiment. The Orbital Raster Scan (ORS) was not used during the experiments.

The hair removal cream was analysed by taking two measurements in triplicate with 60 s acquisition time and 45 mW power.

7.5.4.2 Raman measurements on mice skin placed on CaF_2

After Raman analysis of mice skin, the abdominal or dorsal skin was careful removed with scissors from the mouse. The removed skin was placed on calcium fluoride slides (Crystran Ltd, UK) with the inside skin facing the slide. Raman measurements were obtained as explained previously.

7.5.4.3 Raman measurements of intra-dermal injection of serum and trypanosomes in mice

The lysate was prepared by exsanguinating under anaesthesia a normal BALB/c mouse (without anti-coagulant) for serum. A volume of 1.2 ml blood was obtained which was spun down, and the resulting serum was used to suspend $1x10^7$ cultured *T.b. brucei* 247 cells in 50µl volume.

The back of the recipient mouse cadaver was depilated using a proprietary depilatory cream and the excess cream and hair removed by warm running water. The 50 µl of trypanosomes suspension was injected intradermally at two different sites to produce two blisters and the left-hand side was injected the same way using serum as a control, as shown in Figure 7.1.

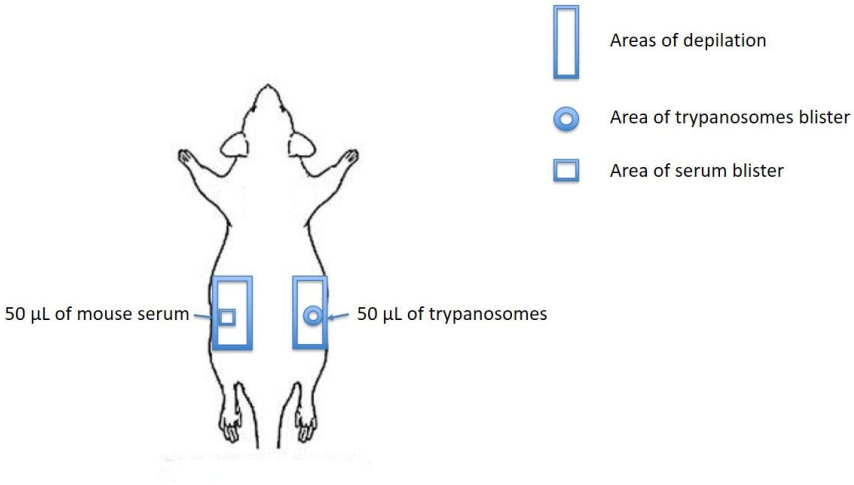

Figure 7.1 Illustration of the experimental procedure for the intradermal injection of trypanosomes and serum in the back region of mouse

Three Raman measurements were made in triplicates on each blister with 60 s acquisition time and 45 mW. Additionally, three Raman measurements made in triplicates were made on a different area from the blisters of the same dorsal skin sample as control.

7.5.4.4 Data processing and spectral comparison

After Raman experiments, data were saved as SPC files and imported in Matlab 2016a (Mathworks®, UK). The three acquisition for each single point measurement were averaged into a single Raman spectrum. Each spectrum was smoothed with Savitzky-Golay smoothing method with a polynomial order of 3 and spectral window of 15, the spectral window was reduced to 599 – 1774 cm^{-1} and data were baseline corrected with a smoothing parameter of 10^5 and asymmetry parameter of 0.01.

The Raman spectra replicates from each mouse were then averaged into a single Raman spectrum representative of the mouse. Finally, each spectrum was normalised to the highest peak intensity and plotted on the same figure for comparison.

7.5.4.5 PCA analysis

In the case of the comparison of hair cream removal, control mice and infected mice measurements shown in Figure 4.2, the three acquisition of each spectrum for the hair removal cream were averaged, which provided two Raman spectra for the cream. The spectral window was reduced to 800 – 1800 cm^{-1} after smoothing method. Data were then processed as explained previously, mean centre and analysed using PCA.

Raman spectra were processed as explained previously and analysed using PCA, with the exception of Figure 4.4, Figure 4.6 and Figure 4.8. To produce these figures, the ten or five replicates obtained across the skin were not averaged into a single Raman spectrum. Individual replicate was normalised to the highest peak intensity, mean centre and analysed using PCA.

7.5.5 Raman time study

Nine C57/BLACK6J mice were used for this study. Eight mice were infected with *T.b. brucei* 247 and one mice was analysed at different time points: 9, 10, 13, 14, 16, 17, 22 and 23 days. The

protocols to prepare the mice, obtained the Raman measurements and analysed them using PCA were described previously. One mouse was not infected and was considered as a control.

7.5.6 Polymerase Chain Reaction (PCR)

PCR measurements were carried out by Dr Annette Macleod's research group at the university of Glasgow.

Mice previously infected with *T.b. brucei* 247 were culled at various time points and a piece of skin from the abdominal area was removed. This skin was frozen and stored at -80 °C.

Genomic DNA (gDNA) was extracted from 25-30 mg frozen tissue following proteinase K digestion and disruption of the tissue using a Qiagen Tissuelyser and adapted method for the Qiagen Dneasy Blood and Tissue Kit (Qiagen, Manchester (UK)). The resulting gDNA was diluted to 4 ng/µl.

Trypanosome load in the skin was determined using Taqman real-time PCR. Taqman PCR, using primers and probe specifically designed to detect the trypanosome *Pfr2* gene, was performed in a 25 µl reaction mix comprising 1xTaqman Brilliant II master mix (Agilent, Stockport, UK), 0.05 pmol/µl forward primer (CCAACCGTGTGTTTCCTCCT), 0.05 pmol/ µl reverse primer (GAAAAGGTGTCAAACTACTGCCG), 0.1 pmol/µl probe (FAM-CTTGTCTTCTCCTTTTTTGTCTCTTTCCCCCT-TAMRA) (Eurofins MWG Operon, Eurofins Genomics, Germany) and 20 ng template DNA.

A standard curve was constructed using a serial dilution (range: 1x 10^6 to 1x 10^1 copies of pCR ®2.1 vector containing the cloned *Pfr2* target sequence (Eurofins MWG Operon, Eurofins Genomics, Germany). The amplification was performed on an Mx Pro 3005 (Agilent, USA) with a thermal profile of 95 °C for 10 minutes followed by 45 cycles of 95 °C for 15 seconds, 60°C for 1 minute and 72 °C for 1 second. The trypanosome load within the skin sample was calculated from the standard curve using the MxPro qPCR software (Agilent, USA).

Values obtained from PCR experiments related to the number of gene copies measured. As the trypanosomes studied (*T.b. brucei*) possessed 4 copies of the gene targeted, dividing the PCR values by 4 had provided the number of trypanosomes present in the sample. Additionally, PCR

values were derived from 20 ng of input DNA, which would equate to 21 µg of skin. Hence, by dividing the number of trypanosomes measured in the sample by 21 provided a concentration of the number of trypanosomes present in 1 µg of skin, giving a representation of their presence in the skin across the mouse.

7.6 Field investigation

7.6.1 Measurements

The same instrument, a Snowy Range benchtop (Snowy Range instruments, UK), model sierra 2.0, 785 nm laser (100 mW), used for the *in situ* analysis of mice skin was used for field investigation on human skin. Measurements were obtained through the bottom aperture of the instrument. In order to keep the focus point and the working distance identical between each measurement, an adaptor was made with a 3D printer (Ultimaker 2+ 3D printer, UK) possessing the exact focal distance and size of the bottom aperture. It also allowed to keep protecting the measurements from natural light.

Raman analysis were performed on the inside forearm and the back of the hand of the patients. Measurements were made with 5 s acquisition time and 5.7 mW power. Five Raman spectra were obtained across each skin area with the Orbital Raster Scan (ORS).

7.6.2 Area under the curve calculation

Raman measurements were saved as SPC files and imported into Matlab 2016a (Mathworks®, UK). Cosmic rays were removed depending on the individual Raman spectrum using a maximum length factor of 9. Data sets was smoothed with Savitzky-Golay smoothing method with a polynomial order of 2 and spectral window of 13, the spectral window was reduced to 599 – 1750 cm^{-1} and the area under the curve for each individual Raman spectrum was calculated in Matlab. The resulted AUC values were exported into an excel file, where the mean and standard deviation of each group were calculated, and their distribution drawn into a table. The student t-test was performed using the data analysis toolbox in Microsoft excel 2018.

Chapter 8 References

(1) Bruce, D. *Preliminary Report on the Tsetse Fly Disease or Nagana, in Zululand*; Bennett & Davis, 1895.

(2) Plimmer, H. G.; Bradford, J. R. A Preliminary Note on the Morphology and Distribution of the Organism Found in the Tsetse Fly Disease. *Proc. R. Soc. London* **1899**, *65*, 274–281.

(3) Forde, R. M. Some Clinical Notes on a European Patient in Whose Blood a Trypanosome Was Observed. *J. Trop. Med.* **1902**, *5*, 261–263.

(4) Dutton, J. E. Preliminary Note upon a Trypanosome Occurring in the Blood of Man. *Thompson Yates Lab. Rep.* **1902**, *4*, 455–468.

(5) Stephens, J. W. W.; Fantham, H. B. On the Peculiar Morphology of a Trypanosome from a Case of Sleeping Sickness and the Possibility of Its Being a New Species (T. Rhodesiense). *Proc. R. Soc. B Biol. Sci.* **1910**, *83* (561), 28–33.

(6) Hoare, C. A. *The Trypanosomes of Mammals. A Zoological Monograph.*; Blackwell Scientific Publications, 1972.

(7) Bruce, D. Classification of the African Trypanosomes Pathogenic to Man and Domestic Animals. *Trans. R. Soc. Trop. Med. Hyg.* **1914**, *8* (1), 1–22.

(8) Cox, F. E. . History of Sleeping Sickness (African Trypanosomiasis). *Infect. Dis. Clin. North Am.* **2004**, *18* (2), 231–245.

(9) Kleine, F. K. Weitere Wissenschaftliche Beobachtungen Über Die Entwicklung von Trypanosomen in Glossinen. *Dtsch Med Wochenschr* **1909**, *11*, 116–139.

(10) Pépin, J.; Méda, H. A. The Epidemiology and Control of Human African Trypanosomiasis. *Adv. Parasitol.* **2001**, *49*, 71–132.

(11) Grebaut, P.; Bodo, J. M.; Assona, A.; Foumane Ngane, V.; Njiokou, F.; Ollivier, G.; Soula, G.; Laveissiere, C. Risk Factors for Human African Trypanosomiasis in the Bipindi Region of Cameroon. *Med. Trop. (Mars).* **2001**, *61* (4–5), 377–383.

(12) Courtin, F.; Jamonneau, V.; Camara, M.; Camara, O.; Coulibaly, B.; Diarra, A.; Solano, P.; Bucheton, B. A Geographical Approach to Identify Sleeping Sickness Risk Factors in a Mangrove Ecosystem. *Trop. Med. Int. Heal.* **2010**, *15* (8), 881–889.

(13) Moloo, S. K. The Distribution of Glossina Species in Africa and Their Natural Hosts. *Int. J. Trop. Insect Sci.* **1993**, *14* (04), 511–527.

(14) Allsopp, R. Options for Vector Control against Trypanosomiasis in Africa. *Trends Parasitol.* **2001**, *17* (1), 15–19.

(15) World Health Organization. Control and Surveillance of Human African Trypanosomiasis. *World Health Organ. Tech. Rep. Ser.* **2013**, No. 984, 1–237.

(16) Steverding, D. The History of African Trypanosomiasis. *Parasit. Vectors* **2008**, *1* (1), 3.

(17) Brun, R.; Blum, J.; Chappuis, F.; Burri, C. Human African Trypanosomiasis. *Lancet* **2010**, *375* (9709), 148–159.

(18) World Health Organization. Control and Surveillance of African Trypanosomiasis. Report of a WHO Expert Committee. *World Health Organ. Tech. Rep. Ser.* **1998**, *881* (I–IV), 1–114.

(19) Simarro, P. P.; Diarra, A.; Postigo, J. A. R.; Franco, J. R.; Jannin, J. G. The Human African Trypanosomiasis Control and Surveillance Programme of the World Health Organization 2000-2009: The Way Forward. *PLoS Negl. Trop. Dis.* **2011**, *5* (2).

(20) World Health Organization. Resolution 50.36, 50th World Health Assembly. In *Fiftieth World Health Assembly*; Geneva, 1997.

(21) Savioli, D. D. and L. Accelerating Work to Overcome the Global Impact of Neglected Tropical Diseases: A Roadmap for Implementation. *World Heal. Organ.* **2012**, 1–42.

(22) Pandey, A.; Atkins, K. E.; Bucheton, B.; Camara, M.; Aksoy, S.; Galvani, A. P.; Ndeffo-Mbah, M. L. Evaluating Long-Term Effectiveness of Sleeping Sickness Control Measures in Guinea. *Parasit. Vectors* **2015**, *8*, 550.

(23) Cecchi, G.; Mattioli, R. C.; Programme Against African Trypanosomiasis. *Geospatial Datasets and Analyses for an Environmental Approach to African Trypanosomiasis*; Food

and Agriculture Organization of the United Nations, 2009.

(24) Swallow, B. Impacts of Trypanosomiasis on African Agriculture. *Int. Livest. Res. Institute, Nairobi, Kenya.* **1999**, No. December 1999, 1–46.

(25) Kristjanson, P. M.; Swallow, B. M.; Rawlands, G. J.; Kruska, R. L.; Leeuw, P. N. Measuring the Cost of African Animal Trypanosomiasis, the Potential Benefits of Control and Returns to Research. *Agric. Syst.* **1999**, *59* (1), 79–98.

(26) Keating, J.; Yukich, J. O.; Sutherland, C. S.; Woods, G.; Tediosi, F. Human African Trypanosomiasis Prevention, Treatment and Control Costs: A Systematic Review. *Acta Trop.* **2015**, *150*, 4–13.

(27) Franco, J. R.; Simarro, P. P.; Diarra, A.; Jannin, J. G. Epidemiology of Human African Trypanosomiasis. *Clin. Epidemiol.* **2014**, *6* (1), 257–275.

(28) Gibson, W. Kinetoplastid Biology and Disease Species Concepts for Trypanosomes : From Morphological to Molecular. *Kinetoplastid Biol. Dis.* **2003**, *2* (10).

(29) Simarro, P. P.; Jannin, J.; Cattand, P. Eliminating Human African Trypanosomiasis: Where Do We Stand and What Comes Next? *PLoS Med.* **2008**, *5* (2), 0174–0180.

(30) Büscher, P.; Cecchi, G.; Jamonneau, V.; Priotto, G. Human African Trypanosomiasis. *Lancet* **2017**, *390* (10110), 2397–2409.

(31) Simo, G.; Asonganyi, T.; Nkinin, S. W.; Njiokou, F.; Herder, S. High Prevalence of Trypanosoma Brucei Gambiense Group 1 in Pigs from the Fontem Sleeping Sickness Focus in Cameroon. *Vet. Parasitol.* **2006**, *139* (1–3), 57–66.

(32) Njiokou, F.; Nimpaye, H.; Simo, G.; Njitchouang, G. R.; Asonganyi, T.; Cuny, G.; Herder, S. Domestic Animals as Potential Reservoir Hosts of Trypanosoma Brucei Gambiense in Sleeping Sickness Foci in Cameroon. *Parasite* **2010**, *17* (1), 61–66.

(33) Njiokou, F.; Laveissière, C.; Simo, G.; Nkinin, S.; Grébaut, P.; Cuny, G.; Herder, S. Wild Fauna as a Probable Animal Reservoir for Trypanosoma Brucei Gambiense in Cameroon. *Infect. Genet. Evol.* **2006**, *6* (2), 147–153.

(34) Jamonneau, V.; Ravel, S.; Koffi, M.; Kaba, D.; Zeze, D. G.; Ndri, L.; Sane, B.; Coulibaly, B.; Cuny, G.; Solano, P. Mixed Infections of Trypanosomes in Tsetse and Pigs and Their Epidemiological Significance in a Sleeping Sickness Focus of Côte d'Ivoire. *Parasitology* **2004**, *129* (Pt 6), 693–702.

(35) Fèvre, E. M.; Coleman, P. G.; Welburn, S. C.; Maudlin, I. Reanalyzing the 1900–1920 Sleeping Sickness Epidemic in Uganda. *Emerg. Infect. Dis.* **2004**, *10* (4), 567–573.

(36) Hide, G. History of Sleeping Sickness in East Africa. *Clin. Microbiol. Rev.* **1999**, *12* (1), 112–125.

(37) Waiswa, C.; Olaho-Mukani, W.; Katunguka-Rwakishaya, E. Domestic Animals as Reservoirs for Sleeping Sickness in Three Endemic Foci in South–eastern Uganda. *Ann. Trop. Med. Parasitol.* **2003**, *97* (2), 149–155.

(38) Kinung'hi, S. M.; Malele, I. I.; Kibona, S. N.; Matemba, L. E.; Sahani, J. K.; Kishamawe, C.; Mlengeya, T. D. K. Knowledge, Attitudes and Practices on Tsetse and Sleeping Sickness among Communities Living in and around Serengeti National Park, Tanzania. *Tanzan. Health Res. Bull.* **2006**, *8* (3), 168–172.

(39) Zoller, T.; Fèvre, E. M.; Welburn, S. C.; Odiit, M.; Coleman, P. G. Analysis of Risk Factors for T. Brucei Rhodesiense Sleeping Sickness within Villages in South-East Uganda. *BMC Infect. Dis.* **2008**, *8* (1), 88.

(40) von Wissmann, B.; Machila, N.; Picozzi, K.; Fèvre, E. M.; deC. Bronsvoort, B. M.; Handel, I. G.; Welburn, S. C. Factors Associated with Acquisition of Human Infective and Animal Infective Trypanosome Infections in Domestic Livestock in Western Kenya. *PLoS Negl. Trop. Dis.* **2011**, *5* (1), e941.

(41) Picozzi, K. Sleeping Sickness in Uganda: A Thin Line between Two Fatal Diseases. *Bmj* **2005**, *331* (7527), 1238–1241.

(42) Simarro, P. P.; Cecchi, G.; Paone, M.; Franco, J. R.; Diarra, A.; Ruiz, J. A.; Fèvre, E. M.; Courtin, F.; Mattioli, R. C.; Jannin, J. G. The Atlas of Human African Trypanosomiasis: A Contribution to Global Mapping of Neglected Tropical Diseases. *Int. J. Health Geogr.* **2010**, *9* (1), 57.

(43) Batchelor, N. A.; Atkinson, P. M.; Gething, P. W.; Picozzi, K.; Fèvre, E. M.; Kakembo, A. S. L.; Welburn, S. C. Spatial Predictions of Rhodesian Human African Trypanosomiasis (Sleeping Sickness) Prevalence in Kaberamaido and Dokolo, Two Newly Affected Districts of Uganda. *PLoS Negl. Trop. Dis.* **2009**, *3* (12), e563.

(44) Picado, A.; Ndung'u, J. Elimination of Sleeping Sickness in Uganda Could Be Jeopardised by Conflict in South Sudan. *Lancet. Glob. Heal.* **2017**, *5* (1), e28–e29.

(45) Vickerman, K. Developmental Cycles and Biology of Pathogenic Trypanosomes. *Br. Med. Bull.* **1985**, *41* (2), 105–114.

(46) Matthews, K. R.; Gull, K. Evidence for an Interplay between Cell Cycle Progression and the Initiation of Differentiation between Life Cycle Forms of African Trypanosomes. *J. Cell Biol.* **1994**, *125* (5), 1147–1156.

(47) Nolan, D. P.; Rolin, S.; Rodriguez, J. R.; Van Den Abbeele, J.; Pays, E. Slender and Stumpy Bloodstream Forms of Trypanosoma Brucei Display a Differential Response to Extracellular Acidic and Proteolytic Stress. *Eur. J. Biochem.* **2000**, *267* (1), 18–27.

(48) Sharma, R.; Gluenz, E.; Peacock, L.; Gibson, W.; Gull, K.; Carrington, M. The Heart of Darkness: Growth and Form of Trypanosoma Brucei in the Tsetse Fly. *Trends Parasitol.* **2009**, *25* (11), 517–524.

(49) Vickerman, K.; Tetley, L.; Hendry, K. A.; Turner, C. M. Biology of African Trypanosomes in the Tsetse Fly. *Biol. cell* **1988**, *64* (2), 109–119.

(50) Dyer, N. A.; Rose, C.; Ejeh, N. O.; Acosta-Serrano, A. Flying Tryps: Survival and Maturation of Trypanosomes in Tsetse Flies. *Trends Parasitol.* **2013**, *29* (4), 188–196.

(51) Kennedy, P. G. E. Clinical Features, Diagnosis, and Treatment of Human African Trypanosomiasis (Sleeping Sickness). *Lancet Neurol.* **2013**, *12* (2), 186–194.

(52) MacGregor, P.; Matthews, K. R. New Discoveries in the Transmission Biology of Sleeping Sickness Parasites: Applying the Basics. *J. Mol. Med. (Berl).* **2010**, *88* (9), 865–871.

(53) Matthews, K. R.; Ellis, J. R.; Paterou, A. Molecular Regulation of the Life Cycle of African Trypanosomes. *Trends Parasitol.* **2004**, *20* (1), 40–47.

(54) Kennedy, P. G. E. Human African Trypanosomiasis of the CNS : Current Issues and Challenges. *J Clin Invest* **2004**, *113* (4), 496–504.

(55) Masocha, W.; Rottenberg, M. E.; Kristensson, K. Migration of African Trypanosomes across the Blood–brain Barrier. *Physiol. Behav.* **2007**, *92* (1–2), 110–114.

(56) Checchi, F.; Filipe, J. A.; Haydon, D. T.; Chandramohan, D.; Chappuis, F. Estimates of the Duration of the Early and Late Stage of Gambiense Sleeping Sickness. *BMC Infect. Dis.* **2008**, *8* (1), 16.

(57) Odiit, M.; Kansiime, F.; Enyaru, J. C. Duration of Symptoms and Case Fatality of Sleeping Sickness Caused by Trypanosoma Brucei Rhodesiense in Tororo, Uganda. *East Afr. Med. J.* **1997**, *74* (12), 792–795.

(58) Blum, J.; Schmid, C.; Burri, C. Clinical Aspects of 2541 Patients with Second Stage Human African Trypanosomiasis. *Acta Trop.* **2006**, *97* (1), 55–64.

(59) Kennedy, P. G. E. The Continuing Problem of Human African Trypanosomiasis (Sleeping Sickness). *Ann. Neurol.* **2008**, *64* (2), 116–126.

(60) MacLean, L.; Chisi, J. E.; Odiit, M.; Gibson, W. C.; Ferris, V.; Picozzi, K.; Sternberg, J. M. Severity of Human African Trypanosomiasis in East Africa Is Associated with Geographic Location, Parasite Genotype, and Host Inflammatory Cytokine Response Profile. *Infect. Immun.* **2004**, *72* (12), 7040–7044.

(61) Sternberg, J. M. Human African Trypanosomiasis: Clinical Presentation and Immune Response. *Parasite Immunol.* **2004**, *26* (11–12), 469–476.

(62) Sudarshi, D.; Lawrence, S.; Pickrell, W. O.; Eligar, V.; Walters, R.; Quaderi, S.; Walker, A.; Capewell, P.; Clucas, C.; Vincent, A.; et al. Human African Trypanosomiasis Presenting at Least 29 Years after Infection—What Can This Teach Us about the Pathogenesis and Control of This Neglected Tropical Disease? *PLoS Negl. Trop. Dis.* **2014**, *8* (12), e3349.

(63) Jamonneau, V.; Ilboudo, H.; Kaboré, J.; Kaba, D.; Koffi, M.; Solano, P.; Garcia, A.; Courtin, D.; Laveissière, C.; Lingue, K.; et al. Untreated Human Infections by Trypanosoma Brucei Gambiense Are Not 100% Fatal. *PLoS Negl. Trop. Dis.* **2012**, *6* (6), e1691.

(64) Naessens, J. Bovine Trypanotolerance: A Natural Ability to Prevent Severe Anaemia and Haemophagocytic Syndrome? *Int. J. Parasitol.* **2006**, *36* (5), 521–528.

(65) Bucheton, B.; Macleod, A.; Jamonneau, V. Human Host Determinants Influencing the Outcome of Trypanosoma Brucei Gambiense Infections. *Parasite Immunol.* **2011**, *33* (8), 438–447.

(66) Woodruff, A. W.; Evans, D. A.; Owino, N. O. A 'Healthy' Carrier of African Trypanosomiasis. *J. Infect.* **1982**, *5* (1), 89–92.

(67) Jamonneau, V.; Bucheton, B.; Kaboré, J.; Ilboudo, H.; Camara, O.; Courtin, F.; Solano, P.; Kaba, D.; Kambire, R.; Lingue, K.; et al. Revisiting the Immune Trypanolysis Test to Optimise Epidemiological Surveillance and Control of Sleeping Sickness in West Africa. *PLoS Negl. Trop. Dis.* **2010**, *4* (12), e917.

(68) Garcia, A.; Jamonneau, V.; Magnus, E.; Laveissière, C.; Lejon, V.; N'Guessan, P.; N'Dri, L.; Van Meirvenne, N.; Büscher, P. Follow-up of Card Agglutination Trypanosomiasis Test (CATT) Positive but Apparently Aparasitaemic Individuals in Côte d'Ivoire: Evidence for a Complex and Heterogeneous Population. *Trop. Med. Int. Health* **2000**, *5* (11), 786–793.

(69) Koffi, M.; Solano, P.; Denizot, M.; Courtin, D.; Garcia, A.; Lejon, V.; Büscher, P.; Cuny, G.; Jamonneau, V. Aparasitemic Serological Suspects in Trypanosoma Brucei Gambiense Human African Trypanosomiasis: A Potential Human Reservoir of Parasites? *Acta Trop.* **2006**, *98* (2), 183–188.

(70) Kanmogne, G. D.; Asonganyi, T.; Gibson, W. C. Detection of Trypanosoma Brucei Gambiense, in Serologically Positive but Aparasitaemic Sleeping-Sickness Suspects in Cameroon, by PCR. *Ann. Trop. Med. Parasitol.* **1996**, *90* (5), 475–483.

(71) Ilboudo, H.; Jamonneau, V.; Camara, M.; Camara, O.; Dama, E.; Léno, M.; Ouendeno, F.; Courtin, F.; Sakande, H.; Sanon, R.; et al. Diversity of Response to Trypanosoma Brucei Gambiense Infections in the Forecariah Mangrove Focus (Guinea): Perspectives for a Better Control of Sleeping Sickness. *Microbes Infect.* **2011**, *13* (11), 943–952.

(72) Philippe; Büscher, P.; Bart, J.-M.; Boelaert, M.; Bucheton, B.; Cecchi, G.; Chitnis, N.; Courtin, D.; Figueiredo, L. M.; Franco, J.-R.; et al. Do Cryptic Reservoirs Threaten

Gambiense-Sleeping Sickness Elimination? *Trends Parasitol.* **2018**, *34* (3), 197–207.

(73) Steverding, D. The Development of Drugs for Treatment of Sleeping Sickness: A Historical Review. *Parasit. Vectors* **2010**, *3* (1), 15.

(74) Fairlamb, A. H. Chemotherapy of Human African Trypanosomiasis: Current and Future Prospects. *Trends Parasitol.* **2003**, *19* (11), 488–494.

(75) Barrett, M. P. Potential New Drugs for Human African Trypanosomiasis: Some Progress at Last. *Curr. Opin. Infect. Dis.* **2010**, *23* (6), 603–608.

(76) Brun, R.; Don, R.; Jacobs, R. T.; Wang, M. Z.; Barrett, M. P. Development of Novel Drugs for Human African Trypanosomiasis. *Future Microbiol.* **2011**, *6* (6), 677–691.

(77) Pohlig, G.; Bernhard, S. C.; Blum, J.; Burri, C.; Mpanya, A.; Lubaki, J.-P. F.; Mpoto, A. M.; Mununga, B. F.; N'tombe, P. M.; Deo, G. K. M.; et al. Efficacy and Safety of Pafuramidine versus Pentamidine Maleate for Treatment of First Stage Sleeping Sickness in a Randomized, Comparator-Controlled, International Phase 3 Clinical Trial. *PLoS Negl. Trop. Dis.* **2016**, *10* (2), e0004363.

(78) Barrett, M. P.; Boykin, D. W.; Brun, R.; Tidwell, R. R. Human African Trypanosomiasis: Pharmacological Re-Engagement with a Neglected Disease. *Br. J. Pharmacol.* **2007**, *152* (8), 1155–1171.

(79) Pépin, J.; Milord, F. The Treatment of Human African Trypanosomiasis. *Adv. Parasitol.* **1994**, *33*, 1–47.

(80) Burri, C.; Brun, R. Eflornithine for the Treatment of Human African Trypanosomiasis. *Parasitol. Res.* **2003**, *90 Supp 1*, S49-52.

(81) Jacobs, R. T.; Nare, B.; Phillips, M. A. State of the Art in African Trypanosome Drug Discovery. *Curr. Top. Med. Chem.* **2011**, *11* (10), 1255–1274.

(82) Simarro, P. P.; Franco, J.; Diarra, A.; Postigo, J. A. R.; Jannin, J. Update on Field Use of the Available Drugs for the Chemotherapy of Human African Trypanosomiasis. *Parasitology* **2012**, *139* (07), 842–846.

(83) Priotto, G.; Kasparian, S.; Mutombo, W.; Ngouama, D.; Ghorashian, S.; Arnold, U.; Ghabri, S.; Baudin, E.; Buard, V.; Kazadi-Kyanza, S.; et al. Nifurtimox-Eflornithine Combination Therapy for Second-Stage African Trypanosoma Brucei Gambiense Trypanosomiasis: A Multicentre, Randomised, Phase III, Non-Inferiority Trial. *Lancet* **2009**, *374* (9683), 56–64.

(84) Tarral, A.; Blesson, S.; Mordt, O. V.; Torreele, E.; Sassella, D.; Bray, M. A.; Hovsepian, L.; Evène, E.; Gualano, V.; Felices, M.; et al. Determination of an Optimal Dosing Regimen for Fexinidazole, a Novel Oral Drug for the Treatment of Human African Trypanosomiasis: First-in-Human Studies. *Clin. Pharmacokinet.* **2014**, *53* (6), 565–580.

(85) Jacobs, R. T.; Nare, B.; Wring, S. A.; Orr, M. D.; Chen, D.; Sligar, J. M.; Jenks, M. X.; Noe, R. A.; Bowling, T. S.; Mercer, L. T.; et al. SCYX-7158, an Orally-Active Benzoxaborole for the Treatment of Stage 2 Human African Trypanosomiasis. *PLoS Negl. Trop. Dis.* **2011**, *5* (6), e1151.

(86) Schwede, A.; Macleod, O.; MacGregor, P. How Does the VSG Coat of Bloodstream Form African Trypanosomes Interact with External Proteins? *PLoS* **2015**, *11* (12), e1005259.

(87) Vickerman, K. On The Surface Coat and Flagellar Adhesion in Trypanosomes. *J. Cell Sci.* **1969**, *5* (1), 163–193.

(88) Cross, G. A. Identification, Purification and Properties of Clone-Specific Glycoprotein Antigens Constituting the Surface Coat of Trypanosoma Brucei. *Parasitology* **1975**, *71* (3), 393–417.

(89) Ferguson, M. The Structure, Biosynthesis and Functions of Glycosylphosphatidylinositol Anchors, and the Contributions of Trypanosome Research. *J Cell Sci* **1999**, *112*, 2799–2809.

(90) Freymann, D.; Down, J.; Carrington, M.; Roditi, I.; Turner, M.; Wiley, D. 2·9 Å Resolution Structure of the N-Terminal Domain of a Variant Surface Glycoprotein from Trypanosoma Brucei. *J. Mol. Biol.* **1990**, *216* (1), 141–160.

(91) Chattopadhyay, A.; Jones, N. G.; Nietlispach, D.; Nielsen, P. R.; Voorheis, H. P.; Mott, H. R.; Carrington, M. Structure of the C-Terminal Domain from Trypanosoma Brucei Variant Surface Glycoprotein MITat1.2. *J. Biol. Chem.* **2005**, *280* (8), 7228–7235.

(92) Blum, M. L.; Down, J. A.; Gurnett, A. M.; Carrington, M.; Turner, M. J.; Wiley, D. C. A Structural Motif in the Variant Surface Glycoproteins of Trypanosoma Brucei. *Nature* **1993**, *362* (6421), 603–609.

(93) Ziegelbauer, K.; Overath, P. Identification of Invariant Surface Glycoproteins in the Bloodstream Stage of Trypanosoma Brucei. *J. Biol. Chem.* **1992**, *267* (15), 10791–10796.

(94) Doyle, J. J.; Hirumi, H.; Hirumi, K.; Lupton, E. N.; Cross, G. A. M. Antigenic Variation in Clones of Animal-Infective Trypanosoma Brucei Derived and Maintained in Vitro. *Parasitology* **1980**, *80* (02), 359–369.

(95) Manna, P. T.; Boehm, C.; Leung, K. F.; Natesan, S. K.; Field, M. C. Life and Times: Synthesis, Trafficking, and Evolution of VSG. *Trends Parasitol.* **2014**, *30* (5), 251–258.

(96) Field, M. C.; Carrington, M. The Trypanosome Flagellar Pocket. *Nat. Rev. Microbiol.* **2009**, *7* (11), 775–786.

(97) Engstler, M.; Thilo, L.; Weise, F.; Grünfelder, C. G.; Schwarz, H.; Boshart, M.; Overath, P. Kinetics of Endocytosis and Recycling of the GPI-Anchored Variant Surface Glycoprotein in Trypanosoma Brucei. *J. Cell Sci.* **2004**, *117* (Pt 7), 1105–1115.

(98) Buelow, R.; Overath, P.; Davoust, J. Rapid Lateral Diffusion of the Variant Surface Glycoprotein in the Coat of Trypanosoma Brucei. *Biochemistry* **1988**, *27* (7), 2384–2388.

(99) Pinger, J.; Chowdhury, S.; Papavasiliou, F. N. Variant Surface Glycoprotein Density Defines an Immune Evasion Threshold for African Trypanosomes Undergoing Antigenic Variation. *Nat. Commun.* **2017**, *8* (1), 828.

(100) Esser, K. M.; Schoenbechler, M. J. Expression of Two Variant Surface Glycoproteins on Individual African Trypanosomes during Antigen Switching. *Science* **1985**, *229* (4709), 190–193.

(101) Cross, G. A. M.; Kim, H.-S.; Wickstead, B. Capturing the Variant Surface Glycoprotein Repertoire (the VSGnome) of Trypanosoma Brucei Lister 427. *Mol. Biochem. Parasitol.* **2014**, *195* (1), 59–73.

(102) Borst, P. Antigenic Variation and Allelic Exclusion. *Cell* **2002**, *109* (1), 5–8.

(103) Hertz-Fowler, C.; Figueiredo, L. M.; Quail, M. A.; Becker, M.; Jackson, A.; Bason, N.; Brooks, K.; Churcher, C.; Fahkro, S.; Goodhead, I.; et al. Telomeric Expression Sites Are Highly Conserved in Trypanosoma Brucei. *PLoS One* **2008**, *3* (10), e3527.

(104) Günzl, A.; Kirkham, J. K.; Nguyen, T. N.; Badjatia, N.; Park, S. H. Mono-Allelic VSG Expression by RNA Polymerase I in Trypanosoma Brucei: Expression Site Control from Both Ends? *Gene* **2015**, *556* (1), 68–73.

(105) Morrison, L. J.; McCulloch, R.; Hall, J. P. J. DNA Recombination Strategies During Antigenic Variation in the African Trypanosome. *Microbiol. Spectr.* **2015**, *3* (2), MDNA3-0016-2014.

(106) Hall, J. P. J.; Wang, H.; Barry, J. D. Mosaic VSGs and the Scale of Trypanosoma Brucei Antigenic Variation. *PLoS Pathog.* **2013**, *9* (7), e1003502.

(107) Engstler, M.; Pfohl, T.; Herminghaus, S.; Boshart, M.; Wiegertjes, G.; Heddergott, N.; Overath, P. Hydrodynamic Flow-Mediated Protein Sorting on the Cell Surface of Trypanosomes. *Cell* **2007**, *131* (3), 505–515.

(108) Russo, D. C.; Grab, D. J.; Lonsdale-Eccles, J. D.; Shaw, M. K.; Williams, D. J. Directional Movement of Variable Surface Glycoprotein-Antibody Complexes in Trypanosoma Brucei. *Eur. J. Cell Biol.* **1993**, *62* (2), 432–441.

(109) Dubois, M. E.; Demick, K. P.; Mansfield, J. M. Trypanosomes Expressing a Mosaic Variant Surface Glycoprotein Coat Escape Early Detection by the Immune System. *Infect. Immun.* **2005**, *73* (5), 2690–2697.

(110) Takahashi, Y.; Miyamoto, H.; Fukuma, T.; Nishiyama, T.; Araki, T.; Shinka, S. In Vivo Interaction between Trypanosoma Gambiense and Leucocytes in Mice. *Ser. A Med. Microbiol. Infect. Dis. Virol. Parasitol.* **1987**, *264* (3–4), 399–406.

(111) Pan, W.; Ogunremi, O.; Wei, G.; Shi, M.; Tabel, H. CR3 (CD11b/CD18) Is the Major Macrophage Receptor for IgM Antibody-Mediated Phagocytosis of African Trypanosomes: Diverse Effect on Subsequent Synthesis of Tumor Necrosis Factor α and Nitric Oxide. *Microbes Infect.* **2006**, *8* (5), 1209–1218.

(112) Macaskill, J. A.; Holmes, P. H.; Jennings, F. W.; Urquhart, G. M. Immunological Clearance

of 75Se-Labelled Trypanosoma Brucei in Mice. III. Studies in Animals with Acute Infections. *Immunology* **1981**, *43* (4), 691–698.

(113) Ponte-Sucre, A. An Overview of Trypanosoma Brucei Infections: An Intense Host-Parasite Interaction. *Front. Microbiol.* **2016**, *7*, 2126.

(114) Stijlemans, B.; Caljon, G.; Van Den Abbeele, J.; Van Ginderachter, J. A.; Magez, S.; De Trez, C. Immune Evasion Strategies of Trypanosoma Brucei within the Mammalian Host: Progression to Pathogenicity. *Front. Immunol.* **2016**, *7*, 233.

(115) Horn, D.; McCulloch, R. Molecular Mechanisms Underlying the Control of Antigenic Variation in African Trypanosomes. *Curr. Opin. Microbiol.* **2010**, *13* (6), 700–705.

(116) Turner, C. M. R.; Aslam, N.; Dye, C. Replication, Differentiation, Growth and the Virulence of Trypanosoma Brucei Infections. *Parasitology* **1995**, *111* (03), 289–300.

(117) La Greca, F.; Magez, S. Vaccination against Trypanosomiasis. *Hum. Vaccin.* **2011**, *7* (11), 1225–1233.

(118) Rayaisse, J. B.; Esterhuizen, J.; Tirados, I.; Kaba, D.; Salou, E.; Diarrassouba, A.; Vale, G. A.; Lehane, M. J.; Torr, S. J.; Solano, P. Towards an Optimal Design of Target for Tsetse Control: Comparisons of Novel Targets for the Control of Palpalis Group Tsetse in West Africa. *PLoS Negl. Trop. Dis.* **2011**, *5* (9), e1332.

(119) Kabayo, J. P. Aiming to Eliminate Tsetse from Africa. *Trends Parasitol.* **2002**, *18* (11), 473–475.

(120) Kgori, P. M.; Modo, S.; Torr, S. J. The Use of Aerial Spraying to Eliminate Tsetse from the Okavango Delta of Botswana. *Acta Trop.* **2006**, *99* (2–3), 184–199.

(121) Green, C. H. The Use of Two-Coloured Screens for Catching Glossina Palpalis Palpalis (Robineau-Desvoidy) (Diptera: Glossinidae). *Bull. Entomol. Res.* **1989**, *79* (01), 81–93.

(122) Esterhuizen, J.; Rayaisse, J. B.; Tirados, I.; Mpiana, S.; Solano, P.; Vale, G. A.; Lehane, M. J.; Torr, S. J. Improving the Cost-Effectiveness of Visual Devices for the Control of Riverine Tsetse Flies, the Major Vectors of Human African Trypanosomiasis. *PLoS Negl. Trop. Dis.* **2011**, *5* (8), e1257.

(123) Vreysen, M. J. B.; Seck, M. T.; Sall, B.; Bouyer, J. Tsetse Flies: Their Biology and Control Using Area-Wide Integrated Pest Management Approaches. *J. Invertebr. Pathol.* **2013**, *112*, S15–S25.

(124) Simarro, P. P.; Cecchi, G.; Franco, J. R.; Paone, M.; Diarra, A.; Ruiz-Postigo, J. A.; Mattioli, R. C.; Jannin, J. G. Mapping the Capacities of Fixed Health Facilities to Cover People at Risk of Gambiense Human African Trypanosomiasis. *Int. J. Health Geogr.* **2014**, *13* (1), 4.

(125) Odiit, M.; Coleman, P. G.; Liu, W.-C.; McDermott, J. J.; Fevre, E. M.; Welburn, S. C.; Woolhouse, M. E. J. Quantifying the Level of Under-Detection of Trypanosoma Brucei Rhodesiense Sleeping Sickness Cases. *Trop. Med. Int. Heal.* **2005**, *10* (9), 840–849.

(126) Odiit, M.; Shaw, A.; Welburn, S. C.; Fèvre, E. M.; Coleman, P. G.; McDermott, J. J. Assessing the Patterns of Health-Seeking Behaviour and Awareness among Sleeping-Sickness Patients in Eastern Uganda. *Ann. Trop. Med. Parasitol.* **2004**, *98* (4), 339–348.

(127) Wembonyama, S.; Mpaka, S.; Tshilolo, L. [Medicine and Health in the Democratic Republic of Congo: From Independence to the Third Republic]. *Med. Trop. (Mars).* **2007**, *67* (5), 447–457.

(128) Simarro, P. P.; Franco, J. R.; Ndongo, P.; Nguema, E.; Louis, F. J.; Jannin, J. The Elimination of Trypanosoma Brucei Gambiense Sleeping Sickness in the Focus of Luba, Bioko Island, Equatorial Guinea. *Trop. Med. Int. Heal.* **2006**, *11* (5), 636–646.

(129) Robays, J.; Bilengue, M. M. C.; Van Der Stuyft, P.; Boelaert, M. The Effectiveness of Active Population Screening and Treatment for Sleeping Sickness Control in the Democratic Republic of Congo. *Trop. Med. Int. Heal.* **2004**, *9* (5), 542–550.

(130) Simarro, P. P.; Sima, F. O.; Mir, M.; Mateo, M. J.; Roche, J. Control of Human African Trypanosomiasis in Luba in Equatorial Guinea:Evaluation of Three Methods. *Bull. World Health Organ.* **1991**, *69* (4), 451–457.

(131) Ruiz, J. A.; Simarro, P. P.; Josenando, T. Control of Human African Trypanosomiasis in the Quiçama Focus, Angola. *Bull. World Health Organ.* **2002**, *80* (9), 738–745.

(132) Chappuis, F.; Stivanello, E.; Adams, K.; Kidane, S.; Pittet, A.; Bovier, P. A. Card

Agglutination Test for Trypanosomiasis (CATT) End-Dilution Titer and Cerebrospinal Fluid Cell Count as Predictors of Human African Trypanosomiasis (Trypanosoma Brucei Gambiense) among Serologically Suspected Individuals in Southern Sudan. *Am. J. Trop. Med. Hyg.* **2004**, *71* (3), 313–317.

(133) Simarro, P. P.; Ruiz, J. A.; Franco, J. R.; Josenando, T. Attitude towards CATT-Positive Individuals without Parasitological Confirmation in the African Trypanosomiasis (T.b. Gambiense) Focus of Quicama (Angola). *Trop. Med. Int. Heal.* **1999**, *4* (12), 858–861.

(134) Malvy, D.; Chappuis, F. Sleeping Sickness. *Clin. Microbiol. Infect.* **2011**, *17* (7), 986–995.

(135) Magnus, E.; Vervoort, T.; Van Meirvenne, N. A Card-Agglutination Test with Stained Trypanosomes (C.A.T.T.) for the Serological Diagnosis of T.b.Gambiense Trypanosomiasis. *Ann. Soc. Belg. Med. Trop. (1920).* **1978**, *58* (3), 169–176.

(136) Chappuis, F.; Loutan, L.; Simarro, P.; Lejon, V.; Büscher, P. Options for Field Diagnosis of Human African Trypanosomiasis. *Clin. Microbiol. Rev.* **2005**, *18* (1), 133–146.

(137) Büscher, P.; Lejon, V.; Magnus, E.; Van Meirvenne, N. Improved Latex Agglutination Test for Detection of Antibodies in Serum and Cerebrospinal Fluid of Trypanosoma Brucei Gambiense Infected Patients. *Acta Trop.* **1999**, *73* (1), 11–20.

(138) Jamonneau, V.; Truc, P.; Garcia, A.; Magnus, E.; Büscher, P. Preliminary Evaluation of LATEX/T. b. Gambiense and Alternative Versions of CATT/T. b. Gambiense for the Serodiagnosis of Human African Trypanosomiasis of a Population at Risk in Côte d'Ivoire: Considerations for Mass-Screening. *Acta Trop.* **2000**, *76* (2), 175–183.

(139) Van Meirvenne, N.; Magnus, E.; Buscher, P. Evaluation of Variant Specific Trypanolysis Tests for Serodiagnosis of Human Infections with Trypanosoma Brucei Gambiense. *Acta Trop.* **1995**, *60* (3), 189–199.

(140) Mitashi, P.; Hasker, E.; Lejon, V.; Kande, V.; Muyembe, J.-J.; Lutumba, P.; Boelaert, M. Human African Trypanosomiasis Diagnosis in First-Line Health Services of Endemic Countries, a Systematic Review. *PLoS Negl. Trop. Dis.* **2012**, *6* (11), e1919.

(141) Enyaru, J. C. K.; Matovu, E.; Akol, M.; Sebikali, C.; Kyambadde, J.; Schmidt, C.; Brun, R.;

Kaminsky, R.; Ogwal, L. M.; Kansiime, F. Parasitological Detection of *Trypanosoma Brucei Gambiense* in Serologically Negative Sleeping-Sickness Suspects from North-Western Uganda. *Ann. Trop. Med. Parasitol.* **1998**, *92* (8), 845–850.

(142) Dukes, P.; Gibson, W. C.; Gashumba, J. K.; Hudson, K. M.; Bromidge, T. J.; Kaukus, A.; Asonganyi, T.; Magnus, E. Absence of the LiTat 1.3 (CATT Antigen) Gene in Trypanosoma Brucei Gambiense Stocks from Cameroon. *Acta Trop.* **1992**, *51* (2), 123–134.

(143) Paquet, C.; Ancelle, T.; Gastellu-Etchegorry, M.; Castilla, J.; Harndt, I. Persistence of Antibodies to Trypanosoma Brucei Gambiense after Treatment of Human Trypanosomiasis in Uganda. *Lancet (London, England)* **1992**, *340* (8813), 250.

(144) Checchi, F.; Chappuis, F.; Karunakara, U.; Priotto, G.; Chandramohan, D. Accuracy of Five Algorithms to Diagnose Gambiense Human African Trypanosomiasis. *PLoS Negl. Trop. Dis.* **2011**, *5* (7), e1233.

(145) Lumsden, W. H.; Kimber, C. D.; Evans, D. A.; Doig, S. J. Trypanosoma Brucei: Miniature Anion-Exchange Centrifugation Technique for Detection of Low Parasitaemias: Adaptation for Field Use. *Trans. R. Soc. Trop. Med. Hyg.* **1979**, *73* (3), 312–317.

(146) Büscher, P.; Mumba Ngoyi, D.; Kaboré, J.; Lejon, V.; Robays, J.; Jamonneau, V.; Bebronne, N.; Van der Veken, W.; Biéler, S. Improved Models of Mini Anion Exchange Centrifugation Technique (MAECT) and Modified Single Centrifugation (MSC) for Sleeping Sickness Diagnosis and Staging. *PLoS Negl. Trop. Dis.* **2009**, *3* (11), e471.

(147) Woo, P. T. The Haematocrit Centrifuge Technique for the Diagnosis of African Trypanosomiasis. *Acta Trop.* **1970**, *27* (4), 384–386.

(148) Woo, P. T. Evaluation of the Haematocrit Centrifuge and Other Techniques for the Field Diagnosis of Human Trypanosomiasis and Filariasis. *Acta Trop.* **1971**, *28* (3), 298–303.

(149) Mumba Ngoyi, D.; Menten, J.; Pyana, P. P.; Büscher, P.; Lejon, V. Stage Determination in Sleeping Sickness: Comparison of Two Cell Counting and Two Parasite Detection Techniques. *Trop. Med. Int. Heal.* **2013**, *18* (6), 778–782.

(150) Stanghellini, A.; Josenando, T. The Situation of Sleeping Sickness in Angola: A Calamity.

Trop. Med. Int. Heal. **2001**, *6* (5), 330–334.

(151) Lejon, V.; Reiber, H.; Legros, D.; Djé, N.; Magnus, E.; Wouters, I.; Sindic, C. J. M.; Büscher, P. Intrathecal Immune Response Pattern for Improved Diagnosis of Central Nervous System Involvement in Trypanosomiasis. *J. Infect. Dis.* **2003**, *187* (9), 1475–1483.

(152) Bonnet, J.; Boudot, C.; Courtioux, B. Overview of the Diagnostic Methods Used in the Field for Human African Trypanosomiasis: What Could Change in the Next Years? *Biomed Res. Int.* **2015**, *2015*, 1–10.

(153) McGovern, T. W.; Williams, W.; Fitzpatrick, J. E.; Cetron, M. S.; Hepburn, B. C.; Gentry, R. H. Cutaneous Manifestations of African Trypanosomiasis. *Arch. Dermatol.* **1995**, *131* (10), 1178–1182.

(154) Trindade, S.; Rijo-Ferreira, F.; Carvalho, T.; Pinto-Neves, D.; Guegan, F.; Aresta-Branco, F.; Bento, F.; Young, S. A.; Pinto, A.; Van Den Abbeele, J.; et al. Trypanosoma Brucei Parasites Occupy and Functionally Adapt to the Adipose Tissue in Mice. *Cell Host Microbe* **2016**, *19* (6), 837–848.

(155) Caljon, G.; Van Reet, N.; De Trez, C.; Vermeersch, M.; Pérez-Morga, D.; Van Den Abbeele, J. The Dermis as a Delivery Site of Trypanosoma Brucei for Tsetse Flies. *PLOS Pathog.* **2016**, *12* (7), e1005744.

(156) Capewell, P.; Cren-Travaillé, C.; Marchesi, F.; Johnston, P.; Clucas, C.; Benson, R. A.; Gorman, T. A.; Calvo-Alvarez, E.; Crouzols, A.; Jouvion, G.; et al. The Skin Is a Significant but Overlooked Anatomical Reservoir for Vector-Borne African Trypanosomes. *Elife* **2016**, *5*, e17716.

(157) Raman, C. V.; Krishnan, K. S. A New Type of Secondary Radiation. *Nature* **1928**, *121* (3048), 501–502.

(158) Carter, J. C.; Angel, S. M.; Brewer, W. E. Raman Spectroscopy for the in Situ Identification of Cocaine and Selected Adulterants. *Appl. Spectrosc. Vol. 54, Issue 12, pp. 1876-1881* **2000**, *54* (12), 1876–1881.

(159) West, M. J.; Went, M. J. The Spectroscopic Detection of Drugs of Abuse in Fingerprints

after Development with Powders and Recovery with Adhesive Lifters. *Spectrochim. Acta Part A Mol. Biomol. Spectrosc.* **2009**, *71* (5), 1984–1988.

(160) Bellot-Gurlet, L.; Pagès-Camagna, S.; Coupry, C. Raman Spectroscopy in Art and Archaeology. *J. Raman Spectrosc.* **2006**, *37* (10), 962–965.

(161) Sandalinas, C.; Ruiz-Moreno, S.; López-Gil, A.; Miralles, J. Experimental Confirmation by Raman Spectroscopy of a Pb - Sn - Sb Triple Oxide Yellow Pigment in Sixteenth-Century Italian Pottery. *J. Raman Spectrosc.* **2006**, *37* (10), 1146–1153.

(162) Yang, D.; Ying, Y. Applications of Raman Spectroscopy in Agricultural Products and Food Analysis: A Review. *Appl. Spectrosc. Rev.* **2011**, *46* (7), 539–560.

(163) Li, Y.-S.; Church, J. S. Raman Spectroscopy in the Analysis of Food and Pharmaceutical Nanomaterials. *J. Food Drug Anal.* **2014**, *22* (1), 29–48.

(164) Ember, K. J. I.; Hoeve, M. A.; McAughtrie, S. L.; Bergholt, M. S.; Dwyer, B. J.; Stevens, M. M.; Faulds, K.; Forbes, S. J.; Campbell, C. J. Raman Spectroscopy and Regenerative Medicine: A Review. *npj Regen. Med.* **2017**, *2* (1), 12.

(165) Kong, K.; Kendall, C.; Stone, N.; Notingher, I. Raman Spectroscopy for Medical Diagnostics - From in-Vitro Biofluid Assays to in-Vivo Cancer Detection. *Adv. Drug Deliv. Rev.* **2015**, *89*, 121–134.

(166) Smith, E.; Dent, G. *Modern Raman Spectroscopy - A Practical Approach*; John Wiley & Sons, Ltd: Chichester, UK, 2004.

(167) Vandenabeele, P.; Peter. *Practical Raman Spectroscopy - An Introduction*; John Wiley & Sons, Ltd: Chichester, UK, 2013.

(168) Ferraro, J. R.; Nakamoto, K.; Brown, C. W.; Ferraro, J. R.; Nakamoto, K.; Brown, C. W. Chapter 1 – Basic Theory. In *Introductory Raman Spectroscopy*; 2003; pp 1–94.

(169) Uzunbajakava, N.; Lenferink, A.; Kraan, Y.; Willekens, B.; Vrensen, G.; Greve, J.; Otto, C. Nonresonant Raman Imaging of Protein Distribution in Single Human Cells. *Biopolymers* **2003**, *72* (1), 1–9.

(170) Krafft, C.; Knetschke, T.; Funk, R. H. W.; Salzer, R. Identification of Organelles and Vesicles in Single Cells by Raman Microspectroscopic Mapping. *Vib. Spectrosc.* **2005**, *38* (1–2), 85–93.

(171) Bonnier, F.; Knief, P.; Lim, B.; Meade, A. D.; Dorney, J.; Bhattacharya, K.; Lyng, F. M.; Byrne, H. J. Imaging Live Cells Grown on a Three Dimensional Collagen Matrix Using Raman Microspectroscopy. *Analyst* **2010**, *135* (12), 3169–3177.

(172) Butler, H. J.; Ashton, L.; Bird, B.; Cinque, G.; Curtis, K.; Esmonde-white, K.; Fullwood, N. J.; Gardner, B.; Martin-, P. L.; Walsh, M. J.; et al. Using Raman Spectroscopy to Characterise Biological Materials. *Nat. Protoc.* **2016**, *11* (4), 1–47.

(173) Li, Z.; Deen, M.; Kumar, S.; Selvaganapathy, P. Raman Spectroscopy for In-Line Water Quality Monitoring—Instrumentation and Potential. *Sensors* **2014**, *14* (12), 17275–17303.

(174) Frank, C. J.; McCreery, R. L.; Redd, D. C. B. Raman Spectroscopy of Normal and Diseased Human Breast Tissues. *Anal. Chem.* **1995**, *67* (5), 777–783.

(175) Yang, S.; Li, B.; Slipchenko, M. N.; Akkus, A.; Singer, N. G.; Yeni, Y. N.; Akkus, O. Laser Wavelength Dependence of Background Fluorescence in Raman Spectroscopic Analysis of Synovial Fluid from Symptomatic Joints. *J. Raman Spectrosc.* **2013**, *44* (8), 1089–1095.

(176) Chen, T.-C.; Shea, D. A.; Morris, M. D. Effect of Hydrogen Peroxide Bleaching on Bone Mineral/Matrix Ratio. *Appl. Spectrosc.* **2002**, *56* (8), 1035–1037.

(177) Yang, B.; Owen, H.; Morris, M. D. Holographic Notch Filter for Low-Wavenumber Stokes and Anti-Stokes Raman Spectroscopy. *Appl. Spectrosc. Vol. 45, Issue 9, pp. 1533-1536* **1991**, *45* (9), 1533–1536.

(178) Harnly, J. M.; Fields, R. E. Solid-State Array Detectors for Analytical Spectrometry. *Appl. Spectrosc.* **1997**, *51* (9), 334A–351A.

(179) Prats Mateu, B.; Harreither, E.; Schosserer, M.; Puxbaum, V.; Gludovacz, E.; Borth, N.; Gierlinger, N.; Grillari, J. Label-Free Live Cell Imaging by Confocal Raman Microscopy Identifies CHO Host and Producer Cell Lines. *Biotechnol. J.* **2017**, *12* (1).

(180) Majzner, K.; Kaczor, A.; Kachamakova-Trojanowska, N.; Fedorowicz, A.; Chlopicki, S.;

Baranska, M. 3D Confocal Raman Imaging of Endothelial Cells and Vascular Wall: Perspectives in Analytical Spectroscopy of Biomedical Research. *Analyst* **2013**, *138* (2), 603–610.

(181) Gierlinger, N.; Keplinger, T.; Harrington, M. Imaging of Plant Cell Walls by Confocal Raman Microscopy. *Nat. Protoc.* **2012**, *7* (9), 1694–1708.

(182) Hashimoto, A.; Yamaguchi, Y.; Chiu, L.; Morimoto, C.; Fujita, K.; Takedachi, M.; Kawata, S.; Murakami, S.; Tamiya, E. Time-Lapse Raman Imaging of Osteoblast Differentiation. *Sci. Rep.* **2015**, *5* (1), 12529.

(183) Kong, L.; Setlow, P.; Li, Y. Observation of the Dynamic Germination of Single Bacterial Spores Using Rapid Raman Imaging. *J. Biomed. Opt.* **2013**, *19* (1), 011003.

(184) Okada, M.; Smith, N. I.; Palonpon, A. F.; Endo, H.; Kawata, S.; Sodeoka, M.; Fujita, K. Label-Free Raman Observation of Cytochrome c Dynamics during Apoptosis. *Proc. Natl. Acad. Sci.* **2012**, *109* (1), 28–32.

(185) Ichimura, T.; Chiu, L.; Fujita, K.; Kawata, S.; Watanabe, T. M.; Yanagida, T.; Fujita, H. Visualizing Cell State Transition Using Raman Spectroscopy. *PLoS One* **2014**, *9* (1), e84478.

(186) Farhane, Z.; Bonnier, F.; Casey, A.; Byrne, H. J. Raman Micro Spectroscopy for in Vitro Drug Screening: Subcellular Localisation and Interactions of Doxorubicin. *Analyst* **2015**, *140* (12), 4212–4223.

(187) Krafft, C.; Knetschke, T.; Siegner, A.; Funk, R. H. W.; Salzer, R. Mapping of Single Cells by near Infrared Raman Microspectroscopy. *Vib. Spectrosc.* **2003**, *32* (1), 75–83.

(188) Kallepitis, C.; Bergholt, M. S.; Mazo, M. M.; Leonardo, V.; Skaalure, S. C.; Maynard, S. A.; Stevens, M. M. Quantitative Volumetric Raman Imaging of Three Dimensional Cell Cultures. *Nat. Commun.* **2017**, *8*, 14843.

(189) Palonpon, A. F.; Ando, J.; Yamakoshi, H.; Dodo, K.; Sodeoka, M.; Kawata, S.; Fujita, K. Raman and SERS Microscopy for Molecular Imaging of Live Cells. *Nat. Protoc.* **2013**, *8* (4), 677–692.

(190) Matthäus, C.; Chernenko, T.; Newmark, J. A.; Warner, C. M.; Diem, M. Label-Free

Detection of Mitochondrial Distribution in Cells by Nonresonant Raman Microspectroscopy. *Biophys. J.* **2007**, *93* (2), 668–673.

(191) Klein, K.; Gigler, A. M.; Aschenbrenner, T.; Monetti, R.; Bunk, W.; Jamitzky, F.; Morfill, G.; Stark, R. W.; Schlegel, J. Label-Free Live-Cell Imaging with Confocal Raman Microscopy. *Biophys. J.* **2012**, *102* (2), 360–368.

(192) Hamada, K.; Fujita, K.; Smith, N. I.; Kobayashi, M.; Inouye, Y.; Kawata, S. Raman Microscopy for Dynamic Molecular Imaging of Living Cells. *J. Biomed. Opt.* **2008**, *13* (4), 044027.

(193) Draux, F.; Jeannesson, P.; Beljebbar, A.; Tfayli, A.; Fourre, N.; Manfait, M.; Sulé-Suso, J.; Sockalingum, G. D. Raman Spectral Imaging of Single Living Cancer Cells: A Preliminary Study. *Analyst* **2009**, *134* (3), 542–548.

(194) Huang, Y. S.; Karashima, T.; Yamamoto, M.; Hamaguchi, H. O. Molecular-Level Investigation of the Structure, Transformation, and Bioactivity of Single Living Fission Yeast Cells by Time- and Space-Resolved Raman Spectroscopy. *Biochemistry* **2005**, *44* (30), 10009–10019.

(195) Swain, R. J.; Jell, G.; Stevens, M. M. Non-invasive Analysis of Cell Cycle Dynamics in Single Living Cells with Raman Micro-spectroscopy. *J. Cell. Biochem.* **2008**, *104* (4), 1427–1438.

(196) Kumar, R.; Singh, G.; Grønhaug, K.; Afseth, N.; de Lange Davies, C.; Drogset, J.; Lilledahl, M. Single Cell Confocal Raman Spectroscopy of Human Osteoarthritic Chondrocytes: A Preliminary Study. *Int. J. Mol. Sci.* **2015**, *16* (12), 9341–9353.

(197) Krishna, C. M.; Sockalingum, G. D.; Kegelaer, G.; Rubin, S.; Kartha, V. B.; Manfait, M. Micro-Raman Spectroscopy of Mixed Cancer Cell Populations. *Vib. Spectrosc.* **2005**, *38* (1–2), 95–100.

(198) Jess, P. R. T.; Smith, D. D. W.; Mazilu, M.; Dholakia, K.; Riches, A. C.; Herrington, C. S. Early Detection of Cervical Neoplasia by Raman Spectroscopy. *Int. J. Cancer* **2007**, *121* (12), 2723–2728.

(199) Yu, C.; Gestl, E.; Eckert, K.; Allara, D.; Irudayaraj, J. Characterization of Human Breast

Epithelial Cells by Confocal Raman Microspectroscopy. *Cancer Detect. Prev.* **2006**, *30* (6), 515–522.

(200) Chan, J. W.; Taylor, D. S.; Zwerdling, T.; Lane, S. M.; Ihara, K.; Huser, T. Micro-Raman Spectroscopy Detects Individual Neoplastic and Normal Hematopoietic Cells. *Biophys. J.* **2006**, *90* (2), 648–656.

(201) Franco, D.; Trusso, S.; Fazio, E.; Allegra, A.; Musolino, C.; Speciale, A.; Cimino, F.; Saija, A.; Neri, F.; Nicolò, M. S.; et al. Raman Spectroscopy Differentiates between Sensitive and Resistant Multiple Myeloma Cell Lines. *Spectrochim. Acta Part A Mol. Biomol. Spectrosc.* **2017**, *187*, 15–22.

(202) Ilin, Y.; Choi, J. S.; Harley, B. A. C.; Kraft, M. L. Identifying States along the Hematopoietic Stem Cell Differentiation Hierarchy with Single Cell Specificity via Raman Spectroscopy. *Anal. Chem.* **2015**, *87* (22), 11317–11324.

(203) Chowdary, M. V. P.; Kumar, K. K.; Thakur, K.; Anand, A.; Kurien, J.; Krishna, C. M.; Mathew, S. Discrimination of Normal and Malignant Mucosal Tissues of the Colon by Raman Spectroscopy. *Photomed. Laser Surg.* **2007**, *25* (4), 269–274.

(204) Mahadevan-Jansen, A.; Mitchell, M. F.; Ramanujamf, N.; Malpica, A.; Thomsen, S.; Utzinger, U.; Richards-Kortumt, R. Near-Infrared Raman Spectroscopy for In Vitro Detection of Cervical Precancers. *Photochem. Photobiol.* **1998**, *68* (1), 123–132.

(205) Rau, J. V.; Fosca, M.; Graziani, V.; Taffon, C.; Rocchia, M.; Caricato, M.; Pozzilli, P.; Onetti Muda, A.; Crescenzi, A. Proof-of-Concept Raman Spectroscopy Study Aimed to Differentiate Thyroid Follicular Patterned Lesions. *Sci. Rep.* **2017**, *7* (1), 14970.

(206) Teh, S.; Zheng, W.; Ho, K.; Teh, M.; Yeoh, K.; Huang, Z. Diagnostic Potential of Near-Infrared Raman Spectroscopy in the Stomach: Differentiating Dysplasia from Normal Tissue. *Br. J. Cancer* **2008**, *98*, 457–465.

(207) Kendall, C.; Stone, N.; Shepherd, N.; Geboes, K.; Warren, B.; Bennett, R.; Barr, H. Raman Spectroscopy, a Potential Tool for the Objective Identification and Classification of Neoplasia in Barrett's Oesophagus. *J. Pathol.* **2003**, *200* (5), 602–609.

(208) Fullwood, L. M.; Clemens, G.; Griffiths, D.; Ashton, K.; Dawson, T. P.; Lea, R. W.; Davis, C.; Bonnier, F.; Byrne, H. J.; Baker, M. J. Investigating the Use of Raman and Immersion Raman Spectroscopy for Spectral Histopathology of Metastatic Brain Cancer and Primary Sites of Origin. *Anal. Methods* **2014**, *6* (12), 3948–3961.

(209) Haka, A. S.; Shafer-Peltier, K. E.; Fitzmaurice, M.; Crowe, J.; Dasari, R. R.; Feld, M. S. Diagnosing Breast Cancer by Using Raman Spectroscopy. *Proc. Natl. Acad. Sci. U. S. A.* **2005**, *102* (35), 12371–12376.

(210) Crow, P.; Stone, N.; Kendall, C. A.; Uff, J. S.; Farmer, J. A. M.; Barr, H.; Wright, M. P. J. The Use of Raman Spectroscopy to Identify and Grade Prostatic Adenocarcinoma in Vitro. *Br. J. Cancer* **2003**, *89* (1), 106–108.

(211) Huang, Z.; McWilliams, A.; Lui, H.; McLean, D. I.; Lam, S.; Zeng, H. Near-Infrared Raman Spectroscopy for Optical Diagnosis of Lung Cancer. *Int. J. Cancer* **2003**, *107* (6), 1047–1052.

(212) Rashid, N.; Nawaz, H.; Poon, K. W. C.; Bonnier, F.; Bakhiet, S.; Martin, C.; O'Leary, J. J.; Byrne, H. J.; Lyng, F. M. Raman Microspectroscopy for the Early Detection of Pre-Malignant Changes in Cervical Tissue. *Exp. Mol. Pathol.* **2014**, *97* (3), 554–564.

(213) Veenstra, M. A.; Palyvoda, O.; Alahwal, H.; Jovanovski, M.; Reisner, L. A.; King, B.; Poulik, J.; Klein, M. D. Raman Spectroscopy in the Diagnosis of Ulcerative Colitis. *Eur. J. Pediatr. Surg.* **2015**, *25* (1), 56–59.

(214) Stevens, O.; Iping Petterson, I. E.; Day, J. C. C.; Stone, N. Developing Fibre Optic Raman Probes for Applications in Clinical Spectroscopy. *Chem. Soc. Rev.* **2016**, *45* (7), 1919–1934.

(215) Utzinger, U.; Richards-Kortum, R. R. Fiber Optic Probes for Biomedical Optical Spectroscopy. *J. Biomed. Opt.* **2003**, *8* (1), 121–147.

(216) Sharma, M.; Marple, E.; Reichenberg, J.; Tunnell, J. W. Design and Characterization of a Novel Multimodal Fiber-Optic Probe and Spectroscopy System for Skin Cancer Applications. *Rev. Sci. Instrum.* **2014**, *85* (8), 083101.

(217) Kourkoumelis, N.; Balatsoukas, I.; Moulia, V.; Elka, A.; Gaitanis, G.; Bassukas, I. D.

Advances in the in Vivo Raman Spectroscopy of Malignant Skin Tumors Using Portable Instrumentation. *Int. J. Mol. Sci.* **2015**, *16* (7), 14554–14570.

(218) Zheng, J.; Pang, S.; Labuza, T. P.; He, L. Evaluation of Surface-Enhanced Raman Scattering Detection Using a Handheld and a Bench-Top Raman Spectrometer: A Comparative Study. *Talanta* **2014**, *129*, 79–85.

(219) Woo, Y. A.; Ahn, J. W.; Chun, I. K.; Kim, H. J. Development of a Method for the Determination of Human Skin Moisture Using a Portable Near-Infrared System. *Anal. Chem.* **2001**, *73* (20), 4964–4971.

(220) Nijssen, A.; Maquelin, K.; Santos, L. F.; Caspers, P. J.; Bakker Schut, T. C.; den Hollander, J. C.; Neumann, M. H. A.; Puppels, G. J. Discriminating Basal Cell Carcinoma from Perilesional Skin Using High Wave-Number Raman Spectroscopy. *J. Biomed. Opt.* **2007**, *12* (3), 034004.

(221) Lieber, C.; Mahadevan-Jansen, A. Development of a Handheld Raman Microspectrometer for Clinical Dermatologic Applications. *Opt. Express* **2007**, *15* (19), 11874–11882.

(222) Lieber, C. A.; Majumder, S. K.; Ellis, D. L.; Billheimer, D. D.; Mahadevan-Jansen, A. In Vivo Nonmelanoma Skin Cancer Diagnosis Using Raman Microspectroscopy. *Lasers Surg. Med.* **2008**, *40* (7), 461–467.

(223) Schleusener, J.; Gluszczynska, P.; Reble, C.; Gersonde, I.; Helfmann, J.; Fluhr, J. W.; Lademann, J.; Röwert-Huber, J.; Patzelt, A.; Meinke, M. C. In Vivo Study for the Discrimination of Cancerous and Normal Skin Using Fibre Probe-Based Raman Spectroscopy. *Exp. Dermatol.* **2015**, *24* (10), 767–772.

(224) Lui, H.; Zhao, J.; McLean, D.; Zeng, H. Real-Time Raman Spectroscopy for In Vivo Skin Cancer Diagnosis. *Cancer Res.* **2012**, *72* (10), 2491–2500.

(225) Bergholt, M. S.; Zheng, W.; Lin, K.; Ho, K. Y.; Teh, M.; Yeoh, K. G.; Yan So, J. B.; Huang, Z. Raman Endoscopy for in Vivo Differentiation between Benign and Malignant Ulcers in the Stomach. *Analyst* **2010**, *135* (12), 3162–3168.

(226) Day, J. C. C.; Bennett, R.; Smith, B.; Kendall, C.; Hutchings, J.; Meaden, G. M.; Born, C.; Yu, S.; Stone, N. A Miniature Confocal Raman Probe for Endoscopic Use. *Phys. Med. Biol.*

2009, *54* (23), 7077–7087.

(227) Shim, M. G.; Wong Kee Song, L.-M.; Marcon, N. E.; Wilson, B. C. In Vivo Near-Infrared Raman Spectroscopy: Demonstration of Feasibility During Clinical Gastrointestinal Endoscopy. *Photochem. Photobiol.* **2000**, *72* (1), 146–150.

(228) Haka, A. S.; Volynskaya, Z.; Gardecki, J. A.; Nazemi, J.; Lyons, J.; Hicks, D.; Fitzmaurice, M.; Dasari, R. R.; Crowe, J. P.; Feld, M. S. In Vivo Margin Assessment during Partial Mastectomy Breast Surgery Using Raman Spectroscopy. *Cancer Res.* **2006**, *66* (6), 3317–3322.

(229) Jermyn, M.; Mok, K.; Mercier, J.; Desroches, J.; Pichette, J.; Saint-Arnaud, K.; Bernstein, L.; Guiot, M.-C.; Petrecca, K.; Leblond, F. Intraoperative Brain Cancer Detection with Raman Spectroscopy in Humans. *Sci. Transl. Med.* **2015**, *7* (274), 274ra19.

(230) Jones, N. G.; Nietlispach, D.; Sharma, R.; Burke, D. F.; Eyres, I.; Mues, M.; Mott, H. R.; Carrington, M. Structure of a Glycosylphosphatidylinositol-Anchored Domain from a Trypanosome Variant Surface Glycoprotein. *J. Biol. Chem.* **2008**, *283* (6), 3584–3593.

(231) Talari, A. C. S.; Movasaghi, Z.; Rehman, S.; Rehman, I. U. Raman Spectroscopy of Biological Tissues. *Appl. Spectrosc. Rev.* **2015**, *50* (1), 46–111.

(232) Stone, N.; Kendall, C.; Smith, J.; Crow, P.; Barr, H.; Montgomery, E.; Bronner, M. P.; Goldblum, J. R.; Greenson, J. K.; Haber, H. M.; et al. Raman Spectroscopy for Identification of Epithelial Cancers. *Faraday Discuss.* **2004**, *126* (0), 141–157.

(233) Huang, N.; Short, M.; Zhao, J.; Wang, H.; Lui, H.; Korbelik, M.; Zeng, H. Full Range Characterization of the Raman Spectra of Organs in a Murine Model. *Opt. Express* **2011**, *19* (23), 22892–22909.

(234) Golcuk, K.; Mandair, G. S.; Callender, A. F.; Sahar, N.; Kohn, D. H.; Morris, M. D. Is Photobleaching Necessary for Raman Imaging of Bone Tissue Using a Green Laser? *Biochim. Biophys. Acta - Biomembr.* **2006**, *1758* (7), 868–873.

(235) Bartossek, T.; Jones, N. G.; Schäfer, C.; Cvitković, M.; Glogger, M.; Mott, H. R.; Kuper, J.; Brennich, M.; Carrington, M.; Smith, A.-S.; et al. Structural Basis for the Shielding Function

of the Dynamic Trypanosome Variant Surface Glycoprotein Coat. *Nat. Microbiol.* **2017**, *2* (11), 1523–1532.

(236) Pelton, J. T.; McLean, L. R. Spectroscopic Methods for Analysis of Protein Secondary Structure. *Anal. Biochem.* **2000**, *277* (2), 167–176.

(237) Tuma, R. Raman Spectroscopy of Proteins: From Peptides to Large Assemblies. *J. Raman Spectrosc.* **2005**, *36* (4), 307–319.

(238) Signorelli, S.; Cannistraro, S.; Bizzarri, A. R. Structural Characterization of the Intrinsically Disordered Protein P53 Using Raman Spectroscopy. *Appl. Spectrosc.* **2017**, *71* (5), 823–832.

(239) Mangialardo, S.; Piccirilli, F.; Perucchi, A.; Dore, P.; Postorino, P. Raman Analysis of Insulin Denaturation Induced by High-Pressure and Thermal Treatments. *J. Raman Spectrosc.* **2012**, *43* (6), 692–700.

(240) Patnaik, P. K.; Field, M. C.; Menon, A. K.; Cross, G. A.; Yee, M. C.; Bütikofer, P. Molecular Species Analysis of Phospholipids from Trypanosoma Brucei Bloodstream and Procyclic Forms. *Mol. Biochem. Parasitol.* **1993**, *58* (1), 97–105.

(241) Carroll, M.; McCrorie, P. Lipid Composition of Bloodstream Forms of Trypanosoma Brucei Brucei. *Comp. Biochem. Physiol. Part B Comp. Biochem.* **1986**, *83* (3), 647–651.

(242) Richmond, G. S.; Gibellini, F.; Young, S. A.; Major, L.; Denton, H.; Lilley, A.; Smith, T. K. Lipidomic Analysis of Bloodstream and Procyclic Form Trypanosoma Brucei. *Parasitology* **2010**, *137* (9), 1357–1392.

(243) Smith, T. K.; Bütikofer, P. Lipid Metabolism in Trypanosoma Brucei. *Mol. Biochem. Parasitol.* **2010**, *172* (2), 66–79.

(244) Serricchio, M.; Bütikofer, P. Trypanosoma Brucei: A Model Micro-Organism to Study Eukaryotic Phospholipid Biosynthesis. *FEBS J.* **2011**, *278* (7), 1035–1046.

(245) Carrington, M.; Miller, N.; Blum, M.; Roditi, I.; Wiley, D.; Turner, M. Variant Specific Glycoprotein of Trypanosoma Brucei Consists of Two Domains Each Having an Independently Conserved Pattern of Cysteine Residues. *J. Mol. Biol.* **1991**, *221* (3), 823–

835.

(246) Gadelha, C.; Zhang, W.; Chamberlain, J. W.; Chait, B. T.; Wickstead, B.; Field, M. C. Architecture of a Host–Parasite Interface: Complex Targeting Mechanisms Revealed Through Proteomics. *Mol. Cell. Proteomics* **2015**, *14* (7), 1911–1926.

(247) Kerr, L. T.; Byrne, H. J.; Hennelly, B. M. Optimal Choice of Sample Substrate and Laser Wavelength for Raman Spectroscopic Analysis of Biological Specimen. *Anal. Methods* **2015**, *7* (12), 5041–5052.

(248) Mariani, M. M.; Lampen, P.; Popp, J.; Wood, B. R.; Deckert, V. Impact of Fixation on in Vitro Cell Culture Lines Monitored with Raman Spectroscopy. *Analyst* **2009**, *134* (6), 1154–1161.

(249) Tfayli, A.; Gobinet, C.; Vrabie, V.; Huez, R.; Manfait, M.; Piot, O. Digital Dewaxing of Raman Signals: Discrimination between Nevi and Melanoma Spectra Obtained from Paraffin-Embedded Skin Biopsies. *Appl. Spectrosc.* **2009**, *63* (5), 564–570.

(250) Faolain, E. . Raman Spectroscopic Evaluation of Efficacy of Current Paraffin Wax Section Dewaxing Agents. *J. Histochem. Cytochem.* **2005**, *53* (1), 121–129.

(251) Bringaud, F.; Rivière, L.; Coustou, V. Energy Metabolism of Trypanosomatids: Adaptation to Available Carbon Sources. *Mol. Biochem. Parasitol.* **2006**, *149* (1), 1–9.

(252) Ter Kuile, B. H.; Opperdoes, F. R. Glucose Uptake by Trypanosoma Brucei. Rate-Limiting Steps in Glycolysis and Regulation of the Glycolytic Flux. *J. Biol. Chem.* **1991**, *266* (2), 857–862.

(253) Black, S.; Vandeweerd, V. Serum Lipoproteins Are Required for Multiplication of Trypanosoma Brucei Brucei under Axenic Culture Conditions. *Mol. Biochem. Parasitol.* **1989**, *37* (1), 65–72.

(254) Coppens, I.; Levade, T.; Courtoy, P. J. Host Plasma Low Density Lipoprotein Particles as an Essential Source of Lipids for the Bloodstream Forms of Trypanosoma Brucei. *J. Biol. Chem.* **1995**, *270* (11), 5736–5741.

(255) Krafft, C.; Neudert, L.; Simat, T.; Salzer, R. Near Infrared Raman Spectra of Human Brain

Lipids. *Spectrochim. Acta Part A Mol. Biomol. Spectrosc.* **2005**, *61* (7), 1529–1535.

(256) Lund-Katz, S.; Phillips, M. C. High Density Lipoprotein Structure-Function and Role in Reverse Cholesterol Transport. *Subcell. Biochem.* **2010**, *51*, 183–227.

(257) Biryomumaisho, S.; Katunguka-Rwakishaya, E.; Rubaire-Akiiki, C. M. Serum Biochemical Changes in Experimental Trypanosoma Congolense and Trypanosoma Brucei Infection in Small East Africa Goats. *Vet. Arh.* **2003**, *73* (3), 167–180.

(258) Adamu, S.; Barde; Abenga, J. N.; Useh, N. M.; Ibrahim; Esievo, K. A. N. Experimental Trypanosoma Brucei Infection-Induced Changes in the Serum Profiles of Lipids and Cholesterol and the Clinical Implications in Pigs. *J. Cell Anim. Biol.* **2009**, *3* (2), 15–20.

(259) Johndrow, C.; Nelson, R.; Tanowitz, H.; Weiss, L.; Nagajyothi, F. Trypanosoma Cruzi Infection Results in an Increase in Intracellular Cholesterol. *Microbes Infect.* **2014**, *16* (4), 337–344.

(260) Tyler, K. M.; Fridberg, A.; Toriello, K. M.; Olson, C. L.; Cieslak, J. A.; Hazlett, T. L.; Engman, D. M. Flagellar Membrane Localization via Association with Lipid Rafts. *J. Cell Sci.* **2009**, *122* (Pt 6), 859–866.

(261) Green, H. P.; Del Pilar Molina Portela, M.; St Jean, E. N.; Lugli, E. B.; Raper, J. Evidence for a Trypanosoma Brucei Lipoprotein Scavenger Receptor. *J. Biol. Chem.* **2003**, *278* (1), 422–427.

(262) Newport, G. R.; Page, C. R.; Ashman, P. U.; Stibbs, H. H.; Seed, J. R. Alteration of Free Serum Amino Acids in Voles Infected with Trypanosoma Brucei Gambiense. *J. Parasitol.* **1977**, *63* (1), 15–24.

(263) Hall, J. E.; Seed, J. R. Increased Urinary Excretion of Aromatic Amino Acid Catabolites by Microtus Montanus Chronically Infected with Trypanosoma Brucei Gambiense. *Comp. Biochem. Physiol. Part B Comp. Biochem.* **1984**, *77* (4), 755–760.

(264) McGettrick, A. F.; Corcoran, S. E.; Barry, P. J. G.; McFarland, J.; Crès, C.; Curtis, A. M.; Franklin, E.; Corr, S. C.; Mok, K. H.; Cummins, E. P.; et al. Trypanosoma Brucei Metabolite Indolepyruvate Decreases HIF-1α and Glycolysis in Macrophages as a Mechanism of

Innate Immune Evasion. *Proc. Natl. Acad. Sci. U. S. A.* **2016**, *113* (48), E7778–E7787.

(265) Wang, Y.; Utzinger, J.; Saric, J.; Li, J. V; Burckhardt, J.; Dirnhofer, S.; Nicholson, J. K.; Singer, B. H.; Brun, R.; Holmes, E. Global Metabolic Responses of Mice to Trypanosoma Brucei Brucei Infection. *Proc. Natl. Acad. Sci. U. S. A.* **2008**, *105* (16), 6127–6132.

(266) Herbert, W. J.; Lumsden, W. H. R. Trypanosoma Brucei: A Rapid "Matching" Method for Estimating the Host's Parasitemia. *Exp. Parasitol.* **1976**, *40* (3), 427–431.

(267) Deng, J. L.; Wei, Q.; Zhang, M. H.; Wang, Y. Z.; Li, Y. Q. Study of the Effect of Alcohol on Single Human Red Blood Cells Using Near-Infrared Laser Tweezers Raman Spectroscopy. *J. Raman Spectrosc.* **2005**, *36* (3), 257–261.

(268) Bastos, I. M. D.; Motta, F. N.; Charneau, S.; Santana, J. M.; Dubost, L.; Augustyns, K.; Grellier, P. Prolyl Oligopeptidase of Trypanosoma Brucei Hydrolyzes Native Collagen, Peptide Hormones and Is Active in the Plasma of Infected Mice. *Microbes Infect.* **2010**, *12* (6), 457–466.

(269) Czamara, K.; Majzner, K.; Pacia, M. Z.; Kochan, K.; Kaczor, A.; Baranska, M. Raman Spectroscopy of Lipids: A Review. *J. Raman Spectrosc.* **2015**, *46* (1), 4–20.

(270) Moulton, J. E. Experimental Trypanosoma Brucei Infection in Deer Mice: Splenic Changes. *Vet. Pathol.* **1980**, *17* (2), 218–225.

(271) Anosa, V. O.; Kaneko, J. J. Pathogenesis of Trypanosoma Brucei Infection in Deer Mice (Peromyscus Maniculatus). *Vet. Pathol.* **1984**, *21* (2), 229–237.

(272) Waema, M. W.; Maina, N. W.; Ngotho, M.; Karanja, S. M.; Gachie, B. M.; Maranga, D. N.; Kagira, J. M. IgM, LgG and IL-6 Profiles in the Trypanosoma Brucei Brucei Monkey Model of Human African Trypanosomiasis. *Acta Trop.* **2017**, *168*, 45–49.

(273) Magez, S.; Stijlemans, B.; Baral, T.; De Baetselier, P. VSG-GPI Anchors of African Trypanosomes: Their Role in Macrophage Activation and Induction of Infection-Associated Immunopathology. *Microbes Infect.* **2002**, *4* (9), 999–1006.

(274) Willert, E.; Phillips, M. A. Regulation and Function of Polyamines in African Trypanosomes. *Trends Parasitol.* **2012**, *28* (2), 66–72.

(275) Achcar, F.; Kerkhoven, E. J.; Barrett, M. P. Trypanosoma Brucei: Meet the System. *Curr. Opin. Microbiol.* **2014**, *20*, 162–169.

(276) Stijlemans, B.; Beschin, A.; Magez, S.; Van Ginderachter, J. A.; De Baetselier, P. Iron Homeostasis and Trypanosoma Brucei Associated Immunopathogenicity Development: A Battle/Quest for Iron. *Biomed Res. Int.* **2015**, *2015*, 819389.

(277) Basu, S.; Horáková, E.; Lukeš, J. Iron-Associated Biology of Trypanosoma Brucei. *Biochim. Biophys. Acta - Gen. Subj.* **2016**, *1860* (2), 363–370.

(278) Smith, T. K.; Bringaud, F.; Nolan, D. P.; Figueiredo, L. M. Metabolic Reprogramming during the Trypanosoma Brucei Life Cycle. *F1000Research* **2017**, *6 (F1000 F*, 683.

(279) Becker, S.; Franco, J. R.; Simarro, P. P.; Stich, A.; Abel, P. M.; Steverding, D. Real-Time PCR for Detection of Trypanosoma Brucei in Human Blood Samples. *Diagn. Microbiol. Infect. Dis.* **2004**, *50* (3), 193–199.

(280) Mugasa, C. M.; Adams, E. R.; Boer, K. R.; Dyserinck, H. C.; Büscher, P.; Schallig, H. D. H. F.; Leeflang, M. M. G. Diagnostic Accuracy of Molecular Amplification Tests for Human African Trypanosomiasis-Systematic Review. *PLoS Negl. Trop. Dis.* **2012**, *6* (1), e1438.

Appendix 1

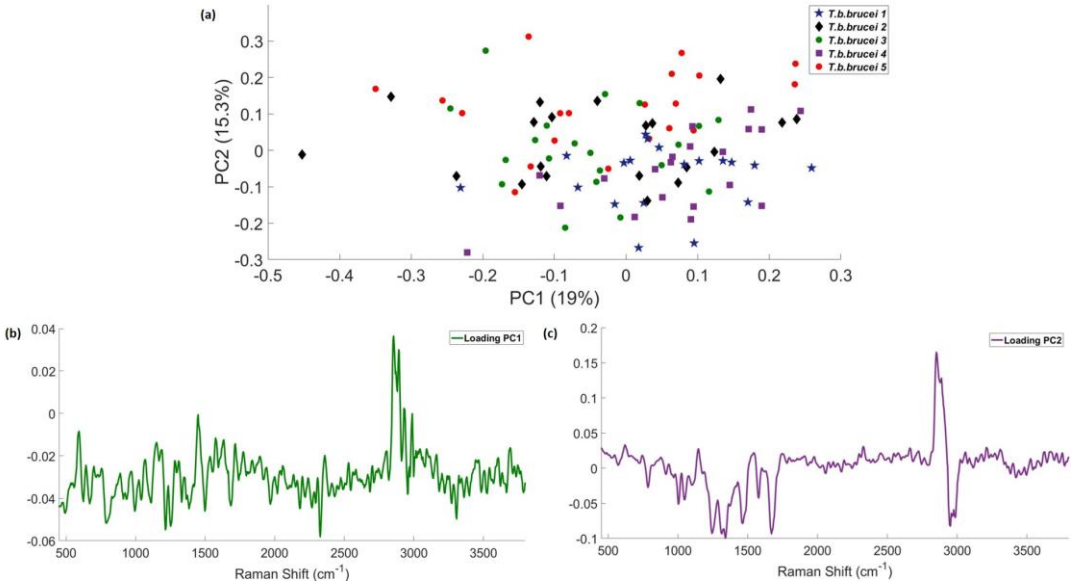

Figure A1.1 Principal component analysis of five different T.b. brucei with 20 spectra each measured with a 532 nm laser. (a) Scores plot of PC1 versus PC2, (b) PC1 loading spectrum, (c) PC2 loading spectrum.

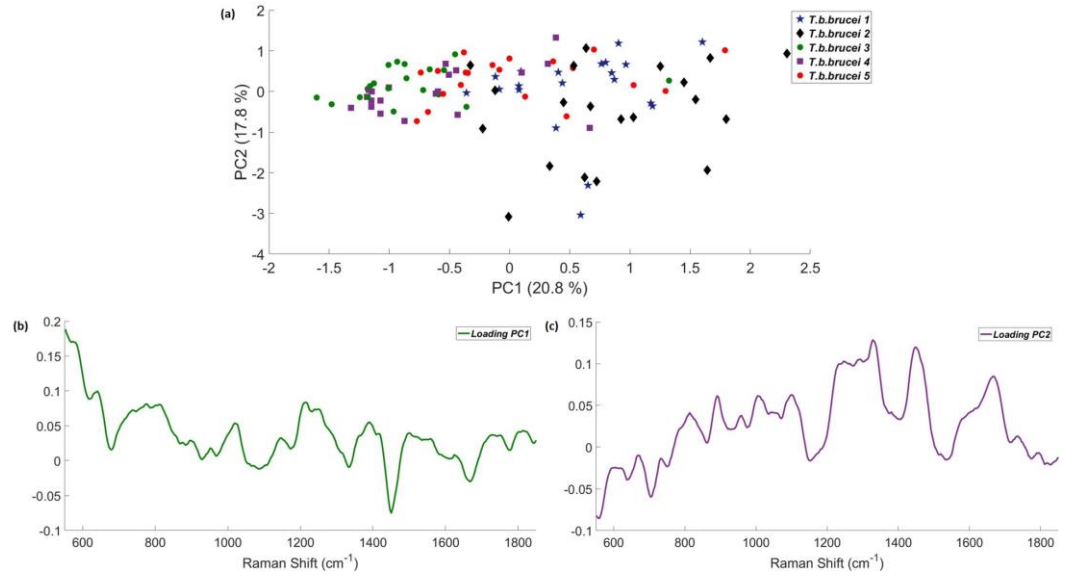

Figure A1.2 Principal component analysis of five different T.b. brucei with 20 spectra each measured with a 785 nm laser between the Raman bands located between the wavenumbers region 550 and 1850 cm^{-1}. (a) Scores plot of PC1 versus PC2, (b) PC1 loading spectrum, (c) PC2 loading spectrum.

Appendix 2

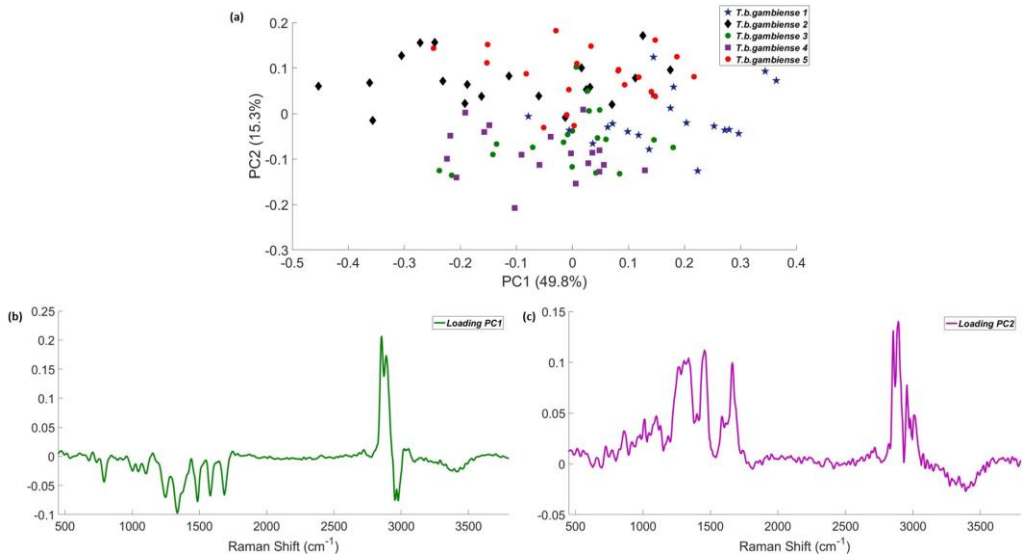

Figure A2.1 Principal component analysis of five different T.b. gambiense with 20 spectra each measured with a 532 nm laser. (a) Scores plot of PC1 versus PC2, (b) PC1 loading spectrum, (c) PC2 loading spectrum.

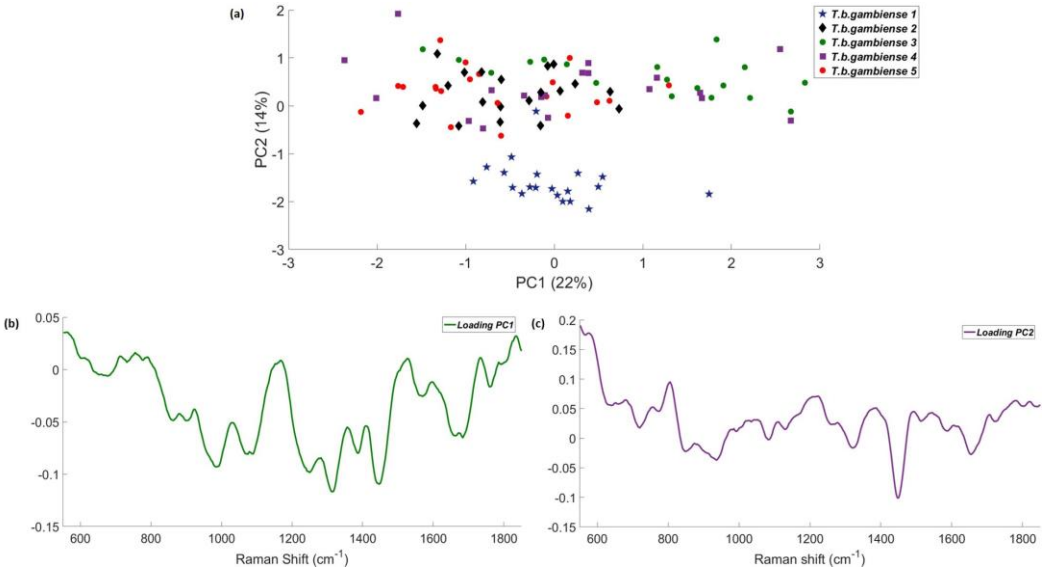

Figure A2.2 Principal component analysis of five different T.b. gambiense with 20 spectra each, measured with a 785 nm laser. (a) Scores plot of PC1 versus PC2, (b) PC1 loading spectrum, (b) PC2 loading spectrum.